DNA damage response pathways in DNA double strand break repair and hepatic metabolism

A Dissertation

Presented to the Faculty of the Graduate School

of Cornell University

In Partial Fulfillment of the Requirements for the Degree of

Doctor of Philosophy

by

Elizabeth S. Moore

May 2019

DNA damage response pathways in DNA double strand break repair and hepatic metabolism

Elizabeth S. Moore, DVM, Ph. D.

Cornell University 2019

The maintenance of genomic integrity and cellular homeostasis relies upon the appropriate selection and coordination of signaling and effector pathways in response to damage or perturbations. The DNA damage response (DDR) is an intricate network of surveillance, signal transduction, checkpoint activation, and repair protein recruitment and function. The DDR is capable of exquisite modulation to appropriately respond to a wide array of damage types, extents, and contexts that depend on cell type, cell cycle stage, cellular metabolic state, and extracellular cues.

One of the most deleterious DNA lesions is a double stranded break (DSB). Multiple repair pathways have evolved to repair DSBs that differ in repair factors, mechanism, kinetics, and fidelity, and pathway choice is incompletely understood. Lower accuracy non-homologous end joining (NHEJ) and high fidelity homologous recombination (HR) are the two major DSB repair mechanisms. We investigated the role of the HUS1 component of the RAD9A-HUS1-RAD1 (9-1-1) DNA damage response clamp in DSB repair. Combined absence of the HR component *Rad54* and *Hus1* deficiency increased genome instability and genotoxin sensitivity, suggesting both *Hus1* and *Rad54* contribute to HR. In contrast, combined loss of the NHEJ component *Prkdc* and *Hus1* deficiency resulted in no significant increase in genomic instability and a partial rescue in genotoxin sensitivity *in vivo*. This suggests that the 9-1-1 clamp may have a role in suppressing inappropriate NHEJ in certain contexts and/or that alternative repair pathways are disinhibited in the absence of NHEJ and

deficiency of *Hus1*. The data suggest the 9-1-1 clamp plays a role in DSB repair pathway selection.

Cell metabolism and genome integrity are intersecting and coordinated, and many canonical DDR proteins also regulate metabolism. This work describes a novel connection between a component of the Fanconi Anemia (FA) DNA repair pathway and hepatic metabolism. Altered energy states have been described in FA deficient cells, and human patients with a defect in the FA pathway are predisposed to metabolic disease through an unknown etiology. Upon challenge with a high fat, high cholesterol diet, FA-deficient *Fancd2*$^{-/-}$ male mice developed hepatic pathology accompanied by altered expression of cholesterol and bile acid metabolism genes and displayed numerous differential abundances of hepatic lipid species, in the absence of significant elevation in DNA damage or DDR activation. This indicates a role for the FA pathway in hepatic metabolic homeostasis.

This work advances our understanding of the molecular function and dynamics of the 9-1-1 DDR repair complex and the mechanisms through which cells respond to DSBs and replication stress. Finessed understanding of the interplay between DDR factors can help us better identify derangements that result in deleterious phenotypes as well as identify DDR pathway components upon which cancer cells have increased reliance, so they may be targeted to increase therapeutic success. This work also advances the known roles of the Fanconi Anemia pathway beyond canonical DNA repair, which may lead to improved understanding of the etiology of FA phenotypes and therapeutic strategies. Elucidating the many connections between the DDR and cellular metabolic homeostasis has broad implications for understanding cancer cell biology.

BIOGRAPHICAL SKETCH

Elizabeth Moore graduated from the University of Kentucky with B.S. degrees in Biotechnology and Biology with a minor in French language. She then achieved admission into the profession she had aspired to since the age of three by completing her DVM from the Cornell University College of Veterinary Medicine. During veterinary school, Elizabeth was drawn to discovery science and the pursuit of advancing biomedical knowledge. She sought to bring her interest in veterinary medicine, comparative biology, and basic research together by completing a residency in laboratory animal medicine with the Cornell Center for Animal Resources and Education and a graduate degree in the Department of Biological and Biomedical Sciences in the laboratory of Dr. Robert Weiss.

ACKNOWLEDGMENTS

I would like to thank my parents who always supported my goals, encouraged my passions, and provided me foundation and example. I also thank my kind and talented husband for his patience and support, and for bringing balance to my life.

I would like to express my gratitude for the mentorship and time investment of my advisor Dr. Weiss, who allowed me to gain experience in his laboratory while I was still a veterinary student and accepted me as a non-traditional part-time student while I was completing my residency. Dr. Weiss is an exemplary scientist and role model, who sets an example with his work ethic, rigorous standards, and thoughtful approaches. I have benefited greatly from his instruction and consider myself incredibly fortunate to have trained with him.

Thank you to my committee members, Drs. Bethany Cummings, Joe Wakshlag, and John Schimenti for committing their time and effort to guiding my training and professional development, and for their insightful comments and suggestions which have improved my projects.

I've been lucky to share my graduate training with many talented colleagues in the Weiss laboratory. It was a privilege to work and learn with you. I have wonderful memories of first working in the lab with Dr. Erin Daugherity, who is a role model and who helped shape my early training choices. I appreciate the hard work and creative ideas of my co-authors, Drs. Pei Xin Lim, Joanna Mleczko, and Amy Lyndaker. I'm so glad to have worked with Dr. Tim Pierpont, who spent hours helping me collect tissue, analyze data, fix every technical problem, and discuss ideas. I had the pleasure of working with Dr. Darshil Patel, a talented scientist and caring person who was always game for an escape off campus for lunch when a break was needed. I've benefited from the insightful ideas of Catalina Pereira, from whom I also learned several techniques. I was lucky to share an office with Irma Fernandez, who brings laughter and encouragement to the lab in addition to her many scientific talents. I am also glad to have shared time

in the lab with Dr. Yashira Abril Negron, Dr. April Blong, and many enthusiastic and talented undergraduates: David Karambizi, Ellen Hong, Charlton Tsai, Brenna Remick, Eric Zhang, Matthew Guo, Michael Downey, and Ravi Dhawan. I thank all of these talented scientists for encouraging, instructing, inspiring and assisting me during my training in the laboratory.

I am grateful for the support and encouragement of Drs. Philippe Baneaux and Mary Martin, who supported my endeavor to combine my residency with graduate training. I would like to thank all of the members of the Cornell Center for Animal Resources and Education for contributing to my training, for their friendship, and for their support in helping me achieve my goals, especially Drs. Erin Daugherity and Wendy Williams, and to my resident-mates Drs. Balu Reddyjarugu, Rohit Rajoria, and Beth Noe who helped make my dual training possible.

TABLE OF CONTENTS

LIST OF FIGURES

LIST OF TABLES

CHAPTER 1

LITERATURE REVIEW

1.1: DNA damage and the DNA Damage Response

The DNA damage response (DDR) is an intricate signal transduction pathway that senses DNA damage and coordinates an array of potential responses, including regulating DNA repair, cell cycle arrest via checkpoint activation, transcription, as well as replication, recombination, chromatin remodeling, and differentiation (1, 2). The DDR consists of sensors of DNA damage, transducers that relay the signal, and effectors. DNA damage occurring anywhere in the genome is recognized and repaired by global genome repair, whereas lesions can also be sensed and repaired in specific manners according to whether they block transcription or replication.

1.1.1: DNA damage

Maintenance of genomic integrity is crucial for survival at both the cellular and organismal level. Failure to maintain genomic integrity can result in cell death, accelerated aging, senescence, loss of function, or transformation. The types of DNA lesions the DDR must counter are many and varied, and it has been estimated that the combination of exogenous and endogenous damages result in approximately 10^4 DNA modifications daily (3, 4). The severity of the consequence resulting from DNA damage will be influenced by the type and extent of DNA lesion(s), their location, the cell type, as well as the stage of the cell cycle and differentiation (5).

Spontaneous DNA damage can result from hydrolysis leading to abasic sites and base deamination, dNTP misincorporation, DNA depurination, and oxidation or other DNA damages caused by products generated from normal cellular metabolism, such as reactive oxygen species, alkylating agents, nitrogen species, and lipid peroxidation products (5). DNA can also be damaged from external sources, such as ultraviolet light (UV), ionizing radiation (IR), and chemical agents, which can create lesions such as the attachment of alkyl groups or other adducts, strand breaks, and the creation of DNA intra and interstrand crosslinks (ICLs). Replication stress can lead to replication fork collapse and the

generation of single and double stranded breaks (DSB). Therefore, many repair mechanisms have evolved.

1.1.2: DNA damage signaling kinases

The main initiators of the DDR signaling networks in mammals are the phosphatidylinositol 3-kinase-like (PIKK) family members and signaling kinases Ataxia-telangiectasia mutated (ATM) and ATM and Rad-3-related (ATR). Though *ATM* is not an essential gene for life, mutations results in a disorder characterized by increased sensitivity to IR and increased cancer risk called ataxia telangietacia (6, 7). Double strand breaks, such as those caused by IR, are sensed by the MRN complex (Mre-11-Rad50-Nsb1), which recruits and activates ATM (2). ATM then phosphorylates many downstream targets, including p53, γH2AX, and Chk2 (8). Loss of ATR is embryonic lethal and results in chromosomal aberrations (9, 10). Mutations in *ATR* in humans result in Seckel syndrome, characterized by physical and cognitive defects (11). Replication protein A (RPA) coated single strand DNA (ssDNA), which could arise from strand breaks or stalled replication forks, recruits ATR along with its binding partner, ATRIP (12, 13). The RAD 17-RFC2-5 clamp loader is also recruited and activated, which loads the toroidal RAD9-Hus1-RAD1 (9-1-1) clamp (12). The 9-1-1 clamp stimulates ATR through its interaction with the ATR activating protein TOPBP1 (12). The ATR kinase can also be activated via interaction with ETAA1, and loss of both TOPBP1 and ETAA1 results in synthetic lethality (14-16). ATR signal transduction results in CHK1 kinase activation, along with phosphorylation of many other chromatin-localized factors and downstream substrates (12), to coordinate cell cycle checkpoint activation and DNA repair.

1.1.3: DNA damage checkpoint signaling

Cell cycle checkpoint signaling is a critical arm of the DDR and ensures that in replicating cells, DNA repair is completed before cell division. Checkpoints have historically been thought of as initiating cell cycle arrest to allow time for DNA repair, however, checkpoint signaling also controls activation of DNA repair pathways, activation of transcriptional programs, chromatin structure and repair protein

localization, and telomere homeostasis (reviewed in (17)). The three major cell cycle divisions regulated by the DNA damage checkpoint are the G1/S transition, S phase progression, and the G2/M transition, with many of the genes necessary for arrest at one stage also necessary at the others (18). Defective checkpoints can lead to increased genome errors, greater rates of genome evolution, formation of secondary lesions (conversion of an unrepaired single strand break to a double strand break), and loss of repair options (fragmentation and loss of a broken chromosome, precluding end-joining) (18).

The G1/S transition checkpoint serves to prevent replication of damaged DNA. The intra-S phase checkpoint decreases the rate of DNA synthesis in response to DNA damage, which can result from regulation of origin initiation and/or replication fork progression (19, 20). Failure of these checkpoints results in consequences associated with replicating a damaged template. For example, replication of a modified base can result in a gap on the daughter strand, and replication of single strand nicks can lead to replication fork collapse and DSB formation (21). Replication across unrepaired lesions may lead to misincorporation of bases. In addition to inhibiting replication in the face of DNA damage, it is also possible that regulating the transition to S phase prevents DNA damage that might arise from inappropriate progression of cells that are not yet able to activate enough replication origins or that have inappropriate nucleotide pools (18, 22).

The G2/M checkpoint prevents initiation of mitosis in cells that still have unrepaired DNA damage after S phase. Mitosis with unrepaired DSBs can be particularly detrimental for cells and lead to chromosome fragments partitioning into separate nuclei, chromosome loss, bridge-breakage-fusion cycles, chromosome rearrangement, and gene amplification (23, 24). G2/M checkpoint failure also precludes the availability of a sister chromatid repair template.

As cell cycle progression is regulated by cyclin dependent kinases and cyclin regulatory proteins, the DNA damage checkpoint can be initiated by DDR proteins that initiate signaling cascades that regulate cyclin dependent kinase (cdk) activity, such as ATM (in response to IR induced DSBs) and ATR (in response to IR, UV, and replication stress) discussed above (25). Downstream of ATM and ATR, the CHK2 and CHK1 kinases have been shown to regulate cyclins. ATM is generally thought to activate CHK2 kinase signaling, and ATR to activate CHK1 kinase signaling, though there is some overlap. Both

CHK1 and CHK2 can phosphorylate CDC25C which results in its cytoplasmic relocalization, preventing dephosphorylation of CDK1/cyclin B and thus maintenance of a G2/M arrest (26, 27). CHK1 and CHK2 can also phosphorylate CDC25A, promoting its degradation, which results in CDK2 remaining phosphorylated and thus inhibited, leading to cell cycle arrest at the G1/S entry phase (28, 29). The checkpoint branch of the DDR is critical in the maintenance of genome integrity.

Thus the DDR allows for both the maintenance of functional integrity in differentiated cells and the faithful passage of information to progeny in replicative cells, preventing deleterious consequences such as cell death or transformation.

1.1.4: DNA repair overview:

1.1.4.1: Direct reversal of DNA damage

Some types of DNA damage do not require multi-step repair, but rather can be directly reversed without incision of the DNA backbone and often by a single protein. Three major direct repair mechanisms are photolysase reversal of UV lesions (separation of fused pyrimidine bases), reversal of an *O*- alkylated DNA damage by O^6-alkylguanine-DNA alkyltransferases, and reversal of *N*-alkylated base adducts by the AlκB family of dioxygenases (30). Few types of DNA lesions can be repaired this way, however, direct reversal is essentially error free.

1.1.4.2: Single strand lesion repair (base excision, nucleotide excision and mismatch repair)

Single stranded DNA damage can be repaired by three main excision repair pathways. Some modifications of DNA, such as oxidative lesions and small alkylation products, can be repaired via base excision repair (BER) throughout the cell cycle. In this process, a damaged base is removed by a glycosylase, followed by strand incision by an AP endonuclease creating a single stranded break that will be repaired by DNA synthesis in short (single nucleotide) or long patch repair (2-10 nucleotides) (5, 31, 32). Nucleotide excision repair (NER) is employed for helix distorting lesions, such as those caused by UV damage (thymine dimers, clyclobutane pyrimidine dimers, and 6,4-photoproducts) and chemotherapeutics, and can be used as part of both global genome repair and transcription coupled repair

(5, 33). A short segment of single stranded DNA is removed, followed by DNA synthesis using the opposite strand as a template and ligation. Defects in NER can result in Xeroderma pigmentosum and Cockayne's syndrome. Mismatch repair (MMR) generally deals with errors of replication and recombination, such as insertions, deletions, and mis-incorporated bases, and involves a mechanism to distinguish the newly synthesized strand which commonly includes replication errors from the parental template strand (34).

1.1.4.3: Damage tolerance

Some DNA errors are tolerated by cells and bypassed. Translesion synthesis (TLS) is a mechanism of damage tolerance. Most DNA lesions unrepaired by S phase block DNA replication. Cells can employ TLS, in which the replicative polymerase is temporarily switched for one of seven identified lower fidelity polymerases to replicate past the lesion and avoid stalled replication forks and DNA breaks (35). Inherent to their ability to replicate damaged templates, the fidelity of TLS polymerases is low, therefore their activity must be tightly controlled to prevent mutagenesis. It is believed that PCNA ubiquitination is the main mechanism for recruitment of TLS polymerases (36). The various TLS polymerases respond to different types of lesions, vary in error rate, have specific mutation signatures, and vary in their ability to extend DNA.

1.1.4.4: Single strand break repair:

Single stranded breaks (SSBs) are discontinuities in one strand, and the 5' and/or 3' termini often have damaged or mismatched bases (37). SSBs can be caused by reactive oxygen species (ROS) which can destroy deoxyribose residues, by irradiation (IR), by aborted activity of some enzymes (such as DNA topoisomerase), and can occur as intermediates of DNA repair, such as BER (38). Some SSBs, such as those caused by ROS may be processed and ligated by the same proteins used in later steps of BER (4). Most SSBs are repaired by a rapid and global SSB repair involving detection, end-processing, gap filling, and ligation.

Detection of SSBs generated from ROS is usually attributed to Poly(ADP-ribose) polymerase-1 (PARP1) (39). PARP1 also protects DNA strand broken ends and prevents erroneous recombination (40). For gap filling and ligation to proceed, the damaged ends must be restored (to 3'-hydroxyl and 5'-phosphate moieties), and several enzymes can participate (such as PNKP, APEX1, Polβ, FEN1, TDP1, APTX, XRCC1, and others), depending on the types of damaged ends (reviewed in (37)). DNA gap filling is often conducted by polymerase beta, though polymerase delta and epsilon are also used (41). If filling is longer than a single nucleotide (short-patch repair), FEN1 can remove the displaced 5' residue as a single-stranded flap (long-patch repair) (41).The ligases LIG1 and LIG3alpha contribute to ligation of nuclear long-patch and short-patch SSB repair respectively (41). Thus SSBs can be repaired by various mechanisms.

Interstrand crosslink (ICL) repair will be discussed in section 1.6.1, but briefly this mechanism repairs covalent cross-links between the two strands of DNA, which prevent strand separation and interfere with transcription and replication. Repair of ICLs involves NER, TLS, and homologous recombination (HR) pathways.

1.1.4.5: DNA double strand break (DSB) repair

The DNA backbone can be broken by both endogenous agents, such as reactive oxygen species, and exogenous sources of damage, such as ionizing radiation. Double strand breaks can also result from replication fork collapse. DSBs exist in different configurations: having two ends or one (Figure 1.1). Unrepaired DSBs lead to unequal distribution of genetic material during mitosis or chromosomal translocations. Such genomic instability can trigger cell death, or lead to cellular transformation via the activation of oncogenes or disruption of tumor suppressor genes (42). DSBs are thus one of the most deleterious DNA lesions.

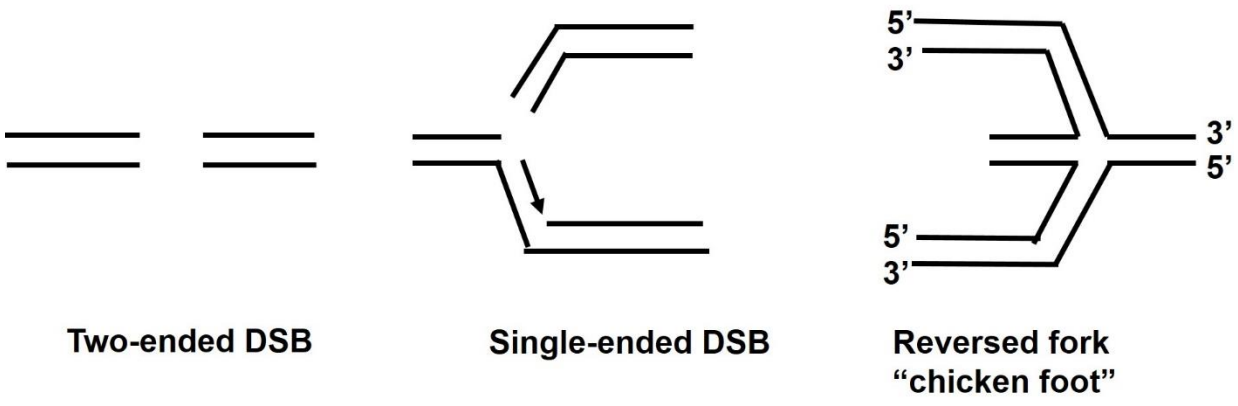

Figure 1.1: Types of DNA double strand breaks (DSBs). Two-ended DNA DSBs can be generated by DNA damaging agents such as irradiation. Single ended DSBs (seDSBs) can be generated by replication fork collapse. Replication fork stalling can lead to replication fork reversal and annealing of the newly synthesized strands in a "chicken foot" structure, which also creates free DNA ends that may be recognized as a DSB.

There are at least four cellular sensors for DSBs (PARP, KU70/80, the MRN complex, and, if some DNA end processing has occurred, RPA (1)), and cells have evolved multiple pathways to repair them. These can be divided into non-homology mediated, minimal end processing pathways: non-homologous end joining (NHEJ) and alternative-end joining (alt-EJ), and homology-directed repair (HDR) pathways that require extensive processing of DNA ends: homologous recombination (HR), single strand annealing (SSA), and break induced replication (BIR). NHEJ and HR are the major pathways responsible for the majority of DSB repair.

1.1.4.5i: Non-homologous end joining (NHEJ)

In NHEJ, broken DNA ends are joined mainly by direct ligation with minimal or no base pairing, which can result in nucleotide insertions, deletions, and substitutions. KU heterodimers (KU70 and KU80) rapidly bind to DNA ends, followed by DNA-PKcs recruitment, stabilizing DNA ends(43). KU interacts with DNA polymerases μ and λ and the XRCC4-DNA ligase IV complex to ligate the ends (44). DNA ends not amenable to direct ligation can be minimally processed by Artemis (reviewed in (45)).

NHEJ is unable to process DNA ends that have been extensively resected with long ssDNA overhangs (46).

1.1.4.5ii: Alternative-end joining (Alt-EJ)

Alternative-end joining appears to encompass more than one process and is thought of as a global rescuing mechanism for DNA ends that are not repaired by NHEJ or HR. Alt-EJ involves a minimal amount of end resection and is mainly functional in late G1 and early S phase, but has been shown to function in G2 (47). Proteins involved in Alt-EJ are generally known to be involved in other DNA repair pathways, particularly HR and single strand annealing (48). PARP1 is required for alt-EJ (49, 50). Other components include ligase III, XRCC1,and PNK (49). CtIP (51) and MRE11 (52) are also implicated in alt- EJ. Though not required, Alt-EJ frequently uses substantial microhomology (5-25 base pairs), resulting in deletion (53).

1.1.4.5iii: Homologous recombination (HR)

HR, which predominates in S and G2 phases, conducts sister chromatid homology-directed, high fidelity repair. HR begins with the MRN complex (MRE11-RAD50-NBS1) localizing to double strand breaks, which stabilizes DNA ends, and is important for initial DNA resection and ATM recruitment (54, 55). CtIP is recruited in an MRN and ATM dependent manner, and is important for end resection (56, 57). EXO1, BLM, and DNA2 continue end resection (58). A 5’ to 3’ resection results in a 3’ ssDNA overhang, which becomes coated and stabilized by RPA (a heterotrimeric complex) (59). RAD51 can then form a filament on the 3’ ssDNA in a BRCA2-dependent manner in combination with PALB2, and perform strand invasion and homology search on the sister chromatid for homologous template directed repair (60). RAD51 paralogs (RAD51B, RAD51C, RAD51D, XRCC2, XRCC3), and the RAD52 epistasis group member RAD54 assist with RAD51 function (61). RAD54 assists multiple stages of HR, including chromatin remodeling for RAD51 filament stabilization, strand invasion, D-loop dissolution and branch migration, and RAD51 dissociation (62). HR repair intermediates can be resolved by BLM/TOPOIII or cleaved by GEN1, MUS81/EME1, or SLX1/SLX4 in either crossover or non-crossover

events (63-66). Unlike two-ended DSBs, which are often repaired by NHEJ, a major function of HR is to repair single-ended DSBs (seDSBs) that occur as a result of replication fork collapse, and to prevent "toxic" NHEJ at these types of seDSBs (67). It is also believed that HR may be preferentially employed to repair DSBs that occur at fragile, highly transcriptionally active sites via R-loop, quadruplex DNA, and topoisomerase-II driven mechanisms (68). Meiotic programmed DSB repair is also HR-predominate.

1.1.4.5iv: Other DSB repair mechanisms

Single strand annealing (SSA) is another homology directed DSB repair pathway in which sequence repeats near a double strand break can be revealed through resection and result in annealing of complementary strands. The region between the repeats is deleted, thus this pathway is mutagenic. This mechanism only involves the DNA duplex and does not need the homologous chromosome or sister chromatid. Roughly half of the mammalian genome consists of repeats, therefore SSA may be an important contributor to mutagenic DNA repair (69).

Break induced replication (BIR) can be used to repair single-ended DSBs (seDSBs), such as those arising at collapsed replication forks. This mutagenic process involves a broken DNA end invading a homologous duplex and using it as a template for DNA synthesis via a migrating bubble, resulting in conservative inheritance of the synthesized DNA. BIR can result in hyper-mutagenesis, loss of heterozygosity, copy number variants, genomic rearrangements and chromosomal translocations (70).

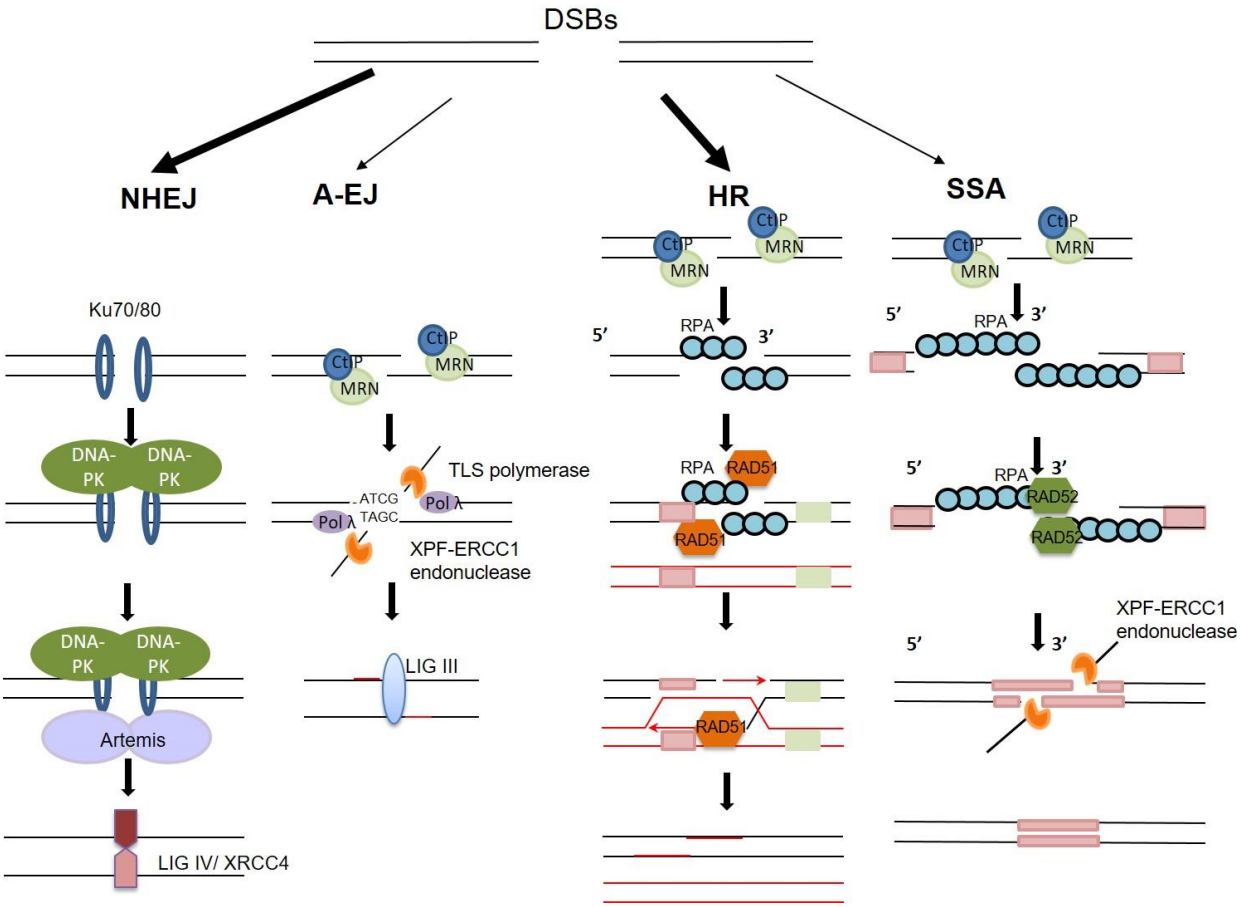

Figure 1.2: DNA double strand break repair pathways. Nonhomologous end-joining (NHEJ) is considered a dominant repair pathway, utilizing highly abundant repair proteins, proceeding with fast kinetics, and being available at all stages of the cell cycle. The KU70/80 heterodimer rapidly localizes to DNA ends, followed by DNA-PK and Artemis recruitment, preventing DNA end resection and tethering the broken ends. Minimal end processing is followed by ligation, resulting in mutagenic repair characterized by insertions/deletions and frameshifts. Homologous recombination (HR) is available only in S/G2 phase, requires initial end processing and resection by endo and exonucleases, and uses the sister chromatid for high fidelity repair via strand invasion mediated by RAD51, synthesis using the sister chromatid as a template, and resolution. Alternative end joining (alt-EJ) utilizes repair proteins also used in other DSB repair pathways, generally results in less end resection than HR, and may use regions of micro-homology. Single strand annealing (SSA) uses long-range resection to reveal regions of homology within the DNA duplex and results in mutagenic repair.

1.1.4.5v: Double strand break repair choice

The mechanisms controlling the repair pathway fate of a DSB are incompletely understood, though repair pathway selection is known to be strongly influenced by the cell cycle. Homologous recombination repair generally repairs breaks during the S and G2 cell cycle stages (replicative and post-replicative phases), at which times a sister chromatid is available for homologous template directed, high fidelity repair. Non-homologous end joining is available throughout the cell cycle (71), though generally thought to occur when a sister chromatid is not present in pre-replicative cells (72-74). Multiple control mechanisms could account for, or contribute to, a cell cycle bias towards HR or NHEJ, including regulation by cyclin-dependent kinase (CDK) activity, regulation by chromosome modifications, and cell cycle dependent control of protein expression and/or protein modifications (75). CDK activity increases at the end of G1 to allow entry into S phase, and is very active at the end of G2 to initiate M phase. Reports in yeast have demonstrated a dependency of HR on CDKs, both for proper 5' → 3' end resection and recruitment of HR components (RPA and RAD51) (76, 77). For damaged DNA to be accessible for end processing enzymes and repair factors, chromatin modifications at the histone and nucleosome level must occur. Chromatin remodeling factors are important for DNA end resection, RAD51 nuclear filament formation, recruitment of DNA repair factors, and in chromatin movement during the homology search (as reviewed in (78, 79)). Cell cycle dependent changes in the protein level or phosphorylation status of DSB repair factors have been demonstrated. For example, CtIP expression is cell cycle dependent (75), and is regulated by MBF transcription factors, which are themselves regulated by CDKs (80). CtIP phosphorylation status, and thus ability to localize at the DSB, is also regulated by CDKs, as reviewed in (81).

The cell cycle-dependent bias for one DSB repair pathway over another does not result in complete segregation; rather, there is some functional and temporal overlap of these two major repair pathways. When one of several NHEJ proteins is knocked out (*Ku70*, *XRCC4*, and *DNA-PKcs*), the frequency of HR increases (82). In multiple contexts, HR and NHEJ can occur at the same time. HR and NHEJ compete in repair of transfected simian viral linear DNA molecules (83). In an analysis of interchromosomal recombination substrates, NHEJ and HR were shown to couple with each other, where

homologous invasion initiated and NHEJ completed the repair (84). DSBs induced by IR in normal G2 cells can be repaired by both NHEJ (~70-80% of DSBs with faster kinetics) and HR (with slower kinetics) (85, 86). Thus, in addition to cell cycle control models, other theories on DSB repair pathway selection have emerged.

One model theorizes that the initial binding of proteins to the DNA ends (KU in the case of NHEJ or RAD52 in the case of HR) determines repair pathway choice, and this initial binding is somewhat stochastic, though also influenced by cell-cycle dependent fluctuations in protein abundance (87, 88). A related theory exists focused on DNA end stability or processing. Through yeast studies, it has been proposed that NHEJ precedes HR temporally and that unprocessed ends might be the exclusive substrate for NHEJ, while 5' strand resection suppresses NHEJ and engages HR (89). NHEJ has been referred to as dominant, since the efficiency of NHEJ doesn't seem impacted by whether NHEJ is the only possibility for repair, however, HR frequency is decreased by about 3 fold in some situations in which it has to compete with NHEJ (89). In vertebrates, pathway determination via end processing may be more complicated, as NHEJ in vertebrates can accommodate cohesive and noncohesive ends (whereas in yeast, NHEJ can only accommodate cohesive ends). However, RAD52 and KU differ in preference for DNA substrates, with KU preferring DNA with free ends and RAD52 preferring single-stranded DNA, suggesting resection occurs before RAD52 binding (90). This supports a dependence of DSB pathway selection on end processing rather than stochastic or competitive DNA end binding.

Other studies indicate that KU, because of its strong-end binding capability and high abundance generally dominates and binds most DSBs, and therefore resection dependent pathways must overcome a "resection block" (91) even during S/G2. KU does indeed bind, though with lower affinity, at seDSBs such as those caused by replication fork encounter of SSBs or replication fork collapse, and DNA ends at reversed forks, even though NHEJ at such ends would be detrimental (92-95). In studying how resection is initiated in the HR-mediated repair of meiotic DSBs induced by SPO11, at which SPO11 remains covalently bound to DNA ends and thus poses a resection block, Garcia et al. identified that MRE11 nicks the strand to be resected up to 300 nucleotides from the 5' terminus of the DSB, enabling resection in a bidirectional manner by EXO1 (5'-3' away from the DSB) and MRE11 (3'-5' towards the DSB end) (96).

Earlier evidence had already suggested that an antagonism between KU and MRE11 at non-meiotic DSBs influences the choice between NHEJ and HR (97, 98). It has since been suggested that initial KU activity and subsequent removal is critical for HR repair of DSBs (91).

Chanut et al. used camptothecin (CPT; a TOP1 inhibitor) to induce seDSBs in U2OS cells and demonstrated that KU transiently binds seDSBs, though its persistence was inhibited by CtIP, in a manner dependent on ATM mediated CtIP phosphorylation (99). They further demonstrated that MRE11 activity was also critical to restrain KU accumulation at seDSBs and cooperates in an epistatic manner with CtIP. Notably, they observed resection and RPA loading onto ssDNA in the presence of bound KU in MRE11 mutant cells. The phosphorylation of RPA was dependent on KU binding and DNA-PK activity. However, RAD51 foci were deficient in the MRE11 mutant cells. This suggests that resection and RPA loading can tolerate KU persistence, though RAD51 loading requires KU removal. It is therefore possible that instead of an antagonism between KU70/80 and HR proteins in the decision between DSB repair pathways, KU binding may actually be the first step in both NHEJ and HR repair at some DSBs. A model in which KU remains bound to a DSB during initial resection until a structure is generated that commits repair to HR and precludes NHEJ is consistent with previous studies that demonstrated IR-induced DSBs can be repaired by both NHEJ and HR in G2 cells, with a ssDNA stretch of significant length being the likely structure committing to HR (86, 91, 100).

A common theme in DSB pathway choice has arisen that reveals both a dependence on proteins required for a particular repair mechanism as well as a dependence on proteins that antagonize competing repair pathways. The proteins 53BP1, which promotes NHEJ, and BRCA1, which promotes HR, are a duo of antagonistic proteins that illustrate this concept. 53BP1 is recruited to DSBs after ATM mediated phosphorylation of histone 2A variant H2 AX via interactions with MDC1 and via the activities of RNF8 and RNF168-dependent chromatin modifications (reviewed in (101)). 53BP1 promotes NHEJ via interactions with PTIP and Artemis to trim DNA ends for ligation, and via interactions with RIF1 to block resection (101). BRCA1 limits the interaction of 53BP1 with chromatin in S phase (102, 103), limits RIF1 accumulation at DSBs that occur during S phase (104), disrupts the 53BP1-RIF1 interaction (105, 106), and promotes the removal of 53BP1 from DNA through its interactions with CtIP (107, 108). The

antagonism between 53BP1 and BRCA1 in regulating DSB repair is further illustrated by the finding that the HR defects and lethality observed in BRCA1 deficient cells are rescued by the loss of 53BP1 (109-111).

Many levels of regulation of DSB repair pathway choice are possible, and likely contribute in various combinations and to contextually-dependent degrees of importance. These include cell cycle/cyclin dependent kinase mediated regulation of protein abundance and post-translational modifications, chromatin state, and the delicate interplay of repair factor activities and affinities that is continually being further elucidated.

1.2: RAD9A-HUS1-RAD1 (9-1-1) clamp

Experiments in both fission and budding yeast identified genes that were essential for DNA replication and DNA damage checkpoint function. In fission yeast, the six genes *hus1*, *rad1*, *rad3*, *rad9*, *rad17*, and *rad26* were shown to be critical for the DDR (112-114). The genetic screens revealed sensitivities to DNA damaging agents in the mutants, which were used to name the genes: hydroxyurea sensitive (*Hus1*), radiation sensitive (*Rad1*, *Rad9*). These proteins were soon shown to be conserved among species and their structure and function extensively explored.

Paralogs of HUS1 (HUS1B) and RAD9 (RAD9B) have been identified in several species (115, 116), and these paralogs may have specialized roles in meiosis (Weiss laboratory unpublished data). In this discussion "RAD9" is used to represent RAD9A.

1.2.1: Structure

The 9-1-1 clamp is a toroidal sliding clamp with structural similarity to the proliferating cell nuclear antigen (PCNA) processivity clamp of DNA replication and repair (117-119). The subunits are highly evolutionarily conserved from yeast to humans (120-122). Crystal structure analysis shows the subunits of both clamps fold into two globular domains that are linked by an interdomain connecting loop and bind in a head to tail orientation (123-125). A distinguishing feature between the two clamps is the presence of a non-PCNA like flexible domain at the C terminus of RAD9, which is critical for checkpoint

signaling (119, 126, 127). The formation of the clamp is dependent on the presence of all three subunits (128). The 9-1-1 clamp is loaded onto DNA by a RAD17-RFC2-5 clamp loader at 5' recessed DNA ends, mainly through interactions of the clamp loader with RAD1 (129-131), while PCNA is loaded by a RFC1-5 clamp loader on 3' recessed ends (132). The RAD9-RAD1 interface appears weakest in stability studies, and thus is thought to open to allow the clamp to encircle DNA, though multiple opening pathways have been described (133).

Like PCNA, the 9-1-1 clamp lacks enzymatic activity. The clamp acts as a molecular scaffold for the recruitment of other DDR proteins, functioning in both checkpoint signaling and DNA repair. Positive residues on the inner surfaces of the clamp facilitate clamp-DNA interactions (134). Early studies of functional similarity between PCNA and the 9-1-1 clamp predicted the conserved residues would be functionally important, which has been supported by subsequent mutagenesis studies (128, 134). Protein binding to PCNA is well understood to occur via interactions between PCNA interacting protein (PIP) boxes of the binding partners and a hydrophobic pocket on PCNA underneath the interdomain connecting loop that bridges the two globular domains of a subunit (135). Some protein interactors of 9-1-1 bind with conserved PIP box like residues, while others bind independently of a PIP motif (reviewed in (136)). In addition to the PCNA-like hydrophobic pocket, a novel hydrophobic pocket of HUS1 is important for survival after DNA damage but not for clamp localization to chromatin (134). The 9-1-1 clamp interacts with factors in multiple DNA repair pathways, including base excision repair, nucleotide excision repair, mismatch repair, homologous recombination, and translesion synthesis, as well as in checkpoint signaling via mediating activation of the DDR kinase ATR (137-150).

1.2.2: 9-1-1 roles in genome integrity

Loss of *Hus1* in mice leads to embryonic lethality and genomic instability (151, 152). Decreased *Hus1* expression in cultured cells results in proliferation defects, checkpoint defects, chromosomal aberrations and increased genotoxin sensitivity. Decreased *Hus1* expression in mouse models results in increased micronuclei in peripheral red blood cells and increased genotoxin sensitivity (142, 151, 153, 154). Thus, *Hus1* is essential for the maintenance of genomic integrity. The Weiss laboratory has

demonstrated that the roles of the 9-1-1 clamp in checkpoint activation and in recruitment of DNA repair proteins are separable ((134) and unpublished data).

The 9-1-1 clamp is critical for ATR-mediated checkpoint signaling. Replication stress and replication fork stalling, as well as certain repair intermediates, generate exposed single stranded DNA (ssDNA), which quickly becomes coated by replication protein A (RPA). The RPA-coated ssDNA recruits the DDR kinase ATR and its binding partner ATRIP to chromatin, as well as the 9-1-1 clamp (13, 155). ATR/ARIP and 9-1-1 recruitment is not interdependent (129, 156). The C terminal tail of RAD9 interacts with the large scaffolding protein TOPBP1 in a manner dependent on the phosphorylation of certain residues in the tail of RAD9 via TOPBP1 BRCT domains (157, 158). TOPBP1 also contains an ATR activation domain (159) and the 9-1-1-TOPBP1-ATR interaction leads to ATR-CHK1 activation and checkpoint signaling (12, 160). Until recently, this 9-1-1 mediated activation of ATR was the only identified means of ATR activation in response to exposed ssDNA. Recently, it was found that an additional protein, ETAA1, can also activate ATR, however, it remains to be characterized how ATR signaling following these two means of activation may differ (14-16).

In additional to checkpoint signaling, the 9-1-1 clamp has direct roles in DNA repair and interacts with repair proteins from many DNA repair pathways. One such pathway is the DNA damage tolerance or translesion synthesis pathway. Hypomutability is a feature of *Hus1* deficient cells (148, 161), suggesting a potential defect in recruitment or activity of TLS polymerases. As previously discussed, translesion polymerases are employed to bypass replication blocking lesions. There is suggestive evidence that 9-1-1 may be important for PCNA regulation, and thus TLS polymerase recruitment. When the 9-1-1 clamp loader RAD17 is knocked down, ubiquitinated PCNA is reduced (162). Additionally, a recent mass spectrometry screen performed in the Weiss laboratory for HUS1 interacting proteins identified USP1 (unpublished data), which is the enzyme responsible for deubiquitinating PCNA (163). Without USP1 there is increased PCNA ubiquitination in the absence of DNA damage as well as after DNA damage, and increased polyubiquitination of PCNA (162). In yeast, 9-1-1 deficiency is associated with decreased TLS activity with a decreased UV-induced mutation rate (161). HUS1 interacts with the TLS polymerase Polζ in yeast, and is required for Polζ chromatin recruitment and Polζ mediated

spontaneous mutagenesis (148).Though *Hus1* deficient cells are hypomutable and *Hus1* has been shown to physically interact with Pol ζ in yeast, it cannot be excluded that TLS defects in *Hus1* deficient cells are not due to a secondary consequence of an ATR mediated checkpoint signaling defect (35).

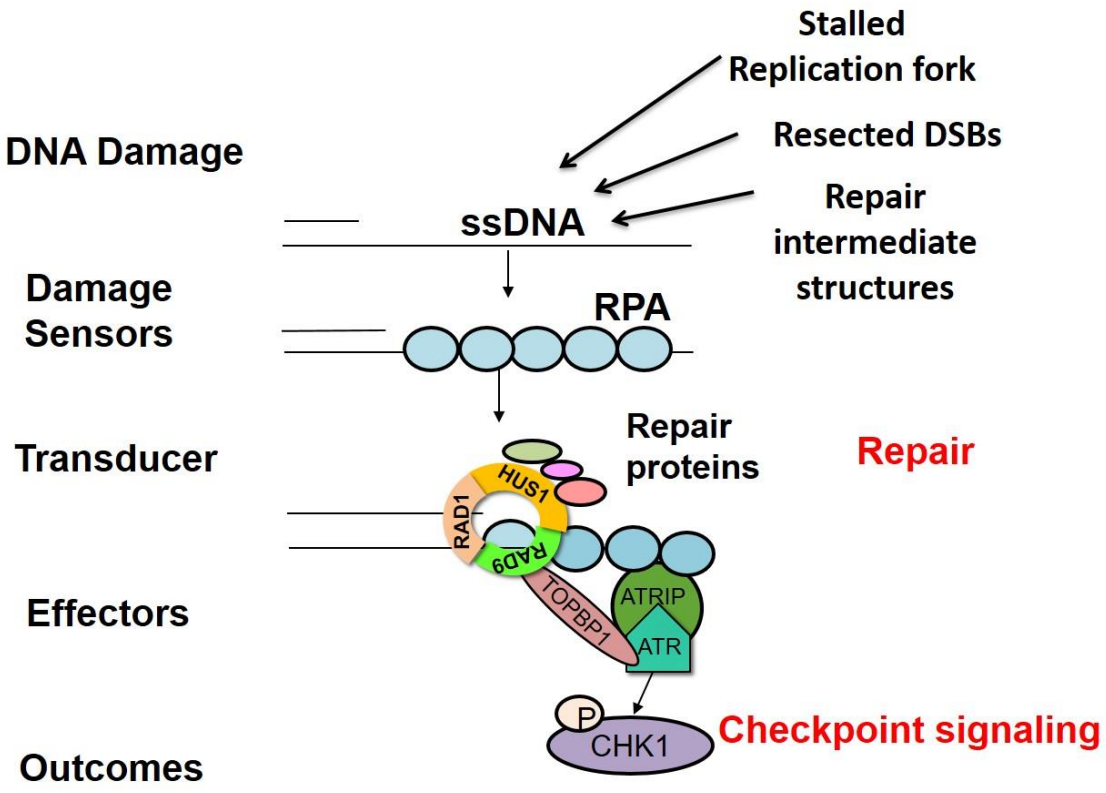

Figure 1.3: The RAD9-HUS1-RAD1 (9-1-1) clamp acts as a molecular scaffold with separable roles in checkpoint signaling and DNA repair. The 9-1-1 clamp is loaded onto replication protein A (RPA) coated single stranded DNA at single stranded-double stranded DNA (ssDNA-dsDNA) junctions with the help of a clamp loader complex. The ssDNA-dsDNA can arise from stalled replication forks, resected double strand breaks (DSBs) and repair intermediates. The 9-1-1 clamp activates the DDR kinase ATR via a RAD9-TopBP1-ATR interaction to initiate checkpoint signaling. The outer surface of the 9-1-1 clamp also physically interacts with DNA repair proteins from various repair pathways, including base excision repair, nucleotide incision repair, mismatch repair, translesion synthesis, and homologous recombination.

1.2.3: Role of the 9-1-1 complex in DSB repair

Several lines of evidence are strongly suggestive that the 9-1-1 complex contributes to homologous recombination repair of double strand breaks, such as physical interactions with HR proteins, including DNA end-processing enzymes, phenotypic features of HUS1 deficient cells, HR DNA repair reporter plasmid analysis, and analysis of meiotic phenotypes in HUS1 deficient germ cells.

DNA end processing at DSBs is critical for determining signaling and repair pathway choices. Resection controls whether an ATM or ATR mediated checkpoint signaling pathway will dominate as well as whether NHEJ or HR will proceed (164). The MRN complex, along with CtIP, initiates resection at DSBs (56). Extensive resection is believed to require the nuclease Exo1 and the nuclease/helicase pair DNA2 and BLM (58). The 9-1-1 checkpoint clamp has been implicated in regulating end processing at DSBs. HUS1 appears to regulate EXO1 and DNA2 in budding yeast, but the relationship between promoting and inhibiting end resection appears dependent on context and on the level of 53BP1 binding. 9-1-1 was found to stimulate resection by DNA2 and EXO1 in human protein extracts and in response to uncapped telomeres in yeast (165). In yeast, HUS1 was found to inhibit DNA2 at DSBs and to stimulate EXO1, and the role of inhibiting DNA2 seemed predominate (166). Unpublished data from the Weiss laboratory suggests that HUS1 is also important for regulating MRE11 mediated DNA resection at stalled replication forks. How HUS1 impacts the activity of these nucleases in higher organisms and the relevance to DSB repair is not yet clear. Additionally, RAD9 knockdown has been reported to decrease phosphorylation of RPA, suggesting decreased ssDNA and decreased resection, as well as increased alt-EJ efficiency (167).

Radial chromosomes are a key feature of *Hus1* deficient cells spontaneously and upon replication stress induction and MMC treatment (153), a feature shared with several other genomic instability syndromes including Fanconi Anemia and Bloom Syndrome. The mechanism of radial formation is still an investigated topic, though generally believed to result from faulty DSB repair. Abrogation of both NHEJ and HR have demonstrated capability of resulting in radial chromosome formation (168). NHEJ and alt-EJ are also capable of generating aberrantly joined chromosomes (169). Alt-EJ, however, is thought to be more likely to result in radials than NHEJ, likely because of its reduced kinetics increasing

the probability of unrelated DNA ends interacting (170). Understanding the mechanism leading to radial formation can characterize the role of *Hus1* in DSB and ICL repair and is discussed further in Chapter 3.

Hus1 deficient cells have decreased HR efficiency in a GFP-I-Sce reporter system, though *Hus1* status does not impact DSB rejoining after IR as assessed by asymmetric field inversion gel electrophoresis (171). It seems, therefore, that *Hus1* deficient cells are capable of normal NHEJ. How *Hus1* deficiency impacts HR proficiency or if *Hus1* impacts NHEJ is not fully known, but discussed further in Chapter 3. *Hus1* may be required for HR to be carried out, or, potentially, *Hus1* is required for HR to be selected as a pathway choice over NHEJ. An example of such a situation exists in *BRCA1* deficient cells. BRCA1 promotes HR, and *BRCA1* deficient cells display HR defects, however, BRCA1 is not absolutely required for HR. When end-resection inhibition is relieved by absence of the end binding, NHEJ-promoting protein 53BP1, the defects in fetal survival, DNA damage sensitivity, and chromosomal aberrancies seen in *BRCA1* deficiency are rescued (109-111).

Meiotic studies have also revealed the importance of the 9-1-1 clamp in DSB repair. Programmed meiotic DSBs, generated by SPO11, and their proper repair, are necessary to ensure accurate chromosome segregation and also result in genetic recombination between homologs (172). Mouse models with conditional 9-1-1 mutations showed severe meiotic phenotypes and germ cell loss (173, 174). In *Hus1* and *Rad9a* conditional knockout models DSBs form with appropriate timing and numbers as assessed by localization of the recombination protein RAD51, however, RAD51 foci persist longer in *Hus1* CKO meiotic spreads than in controls, suggesting unrepaired DSBs (173, 174). *Hus1* deficient primary spermatocytes showed persistent γH2AX (a maker of DNA damage) and RAD51 autosomal foci, and RAD9 co-localized with RAD51 in distinct foci on meiotic chromosomes in a *Hus1* dependent manner (173). This suggests that the 9-1-1 clamp promotes DSB repair in meiosis.

1.3: Cross-talk between the DNA damage response and cellular metabolism

Changes in metabolic pathways can influence DNA repair, and DNA damage can induce metabolic rewiring. Many proteins are known to conduct both DDR functions and to behave as metabolic regulators. The interconnection between the DDR and cellular metabolism is best studied in cancer

biology. In this section I will review some of the known relationships between metabolism and the DDR, and Chapter 3 will describe a connection between deficiency in the Fanconi Anemia DNA repair pathway and altered hepatic bile acid and lipid metabolism.

A large field of study addresses the metabolic re-programming of cancer cells that was first described in the 1920s by Otto Warburg and colleagues which allows them to adapt to altered microenvironments and meet the high metabolic needs associated with increased proliferation (175). A recent review organized cancer-associated metabolic changes into six "hallmarks": amino acid and glucose uptake deregulation, opportunistic nutrient acquisition modes, biosynthesis and NADPH production through glycolysis/TCA cycle intermediates, increased nitrogen demand, metabolite-driven gene regulation changes, and metabolic interactions with the microenvironment (176).

Turgeon et al. recently reviewed three principal mechanisms by which metabolic shifts impact the DDR, namely through chromatin remodeling, nucleotide pool synthesis, and redox homeostasis (177). Post-translational modification of histone proteins (acetylation, methylation, phosphorylation, ubiquitination) and DNA modifications impact DNA folding and thus the ability of repair proteins to access DNA, and may impact DNA repair pathway choice (HR vs NHEJ) (178-180). Metabolic intermediates are the source of the substrates added to histones and DNA (methyl groups from the S-adenosylmethionine pathway, acetyl groups from acetyl coenzyme A) (181, 182). Other metabolites can also impact DNA repair by regulating post-translational modification of histones or DNA. For example, DNA-PK can activate fumarase, increasing the local concentration of fumurate, which then inhibits DKM2B-mediated histone demethylation and promotes the accumulation of Ku70 containing DNA-PK regions for NHEJ repair (183).

Many metabolic pathways contribute to *de novo* nucleotide biosynthesis, including the pentose-phosphate pathway (PPP), and glutamine, aspartate, and glycine metabolism (reviewed in (177)) . The dNTP pool is critical for genome stability, and imbalances can increase mutagenesis (184, 185). Altered dNTP pools impact both the fidelity of DNA synthesis and the DDR (186, 187).

Reactive oxygen species are a source of DNA damage, typically inducing SSBs which may be repaired by NER/BER, or if unrepaired, may lead to replication fork stalling and DSB formation (3). ROS

is generated as a result of cellular metabolic reactions, and cell metabolism also regulates the levels of ROS scavengers, such as glutathione and NADPH (188, 189). Members of the DDR can also impact ROS levels. BRCA1(FANCS) physically interacts with the transcription factor Nrf2, promoting its stability and antioxidant signaling function (190).

In addition to multiple ways cell metabolism impacts DNA repair, there are also many known metabolic regulatory functions of DDR components. For example, the DDR kinase ATM not only regulates DNA repair and checkpoint activation, but also initiates metabolic rewiring. ATM induces the enzyme G6PD to activate the PPP, which in turn leads to increased availability of NADH and ribose-5-phosphate for dNTP synthesis (191, 192). DNA damage can initiate a block in glutamine metabolism via induction of mitochondrial SIRT4, which reduces metabolism of glutamine into the tricarboxylic acid cycle and confers a cell survival benefit (193). The tumor suppressor protein p53, which has DDR functions such as regulating senescence and apoptosis, also regulates energy sensing through AMPK and mTORC1 (194), mitochondrial respiration (195), glycolysis via activation of TIGAR (196), lipid metabolism through regulation of the major fatty acid synthesis regulating transcription factor SREBP (197), and several other metabolic pathways reviewed in (198).

DNA damage and DNA damage response summary:

The integrity of the genome is constantly challenged from both endogenous and exogenous sources. The DDR surveys for damage and initiates signaling and effector pathways to respond in a contextually-dependent manner. DDR signaling can result in cellular apoptosis, senescence, changes in transcription and translation, cell cycle arrest, and/or initiation of DNA repair pathways. Many distinct types of DNA repair exist to respond to the large variety of DNA lesions that can arise. Faulty DNA repair can result in loss of cellular function, cellular apoptosis, or cellular transformation. The 9-1-1 clamp functions in both checkpoint signaling and DNA repair protein recruitment, and is vital to the maintenance of genomic integrity. Among other roles, evidence suggests that the 9-1-1 clamp is important in high fidelity DNA double strand break repair. To gain new insights into these potential functions, I combined *Hus1* deficient mice with mice either lacking the NHEJ component *Prkdc*, or the HR

component *Rad54*, and evaluated the impact of the dual mutations on genomic stability and genotoxin sensitivity *in vivo* and *in vitro*. I found that combined deficiency of *Hus1* and absence of *Rad54* increased genomic instability and sensitivity to genotoxins, while combined deficiency of *Hus1* and absence of *Prkdc* partially rescued genome stability relative to single mutants (Chapter 2). These data suggest that both HUS1 and RAD54 contribute to high fidelity DSB repair and that HUS1 may have a role in inhibiting NHEJ.

1.4: Fanconi Anemia (FA) disease

1.4.1: Disease characteristics, incidence, genetics

The disease of Fanconi Anemia (FA) was first described by the Swiss pediatrician Guido Fanonci in 1927 (199), and was subsequently characterized as a heritable disease of chromosomal instability leading to heterogeneous phenotypes including a predisposition to hematologic and epithelial cancers, bone marrow failure, congenital abnormalities, and endocrine and metabolic disturbances. FA arises when a component of the Fanconi Anemia DNA repair pathway is not intact. There are currently twenty-two known FA genes (*FANCA, -B, -C, D1, D2, E, F, G, I, J, L, M, N, O, P, Q, R, S,* and *T, U, V, W*), and FA can be inherited in an autosomal recessive manner (most FA genes), an autosomal dominant manner (*RAD51*-related FA), or an X-linked manner (*FANCB* related FA). To be designated as a FA gene requires an association with a clinical case of a patient with a mutation in that gene and an FA phenotype.

FA impacts approximately ten in every one million people, and carrier rates are as high as 1:181 people in North America and 1:93 in Israel (200). Founder variants have been identified in certain populations, such as Ashkenazi Jews (*FANCC, BRCA*) and northern Europeans (*FANCC*) (201). The characteristic chromosomal instability of FA is used in its diagnosis in patients suspected of having the disease based on phenotypic presentation. Peripheral blood lymphocytes from patients with FA will show hallmark chromosomal radials and breaks upon exposure to diepoxybutane or mitomycin C, and a diagnosis can then be confirmed with genetic sequencing. The majority of FA patients have biallelic mutation in *FANCA* (60-70%), about 14% have biallelic mutations in *FANCC*, and roughly 10% have

biallelic mutations in *FANCG*, while the other complementation groups each account for less than five percent of FA patients (201). The median age at diagnosis is 6.5 years (202).

1.4.2: FA phenotypes

Roughly 75% of people with a defect in the FA pathway will have some combination of physical features suggestive of the disease, including short stature, abnormal skin pigmentation (40%), microcephaly (20%), skeletal malformations (35%; generally hand and forearm), and ophthalmic (20%) and genitourinary abnormalities (2-25%) (201). Additional findings suggestive of FA include progressive bone marrow failure or cytopenias, myelodysplastic syndrome, acute myelogenous leukemia (AML), early onset solid tumors (squamous cell carcinomas or the genitourinary tract or head and neck, liver tumors), and excessive toxicity from radiation or chemotherapy (201). The average age of onset for bone marrow failure has been reported at 7.6 years, and thrombocytopenia or leukopenia usually precede anemia with pancytopenias worsening over time (201). The median tumor-free survival in FA patients is 29 years with the incidence of head and neck squamous cell carcinomas roughly 500-700 fold higher in FA patients than the general population and the risk of AML roughly 600 fold higher (202). FA patient overall survival has improved with more than 80% of FA patients surviving to at least age 18 and a median survival of 29 years, while prior to 2000, the median survival in case reports was 21 years (202).

In addition to physical, hematologic, and tumor phenotypes, endocrine abnormalities are present in roughly 80% of FA patients (203). The prevalence of diabetes in FA patients is 8-10%, which is higher than the general population, and the frequency of glucose intolerance ranges from 27-68% (204-206). Diabetes is not associated with a particular FA genotype, and has been attributed to both an impairment in pancreatic β-cell function and first phase insulin secretion, characterized by a delayed insulin response and decreased insulin secretion relative to ambient glucose (insulinogenic index) (207), and insulin resistance (203, 206). It has been proposed that increased ROS in pancreatic β-cells may lead to their dysfunction (208), and it must be considered that the androgens and/or corticosteroids used in FA treatments may contribute to insulin and glucose abnormalities (203), however, the FA pathway may also have a role in the maintenance of glucose homeostasis.

FA patients also have an elevated incidence of dyslipidemia and obesity, reportedly as high as 55% and 27%, respectively (206). A separate report described 17% of FA patients to be hypercholesterolemic (204). Metabolic syndrome, which is characterized as dyslipidemia, insulin resistance, and overweight, was present in 21% of FA patients in one report (206). Similar to the general population, there was an association between glucose abnormalities and dyslipidemia in FA patients, with 40% of FA patients who had insulin resistance or hyperglycemia also having serum lipid imbalances (203).

Other endocrine abnormalities are also reported. Short stature is present in roughly 60% of FA patients, (203, 204, 206), and is likely multifactorial in etiology, as growth hormone (GH) deficiency, hypothyroidism, hypogonadism, and pituitary abnormalities are all common in FA patients and can contribute to overall height. However, short stature is also observed in the absence of endocrine deficiencies in some patients with FA, and may also be contributed to by therapies such as androgens (accelerating epiphyseal maturation) and radiation (203). The means of assessing and criteria applied for diagnosing GH deficiency vary between studies, with the more stringent definitions reporting GH deficiency in 12% of FA patients (204) while up to 72% of FA patients were reported to fail a GH stimulation test (205). Primary hypothyroidism, which is not believed to be autoimmune in etiology, but rather proposed to arise from thyroid cell apoptosis resulting from increased DNA and oxidative damage, is reported in about 60% of FA patients (203). FA patients have a high incidence of hypogonadism, impaired fertility, and developmental anomalies of the genital tract (203, 204, 206, 209, 210), which is recapitulated in murine models of FA (211, 212). Growth hormone, thyroid, and gonad abnormalities may also be related to pituitary defects, including small pituitary size (213, 214).

1.4.3: Management of FA disease

Management of FA depends on individual patient symptoms, however, management is complex and requires specialized clinical care involving a hematologist, ophthalmologist, internalist, endocrinologist, geneticist, and others. Therapy guidelines were outlined in a 2014 consensus statement (215). The only curative therapy for hematopoietic failure, myelodysplastic syndrome and AML is a

hematopoietic stem cell transplant. As FA patients are highly sensitive to radiation and chemotherapy, they require specialized pre-transplant care. Anemia and thrombocytopenia can be treated with androgens, though side effects include virilization and hepatic toxicity. Neutropenia may be improved with granulocyte colony-stimulating factor. Non-surgical treatment for solid tumors is complicated by the extreme toxicity of chemotherapeutics and radiation in FA patients. Careful surveillance via routine monitoring for the development of hematopoietic, malignant, or other manifestations is required.

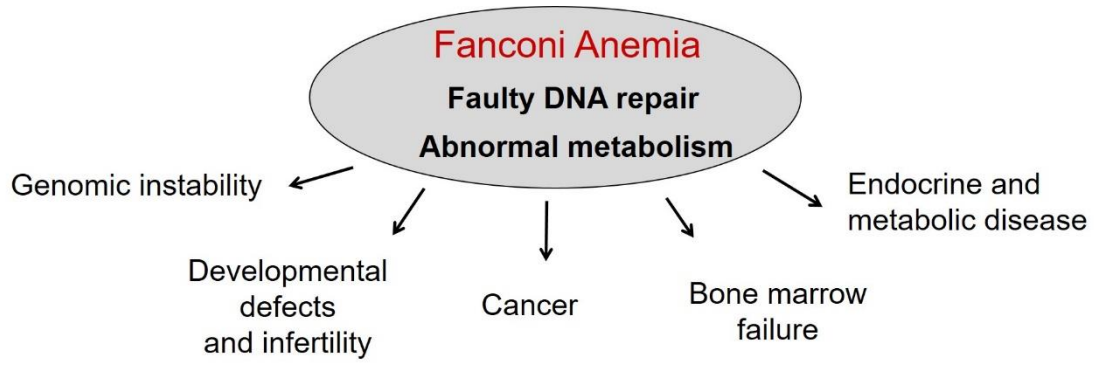

Figure 1.4: Fanconi Anemia (FA) phenotypes. FA phenotypes are heterogeneous and include: a genome instability syndrome resulting in chromosomal instability and chromosomal aberrations in response to mitomycin C and diepoxybutane exposure; developmental defects, hypogonadism, and infertility; a strong cancer predisposition, particularly to hematologic cancer and squamous cell carcinomas of the head and neck; a progressive bone marrow failure driven by hematopoietic stem cell dysfunction; and endocrine and metabolic disease. These phenotypes likely arise from both increased DNA damage accumulation and alterations in cellular metabolic homeostasis in the absence of an intact FA pathway.

1.5: Mouse models of Fanconi Anemia

Mouse models of FA recapitulate some of the phenotypes seen in human FA, though not all, and often show decreased severity of phenotypes. The hematologic manifestations arising from bone marrow dysfunction are a primary component of FA in humans, however, most FA mouse models have

undetectable or mild hematologic function in an unchallenged condition. *Fanca*$^{-/-}$ mice do exhibit thrombocytopenia, but lack deficiencies in granulocyte or macrophage progenitors (216). However, bone marrow progenitors derived from FA deficient mouse models, including *Fancc*, *-g*, *-a*, *d2*, *d1*, display impaired proliferation *in vitro* and/or in repopulation ability (216-220). Developmental abnormalities are also notably less apparent in mouse models of FA, though *Fancd2*$^{-/-}$ and *Fancc*$^{-/-}$ mice are born at sub-Mendelian ratios and several FA mouse models display growth retardation, and defects such as microcephaly and microphthalmia (reviewed in (221)). Gonadal and germ cell defects accompanied by infertility are reported in *Fancc*, *-g*, *-a*, and *-d2* deficient mice (211, 212, 217, 221-224). FA mouse models do develop an array of tumors, including sarcomas, adenosarcomas, lymphoma, ovarian tumors, and epithelial tumors and other carcinomas, though tumor development is reported to occur around the relatively advanced age of 15 months (reviewed in (221)). As seen in human FA patient derived cells, mouse embryonic fibroblasts and bone marrow progenitors derived from FA deficient mouse models are hypersensitive to MMC, though vary in sensitivity to IR (221). Strain background can also impact the severity of phenotypes seen in FA deficient mice, which suggests the presence of phenotype-modifying loci (221). Metabolic phenotypes in FA mouse models are poorly characterized. The similarities between the consequences of FA deficiency observed in humans and mice illustrate the utility of mouse models in studying the functions of the FA pathway, but also indicate that important differences exist in the specific functions of FA components between the species.

1.6: The Fanconi Anemia pathway in genome stability

1.6.1: Pathway components and interstrand crosslink repair

The FA DNA repair pathway consists of 22 known proteins, the canonical function of which is to repair DNA interstrand crosslinks. A subset of eight proteins (FANCA, -B, -C, -E, -F, -G, -L, -M) comprise a core complex which forms from the sequential assembly of sub-complexes (reviewed in (225)). The core complex contains ubiquitin ligase activity and monoubiquitinates a central FANCI-FANCD2 heterodimer upon sensing DNA damage. The activated FANCI-FANCD2 dimer then coordinates endonucleases and DNA repair proteins for resolution of the ICL. In the core complex,

FANCL possess the ubiquitin ligase activity, and functions with FANCT (UBE2T), a ubiquitin conjugating enzyme (226). Activation of the FA pathway also requires phosphorylation of some core complex components, including FANCA and -M, and FANCI, which is believed to be mediated by the ATR kinase (227-229). FANCM contains helicase motifs and DNA-stimulated ATPase activity, and is believed to aid in DNA damage recognition, along with its interacting protein, FAAP24, which is known to recognize branched and single stranded DNA (230, 231). The majority of FA patients have a defect in a gene encoding a member of the core complex, and therefore the majority of FA patients have defective FANCI/D2 monoubiquitination (232).

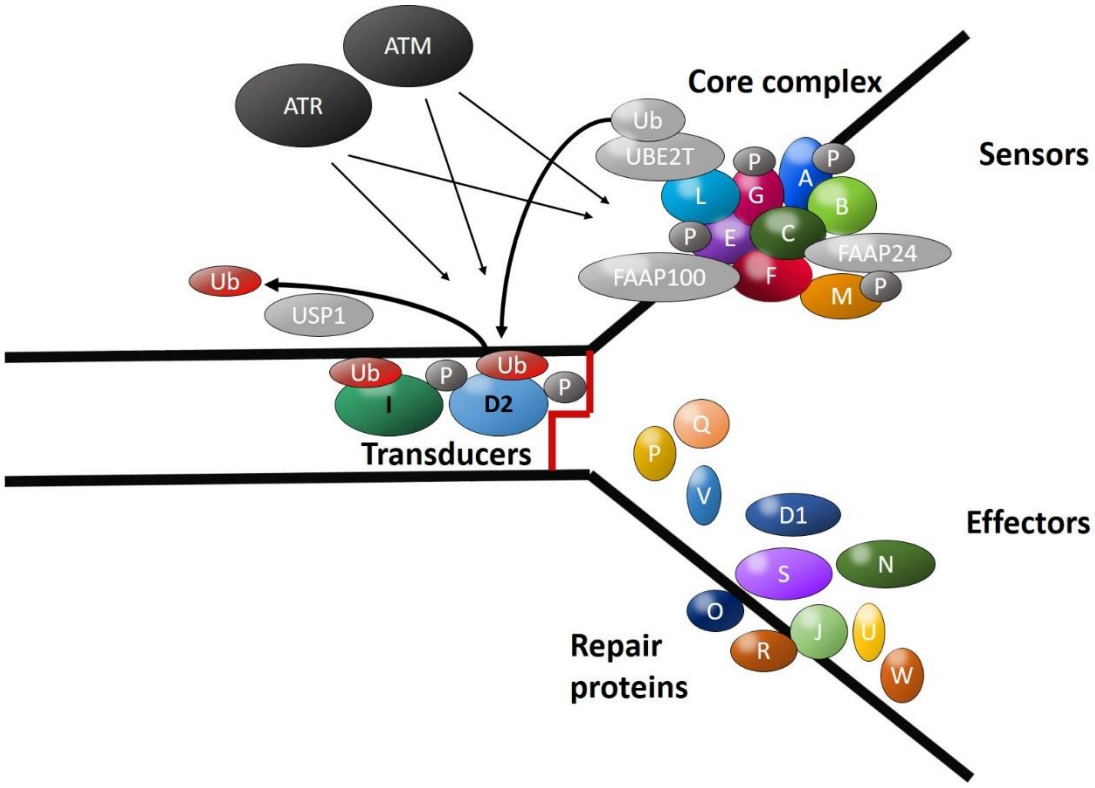

Figure 1.5: Fanconi Anemia Pathway components. The FA core complex, composed of FANCA, -B, -C, -E, -F, -G, -L, -M recognizes and localizes to the site of an ICL. The FANCL ubiquitin ligase, along with UBE2T (FANCT), monoubiquitinates the central FANCI-FANCD2 heterodimer. The DDR kinases

ATM and ATR phosphorylate multiple FA core components as well as the I-D2 dimer. Downstream repair components are then recruited. Modified from (233).

FANCD2 monoubiquitination is used as an indicator of FA pathway activation, allows its subsequent recruitment to sites of DNA damage, and is critical for coordination of ICL repair by additional downstream FA pathway proteins (234). Recruitment of FANCD2 to chromatin in response to mitomycin C also appears dependent on the ICL-interacting and sensing protein UHRF1 (235). De-ubiquitination of FANCD2 by USP1 is also required for normal FANCD2 focus formation and ICL repair (236, 237). Monoubiquitination and focus formation of FANCD2 require, in addition to the FA core complex and ATR, RPA and the ATR-associated protein HCLK2 (238, 239). Required for FANCD2 focus formation, but not monoubiquitination, are BRCA1 and histone H2AX (234, 240). Though not required for cross-linker resistance, FANCD2 phosphorylation by ATM is required for IR resistance and is part of a radiation-induced S phase checkpoint (241).

Downstream of FANCI/D2, FA proteins participate in the unhooking of an ICL (FANCP and FANCQ), translesion synthesis across the strand with the remaining ICL (FANCV) and homologous recombination to repair the remaining break (FANCD1, -J, -N, -O, -R, -S, U) (242). Monoubiquitinated FANCD2 recruits FA-associated nuclease 1 (FAN1) and FANCP (SLX4) to initiate nucleolytic incision at an ICL via their ubiquitin binding domains (243, 244). Cross-link unhooking is also contributed to by the nucleases Mus81-EME1 and XPF-ERCC1 (245). The nucleolytic unhooking of the ICL generates a DNA double strand break. Translesion synthesis allows synthesis past the unhooked crosslink to extend the leading strand. There is evidence of cross-talk between the FA pathway and TLS components, including a relationship between RAD6/RAD18 (the ubiquitin ligase complex that ubiquitinates PCNA, allowing for switching of the active DNA polymerase) and FANCD2 ubiquitination, physical interactions between PCNA with both FANCL and FANCD2, and a role of FANCD2 in recruiting the TLS polymerase Polη (reviewed in (246)).

After TLS synthesis across the leading strand, the double strand break can then be repaired by homologous recombination using the repaired leading strand as a template. Several FA proteins are involved in HR and FA deficient cells are defective in HR (247, 248). The core complex member FANCM appears important for recruitment of end processing proteins CtIP and MRN at ICLs (249). FANCS (BRCA1) excludes the NHEJ protein 53BP1 from broken DNA ends, thus promoting HR (109, 111). FANCD1 (BRCA2) is important in loading of the recombination protein RAD51 (250). FANCN (PALB2) is a regulator of FANCD1 (251) and FANCJ (BACH1/BRIP1) regulates FANCS and prevents inappropriate recombination (252, 253). FANCO (RAD51C) promotes RAD51 loading and Holliday Junction resolution (254, 255). Finally, the remaining adduct/crosslink is removed by nucleotide excision repair.

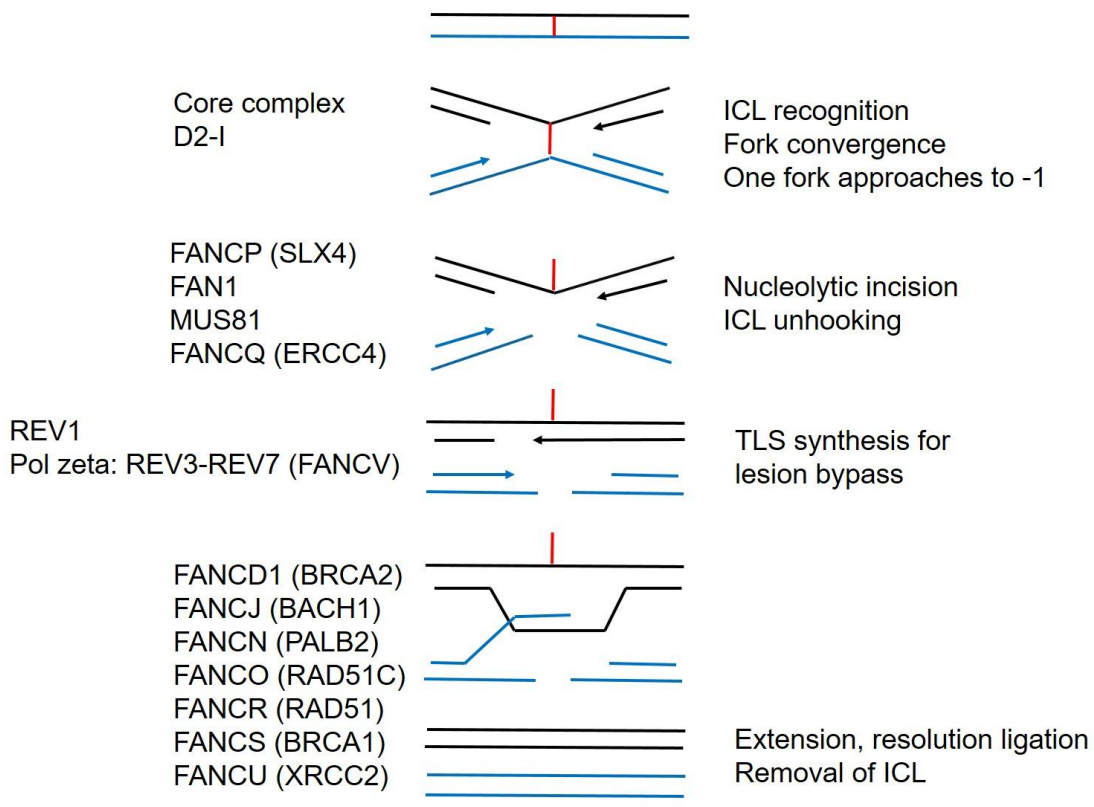

Figure 1.6: Interstrand cross-link (ICL) repair by the Fanconi Anemia pathway. Stages of ICL repair (right) and FA components involved (left). Modified from (256).

1.6.2: FA pathway role in replication stress

In addition to cross-linking agent sensitivity, FA deficient cells are sensitive to other replication stresses that stall the progression of replication forks caused by both exogenous agents (such as hydroxyurea (HU)) and endogenous sources such as re-replication, oncogene induced replication stress, and DNA-protein adducts formed by metabolic byproducts (257-262). Stalled replication forks are unstable structures prone to collapse and contain single stranded DNA which may be exposed to nucleases. Thus stabilizing and repairing stalled forks is crucial for maintenance of genomic integrity.

FANCD2 foci form in response to multiple conditions that induce replication stress, including aphidicolin, hydroxyurea, and UV treatment (reviewed in (225)). A crucial step in preventing mutagenesis and collapse at stalled forks is the prevention of excess base degradation by nucleases. Ubiquitylated FANDC2/I heterodimers localize to stalled forks and have been demonstrated to prevent excessive nucleolytic ssDNA degradation by MRE11 (263-265).

During replication stress in which replication forks stall or slow, cells can fire additional licensed origins (dormant origins) to complete replication in the regions between stalled forks. FANCI interacts with the MCM replicative helicase complex, localizing to replication origins and appears to regulate dormant origin firing (266). While unmodified FANCI was required for dormant origin firing in response to low dose HU treatment, ATR-mediated phosphorylation of FANCI was shown to inhibit dormant origin firing and to promote replication fork restart using DNA fiber analysis (266).

Certain regions of the genome, termed fragile sites, are intrinsically more difficult to replicate. These regions are more prone to damage upon replication stress and frequently show gaps, breaks, or chromosome bridging during metaphase. The FA pathway is implicated in protecting these regions. FANCD2 and FANCI localize to these regions during mitosis (267, 268), though their roles in protection from break formation and/or repair are not characterized. The role of the FA pathway in chromosome separation is discussed further below.

1.6.3: FA pathway and checkpoint responses

In addition to participating directly in DNA repair, the FA pathway contributes to proper cell cycle checkpoint activation. A characteristic phenotype of FA deficient cells is an accumulation of 4N DNA content (spontaneously or with cross-linker treatment), which may be due to failure to activate S phase cell cycle arrest (269). Indeed, FANCD2 deficient cells have a defective replication checkpoint after ICL induction (270). FANCO (RAD51C) deficient cells also have a defective intra-S phase checkpoint triggered by MMC and camptothecin (271). WT complemented cells showed an accumulation of an S-phase population post genotoxin treatment, while the FANCO deficient cells displayed early entry into G2/M. Despite genotoxin treatment, FANCO deficient cells did not show DNA synthesis suppression, and the ability of FANCO to contribute to the intra-S phase checkpoint appeared dependent on CHK2 activity. The FA pathway appears important for the G2/M checkpoint as well, which prevents entry into mitosis with unrepaired DNA damage. FANCC and FANCD2 deficient MEFs were not able to maintain the G2 checkpoint after irradiation induced damage (272). FANCJ (BRCA1) and its interaction with BACH1 were shown to regulate the G2/M checkpoint after irradiation (273). FANCA and FANCD2 are required for the G2/M checkpoint activation after re-replication induced by the DNA replication inhibitor geminin, which prevents apoptosis (260).

1.6.4: FA pathway role in mitosis

The FA pathway plays a crucial role in mitosis. In addition to increased chromosomal breakage, FA is associated with aneuploidy, which arises from chromosome missegregation. Abnormal spindle assembly checkpoint (SAC) function has been demonstrated in FA deficient cells. RNAi of multiple FA genes in HeLA cells resulted in multinucleation upon taxol treatment, suggestive of SAC inactivation, and FA fibroblasts from 12 FA complementation groups also displayed multinuclei in response to taxol (274). This same work showed localization of FANCA, -B, E, G, L, D1, D2, and N to centrosomes during mitosis and reported FA patient fibroblasts to have abnormally high numbers of centrosomes per cell. Additionally, in *Fancd1* (*Brca2*) deficient murine tumors, concurrent mutations in *p53*, *Bub1*, and *Mad3L* with accompanying dysfunction in the SAC were reported (275), suggesting a functional relationship

between the FA pathway and proper spindle assembly during mitosis. An additional connection between the FA pathway and mitosis comes from a report that the mitotic cyclin-dependent kinase CDK1 (*CDC2*), which plays a critical role in the SAC (276), phosphorylates FANCG during mitosis (277).

At later stages of mitosis, it has been suggested that FA proteins FANCD2 and FANCI may participate in resolution of ultrafine chromatin bridges that occur at fragile sites upon replication stress, in association with BLM (267). An association between FANCD2 and BLM was reported by another work, that demonstrated FANC-dependent targeting of BLM to non-centromeric abnormal chromosome structures during anaphase and telophase upon replication stress limits cellular aneuploidy (268). Finally, abnormal cytokinesis has been reported in FA deficient cells. One study reported a higher number of ultrafine bridges and cytokinesis failure resulting in binucleated cells in both human and murine FA deficient cells that proceed past a G2 checkpoint with incompletely replicated DNA (278). They additionally showed FANCM to coat the ultrafine bridges at late mitosis. Thus in addition to repairing DNA damage, such as interstrand crosslinks, the FA pathway is critical for normal cell division.

1.6.5: FA gene mutations and cancer

Increased susceptibility to tumor formation is a hallmark of FA disease, however, the FA pathway is also frequently mutated in tumors from non-FA patients. A 2015 study evaluated the frequency of mutations in the 17 known FA genes at that time using 68 DNA sequence datasets and c-BioPortal. They reported a frequency mostly in the range of 15-35% in a variety of non-FA human cancers with higher rates in bladder, breast, ovarian, head and neck, adrenal, esophageal, liver, lung, pancreatic, and skin tumors, as well as lymphoma (279). Heterozygous or mono-allelic somatic *FANCD1*, *FANCJ*, *FANCN*, and *FANCO* mutations have long been known to increase risk of breast cancer (280). *FANCM*, *FANCP*, *FANCS*, and *FANCC* monoallelic mutations also increase breast and/or ovarian cancer risk (281). For the prototypic *FANCD1* (*BRCA2*) and *FANCS* (*BRCA1*) breast cancer susceptibility genes, mutations result in high life-time risks of 35-60% and 55-85%, respectively, compared to a population risk of about 10% (282, 283). Loss of heterozygosity of *FANCC* and *FANCG* increases sporadic pancreatic cancer incidence (284). In addition to truncating or missense mutations, epigenetic silencing of FA genes is also associated

with increased cancer risk (285). Hypermethylation of *FANCF* may be the most frequent epigenetic change resulting in FA pathway dysfunction in several cancer types (280, 286, 287). Thus, the FA pathway plays a crucial role in the protection against tumorigenesis, and in addition to gene mutation, protein deficiency can result in cancer development.

1.7: **Non-Canonical Roles of the Fanconi Anemia Pathway**

Historically, FA phenotypes were largely viewed in the context of deficient DNA repair and increased chromosomal fragility. Though DNA repair defects do have a well-established role in contributing to FA disease, particularly hematopoetic cell failure and cancer predisposition, it is increasingly recognized that FA phenotypes also arise from the absence of non-canonical roles of the FA pathway outside of DNA repair. Indeed, the complex syndrome of oxidative stress, alterations in energy metabolism, glucose and insulin abnormalities, and serum lipid imbalances are difficult if not impossible to account for merely from a DNA damage accumulation perspective, but rather suggest that the FA pathway is also required for metabolic homeostasis. Multiple FA proteins have been shown to localize outside of the nucleus and to interact with cytosolic proteins, further suggesting that FA proteins function outside of the nucleus and DNA repair (288-292).

1.7.1: FA pathway antioxidant roles

Maintaining proper redox balance is a well-established and long-studied non-DNA repair role of the FA pathway. Nordenson observed that superoxide dismutase and catalase supplementation decreased the frequency of chromosomal breaks in FA deficient cells (293). It was suggested early on that the chromosomal aberrations observed in FA were due not only to lack of proper repair of DNA, but also from a lack of protection from endogenous damage, and it was observed that the degree of chromosomal damage was positively related to oxygen tension (294). Early studies of FA patients reported pro-oxidant states, such as an imbalanced reduced-to-oxidized glutathione ratio, increased 8-hydroxy-deoxyguanosine (8-oxoG), and increased TNF-α (295-297). Interestingly, though FA deficient cells are classically referred to as hypersensitive to DNA crosslinkers, the toxicity of mitomycin C and diepoxybutane involve redox-

dependent mechanisms and are dependent on oxygen levels (298-300). The increased 8-oxoG in FA cells was demonstrated to arise not from a failure of base excision repair of oxidized bases, which did not require FANCD2 or activate FANCD2 monoubiquitination, which suggests that the increased oxidative damage reflects an overproduction of ROS rather than defective repair (301).

Several FA pathway components have interactions with antioxidant proteins, such as FANCC with NADPH cytochrome P-450 reductase (302) and glutathione S-transferase (303). FANCG interacts with cytochrome P450 2E1 (CYP2E1), which is associated with the production of reactive oxygen intermediates, and mitochondrial peroxiredoxin-3 (PRDX3), an antioxidant enzyme (292, 304). FANCD2 has a demonstrated oxidative stress-specific interaction with FOXO3a, a transcription factor and major regulator of oxidative stress, and only FANCD2 corrected, but not mutant cells demonstrated increased cellular resistance to oxidative stress upon FOXO3a overexpression (305). FANCD2 may also regulate the expression of antioxidant genes by protecting the gene promoter regions from oxidative DNA damage via formation of a complex with BRG1, as demonstrated by De et al. in FA bone marrow cells (306). The increased oxidative damage at select antioxidant gene promoter regions and their decreased expression appeared to result not from decreased repair of oxidized bases in FA cells, but rather faulty protection.

Murine FA models also provide evidence for an altered ability to handle oxidative stress in the absence of an intact FA pathway. *Fancd2* mutant mice show improved phenotypes upon antioxidant supplementation. Tempol, which mimics superoxide dismutase, delayed epithelial tumor onset, and resveratrol improved bone marrow phenotypes in *Fancd2* null mice (307, 308). Supportive of the theory that increased oxidative stress is a major driver of FA phenotypes, *Fancc* and superoxide dismutase 1 double mutant mice develop severe, synergistic defects in hematopoiesis (309).

1.7.2: Redox balance and mitochondrial roles of the FA pathway

Redox-balance, energy metabolism, and mitochondrial function are tightly connected, and FA deficient cells are also reported to have mitochondrial dysfunction. FANCD2 null fibroblasts and FANCA and –C null lymphoblasts had decreased mitochondrial membrane potential, decreased ATP production, and abnormal mitochondrial morphology, as well as inactivation of enzymes that function in energy

production (F1F0ATPase and cytochrome C oxidase) and ROS detoxification (SOD1) (310). FANCG was reported to localize to mitochondria and interact with mitochondrial peroxiredoxin-3, and FANG-null cells also showed distorted mitochondria (304). Unlike normal lymphoblasts, FA-A and C lymphoblasts were insensitive to two independent mitochondrial disruptors that result in severe ATP depletion, but were instead very sensitive to two glycolytic metabolism inhibitors, suggesting FA cells may be adapted to abnormal mitochondrial function (311).

FANCC and FANCD2 localize to mitochondria, and deficiency of FANCC and knockdown of several other FA genes *(FANCA*, *-F*, *-L*, *D*1, *-D*2, *-S*) has been linked with impaired mitophagy, or the autophagy of damaged mitochondria (312), independent of the DNA repair functions of the FA pathway. In this study by Sumpter et al., *FANCC* KO HeLA cells showed accumulation of damaged mitochondria post-treatment with two inhibitors of mitochondrial respiration and *Fancc*$^{-/-}$ mice accumulated damaged mitochondria in brain and heart as assessed by EM. Expression of a naturally occurring hypomorphic form of FANCC, in which DNA repair is still defective but hypersensitivity to cytokines is not conferred, was able to rescue mitophagy in KO cells, suggesting the functions in DNA repair and mitophagy are independent. Impaired mitophagy might contribute to the increased ROS, inflammation, and oxidative DNA damage in FA cells.

An additional connection between the FA pathway, energy metabolism, and mitochondria was observed by Jayabal et al. who report a functional connection between FANCD2 and ATP production via its interaction with ATP5α, a subunit of ATP synthase (313). They additionally report that roughly half of cellular ATP5α, normally exclusively present in the inner mitochondrial membrane, is located outside of mitochondria in cells with mutant, non-monoubiquitinated FANCD2, which have significantly reduced ATP production. It is possible the connection between the FA pathway and mitochondrial function is responsible for a significant component of the tumor suppressor function of the pathway.

1.7.3: Regulation of cytokines and inflammatory signaling by the FA pathway

The Fanconi Anemia pathway is important in regulating cytokine signaling, failure of which appears to contribute to FA phenotypes. FA patients frequently have elevated plasma levels of the pro-

inflammatory cytokine tumor necrosis factor-alpha (TNF-alpha), which is also reportedly overproduced by FA lymphoblasts and marrow mononuclear cells (314-317). TNF-alpha signaling can increase ROS via its effects on mitochondria, which can lead to DNA damage (318-320). TNF-alpha also impacts hematopoietic stem cell proliferation, survival, and homing (321).

IL-6, which can be induced by TNF-alpha and in turn suppresses TNF-alpha, was found to be defective in FA lymphoblasts, but when exogenously administered lowered TNF-alpha production (315). Interestingly, IL-6 or anti-TNF-alpha antibody administration prior to MMC treatment decreased the MMC-sensitivity of FA lymphoblasts (315). Another mechanism that appears to contribute to overproduction of TNF-alpha in FA cells involves inappropriate ubiquitinylation, and thus increased activity, of TLR8, a pathogen recognition protein, promoting TNF-alpha production through interleukin 1 receptor associated kinase and IkappaB kinase signaling (322). At least one mechanism of TNF-alpha dependent apoptosis in FA cells appears to be mediated through the redox-dependent protein apoptosis signal-regulating kinase 1 (Ask1). TNF-alpha treatment of FA-C MEFs or hematopoietic progenitors led to Ask1 hyperactivation and inactivation of Ask1 in FA-C MEFs restored survival to WT levels after TNF-alpha treatment (323).

TNF-alpha and interferon gamma (IFN-gamma) contribute to hematopoietic stem cell failure in the context of human aplastic anemia (324), and *in vitro* evidence and mouse models suggest both cytokines likely contribute to bone marrow phenotypes in FA. Cultured bone marrow cells harvested from *Fancc* null mice were hypersensitive to proliferative inhibition by IFN-gamma (217). Both FA-C human and murine hematopoietic stem cells were hypersensitive to IFN-gamma induced expression of *fas* and *interferon response factor* and had an increased apoptotic response, which could be blocked by anti-fas antibodies (325). Additional evidence that the FA pathway intersects with multiple inflammatory cytokine signaling pathways with impacts on BM function comes from a study reporting FA-C hematopoietic progenitor cell proliferation to be decreased by 50% at 50-100 fold lower concentrations of TNF-alpha, IFN gamma, and macrophage inflammatory protein-1alpha vs controls, which was associated with deregulated apoptosis (326). TNF-alpha treatment of *Fancc* null mice led to premature senescence of

hematopoietic stem cells, ROS, and oxidative DNA damage, which could be prevented by TNF-alpha neutralizing antibodies or deletion of its receptor (327).

Transforming growth factor beta (TGF-beta) signaling is also aberrant in FA, and appears to contribute to bone marrow failure. TGF-beta has a precedent for suppressing hematopoiesis (328, 329). An shRNA screen revealed that blocking the TGF-beta pathway improved FA cell survival, and murine (*Fancd2* null) and human (FA-A and FA-D2) hematopoietic stem cell proliferation and function (330). The increased survival was associated with increased high fidelity homologous recombination repair and decreased mutagenic non-homologous end joining of DNA double strand breaks as assessed by a repair reporter plasmid, suggesting aberrant TGF-beta mediated bone marrow attrition may result from DNA damage arising from an altered balance of high fidelity : low fidelity repair (330). Increased TGF-beta may arise from loss of FANCD2-mediated SMAD1 transcriptional regulation (329). The relationship between FA and TGF-beta signaling may be complex, however. A recent study reported an absence of TGF-beta secretion in *FANCD2*-deficient human bone marrow mesenchymal stem cells, a component of the bone marrow niche, which they suggest may promote early senescence (331).

1.7.4: FA pathway roles in energy metabolism and glycolysis

As discussed earlier, FA deficient cells have well established mitochondrial defects that impact not only cellular oxidative stress, but also cellular energy metabolism. Specifically, it appears that FA deficiency (FA-A) is associated with defects in the transfer of electrons from respiratory chain complex I to III, which is part of generating the proton gradient needed for oxidative ATP generation (332). It has been reported that the resulting mitochondrial impairment in oxidative phosphorylation is accompanied by an increase in glycolytic flux, though this doesn't fully compensate for the energy deficit, as FA deficient cells still have a lower ATP/AMP ratio (333). In FA deficient lymphoblasts, AMPK, which senses cellular energy status and stimulates catabolic energy generating processes, was hyperphosphorylated, and the activity of three major glycolytic enzymes was elevated. This is consistent with an earlier reported sensitivity of FA cells to two inhibitors of glycolytic metabolism (311). FA deficient cells may compensate for the decreased efficiency of recycling NADH to NAD^+ via oxidative

phosphorylation through increasing the activity of lactate dehydrogenase, which is also able to recycle NADH to NAD^+. Cappelli et al. reported that the activities of two enzymes involved in glutaminolysis, a process that supplies substrates for aerobic energy metabolism, glutaminase and glutamic dehydrogenase, were lower in FA deficient cells. Therefore, it appears that FA cells are deficient in oxidative phosphorylation, and, similar to Warburg's theory, increase anaerobic metabolism to partially compensate.

A functional association between the Fanconi Anemia pathway and energy metabolism via AMPK was also reported by Chun et al. (334, 335). This group first reported a physical interaction between both FANCA and FANGG, members of the FA core complex, with the alpha subunit of AMPK. They further showed that knockdown of AMPK decreased FAND2 activation and increased cellular sensitivity to MMC treatment, and that MMC treatment lead to AMPK phosphorylation/activation, which was dependent on FANCA. After establishing an FA-AMPK connection in response to MMC, they demonstrated that the AMPK activating drug AICAR induced FANCD2 monoubiquitination and nuclear focus formation, and that FANCD2 repression increased cell death after AICAR treatment. In addition to regulating energy processes, AMPK is also involved in the DDR. It is a downstream substrate of ATM and regulates cell cycle progression, p53, and p21 (336-338). Therefore, though it may be difficult to determine the relative significance of the interaction between the FA pathway and AMPK in the DDR vs energetic metabolism, this physical and functional interaction likely represents another example of a connection between a response to DNA damage and metabolic shifts, and provides further evidence that the FA pathway is involved in regulating cellular energy metabolism.

1.7.5: Influence of the FA pathway on lipid metabolism

Roughly half of FA patients have serum dyslipidemia (206), and this phenotype may be related to cellular lipid imbalances associated with the disease. Recent reports suggest FA cells do indeed have altered lipid metabolism. FANCA deficient lymphoblasts have increased Acetyl CoA concentration as reported by Ravera et al. (339). Acetyl CoA can be produced by both aerobic glucose catabolism and via fatty acid beta-oxidation. As the FA lymphoblasts displayed lower activity of the enzyme that catalyzes

the third step in beta oxidation of fatty acids, 3-hydroxyactyl-CoA dehydrogenase, the authors postulate the increase in acetyl CoA is not due to increased fatty acid oxidation, but potentially due to the known electron transport defect in FA cells, resulting in reduced kinetics of the Krebs cycle and acetyl CoA accumulation. The authors propose the excess Acetyl CoA is converted to fatty acids, and reported an increase in activity of two fatty acid synthesis enzymes, β-ketoacyl-ACP reductase and enoyl-Acyl reductase, in the FA deficient lymphoblasts, as well as an increase in cellular lipid droplets.

Zhao et. al associated invasive characteristics of squamous cell carcinomas of the head and neck (HNSCC) with loss of FA gene function, and reported that transcriptional repression and mutations in FA genes occur in a significant proportion of sporadic HNSCCs (340). They then performed lipidomic profiling of FA-deficient HNSCCs, and reported an elevation of gangliosides, a type of glycosphingolipid and key cell membrane lipid component, that was repressed upon genetic correction (341). They further demonstrated that the HNSCC cell invasion driven by FA pathway loss, and the motility of non-transformed keratinocytes after FA pathway loss was dependent on upregulation of gangliosides. Treatment with the glycosphingolipid synthesis inhibitor NB-DNJ decreased FA-deficient HNSCC cell invasiveness. This suggests that changes in cell surface lipids in response to FA pathway loss stimulate cell invasiveness in HNSCCs and may relate to the increased incidence and poorer prognosis of HNSCC in FA patients. Additionally, this suggests a connection between the FA pathway and ganglioside lipid biosynthesis and cell surface lipid composition.

Abnormal lipid and phospholipid metabolism may also contribute to the bone marrow phenotype of FA. Bone marrow mesenchymal stromal cells (MSCs) and the bone marrow niche have demonstrated importance in the function of hematopoietic stem cells (HSCs) (342). A metabolomics study found glycerophospholipids, a group of MSC-derived metabolites, to be upregulated in FA (*Fancaa* or *Fancd2* null) murine MSCs, and further showed that targeted reduction of these lipids (via administration of TOFA, an inhibitor of acetyl-CoA carboxylase) improved the hematopoietic-supporting function of FA MSCs (343). The report further provided evidence that the increased glycerophospholipids produced by FA MSCs (phosphocholine, phosphoethanolamine, phosphoserine) may lead to HSC dysfunction via activation of their TLR4 receptors and induction of NF-κB signaling.

Fanconi Anemia summary:

The twenty-two currently identified FA genes and their protein network function to maintain genomic integrity and cellular homeostasis. Bi-allelic mutations in FA genes result in heterogeneous phenotypes, such as birth defects, infertility, metabolic and endocrine dysfunction, bone marrow failure and cancer, and are characterized by increased sensitivity to endogenous and exogenous DNA damage and cellular stress. Mono-allelic mutations also result in increased cancer risk. Similar to other DNA repair pathway components that also have identified roles in coordinating non-DNA repair cellular metabolic regulation, a growing list of non-canonical functions of the FA pathway indicates this pathway has functions outside of the nucleus and likely facilitates integration of a response to DNA damage with cellular metabolic changes. To gain insight into the non-canonical roles of the FA pathway, we evaluated how FA deficiency alters the metabolic impacts of challenge with a high fat or a high fat/high cholesterol Paigen diet in mice lacking the FA component *Fancd2*. We found that when fed a Pagien diet, FA deficient male mice were hypersensitive to hepatic pathology, and had altered expression of hepatic cholesterol and bile acid metabolism genes and altered hepatic lipid species abundance in the absence of a significant increase in DNA damage or DNA damage response activation relative to wildtype controls (Chapter 3). These data suggest that the FA pathway plays an important role in hepatic homeostasis in the face of metabolic challenge.

CHAPTER 2

The role of the 9-1-1 complex in DNA double strand break repair

Elizabeth S. Moore†, Pei Xin Lim†, Joanna Mleczko, Amy Lyndaker, Gabriel Balmus, Weishan Huang, Cindy Luan, Eric Zhang, Avery August, Robert Weiss

† co-authors

E.M., P.L. and J.M. conceived and conducted experiments; E.M. wrote the manuscript with support from P.L; A.L. scored testes morphology; G.B., W.H., C.L., E.Z. assisted with experiments and contributed to data analysis; A.A. assisted with data analysis and interpretation; R.W. conceived and supervised the project

2.1: Abstract

The RAD9-HUS1-RAD1 (9-1-1) clamp functions in the DNA damage response, promoting checkpoint signaling and DNA repair. *Hus1* impairment results in chromosome aberrations, hypersensitivity to replication stress, and defects in double strand break (DSB) repair. Several DSB repair pathways exist, including homologous recombination (HR) and non-homologous end joining (NHEJ). To study the role of HUS1 in DSB repair, we combined *Hus1* hypomorph (*Hus1*$^{neo/\Delta 1}$) mice with two DSB repair deficient models: mice null for the HR component *Rad54*, which are mildly impaired for HR, or mice null for the NHEJ component *Prkdc*, which lack mature lymphocytes due to an inability to complete V(D)J recombination. Deficiency of *Hus1* confers mitomycin C (MMC) hypersensitivity, absence of *Rad54* confers mild irradiation (IR) and MMC sensitivity, and absence of *Prkdc* results in hypersensitivity to IR. We show that combined *Rad54* and *Hus1* defects elevate spontaneous and genotoxin-induced genomic instability, suggesting that *Hus1* and *Rad54* both contribute to HR. In contrast, combined *Prkdc* and *Hus1* defects partially rescue some fitness defects, do not significantly elevate spontaneous genomic instability, and confer a partial rescue in genotoxin-induced damage in vivo. We hypothesize that the 9-1-1 complex may have a role in NHEJ inhibition, and/or that in the absence of competent NHEJ, HUS1 loss may relieve inhibition of alternative DSB repair pathways, leading to improved survival and decreased

genotoxin sensitivity. This work suggests the 9-1-1 complex facilitates high fidelity DSB repair and regulates DSB repair pathway choice.

2.2: Introduction

Double stranded DNA breaks (DSBs) are particularly threatening to genomic integrity as they impact both strands of the DNA template, and if unrepaired, can result in chromosome breakage leading to chromosome loss or translocation, cell death, or cell transformation. DSBs can arise from direct damage from ionizing radiation (IR) or chemical mutagens, unrepaired single stranded breaks, and replication fork collapse. Programmed DSBs are also generated by Spo11 during meiosis and as part of V(D)J and class switch recombination in lymphocytes. There are at least four cellular sensors for DSBs: PARP, KU70/80, the MRN complex, and, if some DNA end processing has occurred, RPA (1), and cells have evolved several pathways to repair DSBs. Non-homologous end joining (NHEJ) and homologous recombination (HR) are the major DSB repair pathways, though DSBs can also be repaired by alternative end joining, single strand annealing, and break induced replication. HR and NHEJ are somewhat functionally overlapping as well as mutually-competitive. The regulation of DSB repair pathway choice, though known to be regulated by the cell cycle, DNA end processing, and protein recruitment, is incompletely understood (344-346).

In NHEJ, which is available at all stages of the cell cycle, broken DNA ends are joined by direct ligation with minimal or no base pairing, which can result in nucleotide insertions, deletions, and substitutions. KU70/80 heterodimers rapidly bind to DNA ends, followed by DNA-PKcs (encoded by *Prkdc*) and Artemis recruitment, stabilizing DNA ends (43). Ku interacts with DNA polymerases μ and λ and the XRCC4-DNA ligase IV complex to ligate the ends (44). *Prkdc* deficient mice are NHEJ impaired, immune compromised due to defective T and B lymphocyte differentiation, highly sensitive to IR, and useful for investigating the importance and contribution of NHEJ to DSB repair in varied contexts (347-351).

HR, which predominates in S and G2 phases, involves sister chromatid homology-directed, high fidelity repair, and proceeds more slowly than NHEJ. HR begins with the MRN complex (MRE11-

RAD50-NBS1) localizing to double strand breaks, which stabilizes DNA ends, and is important for initial DNA resection and ATM recruitment (54, 55). CtIP is recruited in an MRN and ATM dependent manner, and is important for end resection (56, 57). EXO1, BLM, and Dna2 continue end resection (58). A 5' to 3' resection results in a 3' ssDNA overhang, which becomes coated and stabilized by replication protein A (RPA) complexes (59). RAD51 can then form a filament on the 3' ssDNA in a BRCA2-dependent manner in combination with PALB2, and perform strand invasion and homology search on the sister chromatid for homologous template directed repair (60). HR repair intermediates can be resolved by BLM/TOPOIII or cleaved by GEN1, MUS81/EME1, or SLX1/SLX4 in either crossover or non-crossover events (63-66). Unlike two-ended DSBs, which are normally repaired by NHEJ, a major function of HR is to repair single-ended DSBs (seDSBs) that occur as a result of replication fork collapse, and to prevent "toxic" NHEJ at these types of seDBS (67).

RAD54, a RAD52 epistasis group member, and RAD51 paralogs (RAD51B, RAD51C, RAD51D, XRCC2, XRCC3) assist with RAD51 function (61). RAD54 is a DNA-interacting protein with translocase activity that uses ATP hydrolysis to alter DNA confirmation (352). RAD54 participates in multiple stages of HR, including chromatin remodeling for RAD51 filament stabilization, strand invasion, D-loop dissolution and branch migration, and RAD51 dissociation (62). *Rad54*-deficient embryonic stem cells show hypersensitivity to IR, the DNA crosslinker mitomycin C (MMC), and the DNA alkylating agent methylmethane sulfonate (MMS), but not towards ultraviolet treatment, consistent with a DSB repair defect (353). Low HR efficiency and reduced MMC-induced sister chromatid exchange in these *Rad54*-deficient ES cells suggest that RAD54 plays a major role in HR (354). Surprisingly, *Rad54*$^{-/-}$ mice do not show increased IR sensitivity at the adult stage, suggesting that the role RAD54 plays in HR is indispensable at early developmental stages, but less so in more differentiated cells (353, 355), though adult *Rad54*$^{-/-}$ mice retain hypersensitivity to MMC, suggesting that at least a mild perturbation in the HR pathway remains. In contrast, deletion of central components of the HR pathway, such as *Rad51*, leads to embryonic lethality (356). This makes the *Rad54* null mouse model suitable for the study of gene function in HR, as already done for Blm (357), as well studying the crosstalk between NHEJ and HR (358).

The highly conserved toroidal RAD9A-HUS1-RAD1 (9-1-1) sliding clamp is a critical component of the DNA damage response and serves as a molecular scaffold with separable functional roles in both cell cycle check point signaling via ATR activation, and DNA repair through direct interaction with DNA repair proteins (119-122, 137-147, 149, 150, 157, 158). Loss of *Hus1* or any clamp component results in embryonic lethality and genomic instability, therefore, we utilize a mouse model with one hypomorphic and one null *Hus1* allele to study decreased HUS1 expression (153). Decreased *Hus1* expression in mouse embryonic fibroblasts (MEFs) leads to proliferation and checkpoint defects, chromosomal aberrations, and hypersensitivity to replication stress-causing agents, while decreased *Hus1* expression in mouse models results in increased micronuclei formation in peripheral blood and hypersensitivity to MMC (151-154). Thus HUS1 and the 9-1-1 clamp are essential for the maintenance of genomic integrity.

Several lines of evidence indicate that HUS1 and the 9-1-1 clamp are important for high fidelity DSB repair, including phenotypic features of HUS1 deficient cells, physical interactions with HR proteins, meiotic phenotypes of HUS1 deficient germ cells, and HR repair DNA reporter plasmid analysis. Radial chromosomes, which are thought to arise from faulty DSB repair, are a key feature of *HUS1* deficient MEFs (153), a phenotype shared with other HR deficient genotypes such as Fanconi Anemia and *Brca1* or *Brca2* deficiency (359, 360). The 9-1-1 clamp has been reported to interact with proteins involved in HR, including RAD51 and EXO1 (141, 361), and to regulate the activity of EXO1 and DNA2 exonucleases in budding yeast (165, 166). These nucleases have critical roles in the DNA end processing at breaks necessary to engage HR. RAD9A colocalizes with RAD51 foci in pachytene of meiotic prophase I, and *Hus1* conditional knockout leads to persistent RAD51 foci and increased γH2AX staining in primary spermatocytes (173). Absence of *Rad9A* also results in meiotic defects, including arrest of spermatocytes in prophase, increased γH2AX staining, and male infertility (174). Additionally, *Hus1* knockdown reduced HR efficiency after IR in mouse kidney fibroblast cells as assessed by a GFP-I-Sce HR repair reporter plasmid (171). These observations suggest that HUS1 and the 9-1-1 clamp play important roles in error-free DSB repair. In this study, we combined a *Hus1* deficient mouse background

with either a mouse model impaired in HR (*Rad54* null) or NHEJ (*Prkdc* null) and assessed the impact of the combined DNA repair deficiencies on genomic integrity and genotoxin sensitivity *in vivo* and *in vitro*.

2.3: Results

2.3.1: Combined loss of *Rad54* and *Hus1* deficiency results in increased genomic instability and genotoxin sensitivity

2.3.1.1: Combined loss of *Rad54* and *Hus1* deficiency results in decreased body size, skeletal defects, and increased spontaneous genomic instability

Initially we hypothesized that simultaneous deletion of *Rad54* and reduction of *Hus1* to the lowest level that still allows viability (*Rad54*$^{-/-}$*Hus1*$^{neo/\Delta 1}$) would cause early embryonal developmental defects and lead to synthetic lethality. *Rad54*$^{-/-}$*Hus1*$^{neo/\Delta 1}$ mice, however, were viable and born at the expected Mendelian ratio (Table 2.S1A). Though viable, *Rad54*$^{-/-}$*Hus1*$^{neo/\Delta 1}$ mice were consistently and significantly underweight compared to the other genotypic groups regardless of gender (Figure 2.1A). We observed that nearly 65% of the *Rad54*$^{-/-}$*Hus1*$^{neo/\Delta 1}$ mice had curly or kinked tails (Figure 2.1 B). These oddly-shaped tails were observed from birth (Figure 2.S1A,B). Skeletal staining and live CT scans of the caudal region revealed vertebral deformities and fusions in *Rad54*$^{-/-}$*Hus1*$^{neo/\Delta 1}$ mice (Figure 2.1C, Figure 2.S1C). These results suggest that perturbing *Hus1* and *Rad54* leads to mild dwarfism and vertebral developmental defects likely due to elevated basal levels of genomic instability throughout development.

We tested the impact of combined *Rad54* and *Hus1* defects on basal genome maintenance by measuring micronucleus formation in peripheral erythrocytes (Figure 2.1D). Using flow cytometry, micronuclei levels were detected as the percentage of CD71-negative/DNA-positive cells, signifying DNA fragment-containing mature erythrocytes. Consistent with previous reports, *Rad54*$^{-/-}$*Hus1*$^{+}$ mice had the same level of micronuclei formation as wildtype mice, whereas *Rad54*$^{+}$*Hus1*$^{neo/\Delta 1}$ mice had a significantly higher number of micronuclei compared to wildtype (153, 353). The double mutant *Rad54*$^{-/-}$ *Hus1*$^{neo/\Delta 1}$ mice had an even higher frequency of micronucleated erythrocytes vs all other genotypic groups, suggesting that loss of *Rad54* and *Hus1* leads to a synergistic increase in spontaneous genomic

instability. These data indicate that combined *Rad54* and *Hus1* perturbations lead to decreased genome stability and deleterious consequences *in vivo*.

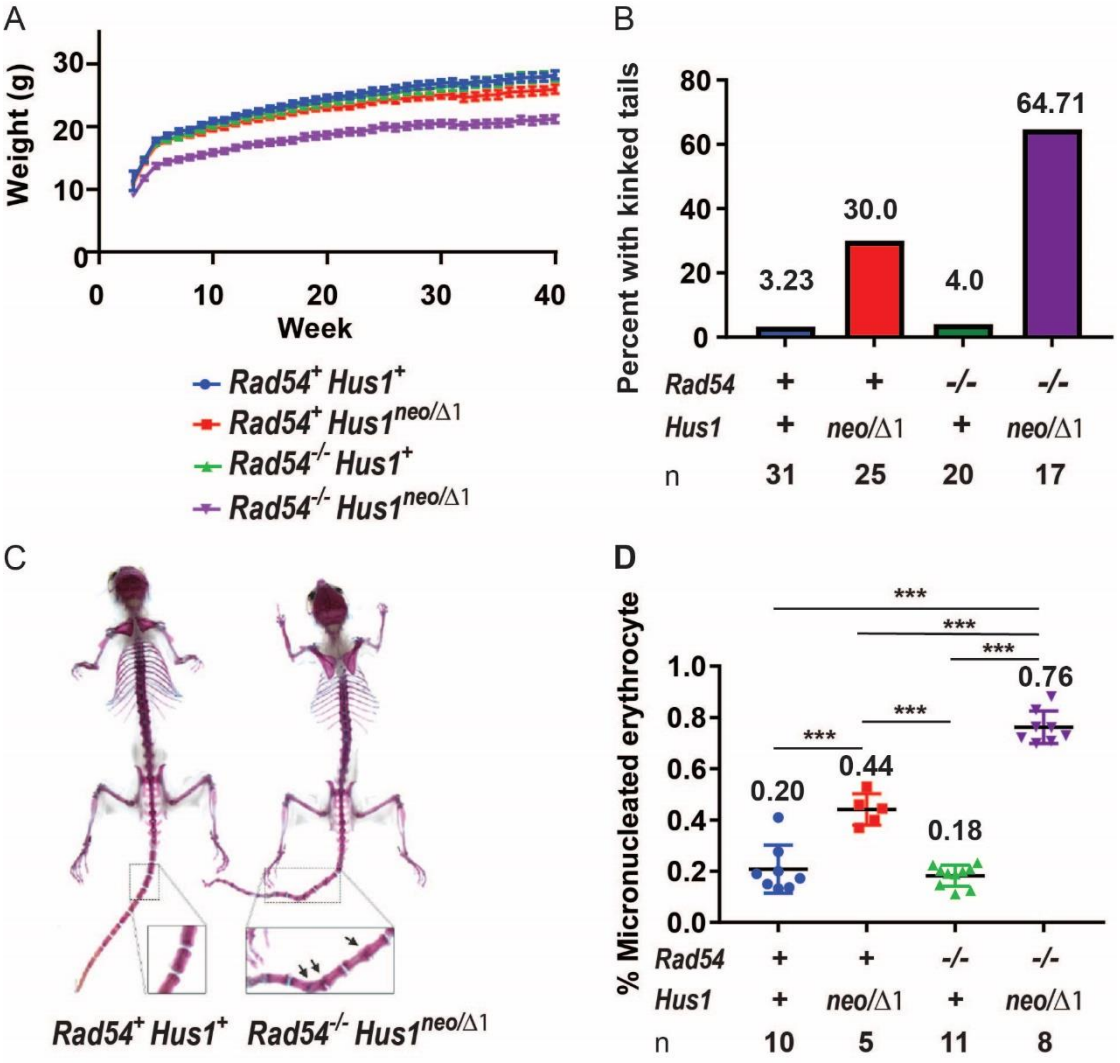

Figure 2.1. Combined loss of *Rad54* and deficiency of *Hus1* results in decreased body size, skeletal defects, and elevated spontaneous genomic instability. A: Double mutant $Rad54^{-/-}Hus1^{neo/\Delta1}$ mice were smaller than the other genotypes beginning at week 4 with all pairwise contrasts involving double mutants having p <0.001 from week 5 to week 39 (week, genotype, and week:genotype were all significant effects with Pr(>F) less than 0.001). This was true for both sexes, therefore data is shown as sexes combined (sex was a significant effect (Pr(>F) less than 0.001); however the interactions sex:genotype and

sex:genoytype:week were not statistically significant). B: *Rad54*$^{+}$*Hus1*$^{neo/\Delta 1}$ mice had an increased incidence of caudal vertebral anomalies relative to wildtype and *Rad54*$^{-/-}$*Hus1*$^{+}$ single mutants, however, double mutant *Rad54*$^{-/-}$*Hus1*$^{neo/\Delta 1}$ mice had an even greater frequency of caudal anomalies. C: Alcian blue stained cleared skeletons of wildtype mouse (left) and double mutant *Rad54*$^{-/-}$*Hus1*$^{neo/\Delta 1}$ mouse (right). Arrows indicate fused vertebrae. D: The percentage of micronucleated circulating erythrocytes was measured via flow cytometry as a proxy of *in vivo* spontaneous genomic instability. As expected, *Rad54*$^{+}$*Hus1*$^{neo/\Delta 1}$ mice had increased micronucleated erythrocytes relative to wildtype and *Rad54*$^{-/-}$*Hus1*$^{+}$ mice. Double mutant *Rad54*$^{-/-}$*Hus1*$^{neo/\Delta 1}$ mice had a synergistic increase in micronucleated erythrocytes.

2.3.1.2: Partial *Hus1* impairment synergizes with *Rad54* deficiency to increase hypersensitivity to genotoxin-induced damage

We hypothesized that simultaneous *Hus1* deficiency and *Rad54* deletion would also cause a synergistic effect on genotoxin-induced genomic instability. *Rad54*$^{-/-}$ mice are hypersensitive to MMC at a 10mg/kg dose, but they are not hypersensitive to IR (355). *Hus1*$^{neo/\Delta 1}$ mice are also hypersensitive to MMC at 4mg/kg but not to IR (154). To determine if the reported preexisting MMC sensitivity in the *Rad54* and *Hus1* single mutant mice would be synergistically increased in the double mutant, we treated mice with 3mg/kg of MMC (Figure 2.2A,B). While none of the mice in control and single mutant groups met endpoint, 5 out of 5 double mutant *Rad54*$^{-/-}$*Hus1*$^{neo/\Delta 1}$ mice met the twenty percent weight loss endpoint by day 6. We also irradiated mice with 8 Gy IR (Figure 2.2C,D). The survival of *Rad54*$^{-/-}$*Hus1*$^{+}$ and *Rad54*$^{+}$*Hus1*$^{neo/\Delta 1}$ single mutant cohorts was not significantly different from the wildtype cohort, consistent with published reports. Interestingly, double mutant *Rad54*$^{-/-}$*Hus1*$^{neo/\Delta 1}$ mice became hypersensitive to IR treatment, and 4 out of 5 mice met endpoint criteria by day 13. This hypersensitivity was also reflected in the severity of weight loss.

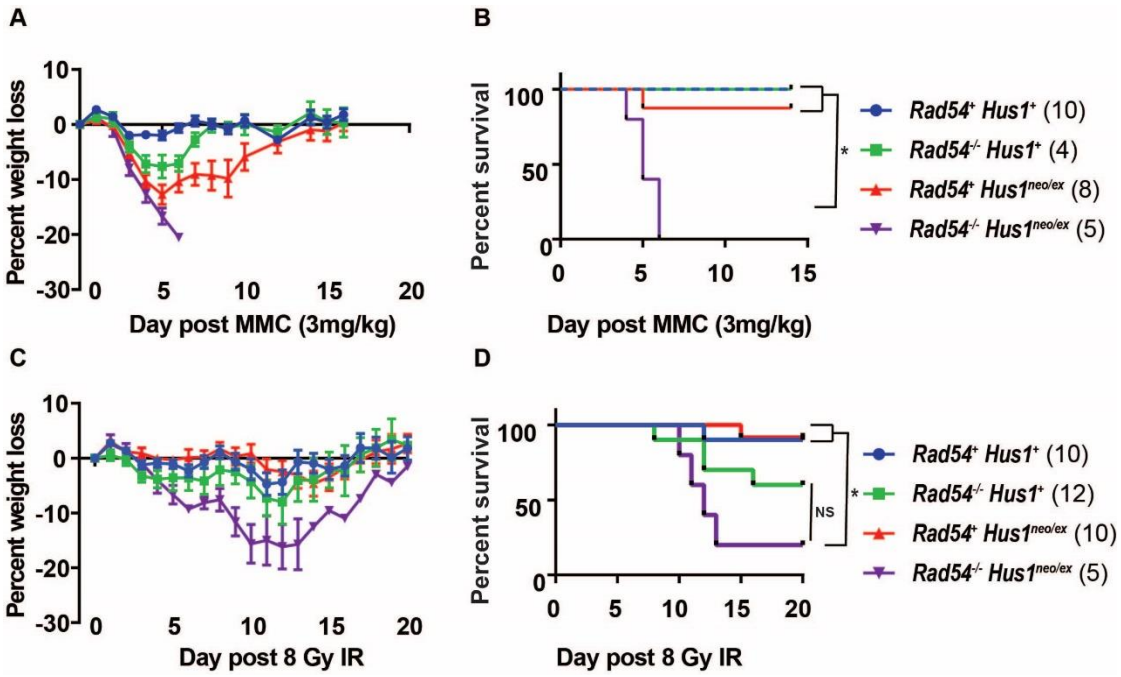

Figure 2.2: Partial loss of *Hus1* in combination with *Rad54* deficiency leads to heightened sensitivity to genotoxin-induced damage *in vivo*. A,C: Averaged percent weight loss for mice of the indicated genotypes after 3 mg/kg MMC and 8 Gy whole body IR. B,D: Kaplan-Meier survival curves for mice of the indicated genotypes after 3 mg/kg MMC and 8 Gy whole body IR treatment, respectively. Log-rank tests with p value adjustment via the Bonferroni method was used for pairwise comparisons. After MMC, double mutant *Rad54*$^{-/-}$*Hus1*$^{neo/\Delta 1}$ mice had a significant reduction in survival vs all other groups. After IR, double mutant *Rad54*$^{-/-}$*Hus1*$^{neo/\Delta 1}$ mice had a significant reduction in survival vs wildtype and *Rad54*$^{+}$*Hus1*$^{neo/\Delta 1}$ mice. Error bars represent SEM.

To evaluate the impact of combined loss of *Rad54* and deficiency of *Hus1* on genome stability and genotoxin sensitivity *in vitro*, we isolated mouse embryonic fibroblasts (MEFs). We evaluated proliferation dynamics in primary MEFs via a population doubling assay (Figure 2.3A). Elevated spontaneous genomic instability often leads to early senescence of primary cells in culture. *Rad54*$^{-/-}$*Hus1*$^{+}$

MEFs proliferated at a reduced rate relative to wildtype, but *Rad54*$^{+}$*Hus1*$^{neo/\Delta 1}$ MEFs began to senesce even earlier at passage 2, as previously reported (153). Importantly, double mutant *Rad54*$^{-/-}$*Hus1*$^{neo/\Delta 1}$ MEFs demonstrated reduced doubling kinetics as early as the first passage and never recovered from senescence, suggesting that combined *Rad54* and *Hus1* perturbations lead to premature cellular senescence *in vitro*.

To further examine the impact of combined *Rad54* loss and *Hus1* deficiency on genotoxin sensitivity, we tested genotoxin sensitivity of LT antigen immortalized MEFs *in vitro*. As expected, *Rad54*$^{-/-}$*Hus1*$^{+}$ and *Rad54*$^{+}$*Hus1*$^{neo/\Delta 1}$ single mutant MEFs were both sensitive to MMC treatment. *Rad54*$^{-/-}$ *Hus1*$^{neo/\Delta 1}$ double mutant MEFs were significantly hypersensitized relative to either single mutant at 0.15µg/ml of MMC (Figure 2.3B), showing a similar trend as the *in vivo* experiment. *Rad54*$^{-/-}$*Hus1*$^{+}$ MEFs showed only a slight reduction in colony forming ability after exposure to the replication stress causing agent aphidicolin, while the *Rad54*$^{+}$*Hus1*$^{neo/\Delta 1}$ MEFs showed increased aphidicolin sensitivity as expected. As with MMC sensitivity, *Rad54*$^{-/-}$*Hus1*$^{neo/\Delta 1}$ double mutant MEFs were significantly hypersensitized to 0.2 and 0.4 µM aphidicolin (Figure 2.3C). Finally, paralleling the *in vivo* data, *Rad54*$^{-/-}$ *Hus1*$^{neo/\Delta 1}$ double mutant MEFs were hypersensitized to 5 Gy IR (Figure 2.3D).

In order to characterize the types of chromosomal aberrations associated with the observed genotoxin hypersensitivity, we examined chromosomal integrity in our MEF lines after genotoxin exposure (Figure 2.3E and Table 2.1). As expected, *Rad54*$^{+}$*Hus1*$^{neo/\Delta 1}$ primary MEFs demonstrated both spontaneous and genotoxin-induced chromosome breaks and radials, indicative of HR repair pathway impairment (153). No metaphase spread analysis of *Rad54*$^{-/-}$ cells has been previously reported. We saw low levels of spontaneous chromosomal abnormalities and a trend towards an increase in number of MMC-induced abnormalities in the *Rad54*$^{-/-}$*Hus1*$^{+}$ MEFs compared to wildtype. Double mutant *Rad54*$^{-/-}$ *Hus1*$^{neo/\Delta 1}$ MEFs had a higher basal level of total chromosomal abnormalities per spread in the untreated condition compared to *Rad54*$^{-/-}$*Hus1*$^{+}$ MEFs. After exposure to MMC, the double mutant MEFs sustained even more chromosomal aberrations, particularly breaks/gaps and radials (Table 2.1). Taken together, these results strongly suggest that partial loss of *Hus1* together with *Rad54* deficiency results in a further

reduction in high fidelity DSB repair efficiency and increased error-prone DSB repair, leading to higher genomic instability.

Figure 2.3: Partial loss of *Hus1* in combination with *Rad54* deficiency leads to a synergistic increase in genotoxin sensitivity *in vitro*. A: Primary mouse embryonic fibroblasts (MEFs) were generated and analysed for proliferation kinetics via a population doubling (PDL) assay. Absence of *Rad54* resulted in a mild reduction in proliferation, while deficiency of *Hus1* resulted in a greater decrease in cumulative PDL. The combined loss of *Rad54* and deficiency of *Hus1* in MEFs led to a further decrease in PDL, the earliest senescence, and a failure to exit senescence. B: After exposure to MMC, both $Rad54^{-/-}Hus1^{+}$ and $Rad54^{+}Hus1^{neo/\Delta 1}$ single mutant MEFs demonstrated decreased colony formation as expected. Double mutant $Rad54^{-/-}Hus1^{neo/\Delta 1}$ MEFs showed an even greater reduction in colony formation. C: As expected after exposure to aphidicolin, $Rad54^{+}Hus1^{neo/\Delta 1}$ single mutant MEFs demonstrated decreased colony formation, however, double mutant $Rad54^{-/-}Hus1^{neo/\Delta 1}$ MEFs showed an even greater reduction in colony formation. D: Double mutant $Rad54^{-/-}Hus1^{neo/\Delta 1}$ MEFs also demonstrated a hypersensitization to the colony reducing impact of IR exposure. E: Metaphase chromosome analyses after MMC exposure demonstrated increased spontaneous and MMC-induced chromosome damage in $Rad54^{+}Hus1^{neo/\Delta 1}$ single mutant MEFs, and increased MMC-induced chromosome damage in $Rad54^{-/-}Hus1^{+}$ MEFs relative to wildtype MEFs. Double mutant $Rad54^{-/-}Hus1^{neo/\Delta 1}$ MEFs had both increased spontaneous and MMC-induced chromosome damage relative to either single mutants.

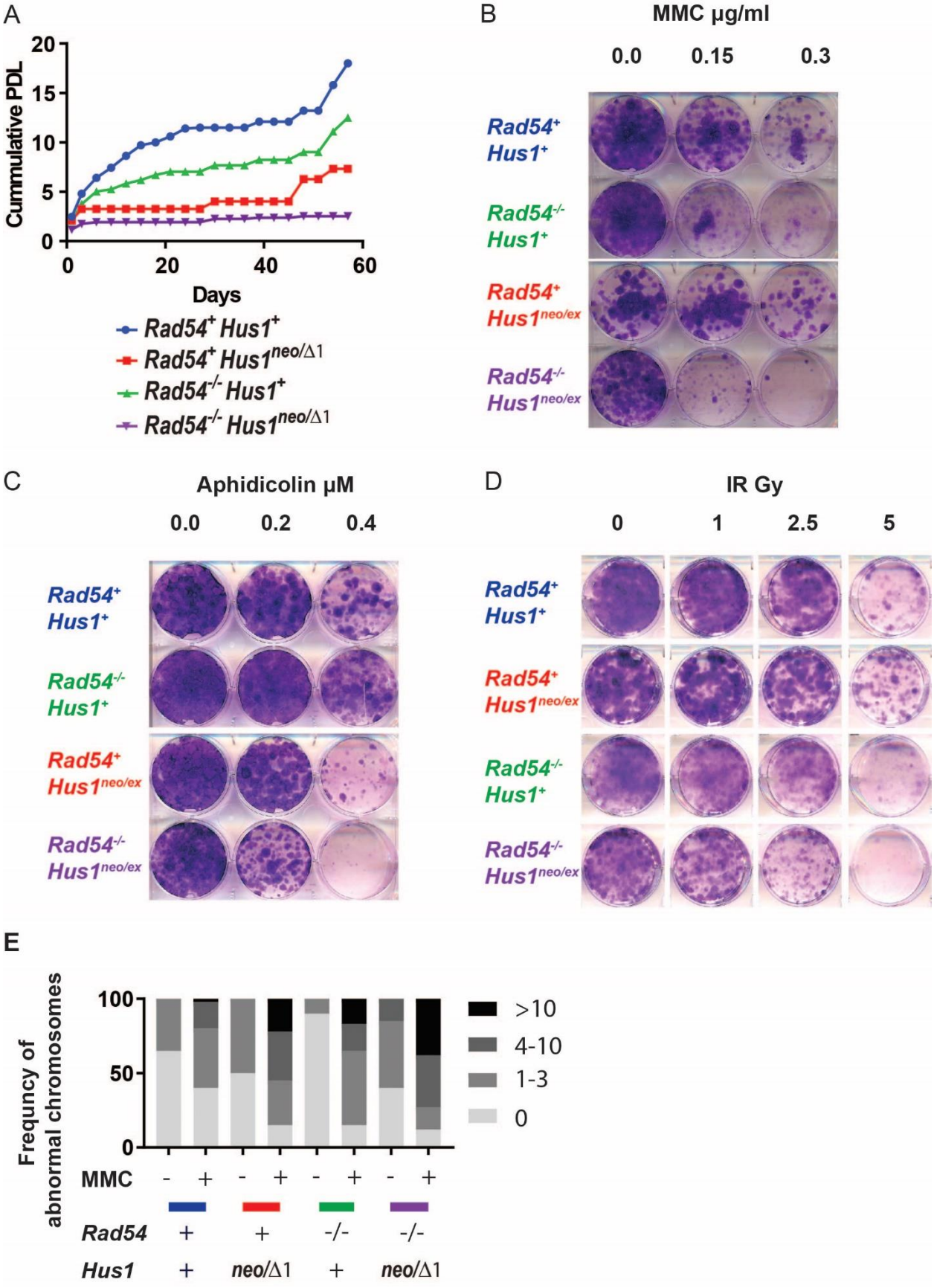
A
Cummulative PDL
20
15
10
5
0
0
20
40
60
Days
Rad54+ Hus1+
Rad54+ Hus1neo/Δ1
Rad54-/- Hus1+
Rad54-/- Hus1neo/Δ1
B
MMC µg/ml
0.0
0.15
0.3
Rad54+ Hus1+
Rad54-/- Hus1+
Rad54+ Hus1neo/ex
Rad54-/- Hus1neo/ex
C
Aphidicolin µM
0.0
0.2
0.4
Rad54+ Hus1+
Rad54-/- Hus1+
Rad54+ Hus1neo/ex
Rad54-/- Hus1neo/ex
D
IR Gy
0
1
2.5
5
Rad54+ Hus1+
Rad54+ Hus1neo/ex
Rad54-/- Hus1+
Rad54-/- Hus1neo/ex
E
Frequncy of abnormal chromosomes
100
50
0
>10
4-10
1-3
0
MMC - + - + - + - +
Rad54 + + -/- -/-
Hus1 + neo/Δ1 + neo/Δ1

Table 2.1. Chromosomal aberrations are increased with simultaneous *Rad54* and *Hus1* impairment. Distribution of MMC-induced chromosomal aberrations. Forty metaphase spreads were randomly imaged and quantified for the number of breaks, fusions, acentric chromosomes, and radials in a manner blinded to genotype. Data shown are the average number of each type of damage per spread.

Genotype	Breaks	Fusions	Acentrics	Radials
Rad54^{+}*Hus1*$^{+}$	1.2	0.5	0.33	0.25
Rad54^{+}*Hus1*$^{neo\Delta 1}$	4.43	1.45	0.98	0.73
Rad54$^{-/-}$*Hus1*$^{+}$	1.98	1.3	0.85	0.7
Rad54$^{-/-}$*Hus1*$^{neo\Delta 1}$	5.6	3.8	0.75	2.25

2.3.1.3: Simultaneous impairment of *Rad54* and *Hus1* causes subfertility and meiotic defects

We aged the mice to 18 months to identify any age-related phenotypes associated with simultaneous impairment of *Rad54* and *Hus1*. However, through necropsy and analyses of histological sections, we did not observe any abnormalities specific to the *Rad54*$^{-/-}$*Hus1*$^{neo/\Delta 1}$ mice, except for smaller testes. We recorded testes weights for mice at 14-days, 4-weeks, 12-weeks and 18-months of age and found that at 12-weeks old, *Rad54*$^{-/-}$*Hus1*$^{neo/\Delta 1}$ mice already had significantly smaller testes (Figure 2.4A). In correlation, 12-week old *Rad54*$^{-/-}$ *Hus1*$^{neo/\Delta 1}$ mice have significantly lower sperm counts (Figure 2.4B). H&E sections of 12-week old *Rad54*$^{-/-}$*Hus1*$^{neo/\Delta 1}$ mice showed that most testicular tubules were smaller, had lost their cellularity and were filled with large vacuoles (Figure 2.4C). Many tubules also lacked mature spermatids in the lumen, and some had pyknotic nuclei or multinucleated cells. Finally, evaluation of the fertility of male *Rad54*$^{-/-}$*Hus1*$^{neo/\Delta 1}$ mice by mating them with wild-type female mice revealed that indeed simultaneous perturbation of *Rad54* and *Hus1* leads to subfertility (Table 2.2). This testicular phenotype suggests that double mutant *Rad54*$^{-/-}$*Hus1*$^{neo/\Delta 1}$ mice are unable to complete meiosis, which could be due to an inability to resolve the programmed DSBs generated by Spo11 and is reminiscent of phenotypes of other HR repair mutants.

Overall, the combined absence of *Rad54* and deficiency of *Hus1* led to a synergistic increase in genome instability and genotoxin hypersensitivity, including decreased body size, skeletal malformations, increased micronucleated red blood cells, increased sensitivity to MMC and IR *in vivo*, increased

chromosomal instability, increased sensitivity to MMC, IR, and aphidicolin *in vitro*, and meiotic impairment.

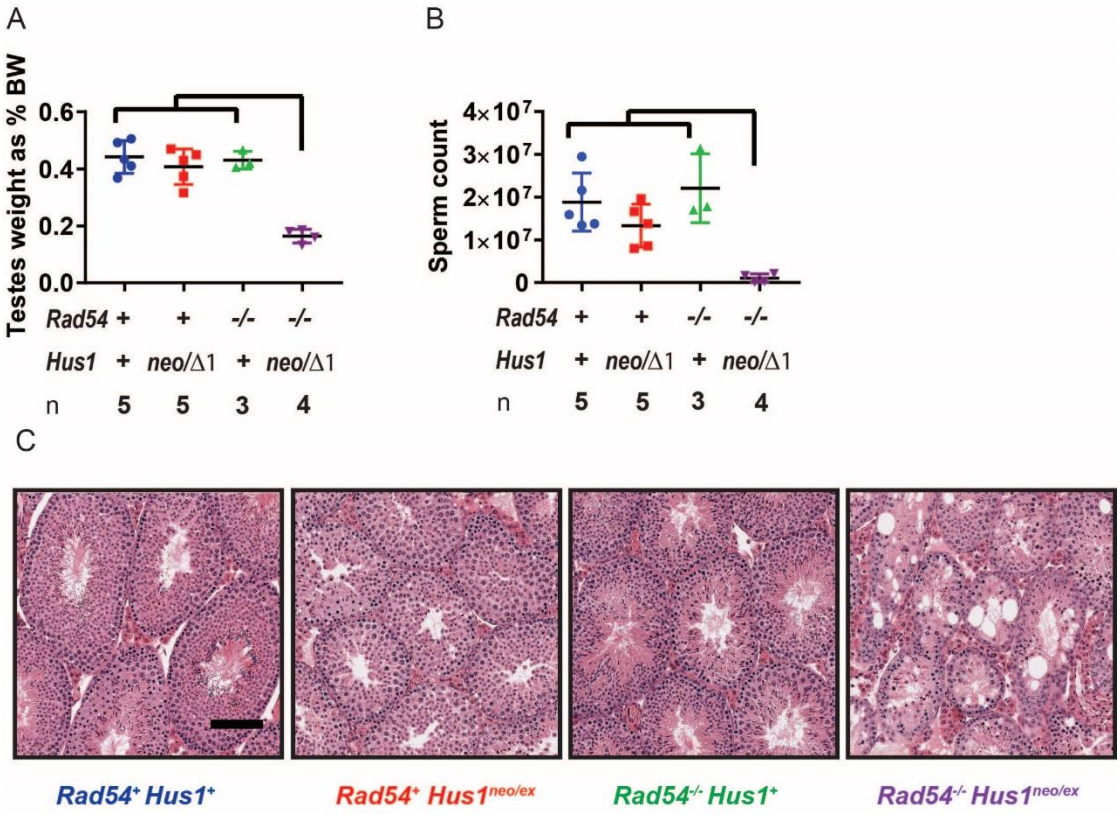

Figure 2.4: *Rad54* deficiency coupled with partial loss of *Hus1* leads to subfertility and testicular defects in male mice. A: Testes weight as percentage of body weight of 12 week old mice of the indicated genotypes. B: Averaged sperm count from the caudal epididymis of mice of the indicated genotypes at 12 weeks old. Data analysed via one way ANOVA with Tukey's method of p value adjustment for post-hoc pairwise comparisons. C: H&E sections of testis tubules showing decreased intraluminal mature sperm in *Rad54*$^{+}$*Hus1*$^{neo/\Delta 1}$ single mutant mice and double mutant *Rad54*$^{-/-}$*Hus1*$^{neo/\Delta 1}$ mice, as well as tubular degeneration in *Rad54*$^{-/-}$*Hus1*$^{neo/\Delta 1}$ mice. Scale bar is 100 micrometers. Error bars represent SEM.

Table 2.2 Simultaneous *Rad54* and *Hus1* impairment decreases fertility. Male mice of the four genotypes were mated with wildtype FVB female mice and the number of plugs, pregnancies and viable pups recorded.

Genotype	Matings	Copulatory plugs	Pregnancies	Viable pups
Rad54^{+}*Hus1*$^{+}$	13	13	12	103
Rad54^{+}*Hus1*$^{neo\Delta 1}$	4	4	3	15
Rad54$^{-/-}$*Hus1*$^{+}$	3	3	3	16
Rad54$^{-/-}$*Hus1*$^{neo\Delta 1}$	16	16	2	12

2.3.2: Combined loss of *Prkdc* and *Hus1* deficiency does not significantly increase spontaneous genomic instability and confers survival benefits post-genotoxin exposure *in vivo*

2.3.2.1: Combined loss of *Prkdc* and *Hus1* deficiency does not significantly increase spontaneous genomic instability and rescues early mortality in *Prkdc*$^{-/-}$ mice

In a complementary strategy, we combined *Hus1* deficiency with absence of the NHEJ component *Prkdc*. Evidence suggests that the 9-1-1 clamp contributes to high fidelity DSB repair, and we hypothesized that roles of the 9-1-1 complex in DSB repair might be further revealed in the absence of the somewhat dominant and competing NHEJ repair pathway. As *Hus1* deficiency is associated with increased chromosome breaks and decreased DSB repair efficiency, we also considered that *Hus1* deficient mice might have an increased reliance on NHEJ repair, and that combined mutation might lead to synthetic lethality. However, *Prkdc*$^{-/-}$*Hus1*$^{neo/\Delta 1}$ mice are viable and were born at the expected Mendelian ratio (Table 2.S1B). *Prkdc*$^{-/-}$*Hus1*$^{neo/\Delta 1}$ double mutant mice did not display a large weight difference from the already reduced weight of the *Prkdc*$^{-/-}$*Hus1*$^{+}$ single mutants (Figure 2.5A). *Prkdc*$^{-/-}$ *Hus1*$^{+}$ single mutant mice were significantly smaller than controls beginning at week 14 through week 40. The double mutant *Prkdc*$^{-/-}$*Hus1*$^{neo/\Delta 1}$ mice were significantly smaller than controls beginning at week 3 until week 40, but were only significantly smaller than *Prkdc*$^{-/-}$*Hus1*$^{+}$ single mutant mice from week 4-9.

The double mutant *Prkdc*$^{-/-}$*Hus1*$^{neo/\Delta 1}$ mice were significantly smaller than *Prkdc*$^{+}$*Hus1*$^{neo/\Delta 1}$ single mutant mice from week 18 through week 40. This indicates that the additional loss of *Prkdc* generally decreased growth rate compared to *Prkdc*$^{+}$*Hus1*$^{neo/\Delta 1}$ single mutant mice, but additional deficiency of *Hus1* did not generally decrease growth rate vs *Prkdc*$^{-/-}$*Hus1*$^{+}$ single mutant mice.

Prkdc$^{-/-}$*Hus1*$^{+}$ single mutant mice had a similar percentage of micronucleated erythrocytes as wildtype mice. As previously reported, *Prkdc*$^{+}$*Hus1*$^{neo/\Delta 1}$ single mutant mice had a significant increase relative to wildtype mice. *Prkdc* loss did not significantly increase the percent of micronucleated erythrocytes relative to *Hus1*-deficient *Prkdc*$^{+}$*Hus1*$^{neo/\Delta 1}$ single mutant mice, though there was a numerical increase in the double mutant (Figure 2.5B).

Unexpectedly, double mutant *Prkdc*$^{-/-}$*Hus1*$^{neo/\Delta 1}$ mice had increased survival in an aging study relative to *Prkdc*$^{-/-}$*Hus1*$^{+}$ single mutant mice, though the survival curves were not statistically different between these groups ($p = 0.035$; corrected p value for statistical significance: $p < 0.008$; Figure 2.5C). During a 300-day aging period, no wildtype or *Prkdc*$^{+}$*Hus1*$^{neo/\Delta 1}$ single mutant mice had mortality events. *Prkdc*$^{-/-}$*Hus1*$^{+}$ single mutant mice had significantly decreased survival relative to wildtype and *Prkdc*$^{+}$*Hus1*$^{neo/\Delta 1}$ single mutant mice. This is most likely attributable to the severe adaptive immune deficiency of mice lacking *Prkdc*. We hypothesized that the trend towards an increase in survival observed in the double mutant *Prkdc*$^{-/-}$*Hus1*$^{neo/\Delta 1}$ mice might be due to a partial rescue in their immune phenotype. To test this, we evaluated lymphocyte maturity in the four genotypic groups via flow cytometry. Contrary to our hypothesis, we did not see an increase in mature T cells from lymphoid tissue in the double mutant *Prkdc*$^{-/-}$*Hus1*$^{neo/\Delta 1}$ mice relative to the *Prkdc*$^{-/-}$*Hus1*$^{+}$ single mutant mice (Figure 2.S2). We observed greater variability in T cell populations in both *Prkdc*$^{-/-}$*Hus1*$^{+}$ and *Prkdc*$^{-/-}$*Hus1*$^{neo/\Delta 1}$ mice, which we predict is due to the known "leakiness" of SCID mice (362, 363). Though the mechanism is unclear, this trend towards a survival benefit in the double mutant *Prkdc*$^{-/-}$*Hus1*$^{neo/\Delta 1}$ mice indicates that deficiency of *Hus1* does not worsen fitness of mice already lacking *Prkdc*, similar to the trend observed in overall growth.

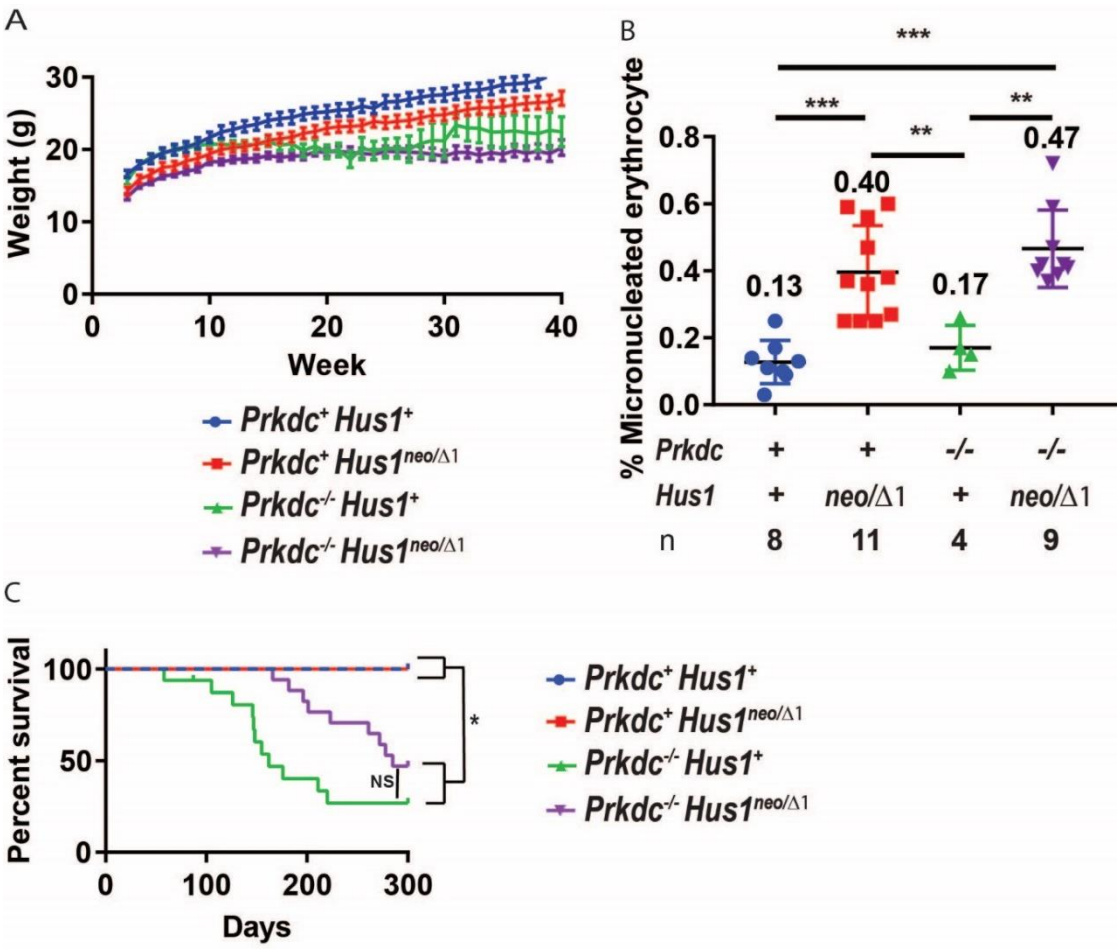

Figure 2.5: Combined loss of *Prkdc* and deficiency of *Hus1* does not worsen phenotypes associated with fitness and spontaneous genome stability already seen in either single mutation. A: Double mutant *Prkdc*$^{-/-}$*Hus1*$^{neo/\Delta1}$ mice had similar growth curves as *Prkdc*$^{-/-}$*Hus1*$^{+}$ single mutant mice. Similar trends were observed for both sexes; therefore, data is shown as sexes combined. One way ANOVA was performed with each set of weekly weights using Kenward-Roger approximation of degrees of freedom and post-hoc adjustments using Tukey's method. B: The percentage of micronucleated circulating erythrocytes was measured via flow cytometry as a proxy of *in vivo* spontaneous genomic instability. As expected, *Prkdc*$^{+}$*Hus1*$^{neo/\Delta1}$ mice had increased micronucleated erythrocytes relative to wildtype and *Prkdc*$^{-/-}$*Hus1*$^{+}$ mice. Double mutant *Prkdc*$^{-/-}$*Hus1*$^{neo/\Delta1}$ mice had a non-significant numerical increase in micronucleated erythrocytes relative to *Prkdc*$^{+}$*Hus1*$^{neo/\Delta1}$ mice. One way ANOVA with Tukey's method of p value adjustment for post-hoc pairwise comparisons. ** $p < 0.01$; *** $p < 0.001$. C: Kaplan-Meir

survival curve of a 300 day aging study showing decreased survival in *Prkdc*$^{-/-}$*Hus1*$^{+}$ mice and a non-significant trend towards improved survival in the double mutant *Prkdc*$^{+}$*Hus1*$^{neo/\Delta 1}$ mice vs mice lacking *Prkdc* alone (Log rank test, $p = 0.035$; Bonferroni corrected p value for statistical significance: $p < 0.008$).

Unlike the testicular degeneration and decreased sperm count observed in the combined *Rad54*$^{-/-}$ *Hus1*$^{neo/\Delta 1}$ mice, the double mutant *Prkdc*$^{-/-}$*Hus1*$^{neo/\Delta 1}$ mice did not differ in testes weight as a percentage of body weight or sperm count relative to any other genotypic group (Figure 2.S3). Overall, these data indicate that the combined absence of *Prkdc* and deficiency of *Hus1* does not worsen phenotypes related to spontaneous genome stability or fitness relative to deficiencies already present in either single mutant.

2.3.2.2: Combined loss of *Prkdc* and *Hus1* deficiency partially rescues the MMC sensitivity of *Hus1* deficient mice and the IR sensitivity of *Prkdc*$^{-/-}$ mice

As mentioned previously, *Hus1*$^{neo/\Delta 1}$ mice are sensitive to MMC at 4mg/kg but not to IR (154) and *Prkdc* null mice are hypersensitive to IR (350). To determine the impact of combined *Prkdc* loss and *Hus1* impairment on the genotoxin sensitivity associated with the single mutations, we treated mice with 4 mg/kg MMC or 2.25 Gray IR. As expected, wildtype and *Prkdc*$^{-/-}$*Hus1*$^{+}$ single mutant mice were not sensitive to 4 mg/kg MMC (Figure 2.6A,B), while the *Prkdc*$^{+}$*Hus1*$^{neo/\Delta 1}$ mice had significantly greater weight loss that wildtype mice from days five through ten, and two out of ten *Prkdc*$^{+}$*Hus1*$^{neo/\Delta 1}$ single mutant mice met the 20% body weight loss endpoint criteria. Interestingly, none of the eight double mutant *Prkdc*$^{-/-}$*Hus1*$^{neo/\Delta 1}$ mice met endpoint and the percent weight loss of the double mutant mice was never statistically different from the single mutant *Prkdc*$^{+}$*Hus1*$^{neo/\Delta 1}$ mice, though the double mutants had significantly greater weight loss than control mice beginning on day two. None of the pairwise comparisons of survival curves between the four genotypic groups revealed statistically significant differences. These data suggest that additional loss of *Prkdc* does not significantly increase hypersensitivity to MMC in a *Hus1*-deficient background.

Upon treatment with the relatively low dose of 2.25 Gray IR, the *Prkdc*$^{-/-}$*Hus1*$^{+}$ single mutant mice had significantly greater weight loss than both wildtype and *Prkdc*$^{+}$*Hus1*$^{neo/\Delta 1}$ mice from days two

through fourteen and seven of the twenty-eight *Prkdc*$^{-/-}$*Hus1*$^{+}$ mice (25%) met endpoint criteria, though none of the pairwise comparisons of survival curves between the four genotypic groups revealed statistically significant differences (Figure 2.6C,D). Notably, the percent weight loss of the double mutant *Prkdc*$^{-/-}$*Hus1*$^{neo/\Delta 1}$ mice was never statistically different from that of single mutant *Prkdc*$^{-/-}$*Hus1*$^{+}$ mice. Only one of the nine double mutant mice met endpoint criteria, though as with the *Prkdc*$^{-/-}$*Hus1*$^{+}$ mice, the double mutant mice lost significantly more weight than control mice from days two through fourteen. Together, the *in vivo* genotoxin studies indicate that reduction in NHEJ efficiency does not increase MMC hypersensitivity in *Hus1* deficient mice, and that *Hus1* deficiency does not increase hypersensitivity to IR observed in the absence of *Prkdc*. This is in contrast to the synergistic increase in genomic instability sometimes observed when two DDR mutations are combined, and could suggest that *Hus1* and *Prkdc* function in competing pathways.

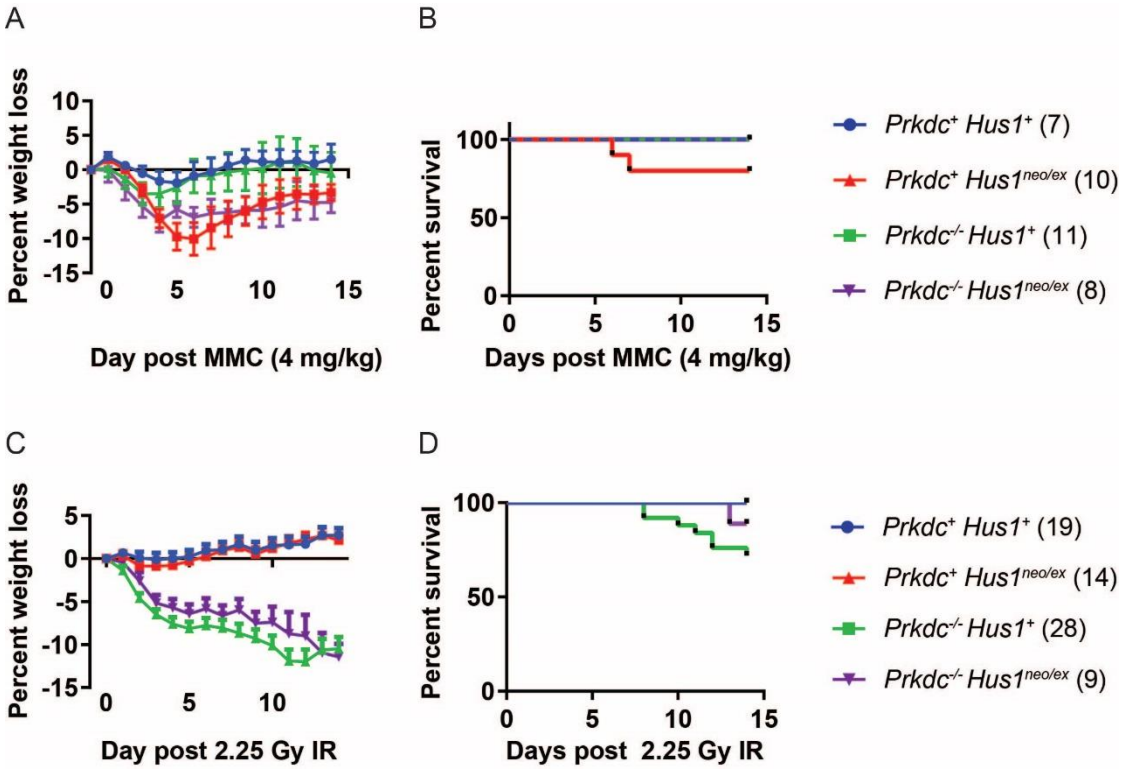

Figure 2.6: Combined absence of *Prkdc* does not worsen MMC-sensitivity associated with *Hus1* deficiency and combined deficiency of *Hus1* does not worsen IR sensitivity associated with absence of *Prkdc*. A,C: Averaged percent weight loss for mice of the indicated genotypes after 4 mg/kg MMC and 2.25 Gy whole body IR. B,D: Kaplan-Meier survival curves for mice of the indicated genotypes after 4 mg/kg MMC and 2.25 Gy whole body IR treatment, respectively. Log-rank tests with p value adjustment via the Bonferroni method was used for pairwise comparisons. None of the pairwise comparisons of survival curves between the four genotypic groups revealed statistically significant differences for either genotoxin. After MMC, $Prkdc^{+}Hus1^{neo/\Delta 1}$ mice had significantly greater weight loss that wildtype mice from days five through ten, and two out of ten $Prkdc^{-/-}Hus1^{+}$ single mutant mice met the 20% body weight loss endpoint criteria. None of the eight double mutant $Prkdc^{-/-}Hus1^{neo/\Delta 1}$ mice met endpoint and the percent weight loss of the double mutant mice was never statistically different from the single mutant

Prkdc^{+}*Hus1*$^{neo/\Delta 1}$ mice After IR, the *Prkdc*$^{-/-}$*Hus1*$^{+}$ single mutant mice had significantly greater weight loss than both wildtype and *Prkdc*$^{+}$*Hus1*$^{neo/\Delta 1}$ mice from days two through fourteen and seven of the twenty-eight *Prkdc*$^{-/-}$*Hus1*$^{+}$ mice met endpoint criteria. The percent weight loss of the double mutant *Prkdc*$^{-/-}$ *Hus1*$^{neo/\Delta 1}$ mice was never statistically different from that of single mutant *Prkdc*$^{-/-}$*Hus1*$^{+}$ mice.

We then tested the impact of combined *Hus1* deficiency and absence of *Prkdc* on genome stability and genotoxin sensitivity *in vitro*. We evaluated the proliferation dynamics of primary MEFs of the *Prkdc* and *Hus1* genotype combinations via a population doubling assay (Figure 2.7A). Wildtype and *Prkdc*$^{-/-}$*Hus1*$^{+}$ single mutant MEFs had similar proliferation kinetics, onset, and recovery from senescence. In contrast, *Prkdc*$^{+}$*Hus1*$^{neo/\Delta 1}$ single mutant MEFs had reduced proliferation kinetics and early senescence, as previously reported. Unlike the phenotype of double mutant *Rad54*$^{-/-}$*Hus1*$^{neo/\Delta 1}$ MEFs, which had the most impaired cumulative population doubling, the double mutant *Prkdc*$^{-/-}$*Hus1*$^{neo/\Delta 1}$ MEFs had a population doubling curve very similar to *Prkdc*$^{+}$*Hus1*$^{neo/\Delta 1}$ single mutant MEFs.

We evaluated genotoxin sensitivity in immortalized MEFs via a colony formation assay. Interestingly, the impact of the double *Prkdc*/*Hus1* deficiency varied based on genotoxin. As expected, wildtype and single mutant *Prkdc*$^{-/-}$*Hus1*$^{+}$ MEFs were not very sensitivity to MMC or aphidicolin, while *Prkdc*$^{+}$*Hus1*$^{neo/\Delta 1}$ MEFs were. The double mutant *Prkdc*$^{-/-}$*Hus1*$^{neo/\Delta 1}$ MEFs had increased sensitivity to MMC relative to the *Prkdc*$^{+}$*Hus1*$^{neo/\Delta 1}$ single mutant MEFs (Figure 2.7B), which was different than the partial rescue in MMC sensitivity seen in double mutant mice. In contrast, after aphidicolin exposure, the double mutant *Prkdc*$^{-/-}$*Hus1*$^{neo/\Delta 1}$ MEFs were less sensitive than *Prkdc*$^{+}$*Hus1*$^{neo/\Delta 1}$ single mutant MEFs (Figure 2.7C). As expected, wildtype and *Prkdc*$^{+}$*Hus1*$^{neo/\Delta 1}$ MEFs displayed a less dramatic reduction in colony formation than *Prkdc*$^{-/-}$*Hus1*$^{+}$ MEFs after IR. Double mutant *Prkdc*$^{-/-}$*Hus1*$^{neo/\Delta 1}$ MEFs demonstrated a greater reduction in colony forming ability after IR relative to *Prkdc*$^{-/-}$*Hus1*$^{+}$ MEFs (Figure 2.7D), which was again different than the partial rescue of IR sensitivity observed in *Prkdc*$^{-/-}$*Hus1*$^{+}$ mice.

As mentioned previously, increased chromosome breaks and radial formation are characteristic of *Hus1* deficient MEFs and thought to arise from faulty DSB repair. We questioned if inappropriate NHEJ

might be contributing to increased radial formation in the absence of *Hus1*. Evaluation of spontaneous and MMC-induced metaphase chromosome damage revealed the expected increase in damage in *Prkdc*$^{+}$*Hus1*$^{neo/\Delta 1}$ MEFs. *Prkdc*$^{-/-}$*Hus1*$^{+}$ single mutant MEFs had fewer breaks and radials than wildtype MEFs upon MMC treatment, which may indicate NHEJ contributes to chromosomal abnormalities even in WT cells treated with MMC. Double mutant *Prkdc*$^{-/-}$*Hus1*$^{neo/\Delta 1}$ MEFs had an increase in the average number of aberrant chromosomes per spread and the average number of radials relative to the *Prkdc*$^{+}$*Hus1*$^{neo/\Delta 1}$ single mutant MEFs (Figure 2.7E and Table 2.3) though the trend towards an increase in total aberrations, radials and breaks was not statistically significant between the *Prkdc*$^{+}$*Hus1*$^{neo/\Delta 1}$ single mutant and the double mutant *Prkdc*$^{-/-}$*Hus1*$^{neo/\Delta 1}$ MEFs. This indicates that radial formation in *Hus1* deficient cells is not dependent on NHEJ.

Figure 2.7: Partial loss of *Hus1* in combination with *Prkdc* deficiency leads to a synergistic reduction in the colony forming ability of mouse embryonic fibroblasts (MEFs) after MMC, but a partial rescue after aphidicolin, and increased genotoxin-induced chromosomal damage *in vitro*. A: Primary mouse embryonic fibroblasts (MEFs) were generated and analysed for proliferation kinetics via a population doubling (PDL) assay. Absence of *Prkdc* did not significantly alter proliferation relative to widltype MEFs, while deficiency of *Hus1* resulted in a decrease in cumulative PDL. The combined loss of *Prkdc* and deficiency of *Hus1* in MEFs did not result in a further decline in population doubling relative to $Prkdc^{+}Hus1^{neo/\Delta 1}$ single mutant MEFs. B: After exposure to MMC, $Prkdc^{+}Hus1^{neo/\Delta 1}$ single mutant MEFs demonstrated decreased colony formation as expected. Double mutant $Prkdc^{-/-}Hus1^{neo/\Delta 1}$ MEFs showed an even greater reduction in colony formation. C: As expected after exposure to aphidicolin, $Prkdc^{+}Hus1^{neo/\Delta 1}$ single mutant MEFs demonstrated decreased colony formation, however, double mutant $prkdc^{-/-}Hus1^{neo/\Delta 1}$ MEFs were more resistant to aphidicolin treatment. D: Double mutant $Prkdc^{-/-}Hus1^{neo/\Delta 1}$ MEFs demonstrated a hypersensitization to the colony reducing impact of IR exposure. E: Metaphase chromosome analyses after MMC exposure demonstrated increased spontaneous and MMC-induced chromosome damage in $Prkdc^{+}Hus1^{neo/\Delta 1}$ single mutant MEFs, and increased MMC-induced chromosome damage in $Prkdc^{-/-}Hus1^{+}$ MEFs relative to wildtype MEFs. Double mutant $Prkdc^{-/-}Hus1^{neo/\Delta 1}$ MEFs had both increased spontaneous and MMC-induced chromosome damage relative to either single mutants.

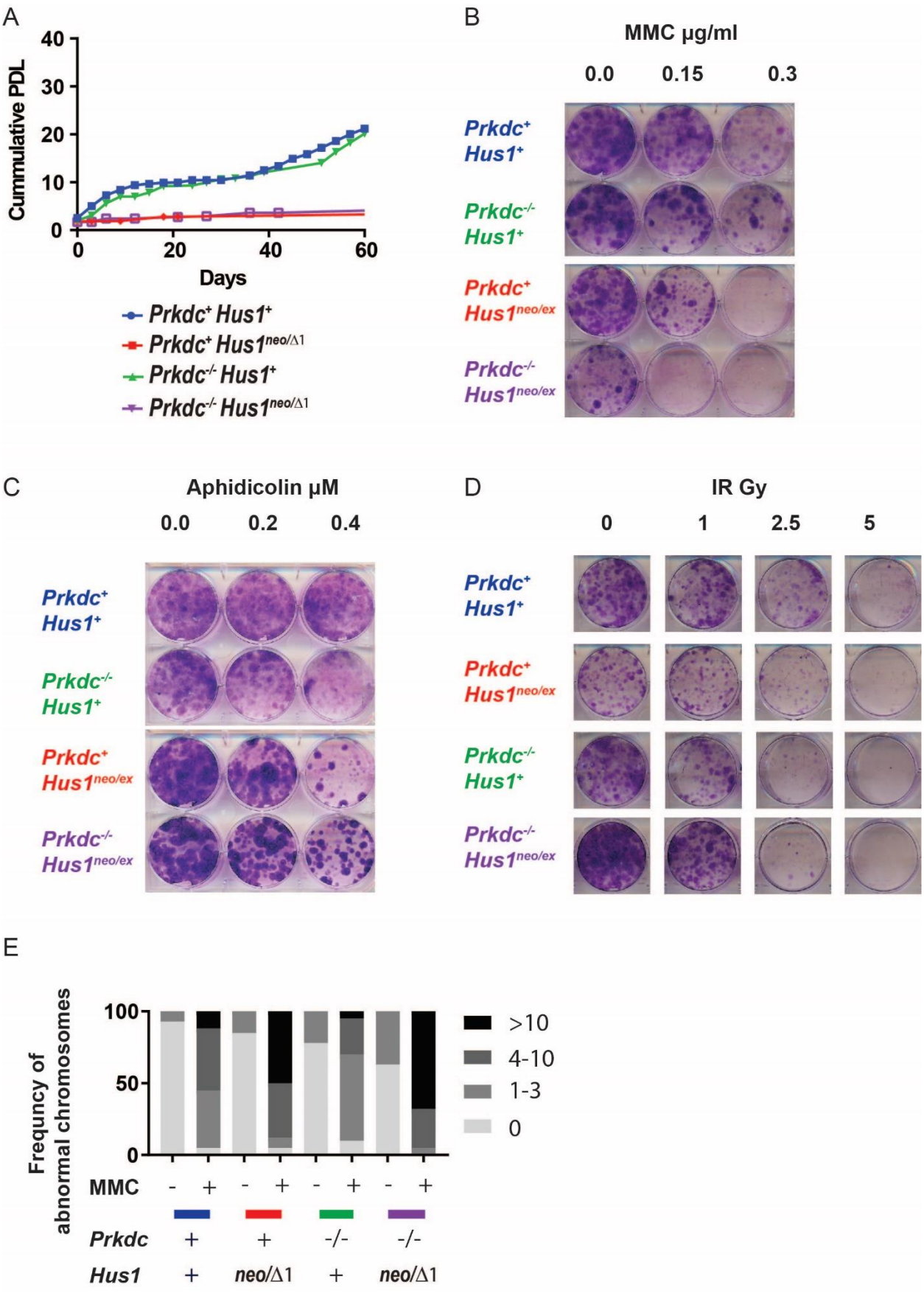
A
Cummulative PDL
40
30
20
10
0
0
20
40
60
Days
Prkdc+ Hus1+
Prkdc+ Hus1neo/Δ1
Prkdc-/- Hus1+
Prkdc-/- Hus1neo/Δ1
B
MMC µg/ml
0.0
0.15
0.3
Prkdc+ Hus1+
Prkdc-/- Hus1+
Prkdc+ Hus1neo/ex
Prkdc-/- Hus1neo/ex
C
Aphidicolin µM
0.0
0.2
0.4
Prkdc+ Hus1+
Prkdc-/- Hus1+
Prkdc+ Hus1neo/ex
Prkdc-/- Hus1neo/ex
D
IR Gy
0
1
2.5
5
Prkdc+ Hus1+
Prkdc+ Hus1neo/ex
Prkdc-/- Hus1+
Prkdc-/- Hus1neo/ex
E
Frequncy of abnormal chromosomes
100
50
0
>10
4-10
1-3
0
MMC - + - + - + - +
Prkdc + + -/- -/-
Hus1 + neo/Δ1 + neo/Δ1

Table 2.3 Combined loss of *Prkdc* and *Hus1* deficiency increases the frequency of chromosomal aberrations. Distribution of MMC-induced chromosomal aberrations. Forty metaphase spreads were randomly imaged and quantified for the number of breaks, fusions, acentric chromosomes, and radials in a manner blinded to genotype. Data shown are the average number of each type of damage per spread.

Genotype	Breaks	Fusions	Acentrics	Radials
$Prkdc^{+}Hus1^{+}$	2.95	0.425	0.225	2.4
$Prkdc^{+}Hus1^{neo\Delta 1}$	4.9	0.525	0.375	2.55
$Prkdc^{-/-}Hus1^{+}$	1.7	0.575	0.175	0.6
$Prkdc^{-/-}Hus1^{neo\Delta 1}$	6.1	0.725	0.575	3.775

2.4: Discussion

In this work, we characterized two distinct outcomes of combining either a background deficient in HR or NHEJ with *Hus1* deficiency. When *Hus1* deficiency was combined with the HR deficient *Rad54* null genotype, double mutant mice showed no decrease in viability, but did have worsening of phenotypes associated with overall fitness, genome stability, and genotoxin hypersensitivity *in vivo* and *in vitro*. The synergistic decrease in body size and skeletal abnormalities observed in $Rad54^{-/-}Hus1^{neo/\Delta 1}$ mice are reminiscent of those observed when *Hus1* deficiency was combined with absence of the DDR kinase ATM (364). Decreased body size is reported in multiple human and murine models of genomic instability, and may arise from increased DNA damage, potentially leading to loss or failure of expansion of certain cell populations, which is proposed to occur in *Atm*-null mice (365-367). Decreased body size associated with other genomic instability syndromes may arise from altered systemic growth signals, such as in mouse models of Cockayne syndrome (368). Vertebral segmentation defects, such as those we observed in the tails of $Rad54^{-/-}Hus1^{neo/\Delta 1}$ mice, have been reported in other genome instability syndromes, such as adrenocortical dysplasia and caudal regression syndrome, and may arise from p53-dependent apoptosis of somatic cells (369). Craniofacial and appendicular abnormalities are also common in genomic instability syndromes, such as Seckel syndrome, Nijmegen breakage syndrome, and Fanconi Anemia (370-373).

Conditional inactivation of *Hus1* in testes in neonatal mice results in meiotic defects and germ cell loss that severely decrease fertility (173). Interestingly, we show that partial loss of *Hus1* in combination with loss of *Rad54* leads to similar testicular defects. This suggests that in the context of decreased HR efficiency, HUS1 level modulates the efficiency of HRR repair. The synergistic effect of the combined *Hus1* and *Rad54* mutations suggests that both genes are important for high fidelity DSB repair, fitting with a model in which both genes support or promote HR, leaving double mutants with reduced ability to maintain genome integrity.

In contrast, *Hus1* deficiency combined with absence of the NHEJ component *Prkdc* resulted in either no significant worsening of phenotypes associated with fitness or genome stability relative to signal mutants, or a partial rescue relative to single mutants. Double mutant $Prkdc^{-/-}Hus1^{neo/\Delta 1}$ mice were not significantly smaller, did not have a significant increase in micronucleated red blood cells, outlived $Prkdc^{-/-}Hus1^{+}$ single mutant mice, and had a partial rescue in sensitivity to both MMC and IR. This suggests that in the context of *Hus1* deficiency, inhibition of NHEJ provides a genome stability benefit. One explanation for this observation is that *Hus1* and the 9-1-1 clamp play a role in suppressing inappropriate or detrimental NHEJ in certain contexts, such as during replication stress. The 9-1-1 clamp interacts with DNA end-processing proteins, as well as numerous DNA repair proteins, and thus may promote the formation of DNA ends that engage HR and limit NHEJ, and/or support recruitment of HR proteins.

Like the 9-1-1 clamp, FANCD2, a component of the Fanconia Anemia (FA) pathway, is known to interact with DNA end processing proteins, such as the Bloom and MRN complexes (374-377). The FA pathway functions in replication fork stability, and homologous recombination and translesion synthesis at DNA interstrand cross links. Similar to the partial rescue we observed in double mutant $Prkdc^{-/-}Hus1^{neo/\Delta 1}$ mice, inhibition of NHEJ has been reported to improve genome stability in response to MMC in FA deficient backgrounds (378). In a separate report, disruption of both FANCC and KU70 suppressed crosslinker sensitivity and chromosome breaks (379). However, the result of combining DDR mutations with FA mutations has varied among groups. Worsening of MMC sensitivity has been reported with combined *Fancd2* and either *53bp1* or *Ku80* mutations (380). Another report describes a failure to

rescue ICL-induced proliferation defects in FA cells by suppression of DNA-PKcs, DNA ligase IV or 53BP1, though 53BP1 partially suppressed FA cell chromosomal abnormalities (381).

Other reports have revealed an improvement in HR deficiency when NHEJ has been inhibited. The HR deficiency associated with loss of *Brca1* can be rescued by loss of *53BP1* (109-111, 380), and NHEJ disabling can improve the lethality of PARP inhibition in cells lacking BRCA2, BRCA1, or ATM (382). Rescue upon NHEJ inhibition in an HR-deficient background suggests that a significant role of these HR proteins is to promote HR and inhibit NHEJ, but also indicates that when NHEJ is non-functional, even cells lacking these HR components have an improvement in high fidelity DNA repair. This would suggest that HR may be able to proceed even in the absence of some of these components, if NHEJ can be repressed.

However, it is not universally observed that NHEJ inhibition provides a genome stability advantage in an HR deficient background. Previous reports of combining an HR-impaired *Rad54* null mouse model with NHEJ deficient mouse models (either *LigIV* or *KU80*) revealed a worsening of phenotypes related to genome stability (358, 383). This fits with the understanding that both HR and NHEJ contribute to the repair of DSBs generated by endogenous and exogenous sources, and, at least in certain contexts, one pathway may be able to compensate for the other.

An alternative hypothesis for the partial rescue seen in some phenotypes related to genome stability in our double mutant *Prkdc*$^{-/-}$*Hus1*$^{neo/\Delta 1}$ mice is that in the absence of NHEJ and deficiency of *Hus1*, alternative DNA repair pathways are disinhibited. Knockdown of the *Rad9* component of the 9-1-1 clamp has been reported to increase alternative end-joining efficiency in repair reporter plasmids (384). Potentially, in the absence of the somewhat dominant NHEJ pathway and with 9-1-1 deficiency, salvage or alternative repair pathways are de-repressed, leading to a partial rescue in genome stability.

Though we observed a partial rescue in genotoxin sensitivity in the double mutant *Prkdc*$^{-/-}$ *Hus1*$^{neo/\Delta 1}$ mice, the double mutant *Prkdc*$^{-/-}$*Hus1*$^{neo/\Delta 1}$ MEFs showed increased sensitivity to MMC and IR, and reduced sensitivity to aphidicolin. The different behavior between the *in vivo* and *in vitro* phenotypes may reflect a differing reliance on select DNA repair pathways among different tissues. The *in vivo* sensitivity to these genotoxins is largely determined by toxicity to the highly proliferative cells of the

intestinal tract and bone marrow, whereas our *in vivo* assays characterized sensitivity in fibroblasts. Additionally, the different sensitivity to MMC vs aphidicolin in the double mutant *Prkdc*$^{-/-}$*Hus1*$^{neo/\Delta 1}$ MEFs may arise from a difference in the roles the 9-1-1 complex plays at specific types of DNA damage (crosslink repair vs replication stress).

The synergistic deleterious effects observed when we combined *Hus1* deficiency and loss of *Rad54* contribute to the evidence that the 9-1-1 clamp is important for promoting high fidelity DSB repair through HR. The partial rescue in genome stability observed when *Prkdc* is absent in a *Hus1* deficient background suggests the 9-1-1 clamp contributes to inhibition of inappropriate NHEJ. Together, our results support that *Hus1* and the 9-1-1 clamp play a role in DSB repair pathway selection.

2.5: Materials and methods

Mouse husbandry and strains: The Cornell University Institutional Animal Care and Use Committee approved all animal procedures and mice were cared for in compliance with the Guide for the Care and Use of Laboratory Animals. Mice were housed under specific pathogen-free conditions in an Association for the Assessment and Accreditation of Laboratory Animal Care International accredited facility. Mice were on a 12:12 light:dark cycle in individually ventilated cages (Mouse Cage PC7115HT, Allentown, Inc., Allentown, NJ) containing ¼ inch autoclaved corn cob bedding (7097A, Harlan Teklad, Frederick, MD), a cardboard hut (Refuge XKA-2450-087, Ketchum Manufacturing Inc, Brockville, Ontario), and a sterile nesting pad (Nestlets, Ancare, Bellmore, NY). Mice received irradiated food (7012 Harlan Teklad LM-485) and reverse osmosis, hyper-acidified water *ad libitum*.

Rad54/Hus1: *Rad54*$^{+/-}$ C57BL/6 mice (353) (provided by Dr. R. Kanaar, Erasmus University Rotterdam) were backcrossed with wildtype 129S6 mouse up to ten generations to unify the genetic background of our *Hus1* hypomorphic mice (153). Then *Rad54*$^{+/-}$ 129 mice were crossed with *Hus1*$^{+/neo}$ and *Hus1*$^{+/\Delta 1}$ 129 mice individually to generate *Rad54*$^{+/-}$*Hus1*$^{+/neo}$ and *Rad54*$^{+/-}$*Hus1*$^{+/\Delta 1}$ mice. Finally, these two genotypes were mated to breed all wanted genotypic groups. *Rad54*$^{-/-}$*Hus1*$^{neo/\Delta 1}$ is designated as the double mutant experimental genotype, *Rad54*$^{-/-}$*Hus1*$^{+/+}$, *Rad54*$^{-/-}$*Hus1*$^{+/neo}$ and *Rad54*$^{-/-}$*Hus1*$^{+/\Delta 1}$ as the *Rad54* single

mutant controls (referred to as *Rad54*$^{-/-}$*Hus1*$^{+}$), *Rad54*$^{+/-}$*Hus1*$^{neo/\Delta 1}$ and *Rad54*$^{+/+}$*Hus1*$^{neo/\Delta 1}$ as the *Hus1* hypomorph controls (referred to as *Rad54*$^{+}$*Hus1* $^{neo/\Delta 1}$), and the rest as wildtype controls.

Prkdc/Hus1: *Prkdc* null mice 129S6 (349) were crossed with *Hus1*$^{+/neo}$ and *Hus1*$^{+/\Delta 1}$ 129S6 mice individually to generate *Prkdc*$^{+/-}$*Hus1*$^{+/neo}$ and *Prkdc*$^{+/-}$*Hus1*$^{+/\Delta 1}$ mice. Finally, these two genotypes were mated to breed all wanted genotypic groups. *Prkdc*$^{-/-}$*Hus1*$^{neo/\Delta 1}$ is designated as the double mutant experimental genotype, *Prkdc*$^{-/-}$*Hus1*$^{+/+}$, *Prkdc*$^{-/-}$*Hus1*$^{+/neo}$ and *Prkdc*$^{-/-}$*Hus1*$^{+/\Delta 1}$ as the *Prkdc* single mutant controls (referred to as *Prkdc*$^{-/-}$*Hus1*$^{+}$), *Prkdc*$^{+/-}$*Hus1*$^{neo/\Delta 1}$ and *Prkdc*$^{+/+}$*Hus1*$^{neo/\Delta 1}$ as the *Hus1* hypomorph controls (referred to as *Prkdc*$^{+}$*Hus1* $^{neo/\Delta 1}$), and the rest as wildtype controls.

The number of viable mice from each genotypic group was recorded and Mendelian ratios were calculated. Mice were weighed weekly. Cohorts were observed for any developmental abnormalities that might occur, including spontaneous tumor development, accelerated aging phenotypes, and diseases. For the *Rad54*/*Hus1* cross, adults of each genotype category were euthanized at 18 months and necropsied to identify any subtle pathological abnormalities. For the *Prkdc*/*Hus1* cross, mice were aged out to 300 days, after which remaining mice were necropsied. A twenty percent body weight loss and/or illness (decreased activity/responsiveness, hunched posture, piloerection, dehydration) were used as humane intervention points for euthanasia and generation of a Kaplan Meier survival curves.

Micronucleus assay: Micronucleus staining was performed as described in (153). Briefly, blood was collected from the facial vein of 6-8 week old female mice into heparin containing tubes and kept in methanol at -80ºC. Blood samples were then washed in ice cold bicarbonate buffer followed by incubation with CD71-FITC and RNAse A in bicarbonate buffer for 45 minutes at 4ºC. Samples were washed in cold bicarbonate buffer, pelleted and resuspended in PI-containing bicarbonate buffer for 10 minutes before flow cytometry analysis (BD LSR II). Gating was optimized using FITC only and PI only labeled samples from a wildtype mouse. Micronucleated normochromatic erythrocytes (evaluated in unchallenged mice) were defined as FITC^{-}PI^{+}, whereas micronucleated reticulocytes (evaluated post-irradiation) were defined as FITC^{+}PI^{+} (385).

In vivo genotoxin sensitivity: As previously described (154), mice (female mice for the *Rad54*/*Hus1* study and both sexes in the *Prkdc*/*Hus1* study) were aged to 6-8 weeks of age and injected

intraperitoneally with mitomycin C dissolved in DMSO at the indicated doses or subjected to whole body irradiation at the indicated doses from a ^{137}C source (JL Shepherd & Associates Mark I Model 68). The mice were monitored and weighed daily for 14 days or until reaching humane endpoint criteria defined as twenty percent body weight loss or morbidity (hunched posture, labored breathing, piloerection, dehydration).

Micro-CT scan: Eighteen month old mice were anesthetized with isofluorane. Micro-CT scans of the tail region were performed using a GE eXplore CT120 micro-CT scanner with a 50 mA current and 100kV voltage. Images were reconstructed at 50 μm^3 voxel dimensions. Scans were converted from the manufacturer's propriety format into DICOM format. 3D reconstruction videos were made using Osirix64 software.

Skeletal Staining: Skeletal staining was done as previously described with minimal alterations (364). Eighteen month old mice were euthanized, eviscerated, and fixed in 95% ethanol for two days. Samples were then stained in Alcian blue solution (Sigma #A3157; 150 µg/ml in 76% ethanol and 20% acetic acid) for one week. Samples were rinsed in fresh 95% ethanol for 24 hours, twice, followed by clearing in 1% KOH solution for six hours. Counterstaining was done in Alizarin red solution (50µg/ml in 1% KO) for 24 hours. Finally, samples were rinsed and kept in 1% KOH for 1-2 months until the desired clarity was reached. The samples were imaged submerged in a tank of water with direct bottom white light with a Canon EOS Rebel XS dSLR camera.

Fertility testing, epididymal sperm count and tests histology: The fertility of the *Rad54*$^{-/-}$*Hus1*$^{neo/\Delta 1}$ mice was evaluated by mating wildtype female mice and recording the number of litters and pups produced. Sperm count and testes histology was evaluated for both *Rad54*/*Hus1* and *Prkc*/*Hus1* cohorts. For sperm counts, both caudal epididymides from each mouse at 12 weeks of age were minced and incubated in 1 ml of 37ºC PBS for 20 min to allow sperm release. A 20 µl aliquot of the sperm-containing PBS was fixed in 480 µl of 10% phosphate buffered formalin (Fisher #SF100-4). Sperm were counted under an inverted microscope using a hemocytometer in triplicate and averaged per mouse. Left and right testes were weighed and averaged per mouse. One testis was fixed in Bouin's fixative (VWR # RC112032) and the other in 10% phosphate buffered formalin overnight, placed in 70% ethanol, then

processed for standard hematoxylin and eosin staining at the Cornell University Animal Health Diagnostic Center. Images of stained sections were obtained with Aperio ScanScope CS.

Lymphocyte analysis: Cervical lymph nodes, thymus, spleen, and femur bone marrow was obtained from *Prkdc*/*Hus1* cohort mice aged 8-16 weeks Spleen, thymus and lymph nodes were ground through a 70 µm nylon mesh filter using the plunger of a 10 ml syringe into RPMI medium and kept on ice. Femur bones were flushed with RMPI via 26 gauge needle and syringe. Filters were rinsed with the flow through an additional time. Cell density of the homogenates was determined. The lymphocyte suspensions were pelleted by centrifugation and resuspended in antibody mix (CD122, CD44, CD8alpha, iNKT, CD4, DX5, B220, γδ, PeCy7, TCPB). All antibodies were used at 1:200 dilution in PBS. FC block was added to all samples at 1:200. Single dye stains were used for compensation controls. FACS analysis was performed on an LSR II and analyzed with FACS DIVA software and FlowJo software.

Mouse embryonic fibroblast (MEF) preparation and immortalization: MEFs were prepared as described previously (153). Briefly, female mice were euthanized thirteen days after detection of a copulatory plug. The uterus was removed and embryos were exteriorized aseptically. Differentiated tissues (head and "red abdominal organs") were removed in a laminar flow hood and the remaining tissue was homogenized in sterile PBS by repeated pipetting. After larger tissue pieces settled, the supernatant was transferred to a 60 mm dish containing media (DMEM with 10% fetal bovine serum, 1% non-essential amino acids, 1% L-glutamine, 1% penicillin-streptomycin). The remaining tissue was used for genotyping. MEFs were allowed to grow for five days with media changes at 24 and 48 hours. On day five, cells were passaged and plated at 250,000 cells in a 60 mm dish for immortalization and 10^6 cells into a 10 cm dish for population doubling (see below; cells in the population doubling experiment were not immortalized). The following day (at roughly 70% confluency), MEFs were infected with retrovirus carrying pBP-LargeT construct (Addgene #14088) overnight with 0.1% polybrene in heat inactivated serum-containing media. Puromycin resistant MEFs were selected in DMEM with 10% bovine calf serum, 1% non-essential amino acids, 1% L-glutamine, 1% penicillin-streptomycin, and 1.25 µg/ml of puromycin.

Population doubling assay: Each MEF line was passaged into a 10 cm dish at 10^6 cells on day five after isolation in duplicate or triplicate. Every three days, cells from each individual dish were trypsinized, dishes of the same genotype were pooled and counted, then reseeded at 10^6 in duplicate or tiplicate until cells entered senescence, after which cells were fed but not passaged until spontaneous immortalization. Population doubling was calculated using the formula $PD = \log2(n_f/n_o)$ where n_o is the initial number of cells plated and n_f is the final number of cells counted at passaging.

Clonogenic survival assay: Cells were plated at low density (1,000-5,000 cells/ well) in six well dishes in triplicate. The following day cells were either left untreated, or irradiated at the indicated doses, treated with Aphidicolin at the indicated doses for 24 hours, or treated with MMC at the indicated does for 1 hour. The media was changed at the end of Aphidicolin/MMC treatment, and again on day 4. On day 7, the media was removed and cells were washed with PBS followed by methanol fixation for 10 minutes. Cells were then stained with either Crystal Violet overnight or Giemsa stain for 1 hour before washing with water. Plates were then scanned.

Metaphase spread/chromosome analysis: Spreads were prepared as previously described (153). Briefly, 24 hours after plating MEFs at 10^6 into a 10 cm dish in duplicate, plates were either left untreated or treated with 0.1 μM of aphidicolin or the indicated dose of mitomycin C (either 60 ng/ml or 42 ng/ml) for 24 hours. Cells were then arrested with 0.15 μg/ml of colcemid (Life Technologies #15210-040) for 1 hour. Cells were trypsinized and centrifuged at 1,500 rpm for 5 min. Cell pellets were resuspended in residual media and hypotonized in 75mM KCL for 6 – 11 min at 37ºC (optimized for individual cohorts of MEFs but consistent within cohorts) followed by the slow addition of 1 ml fixative (75% methanol and 25% acetic acid) while slowly vortexing. Cells were again pelleted and resuspended in 5 ml fresh fixative and incubated at least overnight at -20 ºC. After washing three times with fixative, cells were resuspended in 100-500 μl fixative based on pellet size and spotted onto charged microscope slides (Fisher #12-550-15). Slides were stained with Giemsa (1:50 in Gurr buffer) for 8 minutes, washed with nanopure water three times, and air dried overnight before coverslipping and bright field imaging. For each cell line, chromosomal breaks/gaps, fusions, radials, and acentrics were counted, as well as total aberrations, in 40 randomly selected spreads in a genotype-blinded manner.

Statistical analysis: Body weight gain or loss over time was analysed with a linear mixed effects model with fixed effects of weight, genotype, week, and genotype*week. A random mouse effect was added to control for repeated measures on mice. Fixed model effects were tested using F tests with Kenward Roger approximation of degrees of freedom. Post-hoc tests were performed using Tukey's method. The percentage of erythrocytes containing micronuclei was analysed by a one way ANOVA with Tukey's method used for pair-wise post-hoc tests. Kaplan Meier survival curves were analysed by log rank tests with the p value adjusted using the Bonferroni method. For all comparisons indicated, $p < 0.05$ was considered significant unless a corrected p value was used.

2.6: Supplemental material

Table 2.S1 Double mutant *Rad54*$^{-/-}$*Hus1*$^{neo/\Delta1}$ mice and *Prkdc*$^{-/-}$*Hus1*$^{neo/\Delta1}$ mice were born at expected Mendelian ratios. Frequency of offspring from *Rad54*/*Hus1* (A) and *Prkdc*/*Hus1* (B) crosses. Mice were genotyped by PCR at three weeks of age. Expected values represent combined Mendelian ratios from crosses with different parental genotypes. The observed and expected genotype frequencies are not significantly different (chi squared test p value = 0.73 (A) and p value = 0.79 (B)).

A

Rad54	*Hus1*	Observed	Expected
+/+	+/+	16	12.00
	+/neo	54	50.38
	+/Δ1	17	12.00
	neo/ Δ1	51	50.38
+/-	+/+	21	24.00
	+/neo	101	100.74
	+/Δ1	22	24.00
	neo/ Δ1	95	100.75
-/-	+/+	6	12.00
	+/neo	53	50.38
	+/Δ1	13	12.00
	neo/ Δ1	50	50.38

B

Prkdc	*Hus1*	Observed	Expected
+/+	+/+	46	30
	+/neo	40	30
	+/Δ1	32	30
	neo/ Δ1	28	30
+/-	+/+	68	60
	+/neo	46	60
	+/Δ1	65	60
	neo/ Δ1	49	60
-/-	+/+	22	30
	+/neo	28	30
	+/Δ1	35	30
	neo/ Δ1	21	30

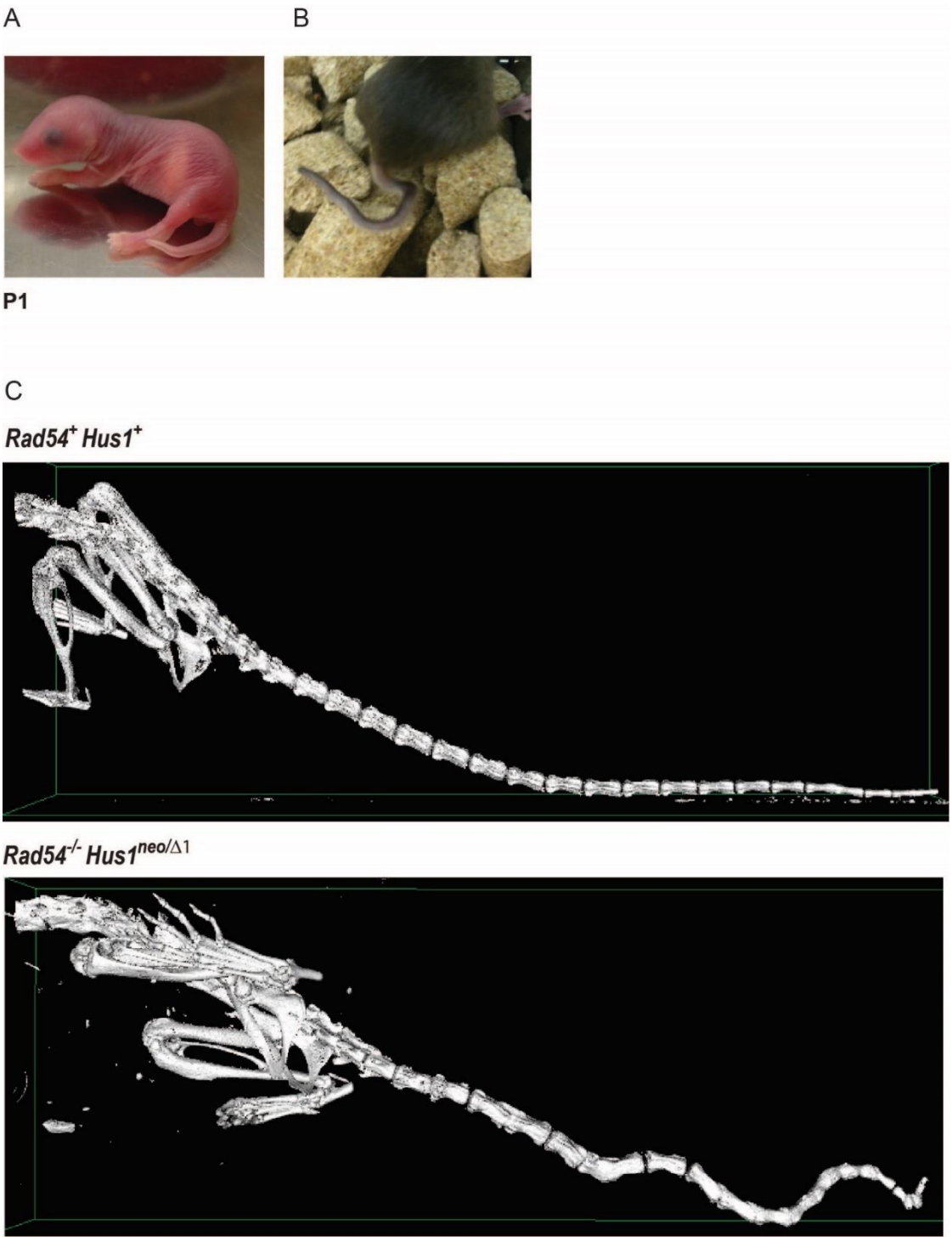

Figure 2.S1: Combined absence of *Rad54* and deficiency of *Hus1* increases the incidence of caudal vertebral anomalies. *Rad54*$^{-/-}$*Hus1*$^{neo/\Delta 1}$ mice had an increased incidence of caudal vertebral anomalies relative to control mice and *Rad54*$^{+}$*Hus1* $^{neo/\Delta 1}$ single mutants. A: One day old pup demonstrating that kinked tails were present from birth and continued into adulthood (B). C: Live CT scan of the pelvis and

tail of a wildtype mouse (top) in comparison with a *Rad54*$^{-/-}$*Hus1*$^{neo/\Delta1}$ mouse (bottom) that has abnormally fused caudal vertebrae.

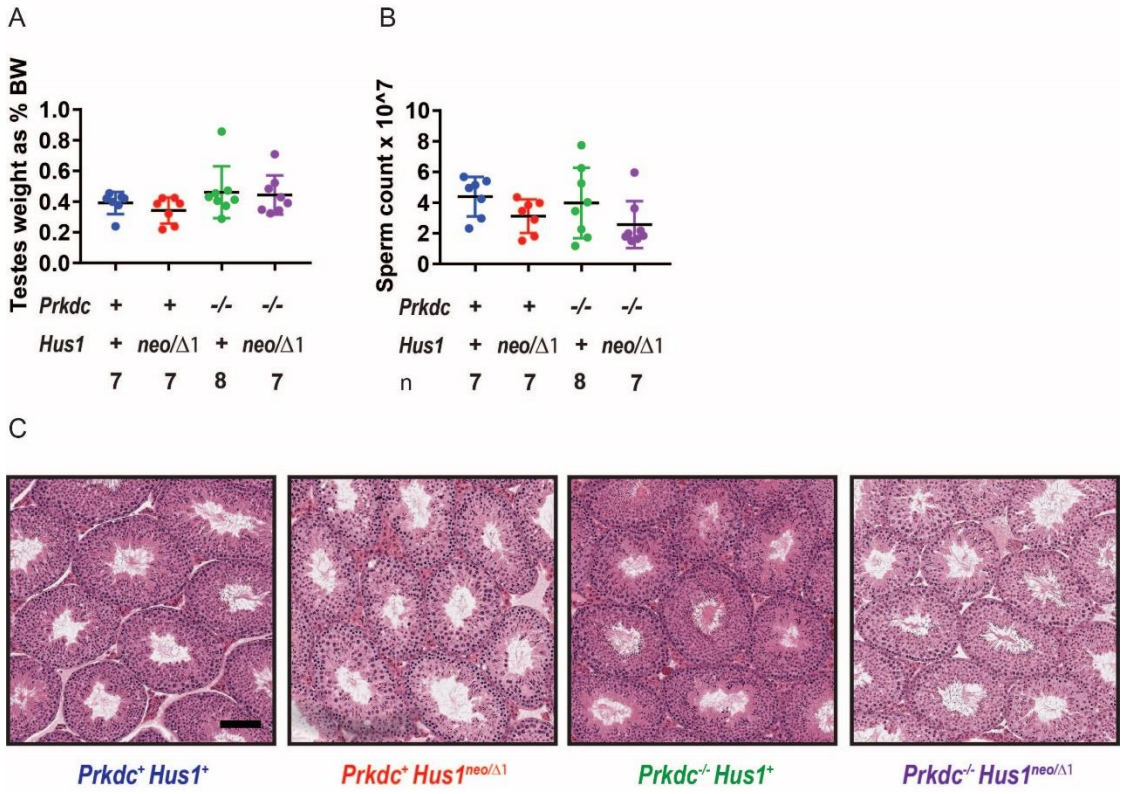

Figure 2.S2: ***Prkdc*** **deficiency coupled with partial loss of** ***Hus1*** **does not impact fertility in male mice.** A: Testes weight as percentage of body weight of 12 week old mice of the indicated genotypes. B: Averaged sperm count from the caudal epididymis of mice of the indicated genotypes at 12 weeks old. C:H&E sections of testis tubules showing similar mild changes in morphology in both *Prkd+*$^{-}$*Hus1*$^{neo/\Delta1}$ and *Prkdc*$^{-/-}$*Hus1*$^{neo/\Delta1}$ mice. Error bars represent SEM.

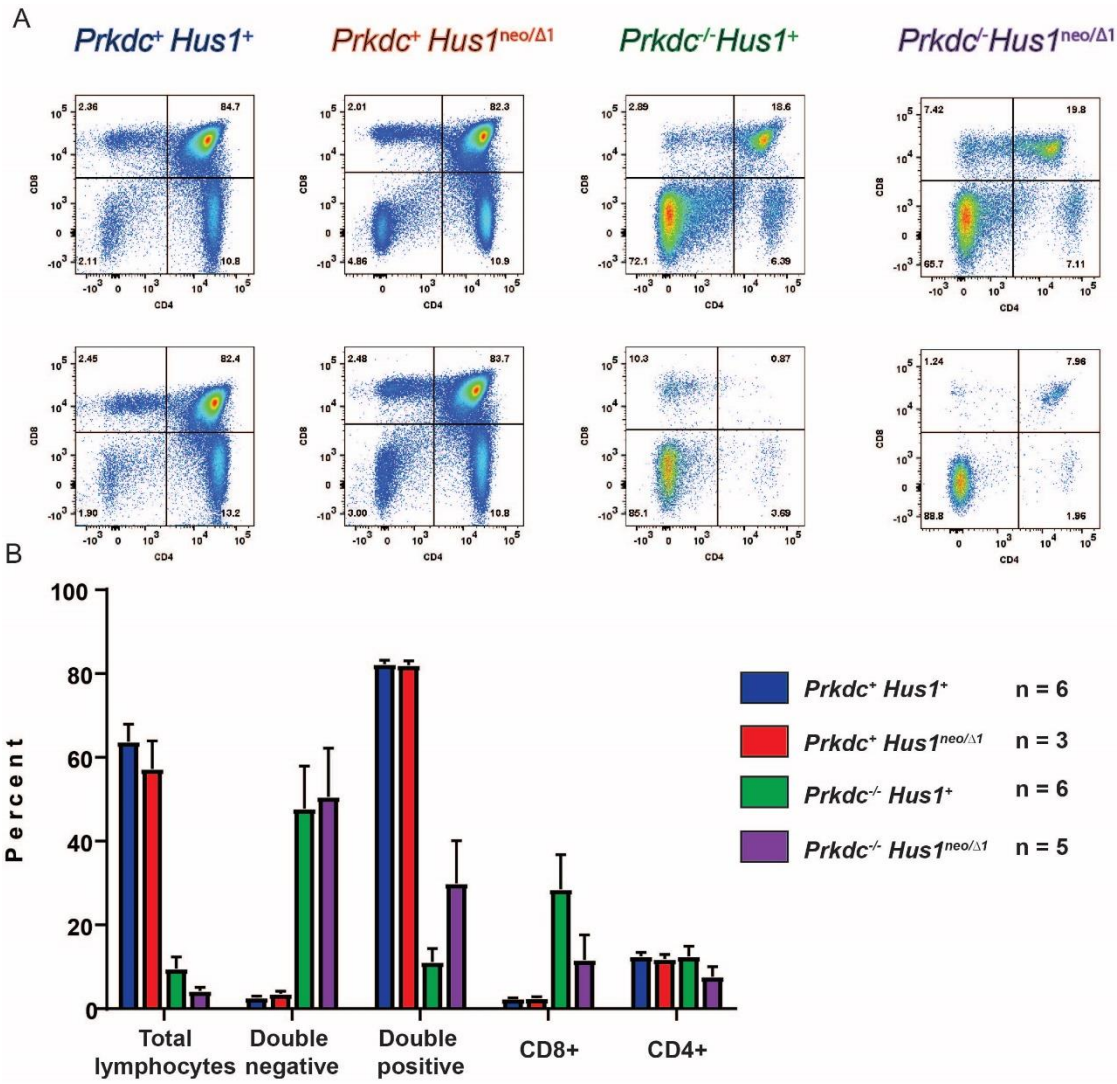

Figure 2.S3: Deficiency of *Hus1* combined with absence of *Prkdc* does not increase T cell maturation relative to loss of *Prkdc* alone. *Prkdc*$^{-/-}$ mice have drastically reduced mature lymphocytes due to failure of V(D)J recombination, which requires NHEJ. We tested if partial rescue of immunodeficiency might account for the improved longevity of double mutant *Prkdc*$^{-/-}$*Hus1*$^{neo/\Delta1}$ mice relative to the early mortality we observed in *Prkdc*$^{-/-}$*Hus*$^{+}$ mice. A: Representative images of CD4/CD8 staining of the indicated genotypes. Wildtype and *Prkdc*$^{+}$*Hus1*$^{neo/\Delta1}$ mice varied little in the relative proportions of double negative, double positive, and single positive cells, whereas *Prkdc*$^{-/-}$*Hus1*$^{+}$ and *Prkdc*$^{-/-}$*Hus1*$^{neo/\Delta1}$ mice varied more, as shown. B: Averaged percent of the indicated T cell populations by genotype. Error bars represent SEM.

CHAPTER 3

Altered hepatic lipid and bile acid metabolism following dietary challenge in *Fancd2*-deficient mice

by authors Elizabeth Moore, Erin Daugherity, David Karambizi, Bethany Cummings, Erica Behling-Kelly, Deanna Schaeffer, Teresa Southard, Joseph McFadden, Joseph W. McFadden, and Robert Weiss is currently in review at the *Journal of Biological Chemistry*.

E.M. conceived and conducted experiments and wrote the manuscript; E.D. contributed to conceptualization and conducted experiments; D.K. contributed to immunohistochemistry; B.C. contributed to conceptualization, supervision, data analysis, and resources; E.B.K. conducted serum lipoprotein analysis; D.S. scored hematology and bone marrow cytology; T.S. scored hepatic pathology; J.M. contributed to data analysis, supervision, resources, and writing; R.W. conceived and supervised the project

3.1: Abstract

Defects in the Fanconi anemia (FA) DNA damage response pathway, canonically known to respond to replication stress, result in genomic instability, developmental defects, hematopoietic failure, cancer predisposition, and metabolic disorders. The endogenous sources of damage contributing to FA phenotypes and the links between FA and metabolic disease remain poorly understood. We tested the hypothesis that the FA pathway protects against metabolic challenges using mice lacking *Fancd2*, a central FA pathway component. *Fancd2*$^{-/-}$ and wildtype (WT) mice were continued on standard diet (SD) or challenged with a diet enriched in fat, cholesterol, and cholic acid (Paigen Diet (PD)), or a diet enriched in lipid alone (Western diet (WD)). *Fancd2*$^{-/-}$ mice developed hepatobiliary disease and exhibited decreased survival when fed PD, but not WD. Male *Fancd2*$^{-/-}$ mice fed PD had significant biliary hyperplasia, increased serum bile acid concentration, and increased hepatic pathology. In contrast, female mice were similarly impacted by PD feeding regardless of *Fancd2* status. Male *Fancd2*$^{-/-}$ mice had

altered expression of genes encoding hepatic bile acid transporters and cholesterol and fatty acid metabolism genes, including, *Scp2/x*, *Abcg5/8*, *Abca1*, *Ldlr*, *Srebf1*, and *Scd-1* upon PD challenge. Untargeted lipidomic profiling in liver tissue revealed 132 lipid species, including sphingolipids, glycerophospholipids and glycerolipids, that differed significantly in abundance depending on *Fancd2* status. These data indicate the FA pathway has sex-specific impacts on hepatic lipid and bile acid metabolism, findings that expand the known cellular functions of the FA pathway and may provide mechanistic insight into the metabolic disease predisposition seen in FA patients.

3.2: Introduction:

Fanconi anemia (FA) is a human genetic disorder characterized by developmental defects, sterility, hematopoeitic failure, cancer predisposition, and metabolic disease. FA is caused by biallelic mutation of any of the 22 genes encoding components of the FA pathway. Canonically, the FA pathway responds to replicative stress, particularly to DNA interstrand crosslinks. FA deficient cells are hypersensitive to genotoxins, such as DNA crosslinking agents, irradiation, alkylating agents, and oxidative stress. Endocrine and metabolic abnormalities are also components of the FA phenotype (203, 205, 206). Close to 80% of FA patients have at least one endocrine abnormality (203). Dyslipidemia has been reported in 55% of FA patients (206) and impaired glucose tolerance in 27-68% of FA patients (203, 204, 206, 207). The endogenous agents contributing to DNA damage and the etiologic connection between FA deficiency and the development of metabolic disease remain incompletely characterized.

FA phenotypes may be the direct result of DNA damage arising from endogenous sources normally counteracted by the FA pathway's DNA repair functions. This is thought to be the mechanism underlying the hypersensitivity of FA deficient cells to aldehydes and formaldehyde byproducts generated as a result of cellular metabolism (386-388). Alternatively, the increased risk of metabolic disease might be attributable to a direct connection between the FA pathway and metabolic homeostasis. Cells have numerous mechanisms to coordinate a DNA damage response (DDR) with metabolic regulation, with several factors having dual roles. For instance, p53 regulates not only DNA repair, cell cycle arrest, and

apoptosis but also oxidative phosphorylation, glycolysis, and bile acid (BA) and fatty acid metabolism (389, 390). ATM, one of the major DDR kinases, coordinates cell cycle arrest and DNA repair, and regulates glucose metabolism by modulating CREB activity, coupling a response to genotoxic stress with metabolism (391).

Evidence for a direct connection between the FA pathway and metabolic homeostasis is accumulating. The FA pathway modulates cellular antioxidant defenses (306, 392). FA deficient cells have altered energy metabolism and increased reliance on glycolysis (333), and the FA pathway regulates energy metabolism via ATP synthesis (313). The FA pathway may also regulate lipid metabolism (reviewed in (393)). FA deficiency has been reported to impact the abundance of lipids, particularly glycosphingolipids, in squamous cell carcinomas, with functional relevance to cell invasion (341). FA deficiency has also been reported to alter Acetyl CoA metabolism, oxidative phosphorylation, fatty acid metabolism, and lipid droplet storage in FA cell lines and lymphoblasts (394). Abnormal production of glycerophospholipids by FA bone marrow mesenchymal stromal cells may contribute to altered hematopoietic cell physiology and bone marrow microenvironment in FA (343). Metabolomic profiling of modified breast cancer cells with reduced FANCC expression revealed altered fatty acid and sphingomyelin metabolites (395). FA mutations are common in bladder cancer, and metabolomics analysis showed distinct metabolite profiles, including differences in fatty acid metabolism between bladder cancer cell lines with an intact or impaired FA pathway (396). MicroRNAs that regulate cholesterol and lipid metabolism, miR-122 and miR-206, have decreased abundance in FA bone marrow mononuclear cells and lymphoblast cell lines (397). Thus regulation of cellular metabolism, including lipid metabolism, may be an important component of the tumor suppression roles of the FA pathway, and may relate to the metabolic phenotypes seen in FA patients.

We evaluated how FA deficiency alters the metabolic impacts of challenge with a high fat or a high fat/high cholesterol diet *in vivo*. The high fat WD is used in obesity and insulin resistance models, whereas the high fat diet with cholesterol and cholic acid (PD) induces steatohepatitis and hepatobiliary disease without obesity (398). We predicted that FA mutant mice would be hypersensitive to hepatic pathology upon challenge with these diets through either increased DNA damage, increased metabolic derangements,

or both. The damaging impacts of excessive lipid metabolism on hepatic physiology include oxidative stress, lipid peroxidation, mitochondrial damage, endoplasmic reticulum stress, cytokine imbalances, and inflammation, factors in non-alcoholic fatty liver disease and steatohepatitis (399). Our data indicate the FA pathway is essential for protection against hepatobiliary disease in the face of PD challenge and impacts hepatic lipid and BA homeostasis in male mice.

3.3: Results:

3.3.1 Male *Fancd2*$^{-/-}$ mice have increased susceptibility to hepatobiliary disease and hepatic damage when fed Paigen diet.

We aimed to test if deficiency for FANCD2, a central component of the FA pathway (256), would be associated with increased sensitivity to hepatic metabolic challenge by feeding mice a high fat, high cholesterol diet with cholic acid (PD), or a diet enriched in lipid alone with 60% kcal derived from fat (WD). PD feeding led to increased morbidity and mortality in *Fancd2*$^{-/-}$ mice compared to WT controls when PD was fed from weaning or beginning at six months of age (Figure 3.1A left and middle panels). No morbidity or mortality were observed in *Fancd2*$^{-/-}$ or WT mice fed WD (Figure 3.1A right panel) or fed SD. These data demonstrate that *Fancd2*$^{-/-}$ mice are hypersensitive to PD feeding, but not WD feeding.

High fat, high cholesterol diets enriched with cholic acid are lithogenic and cause severe hepatic pathology (400). At necropsy, PD-fed mice of both genotypes had significant hepatomegaly characterized by firm, pale livers with rounded margins, while SD fed mice of both genotypes had grossly normal livers (Figure 3.1B). Morbidity in both genotypes fed PD was consistent with liver failure and/or cholestasis. Icterus was an experimental end point, and choleliths and distended gall bladders were found at necropsy. Observed hepatobiliary phenotypes were sex-dependent. In male mice, serum BA concentration increased upon PD feeding in *Fancd2*$^{-/-}$ mice by roughly 9-fold more than in WT mice (Figure 3.1C), while in females, there was no genotype-dependent difference in serum BA concentration upon PD feeding (Figure 3.S1A). Additionally, male *Fancd2*$^{-/-}$ mice fed PD had hepatic biliary hyperplasia, with an

increase in bile duct profiles (Figure 3.1D). Female mice of both genotypes had a non-statistically significant trend towards increased bile ducts upon PD feeding (Figure 3.S1B). Biliary hyperplasia was not observed in either genotype fed WD (WT average 1.15 ± 0.09 ducts/triad; *Fancd2*$^{-/-}$ average 1.15 ± 0.074 ducts/triad on WD) or another DDR deficient mouse model (*Atm*$^{-/-}$) on a FVB/N background Figure 3.S1C) (401). These data indicate that the increased morbidity and mortality observed upon PD feeding in *Fancd2*$^{-/-}$ mice were associated with hepatobiliary disease consistent with biliary outflow obstruction.

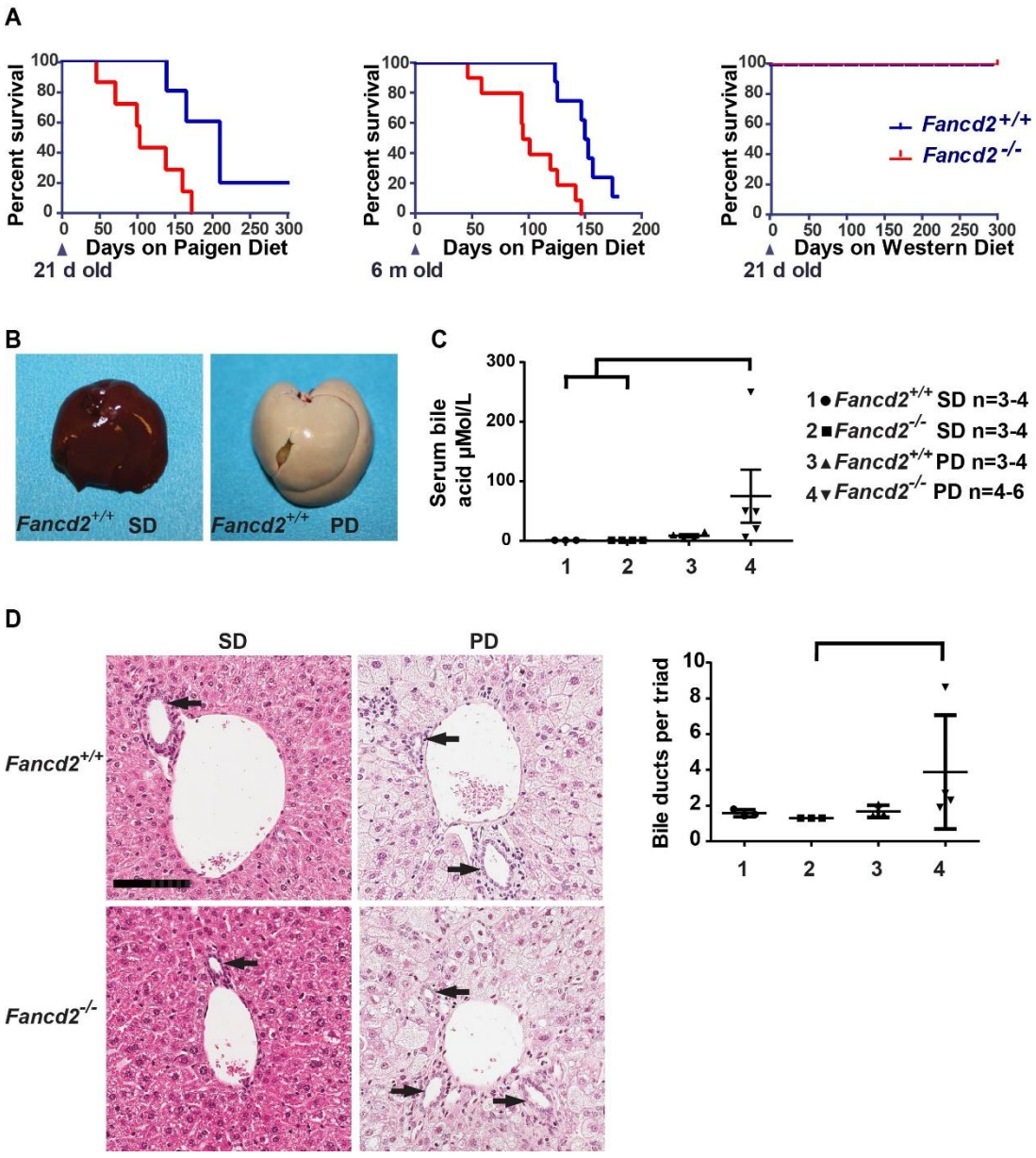

Figure 3.1: Male *Fancd2*$^{-/-}$ mice had increased susceptibility to hepatobiliary disease when fed Paigen diet (PD). A: Kaplan–Meier survival curves showing increased mortality in *Fancd2*$^{-/-}$ mice fed PD beginning at 21 days (left; p = 0.014) or six months (middle; p = 0.001) of age relative to wildtype (WT) mice, and lack of sensitivity to Western high fat diet (WD) (right; p = 1.0). B: Livers were collected from mice fed the indicated diets for 50-55 days, demonstrating PD-induced fatty liver disease. There were no grossly detectable differences between genotypes on either diet. C: Serum was collected from mice at 50-55 days for blood chemistry analysis using an Abaxis VetScan VS2 chemistry analyzer. Bile acid

concentration was significantly increased in male *Fancd2*$^{-/-}$ mice fed PD relative to WT SD fed mice ($p = 0.012$) and *Fancd2*$^{-/-}$ SD fed mice ($p = 0.010$). D: Hematoxylin and eosin (H&E) stained liver sections focusing on portal triads. Bile ducts are lined by cuboidal epithelium (arrows). Scale bar equals 100 μm. Quantification of the average number of bile ducts per hepatic portal triad. *Fancd2*$^{-/-}$ PD fed mice had significantly more bile duct profiles than *Fancd2*$^{-/-}$ SD fed mice ($p = 0.011$) indicating PD feeding induced biliary hyperplasia in *Fancd2*$^{-/-}$ mice.

Concurrent with the biliary phenotype, male *Fancd2*$^{-/-}$ mice fed PD had increased indices of hepatic disease. Male *Fancd2*$^{-/-}$ mice fed PD had an increased liver weight relative to body weight versus *Fancd2*$^{-/-}$ SD fed controls (Figure 3.2A), while PD fed female mice of both genotypes had a similar increase in liver weight (Figure 3.S2A). No difference by genotype was seen in mean liver weight for mice fed WD (WT 2.78 ± 0.3%; *Fancd2*$^{-/-}$ 2.68 ± 0.3%, $p = 0.5476$); we therefore focused subsequent analyses on the PD fed cohort. Male PD fed *Fancd2*$^{-/-}$ mice had significantly fewer hepatocytes per 20x field than SD fed *Fancd2*$^{-/-}$ mice (Figure 3.2B), while PD fed females of both genotypes had a similar number of hepatocytes per field (Figure 3.S2B). These data indicate that PD feeding resulted in greater hepatomegaly and hepatocellular swelling in male *Fancd2*$^{-/-}$ mice.

Plasma was used for liver profile chemistry analysis. The increase in alanine aminotransferase, a marker of hepatocellular injury, was 10.9-fold greater in male *Fancd2*$^{-/-}$ mice than WT mice upon PD challenge (Figure 3.2C left panel). Hepatobiliary disease is also typically associated with elevated alkaline phosphatase. Male *Fancd2*$^{-/-}$ mice fed PD had higher alkaline phosphatase, though it was increased in both WT and *Fancd2*$^{-/-}$ male mice fed PD (Figure 3.2C right panel). In contrast, PD feeding resulted in similar increases in these serologic markers of hepatic pathology in female mice of both genotypes (Figure 3.S2C,D). These data indicate that *Fancd2* deficiency was associated with a greater severity of liver damage upon PD feeding in male mice.

Male *Fancd2*$^{-/-}$ mice fed PD had a significantly higher hepatic parenchymal polymorphonuclear cell (inflammation) score vs WTs (Figure 3.2D,E). Inflammatory cell presence was accompanied by

increased gene expression for transforming growth factor beta (*Tgfb*) and TGFB receptor 2 (*Tgfbr2*) in male *Fancd2*$^{-/-}$ mice upon PD feeding (Figure 3.2F). In contrast, female mice of both genotypes had similar increases in hepatic inflammation score and gene expression of *Tgfb* and *Tgfbr2* (Figure 3.S2E,F). Taken together, these data demonstrate that PD feeding elicits more severe biliary hyperplasia, hepatic injury, and inflammation in male *Fancd2*-deficient mice as compared to *Fancd2*-proficient controls. We therefore focused subsequent mechanistic analyses on male mice.

Figure 3.2: Paigen diet (PD) feeding induced greater hepatomegaly, hepatic damage, and hepatic inflammation in male *Fancd2*$^{-/-}$ mice. Mice were fed PD or standard diet (SD) for 50-55 days and then sacrificed. A: Male *Fancd2*$^{-/-}$ mice had increased liver weight relative to body weight on PD vs SD ($p = 0.002$). B: PD feeding increased hepatocyte size, decreasing the average number of cells across ten 20x fields. Male *Fancd2*$^{-/-}$ mice had marginally significantly larger hepatocytes than male wildtype (WT) mice fed SD ($p = 0.052$) and significantly larger hepatocytes than male *Fancd2*$^{-/-}$ mice fed SD ($p = 0.039$). C: Serum chemistry analysis was performed after 50-55 days of diet feeding using an Abaxis VetScan VS2 chemistry analyzer. Male *Fancd2*$^{-/-}$ mice fed PD had increased serum alanine aminotransferase (ALT) (left panel), a marker of hepatocellular damage, vs WT mice fed SD ($p = 0.0496$) and *Fancd2*$^{-/-}$ mice fed SD ($p = 0.006$). Male *Fancd2*$^{-/-}$ mice fed PD had increased alkaline phosphatase (ALP) (right panel), a marker of hepatobiliary damage, vs WT mice fed SD ($p = 0.011$) and *Fancd2*$^{-/-}$ mice fed SD ($p = 0.038$). WT PD fed mice also had a significant increase in serum ALP vs WT SD fed mice ($p = 0.049$). D, E: Hematoxylin and eosin (H&E) stained liver sections were scored for hepatic parenchymal polymorphonuclear cells (inflammation, arrow). Scale bar equals 100 µm. PD feeding increased hepatic inflammation in male *Fancd2*$^{-/-}$ mice vs all three other groups ($p < 0.005$ for all pairwise comparisons). F: PD feeding was associated with increased expression of the gene encoding the inflammatory marker TGF beta (*Tgfb1*) in *Fancd2*$^{-/-}$ mice vs *Fancd2*$^{-/-}$ mice fed SD ($p = 0.047$). Expression of the gene encoding the TGF beta receptor2 (*Tgfbr2*) increased in *Fancd2*$^{-/-}$ mice fed PD vs *Fancd2*$^{-/-}$ mice fed SD ($p = 0.005$) and WT mice fed SD ($p = 0.014$). Expression presented as fold change relative to the WT SD group. Error bars represent SEM. Box and whisker plots show 25th to 75th percentiles (box) and minimum and maximum (whiskers), with the median indicated by the horizontal bar. $p < 0.05$ for all pairwise comparison indicated.

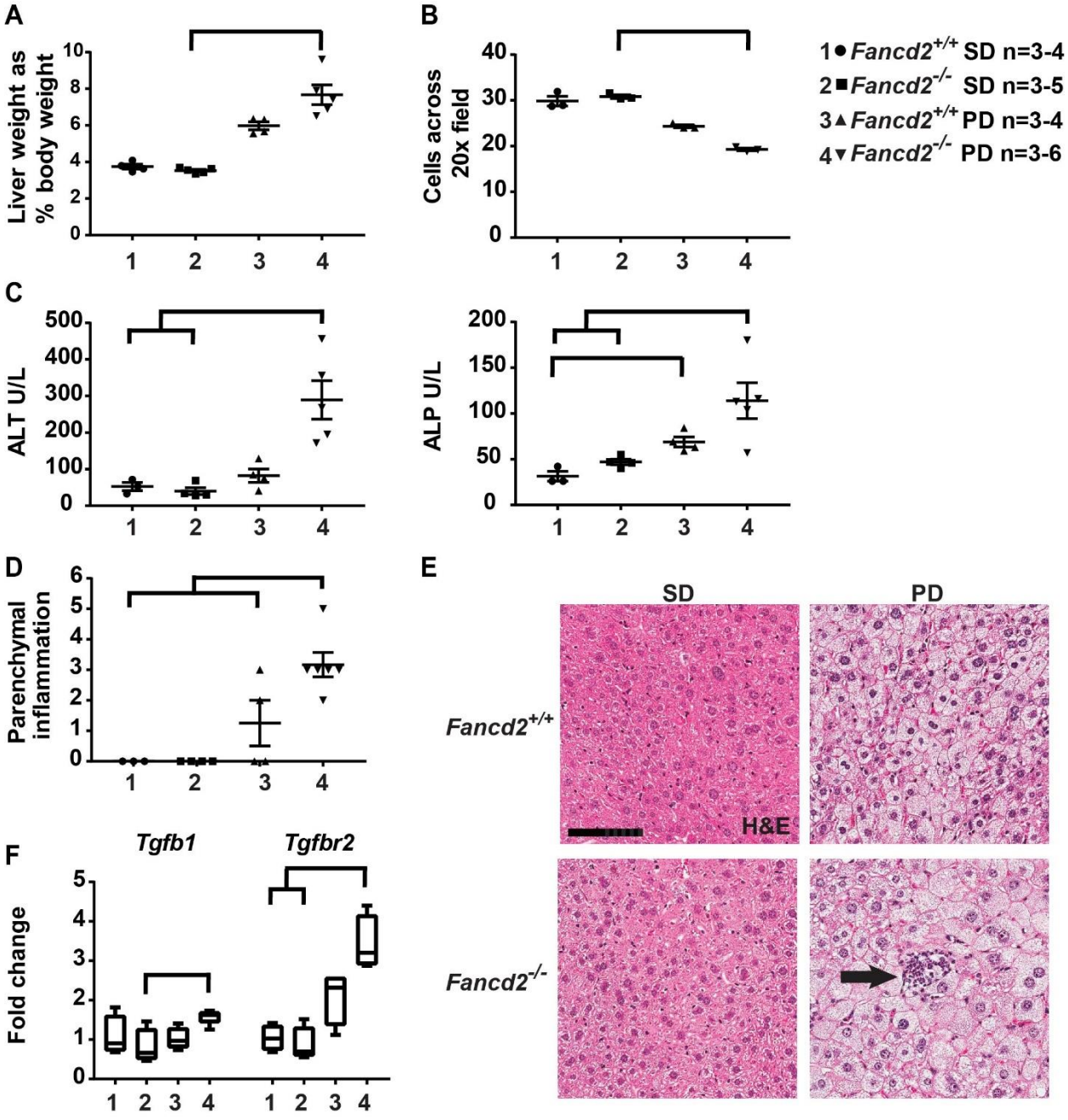
A
Liver weight as % body weight
B
Cells across 20x field
1 ● Fancd2+/+ SD n=3-4
2 ■ Fancd2-/- SD n=3-5
3 ▲ Fancd2+/+ PD n=3-4
4 ▼ Fancd2-/- PD n=3-6
C
ALT U/L
ALP U/L
D
Parenchymal inflammation
E
SD
PD
Fancd2+/+
Fancd2-/-
H&E
F
Tgfb1
Tgfbr2
Fold change

3.3.2 Hepatic DNA damage was only modestly increased by Paigen diet feeding in *Fancd2*-deficient mice relative to controls.

As the canonical function of the FA pathway is in the DDR, we evaluated whether the more severe hepatic phenotypes in PD-fed *Fancd2*$^{-/-}$ mice were associated with elevated hepatic DNA damage. There was a trend towards increased staining for the DNA damage marker γH2AX (Figure 3.3A) in hepatocytes from male *Fancd2*$^{-/-}$ mice fed PD. Apoptosis was also increased as measured by terminal deoxynucleotidyl transferase-mediated deoxyuridine triphosphate nick-end labeling (TUNEL) staining (Figure 3.3B). A similar trend toward increased expression of *p21*, which encodes a cell cycle regulator and indicator of DDR activation, was observed upon PD feeding in *Fancd2*$^{-/-}$ mice, whereas expression of *Puma*, encoding a pro-apoptotic Bcl-2 family member, did not differ by genotype or diet (Figure 3.3C). Though the trends towards increased DNA damage and apoptosis seen in the *Fancd2*$^{-/-}$ PD fed mice are consistent with hepatobiliary pathology from accumulated BA and/or lipids, the magnitude of the changes in the IHC and DDR gene expression data suggest that PD feeding did not elicit a robust DDR in either genotype.

Lipid peroxidation can result in DNA interstrand crosslinks, and FA pathway-directed repair of such lesions involves coordination of translesion synthesis (TLS) DNA polymerases (256, 402). PD feeding was associated with a significant increase in expression of *Polθ*, a TLS polymerase encoding gene, only in *Fancd2*$^{-/-}$ male mice (Figure 3.3D). Additionally, PD feeding was associated with a 3.3 fold greater increase in expression of the TLS encoding gene *Polκ* in *Fancd2*$^{-/-}$ male mice vs WT mice. Neither diet nor genotype impacted expression of the genes encoding TLS polymerases lambda (*Polλ*), eta (*Polη*), beta (*Polβ*), or *Rev1*. Elevated *Polκ* and *Polθ* expression in *Fancd2*$^{-/-}$ mice suggests increased reliance on potentially error-prone DNA damage tolerance mechanisms following PD-induced DNA damage.

Oxidative stress is characteristic of FA deficient cells, and mitochondrial beta oxidation of free fatty acids generates reactive oxygen species (403). To evaluate the potential contribution of oxidative damage to the increased hepatocellular damage seen in *Fancd2*$^{-/-}$ mice fed PD, we quantified expression of genes associated with glutathione metabolism and superoxide detoxification. There were no significant

differences by genotype or diet in gene expression levels of *glutathione peroxidase 1* (*Gpx1*), *glutathioneS-transferase theta* (*Gstt*), *glutathione synthetase* (*Gss*), *sestrin 1*(*Sesn1*), or *sestrin 2* (*Sesn2*) (Figure 3.3E). However, male *Fancd2*$^{-/-}$ mice fed PD had significantly lower *superoxide dismutase 2* (*Sod2*) gene expression than male *Fancd2*$^{-/-}$ mice fed SD. A similar trend was seen in *Sod1* expression. This suggests *Fancd2*$^{-/-}$ mice fed PD may be less able to detoxify superoxide due to lower *Sod1/2* expression; however, upregulation of antioxidant defenses was not observed in either genotype upon PD feeding. Together, these observations that the PD sensitivity phenotype in *Fancd2*$^{-/-}$ mice was not associated with a robust DDR or antioxidant defense response suggested the possibility of a non-canonical metabolic role for the FA pathway.

Figure 3.3: Male *Fancd2*$^{-/-}$ mice showed modestly increased hepatocellular DNA damage when fed Paigen diet (PD). Immunohistochemistry (IHC) or quantitative PCR was performed on livers collected after 50-55 days of PD or standard diet (SD) feeding. Comparisons expressed as fold change relative to the wildtype (WT) SD group. A: IHC on liver sections for γH2AX, a DNA damage marker, and quantification of γH2AX positive hepatocytes (arrow) as a percentage of total hepatocytes. Male *Fancd2*$^{-/-}$ mice fed PD had a trend towards increased γH2AX positive hepatocytes ($p = 0.08$ vs WT SD fed mice). B: IHC of liver sections by TUNEL, which labels DNA nicks associated with apoptosis, and quantification of TUNEL positive apoptotic hepatocytes (arrow) quantified as the percent of total hepatocytes. C: Expression of DNA damage response genes *Cdkn1a* (*p21*) and *Bbc3* (*Puma*). D: Expression of genes encoding translesion synthesis DNA polymerases. Male *Fancd2*$^{-/-}$ PD fed mice had increased expression of *Polκ* relative to WT SD ($p = 0.043$) and *Fancd2*$^{-/-}$ SD ($p = 0.036$) fed mice. Male *Fancd2*$^{-/-}$ PD fed mice had increased expression of *Polθ* relative to *FancdD2*$^{-/-}$ SD fed mice ($p = 0.014$). F: Expression of genes encoding enzymes involved in detoxifying superoxide radicals and glutathione metabolism. Error bars in dot plots represent SEM. Box and whisker plots show 25th to 75th percentiles (box) and minimum and maximum (whiskers), with the median indicated by the horizontal bar. $p < 0.05$ for all pairwise comparison indicated. Scale bars are 100 um.

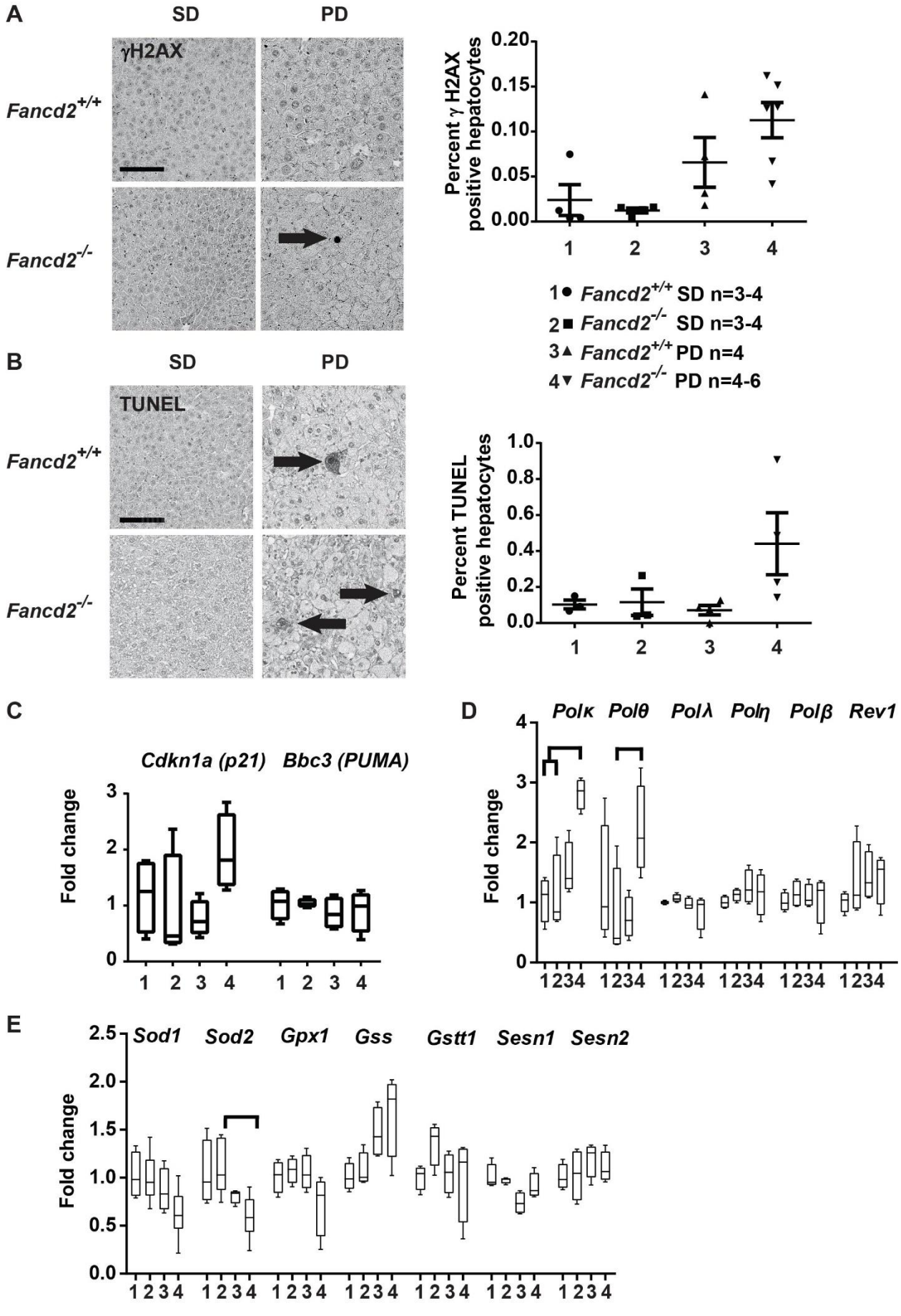
A
SD
PD
γH2AX
Fancd2+/+
Fancd2-/-
Percent γ H2AX positive hepatocytes
0.20
0.15
0.10
0.05
0.00
1
2
3
4
1● Fancd2+/+ SD n=3-4
2■ Fancd2-/- SD n=3-4
3▲ Fancd2+/+ PD n=4
4▼ Fancd2-/- PD n=4-6
B
SD
PD
TUNEL
Fancd2+/+
Fancd2-/-
Percent TUNEL positive hepatocytes
1.0
0.8
0.6
0.4
0.2
0.0
1
2
3
4
C
Cdkn1a (p21)
Bbc3 (PUMA)
Fold change
3
2
1
0
1 2 3 4 1 2 3 4
D
Polκ
Polθ
Polλ
Polη
Polβ
Rev1
Fold change
4
3
2
1
0
1234 1234 1234 1234 1234 1234
E
Sod1
Sod2
Gpx1
Gss
Gstt1
Sesn1
Sesn2
Fold change
2.5
2.0
1.5
1.0
0.5
0.0
1234 1234 1234 1234 1234 1234 1234

3.3.3 Sensitivity to hepatobiliary damage in male *Fancd2*$^{-/-}$ mice fed PD is not due to gene expression differences for rate limiting enzymes in hepatic bile acid synthesis.

As male *Fancd2*$^{-/-}$ mice fed PD had increased susceptibility to hepatobiliary disease, increased serum BA, and biliary hyperplasia, we probed expression of genes involved in hepatic BA, cholesterol, and lipid homeostasis. Expression of *Fxr*, which encodes a nuclear BA receptor that regulates hepatic BA synthesis, and *Shp*, encoding its downstream mediator, did not differ by genotype or diet (Figure 3.4A). There was a slight but statistically significant reduction in expression of *Lxr*, which encodes a nuclear receptor and cholesterol and lipid regulator, in *Fancd2*$^{-/-}$ PD fed male mice. As expected with a cholic acid-enriched diet, expression levels of *Cyp7a1* and *Cyp8b1*, encoding neutral BA synthesis enzymes, were downregulated in WT and *Fancd2*$^{-/-}$ male mice upon PD feeding (Figure 3.4B). *Cyp27A1* and *Cyp7b1*, encoding enzymes that generate oxysterols involved in the acidic BA synthesis pathway, were downregulated upon PD feeding in male mice; however, only *Fancd2*$^{-/-}$ PD fed mice had significantly decreased expression relative to SD fed mice. Expression of *Cyp3A11* and *Sult2A1*, which encode enzymes that modify BA, making them less cytotoxic, was not significantly different by genotype or diet. Thus it appears that *Fancd2*$^{-/-}$ mice are proficient to modulate gene expression following PD challenge to decrease *de novo* BA synthesis and detoxify BA.

We next evaluated expression of hepatic BA exporters. Expression of *Abcb11* (*BSEP*) and *Abcc2* (*Mrp2*), genes encoding canalicular BA exporters, and *Mrp3* (*Abcc3*), which encodes a sinusoidal BA exporter, did not differ significantly by diet or genotype in male mice (Figure 3.4C). Expression of the genes *Abcb1* (MDR1) and *Ostβ* (*Slc51b*), encoding sinusoidal BA exporters, increased upon PD feeding in both genotypes. These findings suggest that the hepatobiliary phenotype seen in *Fancd2*$^{-/-}$ mice upon PD feeding is not due to a failure to export hepatic BA.

As we observed increased serum BA in male *Fancd2*$^{-/-}$ mice fed PD, we quantified expression of genes encoding hepatic BA importers. Male *Fancd2*$^{-/-}$ mice fed PD had a greater decrease in expression of BA importer encoding genes *Slc10a1* (NTCP; 2.59-fold greater decrease), *Slc22a7* (Oat2; 1.95-fold greater decrease), and *Slco1a1* (Oatp1a1; 4.92-fold greater decrease), than WT PD fed mice (Figure 3.4D).

Reduction in these BA import receptors can be interpreted as a compensatory hepatoprotective response to increased intracellular BA accumulation. In addition to being consistent with the observed morbidity, the decreased expression of hepatic BA importer genes in PD fed *Fancd2*$^{-/-}$ mice likely contributed to the observed increase in serum BA.

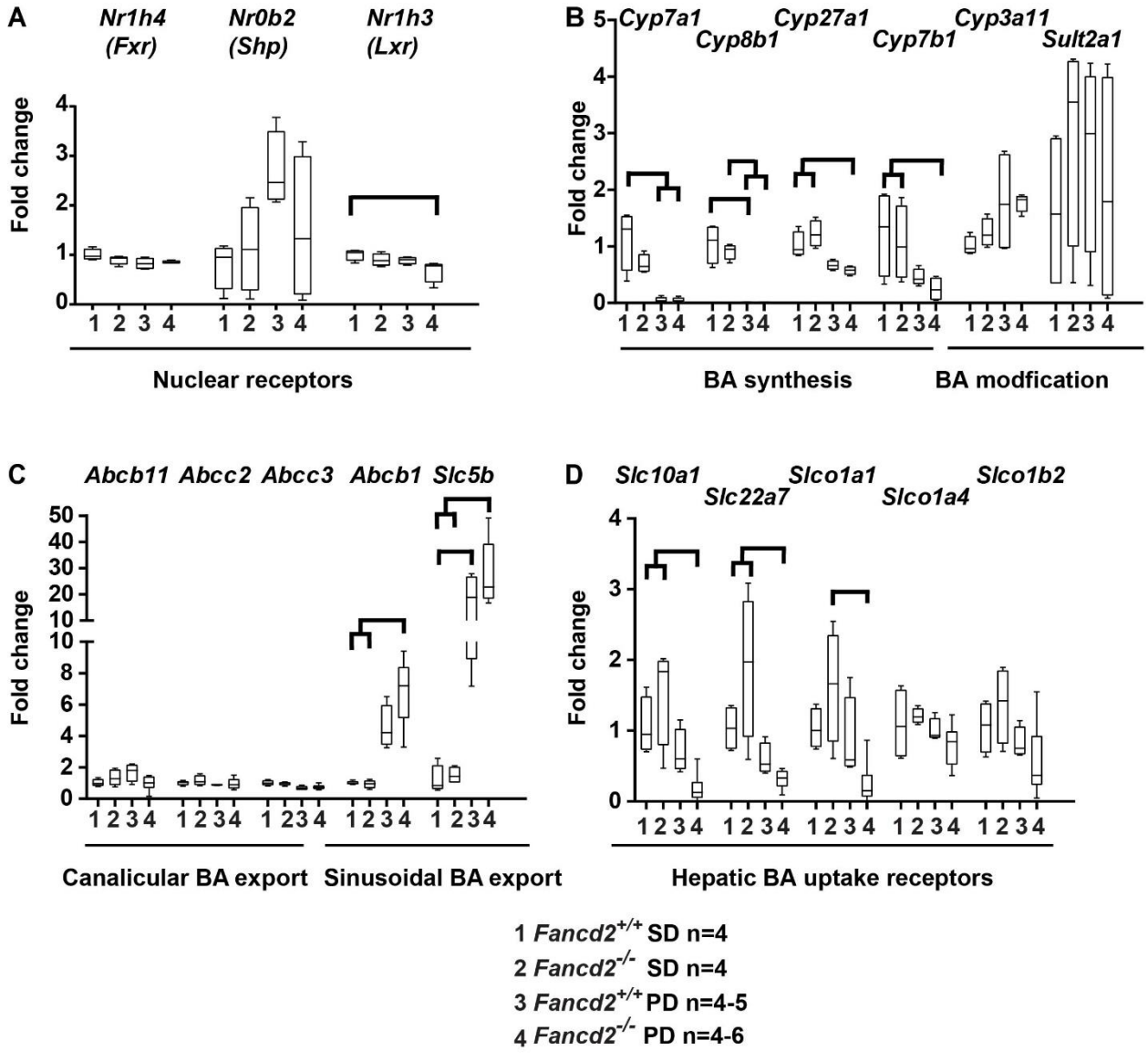

Figure 3.4: Differential expression of genes encoding proteins involved in bile acid (BA) metabolism was unlikely to be the cause of hepatobiliary disease in *Fancd2*$^{-/-}$ mice fed Paigen diet (PD). Mice were sacrificed after feeding PD or standard diet (SD) for 50-55 days, and RNA was extracted from liver, reverse transcribed, and used for quantitative PCR. All comparisons are expressed as fold change relative to the wildtype (WT) SD group. A: Expression of genes encoding the nuclear receptor transcription factors regulating BA (*Fxr* and *Shp*) and cholesterol and lipid (*Lxr*). There was a small, but significant reduction in expression of *Nrlh3* (*Lxr*) in *Fancd2*$^{-/-}$ PD fed mice relative to WT SD fed mice ($p = 0.036$). B: Expression of genes encoding BA synthesis and modification enzymes. WT and *Fancd2*$^{-/-}$ mice downregulated BA synthesis enzyme gene expression when fed PD ($p < 0.05$ for all pairwise comparisons). C: Expression of hepatic canalicular and sinusoidal BA transporter-encoding genes. The expression of the sinusoidal BA exporter encoded by *Abcb1* (*Mdr1*) increased upon PD feeding in both genotypes, but the increase was larger and statistically significant only for *Fancd2*$^{-/-}$ PD fed mice vs SD fed mice ($p < 0.05$ for both pairwise comparisons). The expression of the sinusoidal exporter encoded by *Slc5b* increased upon PD feeding in both genotypes, but to a larger degree in *Fancd2*$^{-/-}$ mice ($p < 0.05$ for all pairwise comparisons indicated). D: Expression of genes encoding hepatic BA uptake receptors. *Fancd2*$^{-/-}$ PD fed mice had a significant reduction in the expression of three hepatic BA uptake receptor-encoding genes (*Slc10a1* (*Ntcp*), *Slc22a7* (*Oat2*) and *Slc1a1*), which is consistent with bile acid accumulation and cytotoxicity. Error bars in dot plots represent SEM. Box and whisker plots show 25th to 75th percentiles (box) and minimum and maximum (whiskers), with the median indicated by the horizontal bar. $p < 0.05$ for all pairwise comparisons indicated.

3.3.4 Male *Fancd2*$^{-/-}$ mice have impaired cholesterol and lipid regulation upon Paigen diet feeding.

As we did not observe differential BA metabolism gene expression that appeared causal for the hepatobiliary pathology in *Fancd2*$^{-/-}$ mice upon PD feeding, we evaluated if the phenotype was associated with impaired cholesterol metabolism. Serum and hepatic total cholesterol increased in a genotype-independent manner upon PD feeding (Figure 3.5A,B), and there was no detectable difference in the

proportion of serum cholesterol HDL and non-HDL subtypes (Figure 3.S3). Expression of *Scarb1* (HDL receptor) did not vary significantly. Expression of *Ldlr* (LDL receptor) decreased in both genotypes on PD; however, the decrease was 1.5-fold greater and statistically significant only in male *Fancd2*$^{-/-}$ mice (Figure 3.5C). These data indicate that the hepatobiliary phenotype observed in male *Fancd2*$^{-/-}$ mice was not associated with gene expression changes predictive of increased serum or hepatic cholesterol; however, factors regulating hepatic uptake of cholesterol may differ by *Fancd2* status.

We subsequently uncovered differential regulation of genes encoding proteins involved in cholesterol transport, export, import, and fatty acid synthesis in male *Fancd2*$^{-/-}$ mice fed PD. The expression level of genes encoding cholesterol synthesis enzymes *Srebf2* (SREBP2) and *Hmgcs2* (HMG-CoA synthase) decreased in both genotypes upon PD feeding, suggesting cholesterol synthesis decreased irrespective of genotype. Expression of genes encoding sterol carrier protein 2/sterol carrier protein-x (SCP-2/SCP-x), which are generated via use of alternative transcriptional start sites and involved in cholesterol trafficking and BA synthesis (404), were differentially regulated by *Fancd2* status. PD feeding was associated with significantly reduced *Scp2* expression and a 10-fold greater reduction in *Scpx* in male *Fancd2*$^{-/-}$ mice (Figure 3.5C), but did not significantly impact expression of *Scp2/x* in WT mice, indicating that *Fancd2* loss impairs hepatic expression of cholesterol transport and enzymatic conversion genes.

Cholesterol is excreted from hepatocytes into bile via ATP-binding cassette family members ABCG5/8 (405). In male WT mice, PD feeding was associated with increased expression of *Abcg5*/*8*; however, male *Fancd2*$^{-/-}$ mice did not demonstrate increased *Abcg5*/*8* expression upon PD feeding. (Figure 3.5C). Cholesterol is also exported to lipoprotein particles in blood. ABCA1 promotes the efflux of cholesterol and phospholipids to lipid poor apoA-I as part of the early formation of HDL particles (406). PD feeding was associated with a significant increase in *Abca1* expression in WT mice only. ABCG1 exports phospholipids and cholesterol to HDL, LDL, and phospholipid particles and is involved in the intracellular movement of cholesterol from the endoplasmic reticulum to the plasma membrane (406, 407). On PD, only *Fancd2*$^{-/-}$ mice significantly upregulated expression of *Abcg1*. These data suggest that cholesterol storage and export dynamics may have been altered in male *Fancd2*$^{-/-}$ mice upon PD challenge.

In addition to assessing genes regulating hepatic BA and cholesterol metabolism, we probed expression of genes encoding proteins involved in fatty acid and triglyceride metabolism. Acetyl-CoA acetyltransferase (*Acat1*) generates acetoacetyl-CoA from acetyl-CoA, and is involved in the metabolism of fatty acids, ketones, and amino acids, and energy metabolism via regulation of the pyruvate dehydrogenase complex in the decision between glycolysis and oxidative phosphorylation (408-410). *Acat1* gene expression was significantly decreased in *Fancd2*$^{-/-}$ mice fed PD, and the decrease observed in *Fancd2*$^{-/-}$ mice fed PD was 3.2 fold greater than the non-significant decrease in *Acat1* expression in WT mice fed PD (Figure 3.5D). SREBP-1c (*Srebf1*) is a transcription factor that regulates hepatic lipogenesis, glucose metabolism, and the expression of genes needed to produce the fatty acid chains esterified to cholesterol (411). PD feeding was associated with increased expression of *Srebf1* in WT, but not *Fancd2*$^{-/-}$, male mice (Figure 3.5D). This alteration in the expression of a fatty acid regulating transcription factor in livers of *Fancd2*$^{-/-}$ mice fed PD may be consistent with previously reported altered fatty acid metabolism in FA lymphoblasts and lymphocytes (339). Stearoyl-Co A desaturase (SCD) is a rate-limiting enzyme that catalyzes the synthesis of monounsaturated fatty acids, primarily oleate and palmitoleate (412). The packaging and export of VLDL from the liver requires oleic acid, either from the diet or synthesized by SCD. Acyl-CoA cholesterol acyltransferase, which esterifies cholesterol to prevent the toxic accumulation of free cholesterol and to make cholesterol available for export in VLDLs, also prefers the substrate oleic acid (412). On PD, WT mice had a significant increase in expression of *Scd-1*, while the non-significant increase in *Scd-1* expression in male *Fancd2*$^{-/-}$ mice was only 0.5 fold that seen in the WTs (Figure 3.5D). *Fancd2* status did not affect expression of *Mlxipl* (ChREBP), encoding a transcription factor regulating triglyceride synthesis, or *Pparα*, which encodes a transcription factor that regulates fatty acid, triglyceride, and glucose metabolism. These data suggest the supply of fatty acids for cholesterol esterification and VLDL formation could have been deficient in *Fancd2*$^{-/-}$ mice, further perturbing cholesterol homeostasis.

Figure 3.5: Male *Fancd2*$^{-/-}$ mice had differential cholesterol and lipid metabolism gene expression upon Paigen diet (PD) feeding. After feeding PD or standard diet (SD) for 50-55 days, livers were collected for RNA extraction and used for quantitative PCR. All comparisons are expressed as fold change relative to the wildtype (WT) SD group. Total serum (A) and hepatic (B) cholesterol increased on PD feeding in both genotypes in male mice ($p < 0.05$ for indicated comparisons). C: Expression of genes encoding proteins involved in cholesterol metabolism and transport. Both genotypes decreased expression of *Srebf2* (*Srebp2*), encoding the major transcription factor regulating cholesterol synthesis and *Hmgcs2*, encoding a cholesterol synthesis enzyme, upon PD feeding. *Fancd2*$^{-/-}$ mice had decreased expression of the cholesterol transporters encoded by *Scp2/x* upon PD feeding and failed to upregulate expression of the cholesterol exporters encoded by *Abcg5/8* and *Abca1* upon PD feeding, as was observed in WT PD fed mice. *Fancd2*$^{-/-}$ but not WT mice had a significantly increased expression of the cholesterol exporter *Abcg1* upon PD feeding. LDL receptor (*Ldlr*) expression decreased in both genotypes upon PD feeding, but decreased significantly only in *Fancd2*$^{-/-}$ mice. D: Expression of genes involved in acetyl-Co A, fatty acid, and triglyceride metabolism. *Fancd2*$^{-/-}$ mice had decreased expression of *Acat1*, which converts two acetyl CoAs to acetoacetyl coA as an early step in lipid, ketone, and amino acid synthesis, while PD feeding did not significantly impact expression of *Acat1* in WT mice. Upon PD feeding, WT but not *Fancd2*$^{-/-}$ mice increased expression of *Srebf1* (*Srebp1c*), the major transcription factor regulating fatty acid synthesis. A trend towards lower expression of *Fasn* (fatty acid synthase), a transcriptional target of SREPB1c, was seen in *Fancd2*$^{-/-}$ mice fed PD. *Ppara*, a gene regulating fatty acid oxidation, decreased upon PD feeding in both genotypes, though the decrease was significant only for *Fancd2*$^{-/-}$ mice fed PD. E: Summary of differential expression of genes encoding proteins involved in cholesterol and lipid metabolism by FANCD2 status upon PD feeding in male WT (left) and *Fancd2*$^{-/-}$ mice (right). Solid lines indicate statistically significant up/downregulation. Dashed lines indicate non-significant trends. Error bars in dot plots represent SEM. Box and whisker plots show 25th to 75th percentiles (box) and minimum and maximum (whiskers), with the median indicated by the horizontal bar. $p < 0.05$ for all pairwise comparisons indicated.

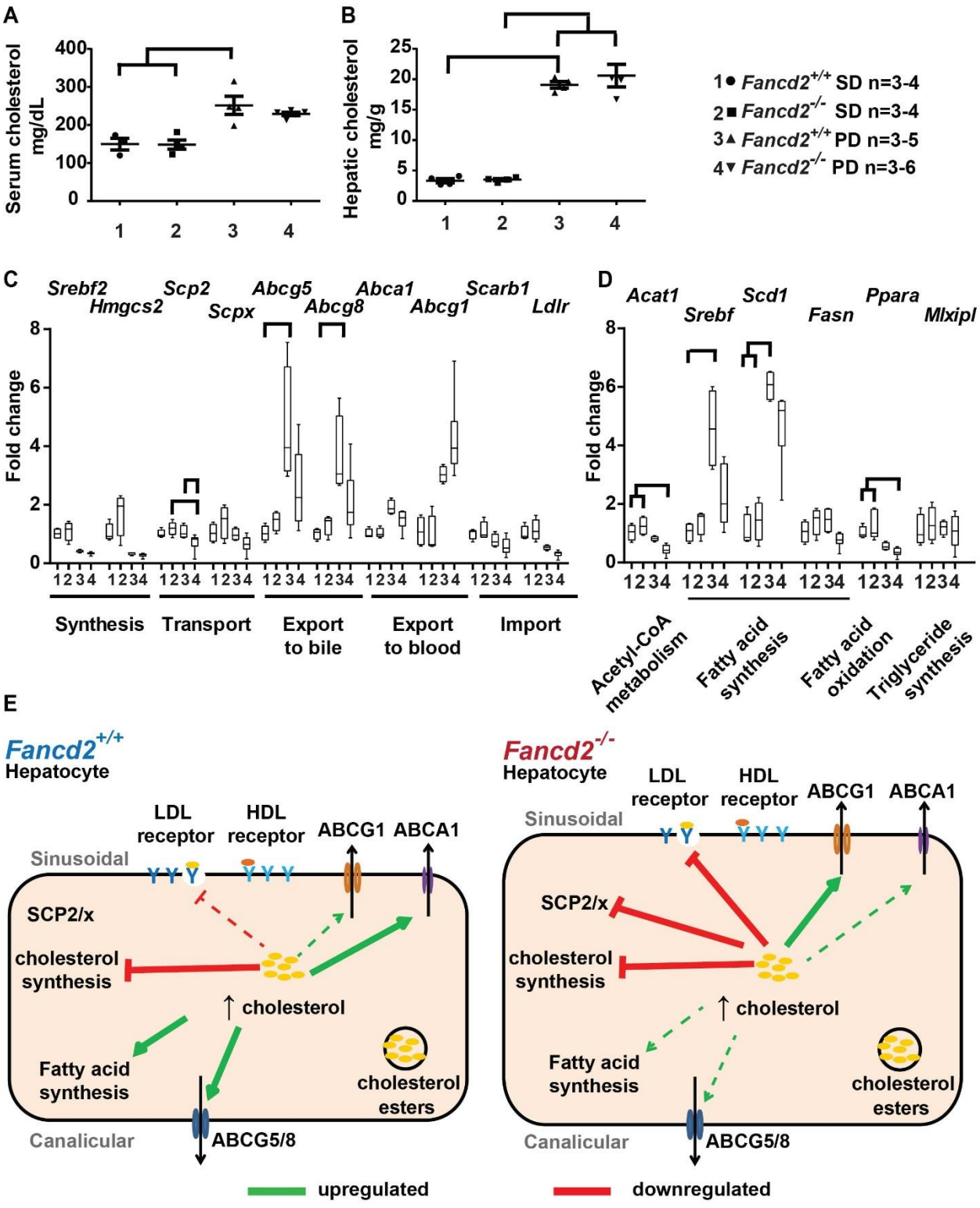
A
Serum cholesterol mg/dL
400
300
200
100
0
1
2
3
4
B
Hepatic cholesterol mg/g
25
20
15
10
5
0
1 Fancd2+/+ SD n=3-4
2 Fancd2-/- SD n=3-4
3 Fancd2+/+ PD n=3-5
4 Fancd2-/- PD n=3-6
C
Srebf2
Hmgcs2
Scp2
Scpx
Abcg5
Abcg8
Abca1
Abcg1
Scarb1
Ldlr
Fold change
Synthesis
Transport
Export to bile
Export to blood
Import
D
Acat1
Srebf
Scd1
Fasn
Ppara
Mlxipl
Fold change
Acetyl-CoA metabolism
Fatty acid synthesis
Fatty acid oxidation
Triglyceride synthesis
E
Fancd2+/+
Hepatocyte
LDL receptor
HDL receptor
ABCG1
ABCA1
Sinusoidal
SCP2/x
cholesterol synthesis
cholesterol
Fatty acid synthesis
cholesterol esters
Canalicular
ABCG5/8
upregulated
Fancd2-/-
Hepatocyte
LDL receptor
HDL receptor
ABCG1
ABCA1
Sinusoidal
SCP2/x
cholesterol synthesis
cholesterol
Fatty acid synthesis
cholesterol esters
Canalicular
ABCG5/8
downregulated

We also fed an additional cohort of male mice PD for a longer ten week period, initiated at 21 days of age, in an attempt to potentially exaggerate the hepatobiliary phenotype. Similar genotype-dependent differences in expression of cholesterol metabolism genes were observed in this cohort as in mice aged to six months and fed PD for 50-55 days (Figure 3.S4). By contrast, transcriptional responses to WD feeding did not generally differ by *Fancd2*$^{-/-}$ status, indicating that the phenotypes are not universal to high fat diets and likely are dependent on the inclusion of cholesterol and/or cholic acid in PD (Figure 3.S5). Together these data suggest that male *Fancd2*$^{-/-}$ mice have alterations in multiple genes involved in cholesterol metabolism in response to PD feeding which may impact hepatic cholesterol storage, intracellular transport, and export, ultimately increasing hepatoxicity (Figure 3.5E).

To further analyze hepatic lipid metabolism in *Fancd2*$^{-/-}$ mice, we performed untargeted lipidomic profiling in positive mode. Partial least squares discriminate analysis revealed distinct clustering of PD fed WT samples relative to *Fancd2*$^{-/-}$ samples (Figure 3.6A). A total of 379 lipid species were detected (Figure 3.S6A), of which approximately 37% (140) showed no significant effect by genotype or diet. Approximately 28% (107) of lipids had a significant diet effect only, and notably, nearly 35% (132) of lipids detected differed between WT and *Fancd2*$^{-/-}$ groups, with the vast majority of genotype differences (105) in lipid abundance occurring on PD (Figure 3.6B). The top lipids contributing to the component scores are shown in Figure 3.S6B,C. *Fancd2*$^{-/-}$ samples had numerous differences in membrane, energy storage, and signaling lipids.

Fancd2$^{-/-}$ mice fed PD had significantly different and largely elevated relative abundances of several species of ceramides (Cer) and sphingomyelins (SM), classes of sphingolipids that are components of cellular membranes and involved in many cellular functions (Figure 3.6C,D, Figure 3.S7A-C). As components of lipid rafts, sphingolipids influence cholesterol trafficking and metabolism (413), promote apoptosis, and impact cell-cell connections (414, 415). Elevated ceramides are associated with insulin resistance and lipotoxicity (reviewed in (416, 417)). Upon PD feeding, we observed elevations in hepatic Cer 18:1/16:0 in *Fancd2*$^{-/-}$ mice, relative to WT. (Figure 3.S7B). Recent work has demonstrated that C16:0-

linked ceramide is considered the principal sphingolipid antagonist of insulin sensitivity (418). Future work should determine whether insulin-stimulated glucose utilization is impaired by ceramide in *Fancd2*$^{-/-}$ mice.

Numerous genotype-dependent differences were detected in the abundance of glycerophospholipids, the major class of lipids in cell membranes. Phosphatidylcholine (PC) species that differed by genotype on PD, which were generally markedly elevated in *Fancd2*$^{-/-}$ mice, are shown in Figure 3.6E, with all PC species shown in Figure 3.S8A. As saturated and unsaturated PC were increased in PD-fed *Fancd2*$^{-/-}$ mice, we expect that the CDP-choline and phosphatidylethanolamine *N*-methyltransferase pathways were fully functional (419). Considering that PC is required for VLDL assembly and secretion (420), the ability of *Fancd2*$^{-/-}$ mice to modulate VLDL export deserves further investigation.

Lysophosphatidylcholines (LPC) and phosphatidylethanolamines (PE) also differed by diet and genotype (Figure 3.S8B-E). *Fancd2*$^{-/-}$ mice fed SD or PD had higher hepatic concentrations of LPC (e.g., LPC 16:0 or 18:0). These findings are of potential significance when we consider the ability of long-chain LPC to regulate innate immunity and inflammatory processes (421), and the observed elevation in hepatic inflammation in male *Fancd2*$^{-/-}$ mice. Changes in glycerophospholipid metabolism can alter membrane dynamics (422, 423) and our finding of differential abundance of sphingolipids and glycerophospholids in livers of *Fancd2*$^{-/-}$ mice is consistent with alterations in these lipid classes reported in other cell types deficient in the FA pathway (341, 343).

Glycerolipids differed by *Fancd2* status as well. Triacylglycerols (TG) were the most frequently detected lipids, and many differed in abundance between genotypes on PD (Figure 3.6F and Figure 3.S9A). Increased TG is associated with lipotoxicity and insulin resistance (424), though interestingly, many TG species were reduced in livers from *Fancd2*$^{-/-}$ mice fed PD. Total hepatic TG was not impacted by diet or genotype (Figure 3.S9B). Several diacylglycerols (DG), which can be reacylated and converted to TG, as well as function as signaling molecules (reviewed in (423)), were differentially impacted by diet and genotype (Figure 3.S10A,B). In addition to ceramides, DG also contribute to increased hepatic insulin resistance (425, 426). Collectively, it would appear that fatty acids were partitioned away from neutral lipid synthesis and towards sphingolipid and glycerophospholipid production in *Fancd2*$^{-/-}$ mice.

Cholesterols can exist as free or esterified forms. Esterified forms are generated by acyl-coenzymeA cholesterol acyltransferase and are considered an inert storage form that protects cells from free cholesterol accumulation (427). Seven cholesterol esters were detected in our lipidomic screen, two of which (ChE 20:4NH4 and ChE 22:6NH4) were significantly different between WT mice fed PD, in which they increased, and *Fancd2*$^{-/-}$ mice fed PD, in which they decreased (Figure 3.S10C), suggesting that cholesterol esterification and storage was altered in *Fancd2*$^{-/-}$ hepatocytes upon PD feeding. Sphingolipid, glycerophospholipid and glycerolipid metabolism are interconnected (423), and these data indicate that altered lipid metabolism was characteristic of FA hepatocytes, particularly when faced with dietary metabolic challenge.

Figure 3.6: Male *Fancd2*$^{-/-}$ differed in hepatic sphingolipid, glycerophospholipid, and glycerolipid species abundance, particularly upon Paigen diet (PD) feeding. After feeding Paigen diet (PD) or standard diet (SD) for 50-55 days, livers were collected and lipids extracted for untargeted lipidomics. **A**: Partial least squares discriminant analysis revealing partial separation of WT and *Fancd2*$^{-/-}$ mice on SD and separation of the genotypes on PD. **B**: Proportions of the 379 lipid species detected that differed significantly by diet or genotype. Heatmaps of lipid species with significantly different abundances between WT and *Fancd2*$^{-/-}$ mice on PD: ceramides (Cer) (**C**), sphingomyelins (SM) (**D**), phosphatidylcholines (PC) (**E**), and triacylglycerols (TG) (**F**).

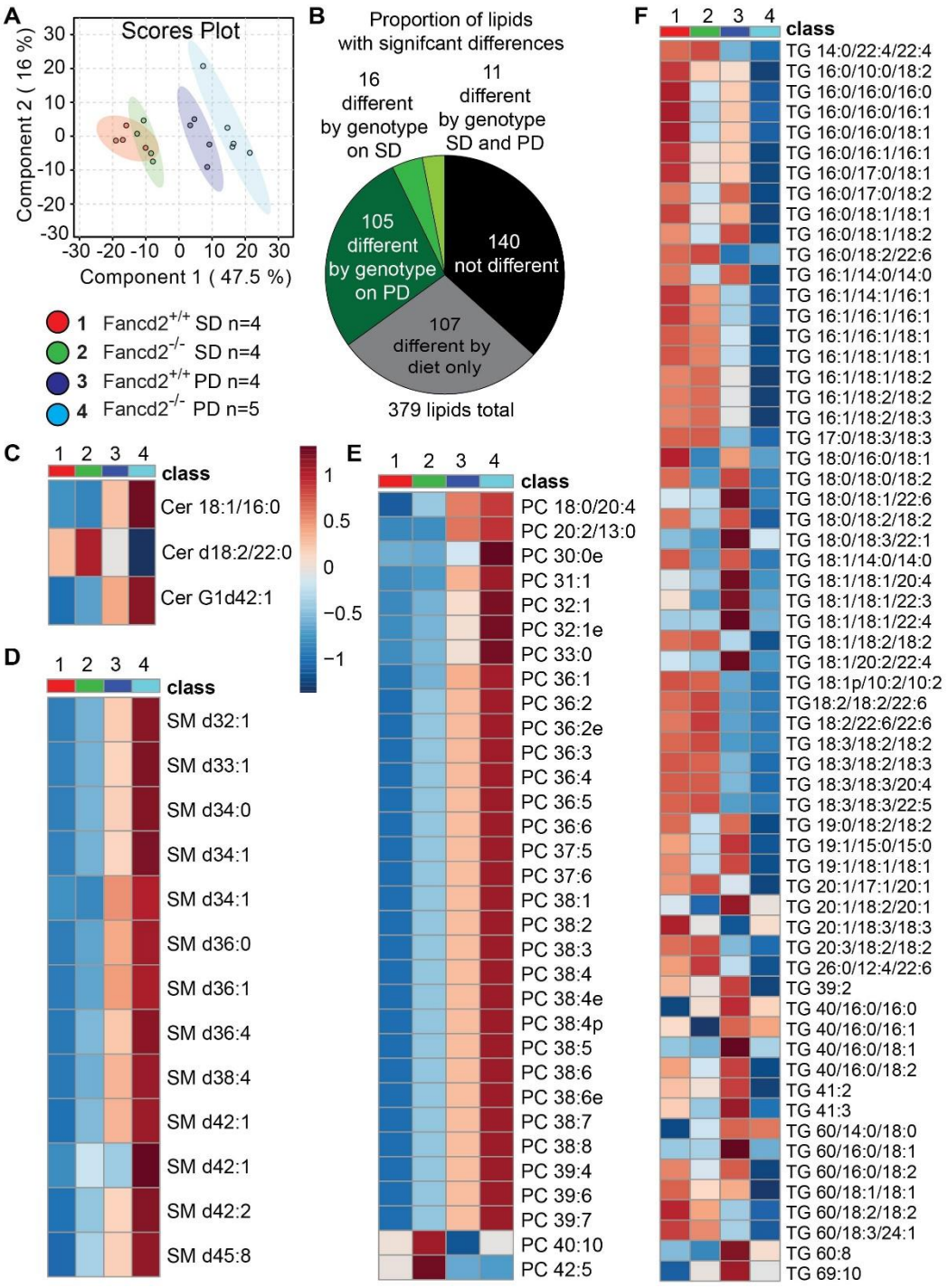
A
Scores Plot
Component 2 (16 %)
Component 1 (47.5 %)
1 Fancd2+/+ SD n=4
2 Fancd2-/- SD n=4
3 Fancd2+/+ PD n=4
4 Fancd2-/- PD n=5
B
Proportion of lipids with signifcant differences
16 different by genotype on SD
11 different by genotype SD and PD
105 different by genotype on PD
140 not different
107 different by diet only
379 lipids total
C
class
Cer 18:1/16:0
Cer d18:2/22:0
Cer G1d42:1
D
class
SM d32:1
SM d33:1
SM d34:0
SM d34:1
SM d34:1
SM d36:0
SM d36:1
SM d36:4
SM d38:4
SM d42:1
SM d42:1
SM d42:2
SM d45:8
E
class
PC 18:0/20:4
PC 20:2/13:0
PC 30:0e
PC 31:1
PC 32:1
PC 32:1e
PC 33:0
PC 36:1
PC 36:2
PC 36:2e
PC 36:3
PC 36:4
PC 36:5
PC 36:6
PC 37:5
PC 37:6
PC 38:1
PC 38:2
PC 38:3
PC 38:4
PC 38:4e
PC 38:4p
PC 38:5
PC 38:6
PC 38:6e
PC 38:7
PC 38:8
PC 39:4
PC 39:6
PC 39:7
PC 40:10
PC 42:5
F
class
TG 14:0/22:4/22:4
TG 16:0/10:0/18:2
TG 16:0/16:0/16:0
TG 16:0/16:0/16:1
TG 16:0/16:0/18:1
TG 16:0/16:1/16:1
TG 16:0/17:0/18:1
TG 16:0/17:0/18:2
TG 16:0/18:1/18:1
TG 16:0/18:1/18:2
TG 16:0/18:2/22:6
TG 16:1/14:0/14:0
TG 16:1/14:1/16:1
TG 16:1/16:1/16:1
TG 16:1/16:1/18:1
TG 16:1/18:1/18:1
TG 16:1/18:1/18:2
TG 16:1/18:2/18:2
TG 16:1/18:2/18:3
TG 17:0/18:3/18:3
TG 18:0/16:0/18:1
TG 18:0/18:0/18:2
TG 18:0/18:1/22:6
TG 18:0/18:2/18:2
TG 18:0/18:3/22:1
TG 18:1/14:0/14:0
TG 18:1/18:1/20:4
TG 18:1/18:1/22:3
TG 18:1/18:1/22:4
TG 18:1/18:2/18:2
TG 18:1/20:2/22:4
TG 18:1p/10:2/10:2
TG18:2/18:2/22:6
TG 18:2/22:6/22:6
TG 18:3/18:2/18:2
TG 18:3/18:2/18:3
TG 18:3/18:3/20:4
TG 18:3/18:3/22:5
TG 19:0/18:2/18:2
TG 19:1/15:0/15:0
TG 19:1/18:1/18:1
TG 20:1/17:1/20:1
TG 20:1/18:2/20:1
TG 20:1/18:3/18:3
TG 20:3/18:2/18:2
TG 26:0/12:4/22:6
TG 39:2
TG 40/16:0/16:0
TG 40/16:0/16:1
TG 40/16:0/18:1
TG 40/16:0/18:2
TG 41:2
TG 41:3
TG 60/14:0/18:0
TG 60/16:0/18:1
TG 60/16:0/18:2
TG 60/18:1/18:1
TG 60/18:2/18:2
TG 60/18:3/24:1
TG 60:8
TG 69:10

3.4: DISCUSSION

The etiologic connection between a FA DDR pathway defect and the metabolic abnormalities observed in FA patients and cells is not understood. Further, the specific DNA lesions and cellular aberrations that arise and contribute to disease phenotypes in the absence of an intact FA pathway are incompletely characterized. Recent work suggests the FA pathway regulates multiple components of cellular metabolism, including energy and lipid metabolism, in addition to its canonical functions in DNA repair (313, 333, 339, 341). In this study, we tested the *in vivo* sensitivity of FA deficient mice to challenge with a high lipid diet (WD) or a high fat, high cholesterol, cholic acid enriched diet (PD) to probe if FA deficiency would result in increased DNA damage accumulation and/or altered cellular metabolism after these two distinct metabolic challenges. We show that male *Fancd2*$^{-/-}$ mice are highly sensitive to PD-induced hepatobiliary pathology relative to WT mice in a sex-dependent manner, and differ in hepatic lipid metabolism.

FA deficiency is known to cause hypersensitivity to aldehydes produced from ethanol metabolism, particularly in hematopoietic stem cells (387). We predicted that metabolic byproducts of lipid metabolism, such as reactive oxygen species and lipid peroxidation products, might also be sources of damage to which FA deficient cells would be sensitive. We found no evidence that PD feeding leads to altered bone marrow or blood cell counts, suggesting that metabolic byproducts resulting from lipid metabolism did not overtly impact hematopoietic cells in *Fancd2*$^{-/-}$ mice (Supporting Results and Figure 3.S11). However, male *Fancd2*$^{-/-}$ mice did demonstrate hepatocellular sensitivity to PD feeding, showing increased serum BA and markers of hepatobiliary damage, biliary hyperplasia, greater hepatomegaly and hepatocellular swelling, and increased hepatic inflammation. Though it is possible that some pathologies were common to both WT and *Fancd2*$^{-/-}$ mice but differed in severity, several of the PD-induced pathologies were apparent only in *Fancd2*$^{-/-}$ mice.

We initially evaluated evidence that canonical FA pathway functions in DNA damage and oxidative stress responses limited hepatic pathology in PD fed mice. It has been proposed that redox imbalances and oxidative stress contribute to cellular and organismal FA phenotypes, potentially including the metabolic

phenotypes seen in FA (203, 208, 428). However, we found only mildly increased DNA damage in PD-fed *Fancd2*$^{-/-}$ mice and no genotype specific PD-induced changes in antioxidant gene expression. We also report the novel finding of increased expression of genes encoding TLS polymerases Polθ and Polκ upon PD feeding in male *Fancd2*$^{-/-}$ mice. It has been reported that *Fancd2* and *Polθ* expression are correlated in ovarian carcinoma, and that homologous recombination deficient tumors are hypersensitive to inhibition of Polθ mediated repair (429, 430). Our results are consistent with increased reliance on lower fidelity repair pathways, such as alternative end-joining, in *Fancd2*$^{-/-}$ mice upon PD feeding. However, the severity of the hepatobiliary phenotype led us to explore additional roles for FANCD2 in hepatic metabolism.

As PD fed male *Fancd2*$^{-/-}$ mice were hypersensitive to hepatic and biliary pathology, we quantified expression of genes involved in hepatic BA and cholesterol metabolism. We found no BA gene expression differences that appeared causal of the phenotype. More likely to contribute to the PD sensitivity, we report multiple cholesterol and lipid metabolism gene expression differences in *Fancd2*$^{-/-}$ mice fed PD, including decreased hepatic expression *of Ldlr* (LDL receptor), and *Scpx/2* (cholesterol transporters), and a lack of a significant increase in *Abcg5/8* (cholesterol exporters) and *Srebf* and *Scd1* (fatty acid synthesis regulators). Though we did not detect differences in serum or hepatic bulk cholesterol or differential proportions of serum cholesterol species, untargeted lipidomic profiling revealed differences across sphingolipid, glycerophospholipid, and glycerolipid classes. Altered lipid accumulation may have led to the increase in hepatocyte size observed in *Fancd2*$^{-/-}$ mice upon PD challenge.

Altered hepatic lipid metabolism is correlated with insulin and glucose homeostasis. Though we did not observe differences in fasting glucose between diets or genotypes in either sex, gluconeogenesis enzymes encoded by *G6pc* and *Pck1* trended towards lower expression in *Fancd2*$^{-/-}$ male mice fed PD (Figure 3.S12). We did not fully characterize insulin and glucose homeostasis in this model, and it is possible that altered lipid metabolism associated with FA defects (i.e. ceramide accumulation) may impact glucose regulation in human FA patients.

Altered lipid abundances could both contribute to the hepatobiliary phenotype observed in *Fancd2*$^{-/-}$ mice upon PD feeding, as well as result from hepatoprotective compensatory responses. Components of

cholesterol-glycosphingolipid rafts are protective against the cytotoxic effects of bile acids (431, 432) and the ratio of PC and PE may be important in hepatocyte protection from cholestatic liver injury (433).

Two independent cohorts fed PD for 55 days or 10 weeks showed the genotype-dependent differences in cholesterol gene expression (Figure 3.S4), suggesting these cholesterol metabolism differences are intrinsic phenotypes in *Fancd2*$^{-/-}$ mice upon PD challenge. Genotype-dependent expression differences in TLS polymerases and inflammation markers were not seen in the 10 week cohort, which may be due to increased damage in both genotypes after the longer 10 week challenge. The transcriptional differences were specific to PD feeding, as a distinct high fat diet, WD, did not elicit the same genotype-dependent cholesterol gene expression differences (Figure 3.S5).

Several of the cholesterol and lipid metabolism genes with increased expression in WT but not *Fancd2*$^{-/-}$ mice fed PD are transcriptional targets positively regulated by the nuclear receptor LXR, including *Abcg5*/8, *Srebf*, *Scd-1*, *Acat1*, and *Lxr* itself (412, 434, 435), suggesting some LXR-dependent transcriptional pathways are differentially regulated in *Fancd2*$^{-/-}$ mice. LXR also regulates *Cyp7a1* (434), which was decreased in PD-fed mice of both genotypes, but had roughly half the expression in WD-fed *Fancd2*$^{-/-}$ vs WT mice. Expression of *Abcg1*, which is also positively regulated by LXR, was an exception, as only *Fancd2*$^{-/-}$ mice significantly increased its expression following PD. However, when treated with the synthetic LXR agonist T0901317, male WT and *Fancd2*$^{-/-}$ mice had similar upregulation in LXR target gene expression, indicating that *Fancd2*$^{-/-}$ mice are capable of appropriate LXR transcriptional activity when LXR is activated by this agonist (Figure 3.S13). Our finding of altered LXR target gene expression is also interesting in light of reports that miR-206, which represses LXR activity, is reduced in FA cells (393, 397). Multiple transcriptional corepressors and coactivators have ligand-dependent interactions with LXR (436), thus differential expression of LXR targets in *Fancd2*$^{-/-}$ mice could arise from differential context-dependent activity of these cofactors. Additionally, as we have shown many lipid species are present at altered levels in PD fed *Fancd2*$^{-/-}$ livers, the endogenous ligands of LXR may be present at different levels in *Fancd2*$^{-/-}$ mice.

Interestingly, the hepatocellular sensitivity to PD feeding was specific to male *Fancd2*$^{-/-}$ mice. Female mice of both genotypes were similarly impacted by PD feeding (Supporting Results and Supporting Figure 3.S1,2,14-16). The mechanism for the sex-specific effects of PD feeding is unknown but may relate to differences in hepatic metabolism. Numerous reports exist of sex-dependent differences in mouse BA and cholesterol metabolism (437-440). Sex hormones may also play a role. Testosterone is potentially protective in the context of PD feeding, as PD feeding impacted WT males less negatively than *Fancd2*$^{-/-}$ males or females of either genotype. Gonadal dysfunction is common in FA (206), and *Fancd2*$^{-/-}$ mice show testis degeneration and germ cell loss. With the exception of one individual, male *Fancd2*$^{-/-}$ mice in our study tended to have lower serum testosterone than WT males, though individual mice varied significantly (Figure 3.S17). Whether the sex-dependent differences in hepatic metabolism observed in our FA deficient mouse model are also present in human FA patients remains to be determined.

Many FA patients have abnormalities in insulin and glucose metabolism, dyslipidemia, and metabolic syndrome (203). Our data revealing important impacts of FANCD2 in lipid and BA metabolism may be mechanistically related to these FA patient phenotypes, and suggest FA patients may respond to conventional therapy for metabolic syndrome differently than the general population. It is not yet clear what components of the metabolic alterations in FA cells are due to primary roles of the FA pathway or secondary to other defects, and the mechanism of how the FA pathway regulates lipid metabolism is unknown. The transcriptional differences in cholesterol and lipid metabolism genes indicate that at least some of the differences arise at the gene expression level. Although we did not detect transcriptional differences in TG metabolism genes, lipidomics revealed many differences in the relative abundance of triglyceride species. Likely a combination of alterations in gene expression and enzymatic activities perturbs hepatic lipid metabolism in FA.

Metabolic derangements are a hallmark of cancer cells, and it is possible some of the pre-existing metabolic phenotypes of FA cells may be relevant to their genomic instability and tumor predisposition. Potentially targeting these metabolic perturbations as part of managing FA patients could reduce their risk of cancer development. It is also possible that combining metabolism-altering therapies with genotoxic

chemotherapy may improve treatment for FA cancer patients, who are particularly sensitive to the toxic effects of common chemotherapeutic agents (201). Further exploration of the role the FA pathway plays in hepatic and systemic metabolism may reveal therapeutic targets for treatment and continue to expand the known roles of the FA pathway beyond its function in DNA repair and our understanding of the connection between the DDR and cellular metabolism.

3.5: Materials and Methods

Animal care: *Fancd2*$^{-/-}$ mice on a 129S4 background (441) were crossed onto a 129S6 background. *Fancd2*$^{-/-}$ and WT littermates were generated from *Fancd2* heterozygote crosses. The Cornell University Institutional Animal Care and Use Committee approved all animal procedures and mice were cared for in compliance with the Guide for the Care and Use of Laboratory Animals. Mice were fed one of three diets: a SD, a high fat diet enriched in cholesterol with cholic acid (PD), or a diet high in lipid alone (WD). For detailed diet composition, housing conditions and pathogen status, see Supporting Information. Male and female mice were fed diets for 50-55 days or ten weeks (if diet was started at six months of age or weaning, respectively), and fasted twelve hours during the dark cycle before euthanasia, which occurred during the light cycle.

Tissue analysis: Mice were euthanized with CO_2 and weighed. Blood was collected via cardiac puncture into microtubes containing heparin for serum chemistry or EDTA for serum lipid analysis. The liver was removed aseptically and weighed. A portion of the median lobe was frozen in liquid nitrogen for RNA isolation. Portions of the remaining liver tissue were fixed in paraformaldehyde, processed and stained with hematoxylin and eosin or immunohistochemistry (IHC). Tissues were scored for inflammation by a boarded veterinary pathologist blinded to sample identity. To assess hepatocellular swelling, the number of hepatocytes across ten 20x fields was counted. To avoid confounding differences in hepatocyte size between liver zones, fields were chosen to center around a central vein of 60-70 μm in diameter.

Serum chemistry: Plasma was separated by centrifugation, flash frozen in liquid N_2 and stored at -80ºC until analysis. An Abaxis VetScan VS2 chemistry analyzer and the VetScan VS2 Mammalian Liver

Profile kit was used to measure alkaline phosphatase, alanine aminotransferase, total BA concentration, and cholesterol in 100 ul of plasma.

Bone marrow and blood analysis: Heparinized blood was collected for hematocrit quantification. Fresh blood smear and bone marrow slides were stained with Wright's stain. The opposite femur and sternum were fixed in paraformaldelyde for bone marrow histopathology. Blood and bone marrow slides were scored by a boarded veterinary pathologist blinded to sample identity. See Supporting Information for the indices scored.

Immunohistochemistry: IHC was performed on paraformaldehyde-fixed, paraffin embedded 5 μm liver sections. See Supporting Information for details. DNA damage was assessed by γH2AX staining at 1:200 (Millipore). Secondary biotinylated anti-rabbit antibody (Invitrogen, Histostain) incubation was followed by staining with 3,3'-diaminobenzidine tetrahydrochloride (DAB) (Invitrogen) to detect positive cells. Hepatocyte apoptosis was quantified by terminal deoxynucleotidyl transferase-mediated deoxyuridine triphosphate nick-end labeling per manufacturers recommendation (TUNEL; ApopTag Kit; Millipore).

Quantitative PCR: RNA was extracted from liver samples using RNA Stat-60 (Tel-Test, Inc). Complimentary DNA (High Capacity cDNA Reverse Transcription Kit; Applied Biosystems) was synthesized from total RNA and used for qPCR (C1000 Touch Thermal Cycler, CFX96 Real-Time System, Bio Rad). Gene expression was normalized to *Rplp0* (*Arbp)* and/or *Tbp* expression. Quantification was determined via the $\Delta\Delta C_T$ method using the *Fancd2*$^{+/+}$ SD group as the comparative delta value. See Supporting Information for additional details and Supporting Table S1 for primer sequences.

Serum lipoprotein agarose electrophoresis: Lipoproteins were quantified as described in (442). See Supporting Information for details.

Serum testosterone quantification: Testosterone was measured in heparinized plasma via radioimmunoassay using ImmuChem™ Double Antibody Testosterone 125 RIA kit (MP Biomedicals) following manufacturer's protocol.

Hepatic cholesterol quantification and triglyceride: Lipid extraction was modified from (443) (see Supporting Information). Cholesterol was measured using Infinity™ Cholesterol Liquid Stable Reagent (Thermo Scientific), and triglyceride was measured with Infinity™ Triglyceride kit (Thermo Scientific) with Data-Cal™ Chemistry Calibrator (Thermo Scientific) for calibration. Absorbance was read at 500 nm on a SpectraMax190 (Molecular Devices) 96 well plate reader.

LXR agonist administration: T0901317 (Caymen Chemical) was dissolved in DMSO to 50 mg/ml, which was then diluted 2:1 with sterile phosphate buffered saline on the day of injection. Drug or DMSO only was administered at 50 mg/kg via intraperitoneal injection to adult male mice of both genotypes on the morning of day one and day two, then mice were euthanized and liver tissue was collected on the evening of day two following an eight hour fast.

Lipidomic profiling: Lipid extraction was performed as follows: Snap-frozen liver tissues (10 mg) were homogenized in 300 µL cold 50% methanol, followed by addition of 50 µL of internal standard (25 µg/ml each of TG $(15:0)_3$, PC $(17:0)_2$, phosphatidylglycerol $(14:0)_2$, LPC (20:0), phosphatidylserine $(16:0)_2$, fatty acid (18:1), C17 ceramide (d18:1/17:0) and ChE (17:0). Then 600 µL of dichloromethane was added and mixture was vortexed for 10 seconds. 300µL of liquid chromatography-mass spectrometry (LCMS) grade water was then added and vortexed again for 10 sec. The tissue homogenates were centrifuged at 13000g for 15 min at 4C. A total of 370 µL of the lower lipid-rich dichloromethane layer was then collected into silica tubes, and the solvent was evaporated to dryness under vacuum. Samples were reconstituted in 150 µL of acetonitrile/isopropanol/H2O (65:30:5 v/v/v) prior to injection. Two uL was injected for LCMS, which was performed on a Vanquish ultra-high performance liquid chromatography system with an Accucore C30, 2.6 µm column (2.1 mm id x 150mm) coupled to a Q Exactive™ Hybrid Quadrupole-Orbitrap High Resolution Mass Spectrometer (Thermo Fisher Scientific, San Jose, CA). Data analysis was conducted with Lipidsearch™ (ThermoFisher) and Metaboanalyst 4.0 software (444, 445). For additional details, see Supporting Information.

Statistical analyses: Data were analyzed nonparametrically with Kruskal-Wallis tests followed by Dunn post hoc tests for multiple comparisons with p values adjusted with the Benjamini-Hochberg method. For

histology and IHC data, an average number per mouse was used with the exception of bile duct quantification, in which case all counts were included in the analysis and a random mouse effect was included in the linear mixed effects model. Kaplan Meier survival curves were compared by log rank test. qPCR comparisons were performed on ΔC_T values per mouse. *p* values of ≤ 0.05 were considered statistically significant. Data are presented as mean ± standard error of the mean, or as box and whisker plots showing 25^{th} to 75^{th} percentiles (box) and minimum and maximum (whiskers), with the median indicated by the horizontal bar. All analyses were made with R-3.4.1 (R Core Team (2015)) and GraphPad Prism version 7.03 for Windows (GraphPad Software). For lipidomics, analyses of normalized data collected in positive ion mode were summed within lipid species. Data were then generalized log-transformed, auto-scaled and subject to partial least squares discriminant analysis and ANOVA with an adjusted p vale (FDR) cutoff of 0.05 and post-hoc analyses by Fischer's least significant difference test. Heat maps were generated using Euclidean distance measure and Ward clustering algorithm. All lipidomics analyses were performed in Metaboanalyst 4.0 software (444, 445).

3.6 Supplemental Material

3.6.1 Supporting Experimental Procedures

Animal husbandry and diets: Mice were housed under specific pathogen-free conditions in an Association for the Assessment and Accreditation of Laboratory Animal Care International accredited facility and cared for in compliance with the Guide for the Care and Use of Laboratory Animals (446). Mice were on a 12:12 light:dark cycle in individually ventilated cages (Mouse Cage PC7115HT, Allentown, Inc., Allentown, NJ) containing ¼ inch autoclaved corn cob bedding (7097A, Harlan Teklad, Frederick, MD), a cardboard hut (Refuge XKA-2450-087, Ketchum Manufactoring Inc, Brockville, Ontario), and a sterile nesting pad (Nestlets, Ancare, Bellmore, NY). Mice were free of Sendai virus, mouse hepatitis virus, mouse parvovirus, minute virus of mice, epizootic diarrhea of infant mice, reovirus type 3, pneumonia virus of mice, ectromelia virus, Theiler murine encephalomyelitis virus, lymphocytic choriomeningitis virus, mouse adenovirus, polyoma virus, Mycoplasma pulmonis, cilia-associated

respiratory bacillus, murine pinworms (Aspicularis and Syphacia spp.) and mouse ectoparasites. Mice received irradiated food and reverse osmosis, hyper-acidified water ad libitum. Mice were fed one of three diets: the normal chow used in Cornell animal facilities referred to as standard diet (SD) (0% cholesterol, 0% cholic acid, 5.8% triglyceride; 7012 Harlan Teklad LM-485 Mouse/Rat Sterilizable Diet), a high fat Paigen diet (PD) (1.25% cholesterol, 0.5% cholic acid, 15.8% triglyceride; TD.880511, Harlan, Teklad Lab Animal Diets), or a western diet (WD) (~0.028% cholesterol, 0% cholic, 34.9% triglyceride; D12492 Research Diets Inc.).

Bone marrow and blood smear analysis: Blood smear cytologic analysis included a white blood cell and platelet estimate, and differential counts (percentages) of neutrophils, band neutrophils, lymphocytes, monocytes, eosinophils, and basophils. A fresh bone marrow slide was prepared for cytology from the distal femur via the paintbrush technique as described in (447) and Wright's stained. Bone marrow cytology included a myeloid:erythroid ratio, and percentages of lymphocytes, plasma cells, and macrophages based on a 500 cell differential count. Bone marrow histopathology included an estimated cellularity (estimated in ten percent increments of hematopoietic cells relative to the percentage of fat), and an average count of megakaryocytes in ten high power (400x) fields.

Histology and Immunohistochemistry: Sections on Superfrost Plus slides (Fisher) were first deparaffinized and rehydrated. After heat mediated antigen retrieval in citrate buffer, endogenous peroxidase was quenched via incubation in a solution of 30% hydrogen peroxide 1:9 in absolute methanol. Slides were blocked with a 4% bovine serum albumin solution followed by incubation with the primary γH2AX antibody overnight at 1:200 (Millipore). Secondary biotinylated anti-rabbit antibody (Invitrogen, Histostain) incubation was followed by staining with 3,3'-diaminobenzidine tetrahydrochloride (DAB) (Invitrogen) to detect positive cells. Sections were counterstained with hematoxylin, cover-slipped, and images were obtained using an Aperio Scanscope (Aperio Technologies, USA) and Fiji software (ImageJ) for random field selection. The number of positive and negative γH2AX, and TUNEL hepatocytes was counted and expressed as the percentage of positive cells in ten randomly chosen 20x fields per mouse, with the exception that fifteen random 20x fields per male mouse were quantified for TUNEL staining. To be selected for bile duct quantification in H&E stained sections,

the portal vein of the triad had to be in cross section and between 65 μm and 200 μm in diameter. The number of bile duct profiles was counted in the maximum number of qualifying triads (ten to nineteen triads per mouse). Samples from *Atm*-deficient mice and matched controls were from a previous study (401).

Quantitative PCR: The GeNorm procedure outlined in Vandesompele et al (448) lead to the selection of ARBP and TBP as the best normalization genes, therefore, gene expression levels were normalized to Rplp0 (ARBP) and/or TBP expression. The following primer sequences were acquired from published work: Scl22a7, Sclo1a1, Slco1a4 from (449), Srb1 (Scarb1) from (450), and G6pc from (451). Primer sequences are listed in Supporting Table S1.

Serum lipoprotein agarose electrophoresis: Blood from cardiac puncture was collected in heparin containing microtubes and serum was separated by centrifugation. Samples were loaded by volume into a 1% agarose gel and separated by horizontal electrophoresis at 80V for 55 min in 60 mM sodium barbital buffer. Gels were stained overnight in 0.18% Sudan black B in 70% ethanol, then destained with 15% acetic acid/20% acetone before scanning and quantification via converting pixel intensity to a linear peak followed by area under the curve calculation with Image J software.

Hepatic cholesterol and triglyceride quantification: Procedures for lipid extraction were modified from (443). Roughly 100mg of frozen liver was weighed and homogenized with 4 g of sodium sulfate in a mortar and pestle and transferred to a glass tube, to which 4 ml of methanol and 8 ml of choloroform were added. The mixture was vortexed for one minute and stored at 4◦ C for 24 hours. The following day, 2.4 ml of 0.7% NaCl was added without agitation. The solution was stored for an additional 24 hours at 4◦ C. The supernatant was then removed by aspiration and 5 ml of the chloroform was transferred to a new glass tube and evaporated under 100% nitrogen gas. After all chloroform had evaporated, 250 ul of 2-propanol was added to each tube followed by 1 minute of vortexing. The sample was centrifuged at 10,000 g for 1 min to remove any tissue debris.

Lipidomics of liver tissue:

Sample preparation: Stock lipid standards were prepared by dissolving them in dichloromethane (DCM)/methanol (MeOH; 2:1 v/v) at concentration ranging 1 to 5 mg/ml which were stored at -20°C.

The final internal standard mixture which was spiked into each sample before extraction consisted of 25 μg/mL of Triglycerides 15:0/15:0/15:0, Phosphatidylcholine 17:0/17:0, Phosphatidylglycerol 14:0/14:0, Lysophosphatidylglycerol 20:0, Phosphatidylserine PS $(16:0)_2$ PS (16:0), Oleic acid (Fatty acid 18:1 (n-9)), Ceramide (d18:1/17:0) and 17:0 Cholesteryl ester. Thirty microliters of internal standard mixture were added to 30 μL sample followed by 190 μL of MeOH. Samples were then vortexed for 20 s. Next, 380 μL of DCM was added, the sample was vortexed for 20 s, and 120 μL of water was added to induce phase separation. The samples were then vortexed for 10 s and allowed to equilibrate at room temperature for 10 min before centrifugation at 8,000 × g for 10 min at 10°C. A total of 370 μL of the lower lipid-rich DCM layer was then collected and the solvent was evaporated to dryness under vacuum. Samples were reconstituted in 100 μL of acetonitrile (ACN)/2-propanol (IPA)/water (65:30:5 v/v/v) before chromatographic separation.

Liquid chromatography – mass spectrometry analysis: Chromatographic separation was performed on a Vanquish UHPLC system with an Accucore C30, 2.6 μm column (2.1 mm id x 150mm) coupled to a Q Exactive™ Hybrid Quadrupole-Orbitrap High Resolution Mass Spectrometer (Thermo Fisher Scientific, San Jose, CA). The mobile phase consisted of (solution A) 60% ACN, 40% water, 10 mM ammonium formate with 0.1% formic acid and (solution B) 90% IPA, 10% ACN, 10 mM ammonium formate with 0.1% formic acid. The gradient was as follows: 0–1.5 min, 32% solvent B; 1.5-4 min,32-45% solvent B; 4-5min, 45-52% solvent B; 5-8min 52-58% solvent B; 8-11min, 58-66%solvent B; 11-14 min, 66-70% solvent B; 14-18 min, 70-75% solvent B; 21-25min, isocratic 97% solvent B, 25-25.1min 97-32% solvent B; followed by 4 min of re-equilibration of the column before the next run. The flow rate was 260 μl/min. All of the samples were analyzed by electrospray ionization in data-dependent MS-MS mode, nitrogen as sheath, auxiliary, and sweep gas was set at 50, 5, and 1 U, respectively. Other conditions included: resolution, 120,000 full width at half maximum; automatic gain control target, 3e6 ions; maximum injection time, 100 ms; scan range, 67-1000 *m/z*; spray voltage, 3.50 kV; and capillary temperature, 275°C. Data-dependent MS-MS spectra were generated through the use of the following conditions: resolution, 15,000 full width at half maximum; automatic gain control target, 1e5 ions; maximum

injection time, 50 ms; isolation window, 0.4m/z; and stepped normalized collision energies 25 and 35. To avoid possible bias, the sequence of injections were randomized.

Acquired data were processed using LipidSearch™ software version 4.1 (Thermo Scientific) with the following workflow: First, the individual data files were searched for product ion MS/MS spectra of lipid precursor ions. MS/MS fragment ions were predicted for all precursor adduct ions measured within ± 5 ppm. The product ions that matched the predicted fragment ions within a ± 5 ppm mass tolerance was used to calculate a match-score, and those candidates providing the highest quality match were determined. Next, the search results from the individual positive ion files from each sample group were aligned within a retention time window (± 0.1 min) and the data were merged for each annotated lipid. The annotated lipids were then filtered to reduce false positives using criteria such as those listed on Table S2. Lipids were then normalized by class using the internal standard mix added before the extraction and normalized to weight of liver tissue analyzed.

3.6.2 Supporting results

Paigen diet challenge in the absence of FANCD2 does not impact hematopoiesis.

Anemia and bone marrow defects are important components of the FA phenotype in humans, though unchallenged FA deficient mice have subtler bone marrow phenotypes. Products of cellular metabolism, such as aldehydes, have been reported to contribute to anemia and hematopoietic stem cell damage in FA deficient mice (452). As the metabolism of lipids also leads to the production of potentially damaging metabolic byproducts, we evaluated peripheral blood and bone marrow smears made at terminal collection, and bone marrow histology. Neither Paigen diet (PD) nor Western diet (WD) feeding led to changes in peripheral blood cell counts or bone marrow cytology/histology in either genotype or sex (Figure 3.S11). This indicates that neither feeding the high fat, high cholesterol, cholic acid diet nor the high lipid diet has a substantial impact on bone marrow or hematopoietic stem cell function in Fancd2-/- mice.

Fancd2 genotype-dependent differences in Paigen diet induced hepatic pathology and cholesterol metabolism gene expression were observed in male mice only.

The difference in response to PD feeding between WT and *Fancd2*$^{-/-}$ mice was specific to males. In male *Fancd2*$^{-/-}$ mice, we observed increased morbidity/mortality, increased serum BA (bile acids) and liver enzymes, increased hepatomegaly and hepatocellular swelling, increased hepatic inflammation, decreased expression of hepatic BA uptake receptors and differential expression of hepatic cholesterol metabolism genes upon PD challenge. In female mice, PD feeding resulted in indices of hepatobiliary damage in both genotypes, including increased serum BA and hepatic bile duct profiles (Figure 3.S1A,B), trends towards increased hepatomegaly and hepatocellular size, elevated plasma levels of ALT and ALP, increased hepatic parenchymal polymorphonuclear cell scores and inflammatory markers (Supporting Figure S2A-F), and increased γH2AX and TUNEL positive hepatocytes (Figure 3.S14A, B). Similar to findings in male mice, there were no significant differences in expression of *p21* or *PUMA* by diet or genotype (Figure 3.S14C). In contrast to findings in males, in females PD feeding resulted in a non-statistically significant trend towards increased *Polθ* and *Polκ* expression in both genotypes, however, the increase was generally greater in WT mice (Figure 3.S14D). Unlike findings in male mice, in which Sod1 and *Sod2* expression tended to decrease more in *Fancd2*$^{-/-}$ mice upon PD feeding, in females *Sod1* and *Sod2* expression decreased to similar degrees in both genotypes (Figure 3.S14E).

In female mice, neither genotype nor diet impacted expression of *Fxr* and *Lxr*, and in contrast to males, PD feeding resulted in a non-statistically significant increase in *Shp* expression in both genotypes (Supporting Figure 3.S15A). As in males, PD feeding was associated with decreased expression of *Cyp7a1* and *Cyp8b1* in female mice of both genotypes (Figure 3.S15B). *Cyp27A1* expression showed a similar response to PD feeding as in males, and there were no statistically significant differences in *Cyp7b1* expression by genotype or diet (Figure 3.S15B). In contrast to males, *Sult2A1* expression in female mice decreased upon PD feeding in both genotypes (Figure 3.S15B). Differential expression of *Sult2A1* between the sexes has been previously reported (453, 454). As in male mice, *Abcb11* and *Abcc2* expression was not different by diet or genotype and *Ostβ* expression was significantly increased upon PD feeding in both genotypes (Figure 3.S15C). In contrast to males, *Abcb1* (*MDR1*) expression increased in

females of both genotypes upon PD feeding (Figure 3.S15C). In female mice, the impact of diet and genotype on the expression level of BA importers was generally less dramatic than in male mice; however, expression of *Slco1a1* was differentially impacted by PD feeding in males, in which its expression decreased in

Fancd2$^{-/-}$ mice, and in females, in which PD feeding was associated with a non-statistically significant increase in *Slco1a1* expression in WT mice but did not impact its expression in *Fancd2*$^{-/-}$ mice (Figure 3.S8D). As in males, in female mice, there was an increase in serum cholesterol upon PD feeding as expected, however, there was no difference in total serum cholesterol between genotypes (Figure 3.S16A). There were no genotype dependent differences in expression of cholesterol, fatty acid, triglyceride, or glucose metabolism genes in female mice on either diet, though there were diet-dependent gene expression changes (Figure 3.S16B,C,D). These data indicate that the hepatobiliary disease sensitivity and differential hepatic cholesterol and BA metabolism gene expression upon PD feeding in *Fancd2*$^{-/-}$ mice is sex specific.

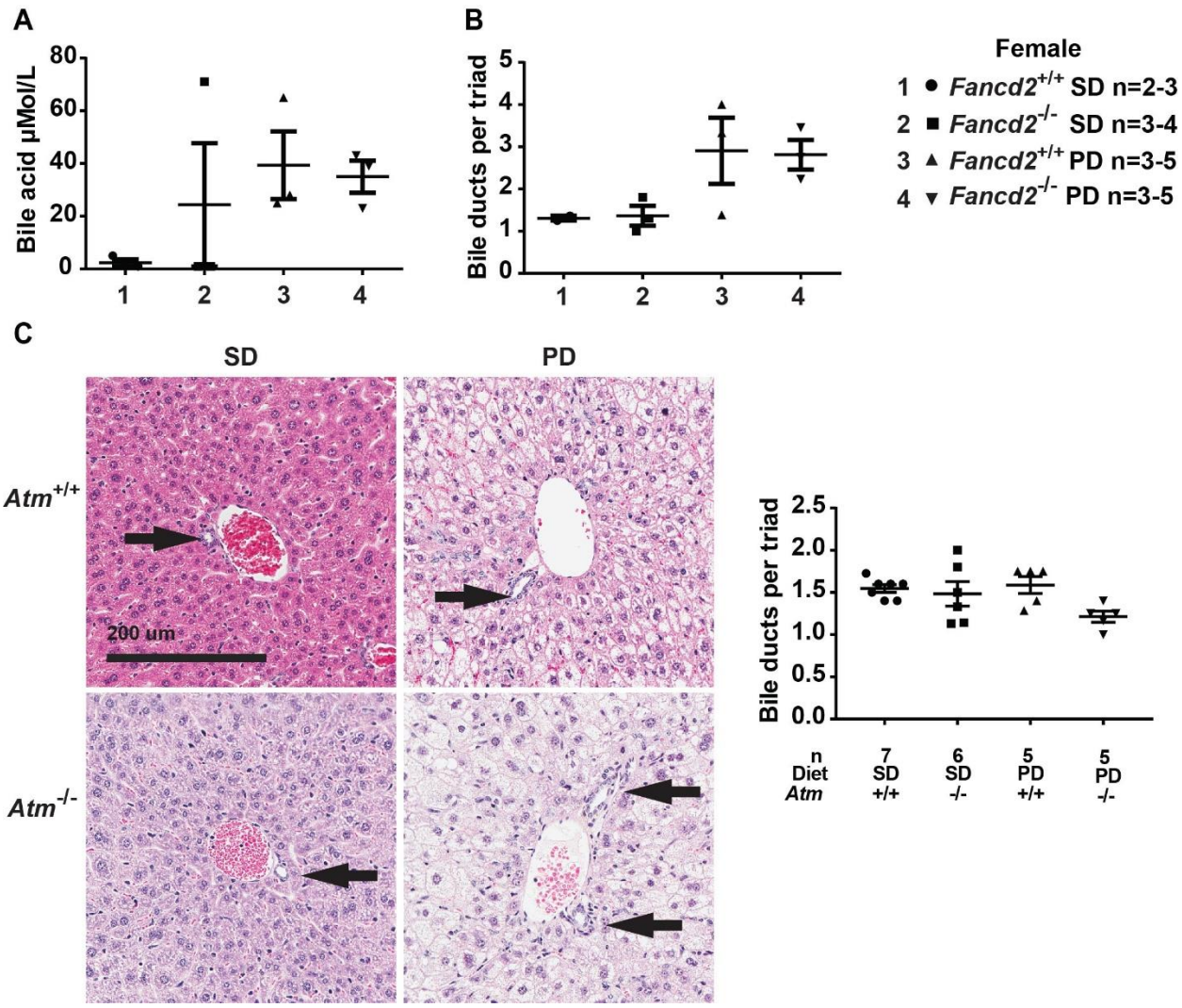

Figure 3.S1: FANCD2 status did not impact serum bile acid (BA) or biliary hyperplasia in female mice fed Paigen diet (PD), and biliary hyperplasia is not seen in all DNA damage response deficient mouse models fed PD. Mice were fed PD or standard diet (SD) for 50-55 days before terminal blood collection and liver collection. A: Serum BA did not differ significantly by genotype or diet, however, in female mice PD feeding was associated with increased serum BA in both wildtype (WT) and *Fancd2*$^{-/-}$ mice. B: Quantification of the average number of bile ducts per hepatic portal triad revealed a non-significant increase in bile duct profiles in both WT and *Fancd2*$^{-/-}$ female mice upon PD feeding. C: Biliary hyperplasia was not present upon PD feeding in an ATM deficient mouse model on a FVB/N

background. Hematoxylin and eosin stained liver sections showing hepatic portal triads and bile duct quantification. Error bars represent SEM.

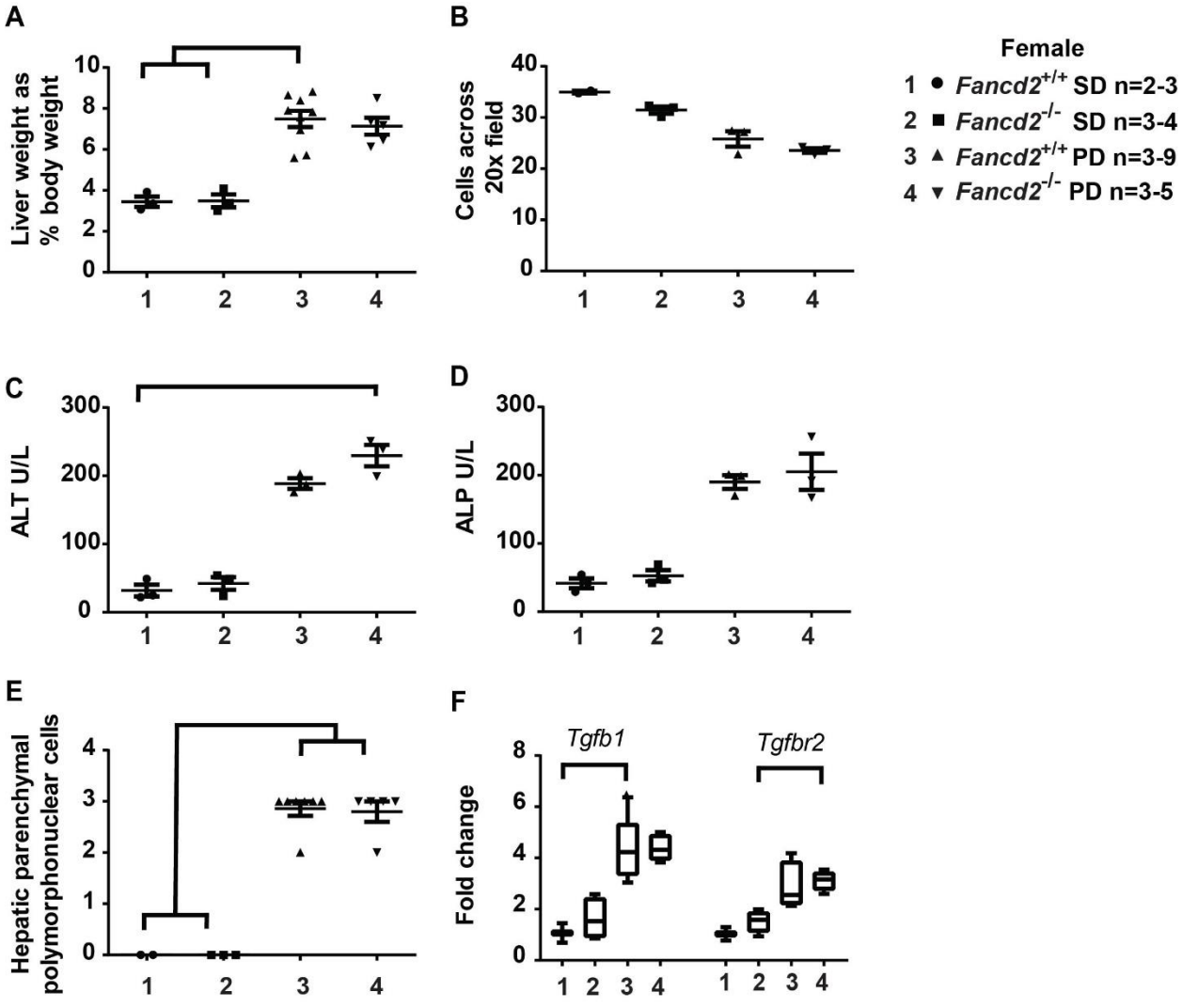

Figure 3.S2: Paigen diet (PD) feeding induced hepatomegaly, hepatic damage, and hepatic inflammation in both wildtype (WT) and *Fancd2*$^{-/-}$ female mice. PD or standard diet (SD) was fed for 50-55 days before terminal blood collection and liver collection. Serum chemistry was analyzed using an Abaxis VetScan VS2 chemistry analyzer. A: PD feeding was associated with an increased liver weight

relative to body weight in both WT and *Fancd2*$^{-/-}$ mice, though the difference was statistically significant only for WT PD fed mice vs WT standard diet (SD) ($p = 0.038$) and *Fancd2*$^{-/-}$ SD fed mice ($p = 0.024$). B: PD feeding increased hepatocyte size, decreasing the average number of cells across ten 20x fields in both WT and *Fancd2*$^{-/-}$ mice, though the trends were not significant. C: Female WT and *Fancd2*$^{-/-}$ mice fed PD had increased serum alanine aminotransferase (ALT), a marker of hepatocellular damage, though the difference was only significant in *Fancd2*$^{-/-}$ mice fed PD vs WT SD fed mice ($p = 0.046$). D: Female WT and *Fancd2*$^{-/-}$ mice fed PD had a trend towards increased alkaline phosphatase (ALP), a marker of hepatobiliary damage, though there were no statistically significant differences by diet or genotype. E: Scores for hepatic parenchymal polymorphonuclear cells (inflammation) obtained from hematoxylin and eosin stained liver sections demonstrating that PD feeding was associated with increased hepatic inflammation regardless of genotype in female mice (F value for impact of diet = 5.91E-06). F: PD feeding resulted in similar increased expression of genes encoding the inflammatory marker TGF beta (Tgfb1) and its receptor Tgfbr2 in WT and *Fancd2*$^{-/-}$ female mice ($p < 0.05$). Expressed as fold change relative to WT SD fed mice. Error bars represent SEM. Box and whisker plots show 25th to 75th percentiles (box) and minimum and maximum (whiskers), with the median indicated by the horizontal bar.

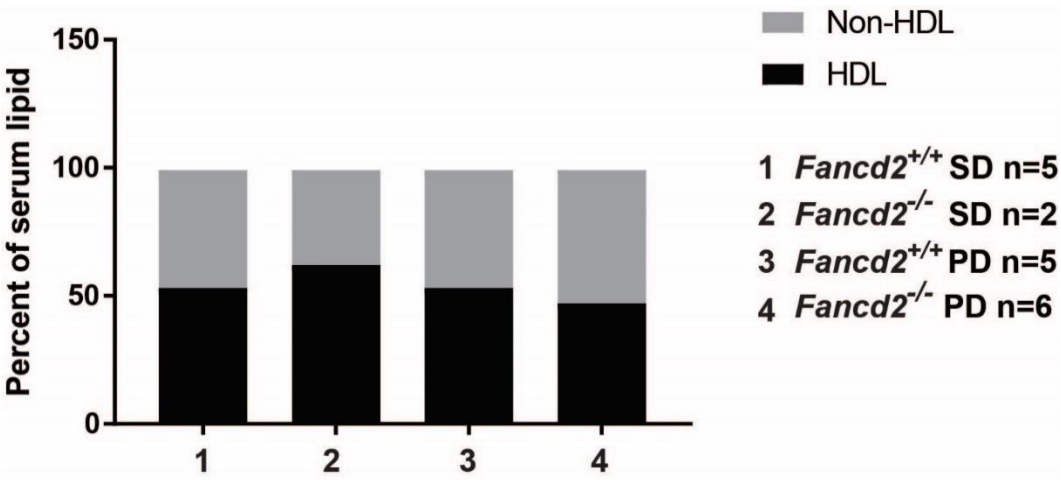

Figure 3.S3: The proportions of serum high density lipoproteins (HDL) and non-HDL did not differ by Fancd2-status or diet. Male mice of the indicated genotypes were fed standard diet (SD) or Paigen diet (PD) for 55 days before terminal cardiac blood collection and serum lipoprotein analysis via gel electrophoresis and Sudan black staining following by lipoprotein band quantification. Data shown as the percent of total serum lipoproteins.

Figure 3.S4: *Fancd2* dependent differential expression of genes involved in cholesterol metabolism are also present in male mice fed Paigen diet (PD) for ten weeks. In addition to the cohort of mice fed PD for 50-55 days starting at weaning (main figures), a cohort of male mice was fed PD or standard diet (SD) for ten weeks starting at 21 days of age. RNA extracted from liver was used for quantitative PCR. Comparisons expressed as fold change relative to the WT SD group. A: PD feeding for ten weeks was associated with increased expression of genes encoding the inflammatory marker TGF beta (Tgfb1) and its receptor Tgfbr2 in wildtype (WT) and *Fancd2*$^{-/-}$ male mice. B: Both WT and *Fancd2*$^{-/-}$ male mice had increased expression of *Cdkn1a*, encoding the DNA damage response marker p21, and translesion DNA polymerase encoding genes Polκ and Polθ when fed PD for ten weeks. C: No significant differences were found by diet or genotype in the expression of hepatic nuclear receptor genes. D: Similar to the cohort of male mice fed PD for 50-55 days, PD feeding for ten weeks was associated decreased expression of three hepatic bile acid (BA) uptake receptor encoding genes (*Slc10a1* (*NTCP*), *Slc22a7* (*OAT2*) and *Slc1a1*) in male *Fancd2*$^{-/-}$ mice relative to standard diet (SD) fed mice, which is consistent with accumulated bile acids and associated cytotoxicity. E: As observed in the cohort fed PD for 50-55 days, male *Fancd2*$^{-/-}$ mice fed PD for ten weeks showed differential expression of genes involved in cholesterol transport, export, and import. F: Similar to the cohort of mice fed PD for 50-55 days, ten weeks of PD feeding resulted in decreased *Acat1* expression in male *Fancd2*$^{-/-}$ mice, and a trend towards increased expression of *Srebf1*, encoding a fatty acid regulating transcription factor, in male WT mice but not in *Fancd2*$^{-/-}$ mice. Also consistent with the main cohort, *Fancd2*$^{-/-}$ male mice fed PD for ten weeks had decreased expression of *Fasn*. Box and whisker plots show 25th to 75th percentiles (box) and minimum and maximum (whiskers), with the median indicated by the horizontal bar. $p < 0.05$ for all pairwise comparisons indicated.

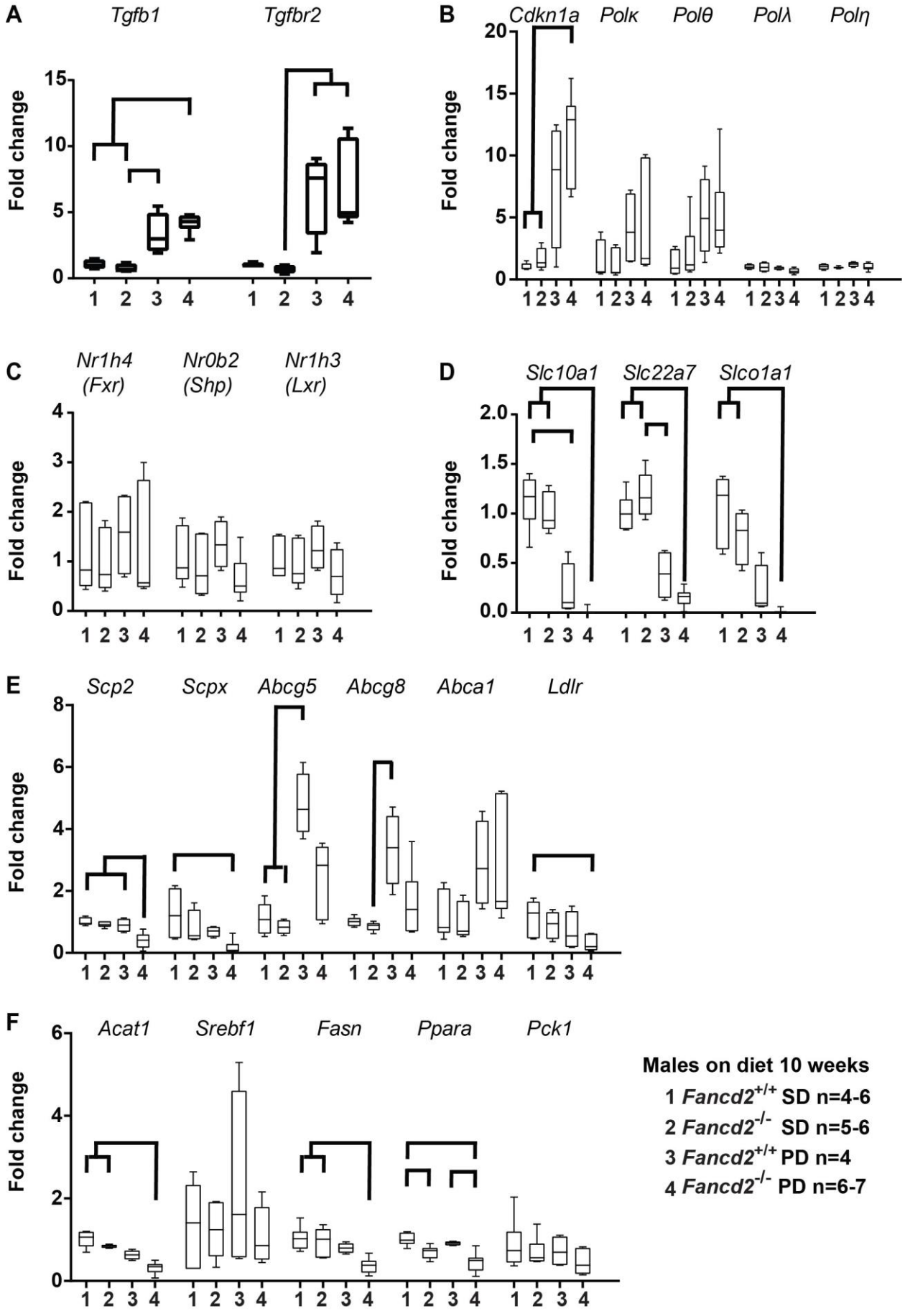
A
Tgfb1
Tgfbr2
Fold change
B
Cdkn1a
Polκ
Polθ
Polλ
Polη
C
Nr1h4 (Fxr)
Nr0b2 (Shp)
Nr1h3 (Lxr)
D
Slc10a1
Slc22a7
Slco1a1
E
Scp2
Scpx
Abcg5
Abcg8
Abca1
Ldlr
F
Acat1
Srebf1
Fasn
Ppara
Pck1
Males on diet 10 weeks
1 Fancd2+/+ SD n=4-6
2 Fancd2-/- SD n=5-6
3 Fancd2+/+ PD n=4
4 Fancd2-/- PD n=6-7

Figure 3.S5: *Fancd2*-dependent differential expression of genes involved in the DNA damage response, inflammation and hepatic metabolism are specific to Paigen diet (PD) feeding and not present with Western diet (WD) feeding. In addition to PD diet feeding, which is enriched in cholesterol and contains cholic acid, wildtype (WT) and *Fancd2*$^{-/-}$ mice were also fed a high lipid WD, which is not enriched in cholesterol and does not contain cholic acid. RNA extracted from liver was used for quantitative PCR. A-E show expression in male mice of select genes in which genotype dependent differences were observed upon PD feeding as fold change relative to WT standard diet (SD) fed mice, including both PD and WD fed mice. The gene expression data of SD and PD fed mice were already represented in Figures 2-5. With WD feeding, both WT and Fancd2$^{-/-}$ mice have similar expression of the DNA damage response marker cdkn1a (p21), the genes encoding translesion DNA polymerases Polκ, and Polθ (A), and the genes encoding the inflammatory marker Tgfb1 and its receptor Tgfbr2 (B). C: Similarly, expression of genes encoding nuclear receptors Nrlh4 (FXR), Nr0b2 (SHP), and Nrlh3 (LXR) were not significantly different between WT and *Fancd2*$^{-/-}$ mice fed WD. D: A single bile acid (BA) synthesis enzyme encoding gene, *Cyp7a1*, trended towards differential expression between genotypes on WD, which was not discernable on PD (where both genotypes drastically decreased expression). E: In contrast to what was observed with PD feeding, expression of genes encoding BA importers was similar between genotypes fed WD. F: Unlike with PD feeding, WT and *Fancd2*$^{-/-}$ mice had similar expression of cholesterol metabolism genes when fed WD. Box and whisker plots show 25th to 75th percentiles (box) and minimum and maximum (whiskers), with the median indicated by the horizontal bar. $p < 0.05$ for all pairwise comparisons indicated.

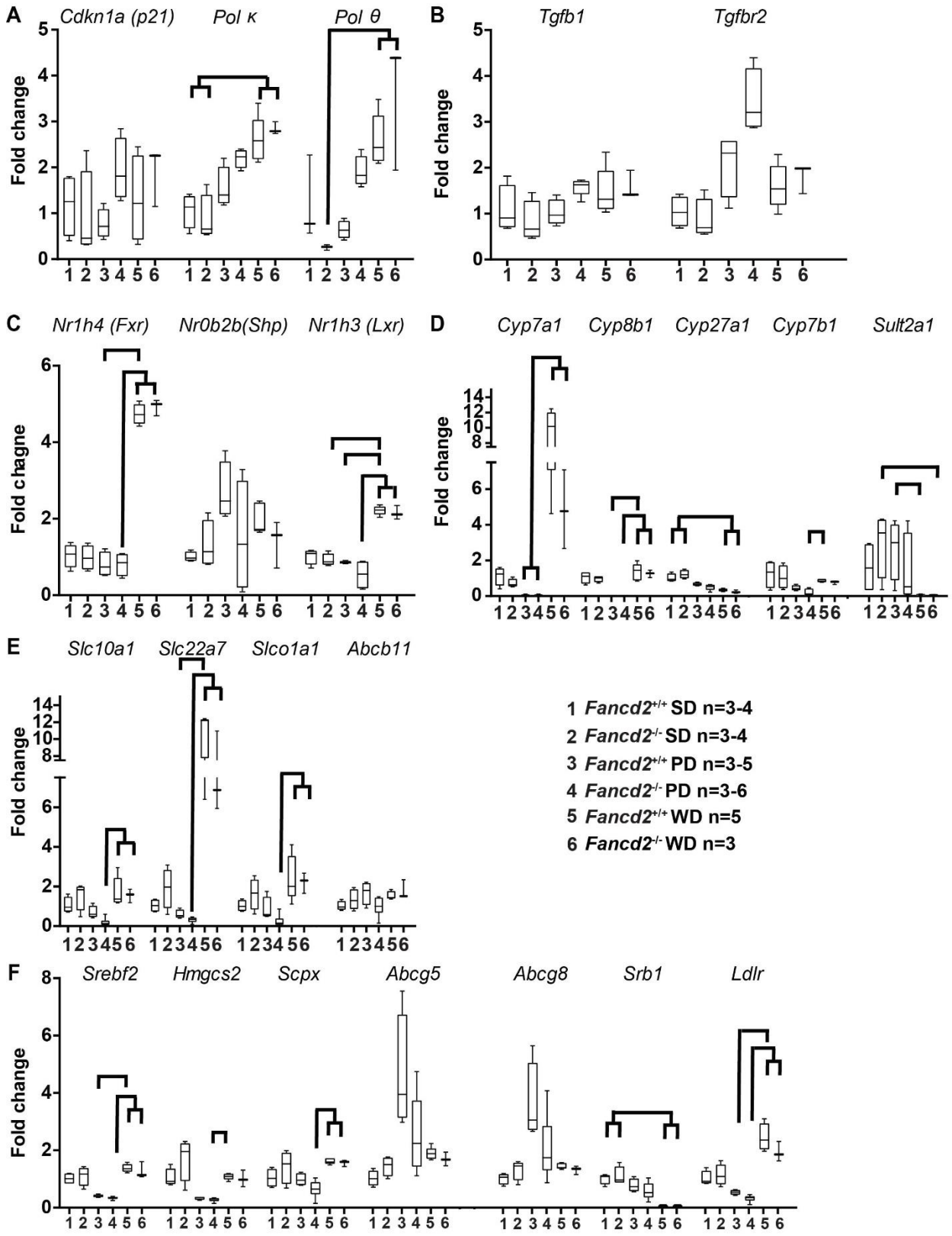
A
Cdkn1a (p21)
Pol κ
Pol θ
Fold change
B
Tgfb1
Tgfbr2
Fold change
C
Nr1h4 (Fxr)
Nr0b2b(Shp)
Nr1h3 (Lxr)
Fold chagne
D
Cyp7a1
Cyp8b1
Cyp27a1
Cyp7b1
Sult2a1
Fold change
E
Slc10a1
Slc22a7
Slco1a1
Abcb11
Fold change
1 Fancd2+/+ SD n=3-4
2 Fancd2-/- SD n=3-4
3 Fancd2+/+ PD n=3-5
4 Fancd2-/- PD n=3-6
5 Fancd2+/+ WD n=5
6 Fancd2-/- WD n=3
F
Srebf2
Hmgcs2
Scpx
Abcg5
Abcg8
Srb1
Ldlr
Fold change

Figure 3.S6: Lipidomics revealed that male *Fancd2*$^{-/-}$ mice differed in hepatic sphingolipid, glycerophospholipid, and glycerolipid species abundance, particularly upon Paigen diet (PD) feeding. After feeding Paigen diet (PD) or standard diet (SD) for 50-55 days, livers were collected and lipids extracted for untargeted lipidomics. **A**: Proportions of detected lipids in each class. **B**: Variable importance in the projection (VIP) scores of the top 20 lipid species. **C**: Heat map of the top 20 lipid species with significantly different abundances on PD. Ceramides (Cer); Cholesterol esters (Chol E); Coenzyme Q (CoQ); Diacylglycerols (DG); Lysophosphatidylcholine (LPC); Phosphatidlycholines (PC); Phosphatidylethanolamines (PE); Phosphatidylglycerol (PG); Sphingomyelins (SM); Triacylglycerols (TG).

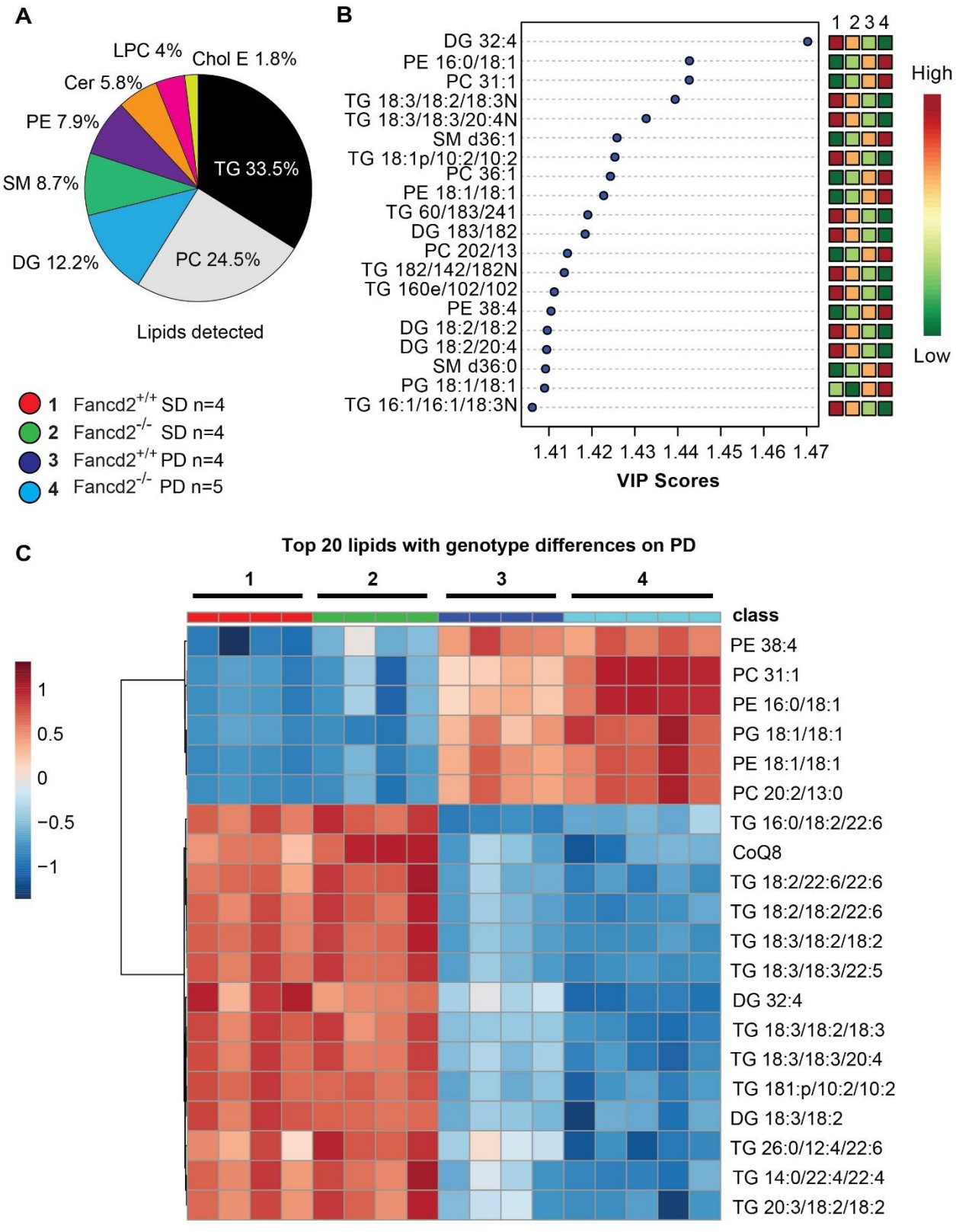
A
LPC 4%
Chol E 1.8%
Cer 5.8%
PE 7.9%
SM 8.7%
TG 33.5%
DG 12.2%
PC 24.5%
Lipids detected
1 Fancd2+/+ SD n=4
2 Fancd2-/- SD n=4
3 Fancd2+/+ PD n=4
4 Fancd2-/- PD n=5
B
DG 32:4
PE 16:0/18:1
PC 31:1
TG 18:3/18:2/18:3N
TG 18:3/18:3/20:4N
SM d36:1
TG 18:1p/10:2/10:2
PC 36:1
PE 18:1/18:1
TG 60/183/241
DG 183/182
PC 202/13
TG 182/142/182N
TG 160e/102/102
PE 38:4
DG 18:2/18:2
DG 18:2/20:4
SM d36:0
PG 18:1/18:1
TG 16:1/16:1/18:3N
1 2 3 4
High
Low
1.41 1.42 1.43 1.44 1.45 1.46 1.47
VIP Scores
C
Top 20 lipids with genotype differences on PD
1
2
3
4
class
1
0.5
0
−0.5
−1
PE 38:4
PC 31:1
PE 16:0/18:1
PG 18:1/18:1
PE 18:1/18:1
PC 20:2/13:0
TG 16:0/18:2/22:6
CoQ8
TG 18:2/22:6/22:6
TG 18:2/18:2/22:6
TG 18:3/18:2/18:2
TG 18:3/18:3/22:5
DG 32:4
TG 18:3/18:2/18:3
TG 18:3/18:3/20:4
TG 181:p/10:2/10:2
DG 18:3/18:2
TG 26:0/12:4/22:6
TG 14:0/22:4/22:4
TG 20:3/18:2/18:2

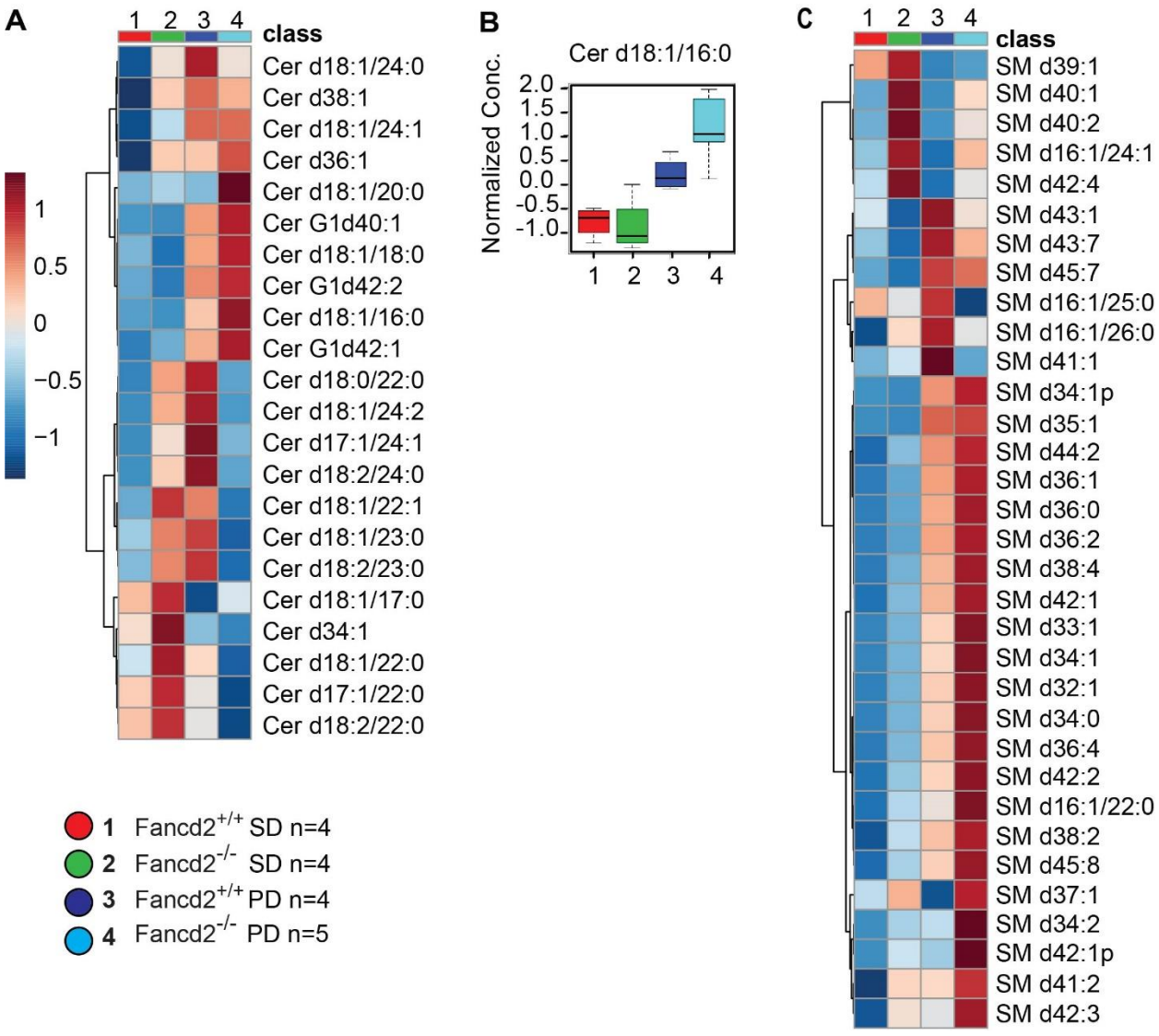

Figure 3.S7: Heatmaps of sphingolipids detected by untargeted lipidomics. After feeding Paigen diet (PD) or standard diet (SD) for 50-55 days, livers were collected and lipids extracted for untargeted lipidomics. **A**: Heatmap of all ceramide species (Cer) detected. Cer with significantly different abundances between genotypes fed PD are show in Main Fig. 6C. **B**: Normalized concentration of Cer 18:1/16:0. C: Heat map of all sphingomyelin species (SM) detected. SM with significantly different abundances between genotypes fed PD are show in Main Fig. 6C

Figure 3.S8: Heatmaps of glycerophospholipids detected by untargeted lipidomics. After feeding Paigen diet (PD) or standard diet (SD) for 50-55 days, livers were collected and lipids extracted for untargeted lipidomics. **A:** Heatmaps of all phosphatidylcholines (PC) species detected. Phosphatidylcholines with significantly different abundances between genotypes fed PD are shown in Main Fig. 6E. Heatmaps of all lysophosphatidylcholines (LPC) species detected (**B**) and lysophosphatidylcholines with significantly different abundances between genotypes on either diet (**C**). Heatmaps of all phosphatidylethanolamines (PE) species detected (**D**) and phosphatidylethanolamines with significantly different abundances between genotypes on either diet (**E**).

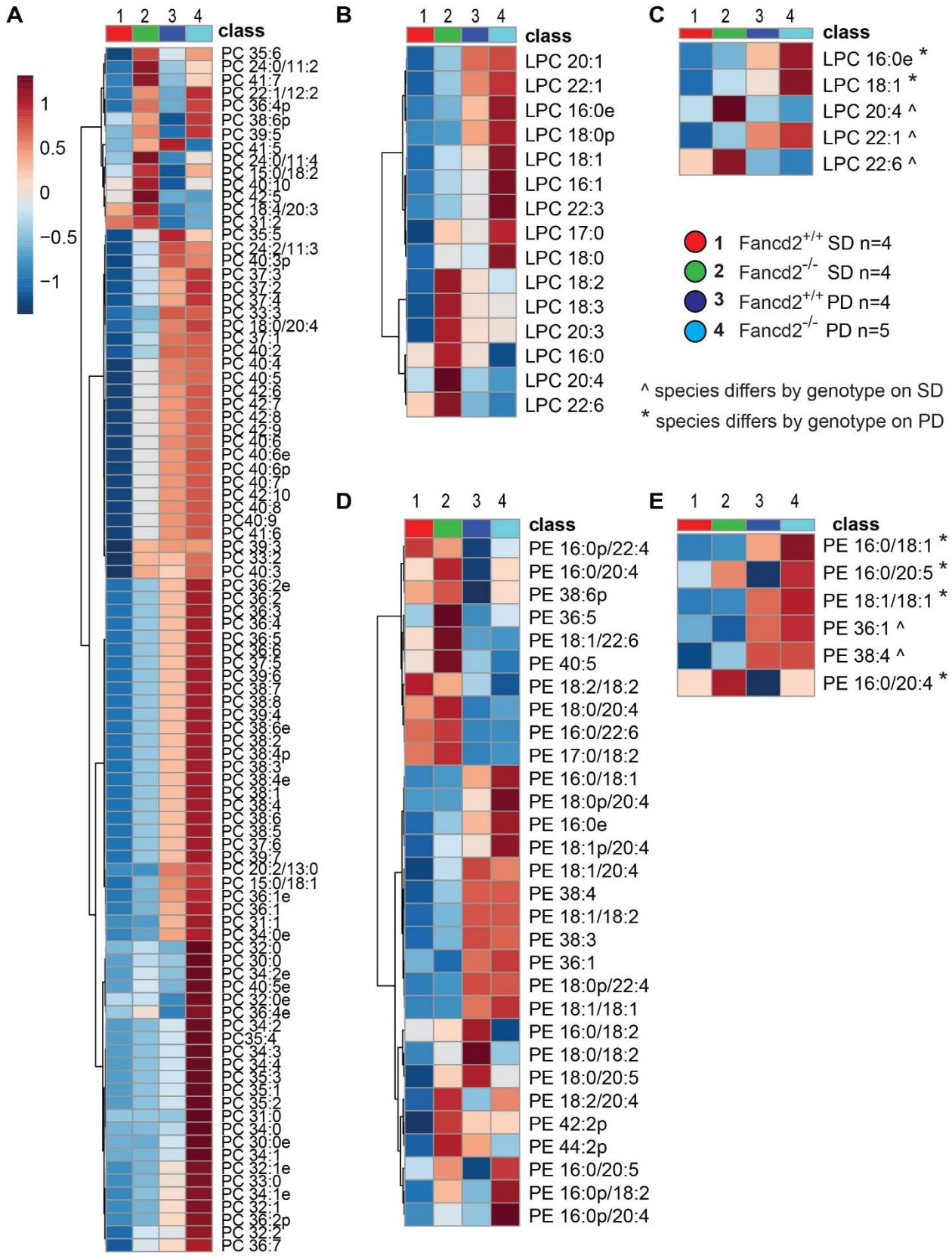
A
1 2 3 4
class
1
0.5
0
−0.5
−1
PC 35:6
PC 24:0/11:2
PC 41:7
PC 22:1/12:2
PC 36:4p
PC 38:6p
PC 39:5
PC 41:5
PC 24:0/11:4
PC 15:0/18:2
PC 40:10
PC 42:5
PC 16:4/20:3
PC 31:2
PC 35:5
PC 24:2/11:3
PC 40:3p
PC 37:3
PC 37:2
PC 37:4
PC 33:3
PC 16:0/20:4
PC 37:1
PC 40:2
PC 40:4
PC 40:5
PC 42:6
PC 42:7
PC 42:8
PC 42:9
PC 40:6
PC 40:6e
PC 40:6p
PC 40:7
PC 42:10
PC 40:8
PC40:9
PC 41:6
PC 39:3
PC 33:2
PC 40:3
PC 36:2e
PC 36:2
PC 36:3
PC 36:4
PC 36:5
PC 36:6
PC 37:5
PC 39:6
PC 38:7
PC 38:8
PC 39:4
PC 38:6e
PC 38:2
PC 38:4p
PC 38:3
PC 38:4e
PC 38:1
PC 38:4
PC 38:6
PC 38:5
PC 37:6
PC 39:7
PC 20:2/13:0
PC 15:0/18:1
PC 36:1e
PC 36:1
PC 31:1
PC 34:0e
PC 32:0
PC 30:0
PC 34:2e
PC 40:5e
PC 32:0e
PC 36:4e
PC 34:2
PC35:4
PC 34:3
PC 34:4
PC 35:3
PC 35:1
PC 35:2
PC 31:0
PC 34:0
PC 30:0e
PC 34:1
PC 32:1e
PC 33:0
PC 34:1e
PC 32:1
PC 36:2p
PC 32:2
PC 36:7
B
1 2 3 4
class
LPC 20:1
LPC 22:1
LPC 16:0e
LPC 18:0p
LPC 18:1
LPC 16:1
LPC 22:3
LPC 17:0
LPC 18:0
LPC 18:2
LPC 18:3
LPC 20:3
LPC 16:0
LPC 20:4
LPC 22:6
C
1 2 3 4
class
LPC 16:0e *
LPC 18:1 *
LPC 20:4 ^
LPC 22:1 ^
LPC 22:6 ^
1 Fancd2+/+ SD n=4
2 Fancd2-/- SD n=4
3 Fancd2+/+ PD n=4
4 Fancd2-/- PD n=5
^ species differs by genotype on SD
* species differs by genotype on PD
D
1 2 3 4
class
PE 16:0p/22:4
PE 16:0/20:4
PE 38:6p
PE 36:5
PE 18:1/22:6
PE 40:5
PE 18:2/18:2
PE 18:0/20:4
PE 16:0/22:6
PE 17:0/18:2
PE 16:0/18:1
PE 18:0p/20:4
PE 16:0e
PE 18:1p/20:4
PE 18:1/20:4
PE 38:4
PE 18:1/18:2
PE 38:3
PE 36:1
PE 18:0p/22:4
PE 18:1/18:1
PE 16:0/18:2
PE 18:0/18:2
PE 18:0/20:5
PE 18:2/20:4
PE 42:2p
PE 44:2p
PE 16:0/20:5
PE 16:0p/18:2
PE 16:0p/20:4
E
1 2 3 4
class
PE 16:0/18:1 *
PE 16:0/20:5 *
PE 18:1/18:1 *
PE 36:1 ^
PE 38:4 ^
PE 16:0/20:4 *

Figure 3.S9: Heatmaps of triacylglycerols detected by untargeted lipidomics and bulk hepatic triglyceride measurements. After feeding Paigen diet (PD) or standard diet (SD) for 50-55 days, livers were collected and lipids extracted for untargeted lipidomics or triglyceride measurement. **A:** Heatmaps of all triacylglyceride (TG) species detected. Triacylglycerides with significantly different abundances between genotypes fed PD are show in Main Fig. 6F. (**B**) Bulk hepatic triacylglyceride measurement, showing no significant differences between diets or gentoypes in total triacylglyceride. Error bars represent SEM.

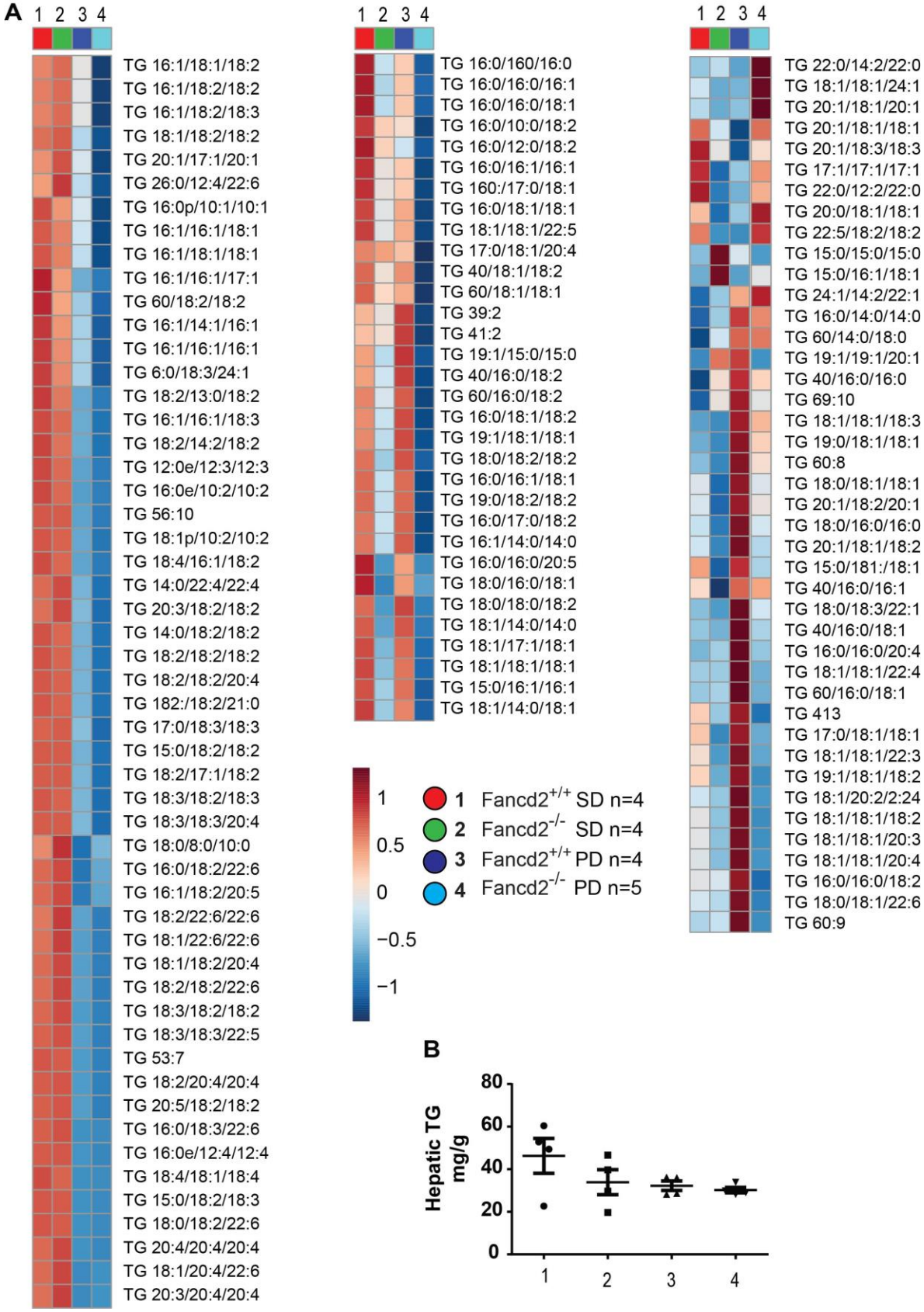
A
1 2 3 4
TG 16:1/18:1/18:2
TG 16:1/18:2/18:2
TG 16:1/18:2/18:3
TG 18:1/18:2/18:2
TG 20:1/17:1/20:1
TG 26:0/12:4/22:6
TG 16:0p/10:1/10:1
TG 16:1/16:1/18:1
TG 16:1/18:1/18:1
TG 16:1/16:1/17:1
TG 60/18:2/18:2
TG 16:1/14:1/16:1
TG 16:1/16:1/16:1
TG 6:0/18:3/24:1
TG 18:2/13:0/18:2
TG 16:1/16:1/18:3
TG 18:2/14:2/18:2
TG 12:0e/12:3/12:3
TG 16:0e/10:2/10:2
TG 56:10
TG 18:1p/10:2/10:2
TG 18:4/16:1/18:2
TG 14:0/22:4/22:4
TG 20:3/18:2/18:2
TG 14:0/18:2/18:2
TG 18:2/18:2/18:2
TG 18:2/18:2/20:4
TG 182:/18:2/21:0
TG 17:0/18:3/18:3
TG 15:0/18:2/18:2
TG 18:2/17:1/18:2
TG 18:3/18:2/18:3
TG 18:3/18:3/20:4
TG 18:0/8:0/10:0
TG 16:0/18:2/22:6
TG 16:1/18:2/20:5
TG 18:2/22:6/22:6
TG 18:1/22:6/22:6
TG 18:1/18:2/20:4
TG 18:2/18:2/22:6
TG 18:3/18:2/18:2
TG 18:3/18:3/22:5
TG 53:7
TG 18:2/20:4/20:4
TG 20:5/18:2/18:2
TG 16:0/18:3/22:6
TG 16:0e/12:4/12:4
TG 18:4/18:1/18:4
TG 15:0/18:2/18:3
TG 18:0/18:2/22:6
TG 20:4/20:4/20:4
TG 18:1/20:4/22:6
TG 20:3/20:4/20:4
1 2 3 4
TG 16:0/160/16:0
TG 16:0/16:0/16:1
TG 16:0/16:0/18:1
TG 16:0/10:0/18:2
TG 16:0/12:0/18:2
TG 16:0/16:1/16:1
TG 160:/17:0/18:1
TG 16:0/18:1/18:1
TG 18:1/18:1/22:5
TG 17:0/18:1/20:4
TG 40/18:1/18:2
TG 60/18:1/18:1
TG 39:2
TG 41:2
TG 19:1/15:0/15:0
TG 40/16:0/18:2
TG 60/16:0/18:2
TG 16:0/18:1/18:2
TG 19:1/18:1/18:1
TG 18:0/18:2/18:2
TG 16:0/16:1/18:1
TG 19:0/18:2/18:2
TG 16:0/17:0/18:2
TG 16:1/14:0/14:0
TG 16:0/16:0/20:5
TG 18:0/16:0/18:1
TG 18:0/18:0/18:2
TG 18:1/14:0/14:0
TG 18:1/17:1/18:1
TG 18:1/18:1/18:1
TG 15:0/16:1/16:1
TG 18:1/14:0/18:1
1 0.5 0 −0.5 −1
1 Fancd2+/+ SD n=4
2 Fancd2-/- SD n=4
3 Fancd2+/+ PD n=4
4 Fancd2-/- PD n=5
1 2 3 4
TG 22:0/14:2/22:0
TG 18:1/18:1/24:1
TG 20:1/18:1/20:1
TG 20:1/18:1/18:1
TG 20:1/18:3/18:3
TG 17:1/17:1/17:1
TG 22:0/12:2/22:0
TG 20:0/18:1/18:1
TG 22:5/18:2/18:2
TG 15:0/15:0/15:0
TG 15:0/16:1/18:1
TG 24:1/14:2/22:1
TG 16:0/14:0/14:0
TG 60/14:0/18:0
TG 19:1/19:1/20:1
TG 40/16:0/16:0
TG 69:10
TG 18:1/18:1/18:3
TG 19:0/18:1/18:1
TG 60:8
TG 18:0/18:1/18:1
TG 20:1/18:2/20:1
TG 18:0/16:0/16:0
TG 20:1/18:1/18:2
TG 15:0/181:/18:1
TG 40/16:0/16:1
TG 18:0/18:3/22:1
TG 40/16:0/18:1
TG 16:0/16:0/20:4
TG 18:1/18:1/22:4
TG 60/16:0/18:1
TG 413
TG 17:0/18:1/18:1
TG 18:1/18:1/22:3
TG 19:1/18:1/18:2
TG 18:1/20:2/2:24
TG 18:1/18:1/18:2
TG 18:1/18:1/20:3
TG 18:1/18:1/20:4
TG 16:0/16:0/18:2
TG 18:0/18:1/22:6
TG 60:9
B
Hepatic TG mg/g
80
60
40
20
0
1
2
3
4

Figure 3.S10: Heatmaps of diacylglycerols and cholesterol esters detected by untargeted lipidomics. After feeding Paigen diet (PD) or standard diet (SD) for 50-55 days, livers were collected and lipids extracted for untargeted lipidomics or triglyceride measurement. Heatmap of all diacylglyceride (DG) species detected (**A**) and diacylglycerides with significantly different abundances between genotypes on either diet (**B**). **C**: Cholesterol esters detected by untargeted lipidomics with those that differed significantly by genotype indicated.

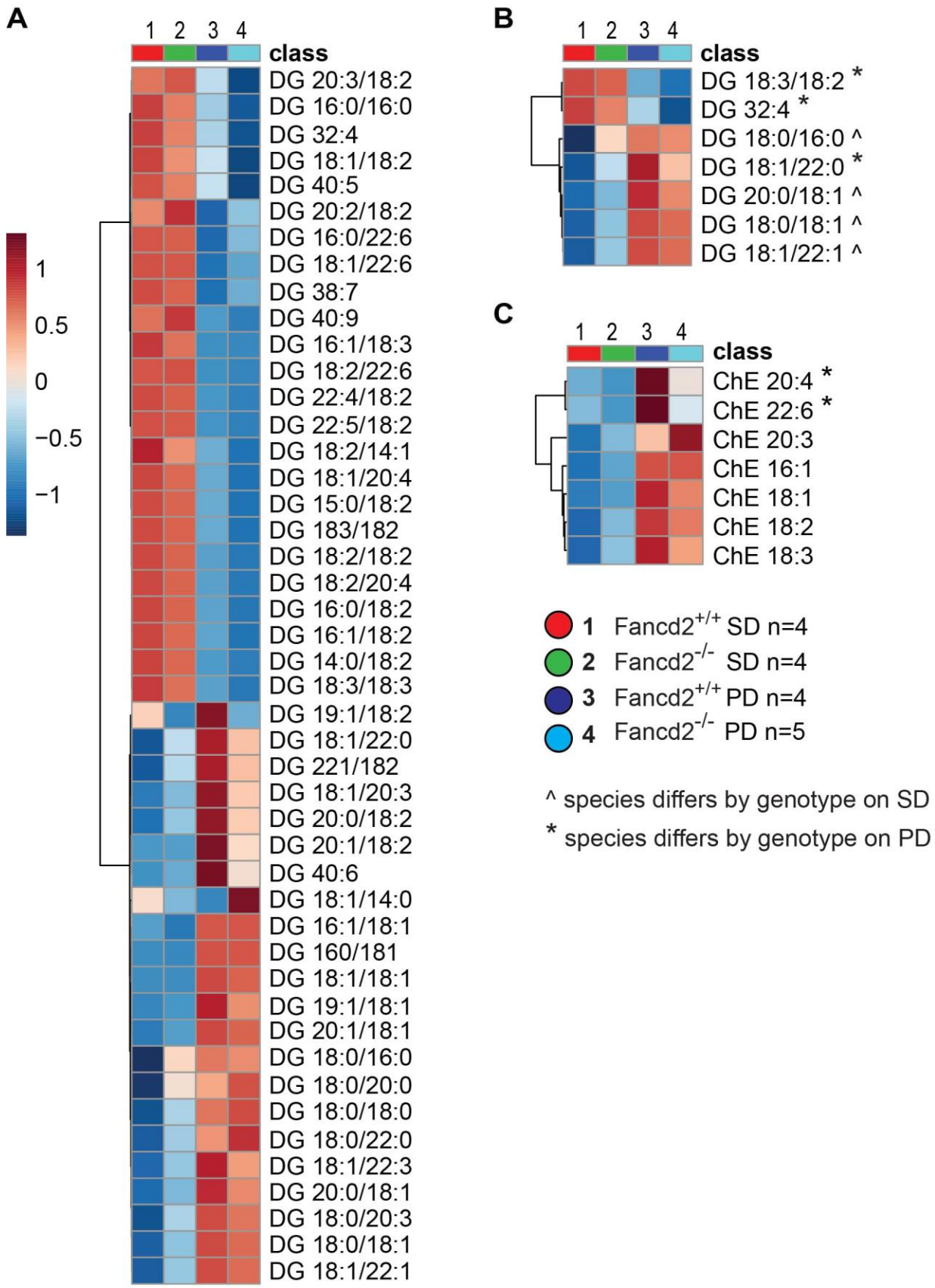
A
1 2 3 4
class
DG 20:3/18:2
DG 16:0/16:0
DG 32:4
DG 18:1/18:2
DG 40:5
DG 20:2/18:2
DG 16:0/22:6
DG 18:1/22:6
DG 38:7
DG 40:9
DG 16:1/18:3
DG 18:2/22:6
DG 22:4/18:2
DG 22:5/18:2
DG 18:2/14:1
DG 18:1/20:4
DG 15:0/18:2
DG 183/182
DG 18:2/18:2
DG 18:2/20:4
DG 16:0/18:2
DG 16:1/18:2
DG 14:0/18:2
DG 18:3/18:3
DG 19:1/18:2
DG 18:1/22:0
DG 221/182
DG 18:1/20:3
DG 20:0/18:2
DG 20:1/18:2
DG 40:6
DG 18:1/14:0
DG 16:1/18:1
DG 160/181
DG 18:1/18:1
DG 19:1/18:1
DG 20:1/18:1
DG 18:0/16:0
DG 18:0/20:0
DG 18:0/18:0
DG 18:0/22:0
DG 18:1/22:3
DG 20:0/18:1
DG 18:0/20:3
DG 18:0/18:1
DG 18:1/22:1
1
0.5
0
−0.5
−1
B
1 2 3 4
class
DG 18:3/18:2 *
DG 32:4 *
DG 18:0/16:0 ^
DG 18:1/22:0 *
DG 20:0/18:1 ^
DG 18:0/18:1 ^
DG 18:1/22:1 ^
C
1 2 3 4
class
ChE 20:4 *
ChE 22:6 *
ChE 20:3
ChE 16:1
ChE 18:1
ChE 18:2
ChE 18:3
1 Fancd2+/+ SD n=4
2 Fancd2-/- SD n=4
3 Fancd2+/+ PD n=4
4 Fancd2-/- PD n=5
^ species differs by genotype on SD
* species differs by genotype on PD

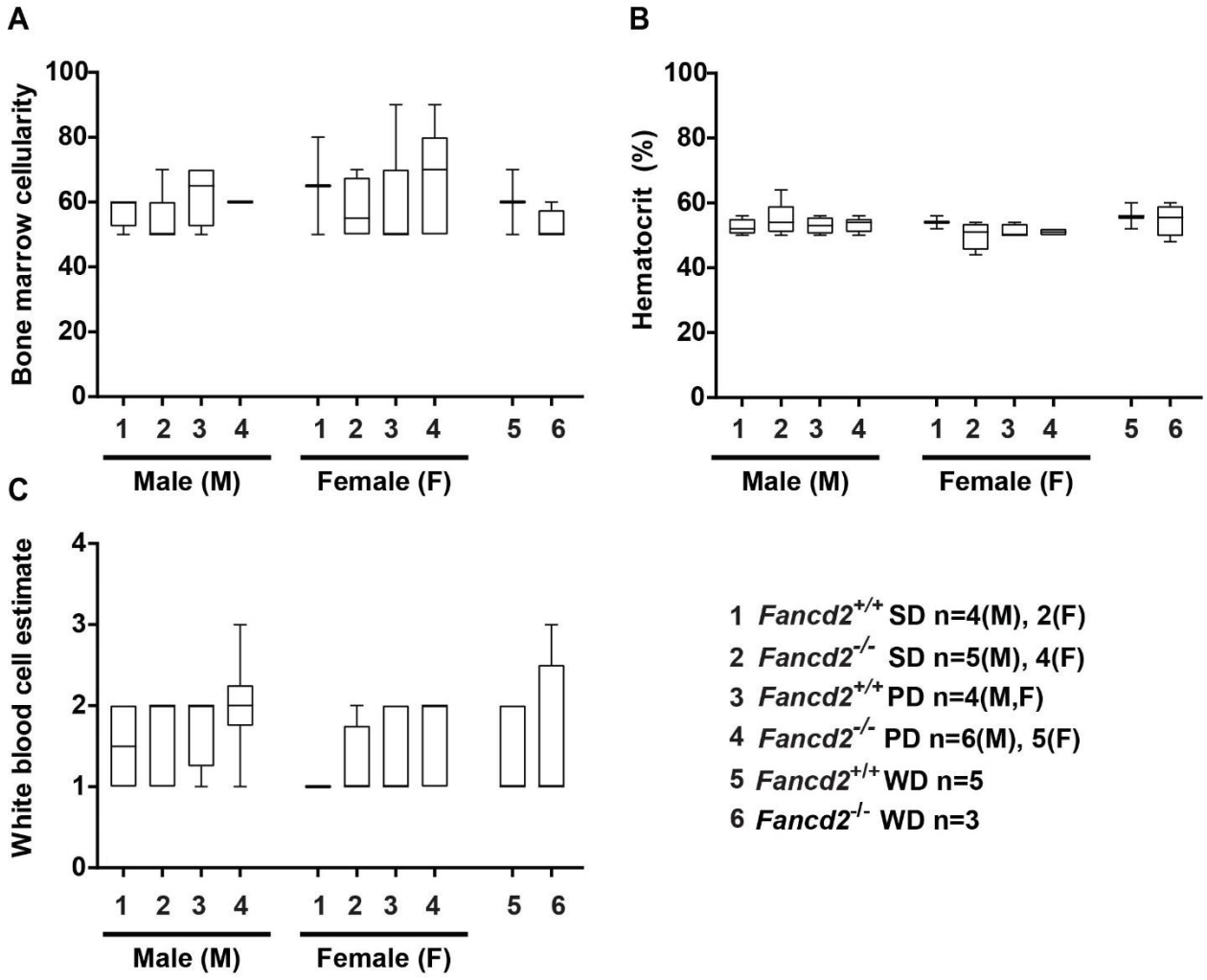

Figure 3.S11: Neither Paigen diet (PD) nor Western diet (WD) feeding induced bone marrow or peripheral blood cell deficiencies in *Fancd2*$^{-/-}$ mice of either sex. PD, WD, or standard diet (SD) was fed for 50-55 days before blood was collected, a fresh bone marrow smear was created, and bone marrow was fixed. A: Bone marrow cellularity scored as the percent of hematopoietic cells relative to the percentage of fat from fixed femur and sternum revealed no significant differences by diet, genotype or sex. B: Hematocrit did not differ by diet, genotype or sex. C: Blood smear cytology estimate of white

blood cells showed a trend towards increased white blood cells upon PD feeding in both genotypes, though no differences were significant. Error bars represent SEM.

Figure 3.S12: **No differences in fasting blood glucose were observed by diet or genotype in either sex.** Paigen diet (PD), or standard diet (SD) was fed for 50-55 days before blood and liver were collected. Blood glucose was measured after terminal cardiac puncture, preceded by a twelve-hour fast. Neither males (**A**) nor females (**C**) differed in blood glucose between groups. Expression of gluconeogenesis and glycolysis genes in males (**B**) and females (**D**). Expression of *Pck1* decreased significantly in male *Fancd2*$^{-/-}$ mice only. In females, *Pck1* expression decreased upon PD feeding in both genotypes, though the difference was significant for WT mice only. Error bars in dot plots represent SEM. Box and whisker plots show 25th to 75th percentiles (box) and minimum and maximum (whiskers), with the median indicated by the horizontal bar. $p < 0.05$ for both pairwise comparisons indicated.

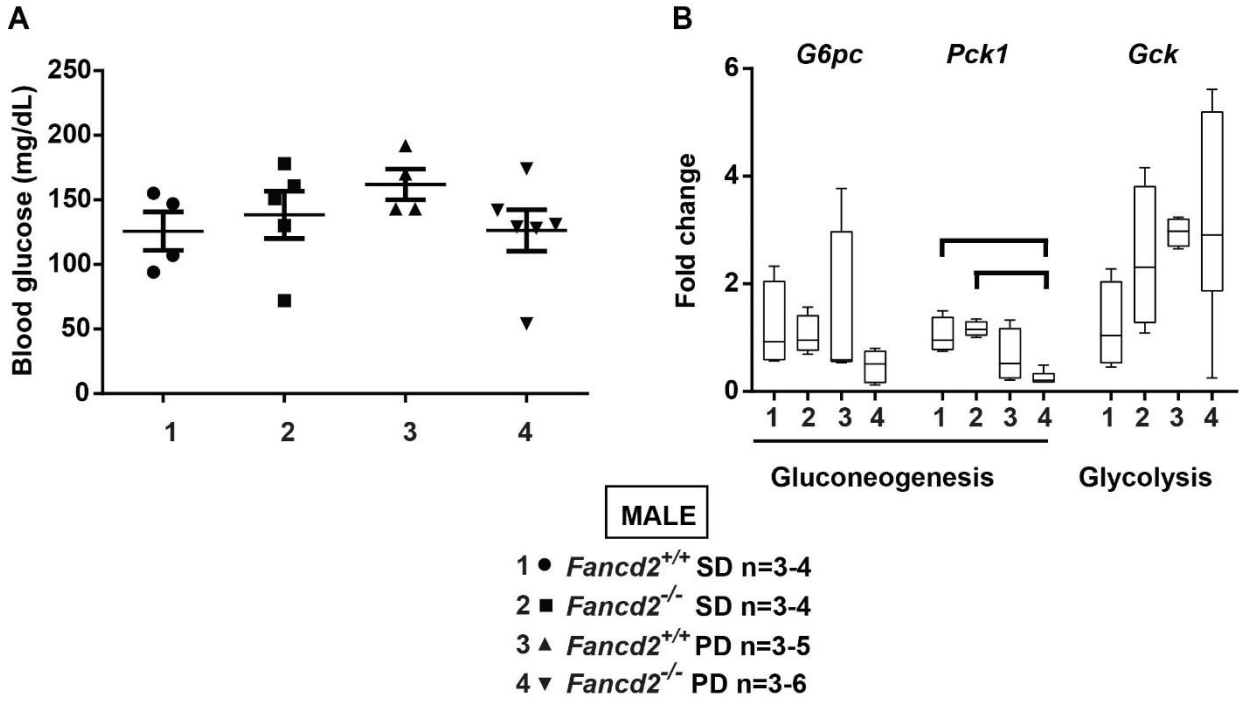
A
Blood glucose (mg/dL)
250
200
150
100
50
0
1
2
3
4
B
G6pc
Pck1
Gck
Fold change
6
4
2
0
1 2 3 4 1 2 3 4 1 2 3 4
Gluconeogenesis
Glycolysis
MALE
1 ● Fancd2+/+ SD n=3-4
2 ■ Fancd2-/- SD n=3-4
3 ▲ Fancd2+/+ PD n=3-5
4 ▼ Fancd2-/- PD n=3-6

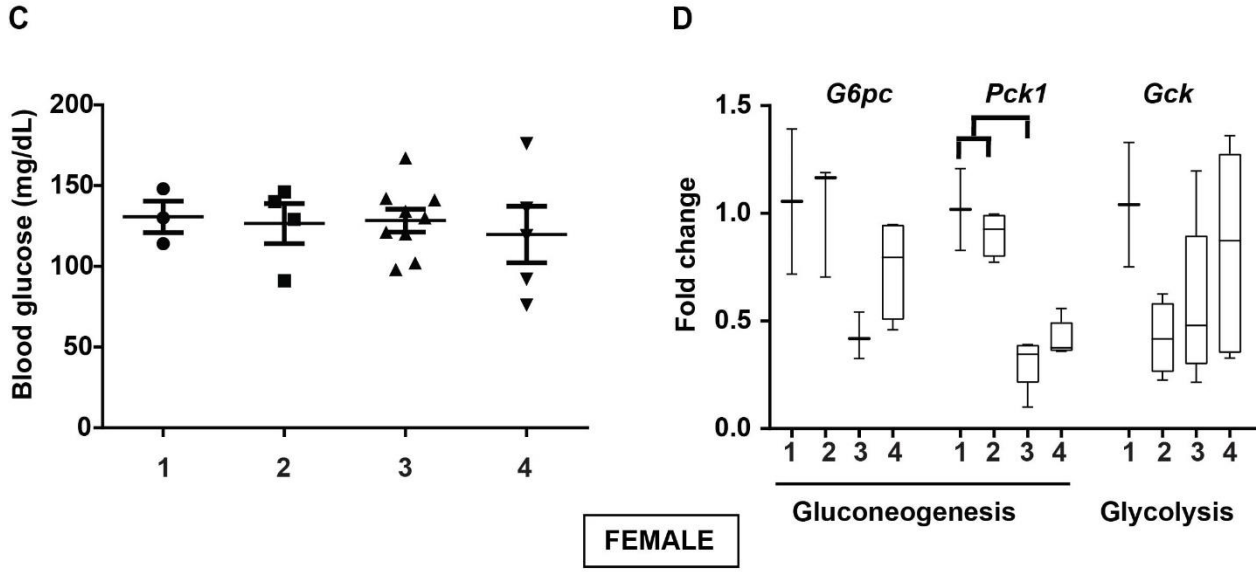
C
Blood glucose (mg/dL)
200
150
100
50
0
1
2
3
4
D
G6pc
Pck1
Gck
Fold change
1.5
1.0
0.5
0.0
1 2 3 4 1 2 3 4 1 2 3 4
Gluconeogenesis
Glycolysis
FEMALE
1 ● Fancd2+/+ SD n=2-3
2 ■ Fancd2-/- SD n=3-4
3 ▲ Fancd2+/+ PD n=3-5
4 ▼ Fancd2-/- PD n=3-5

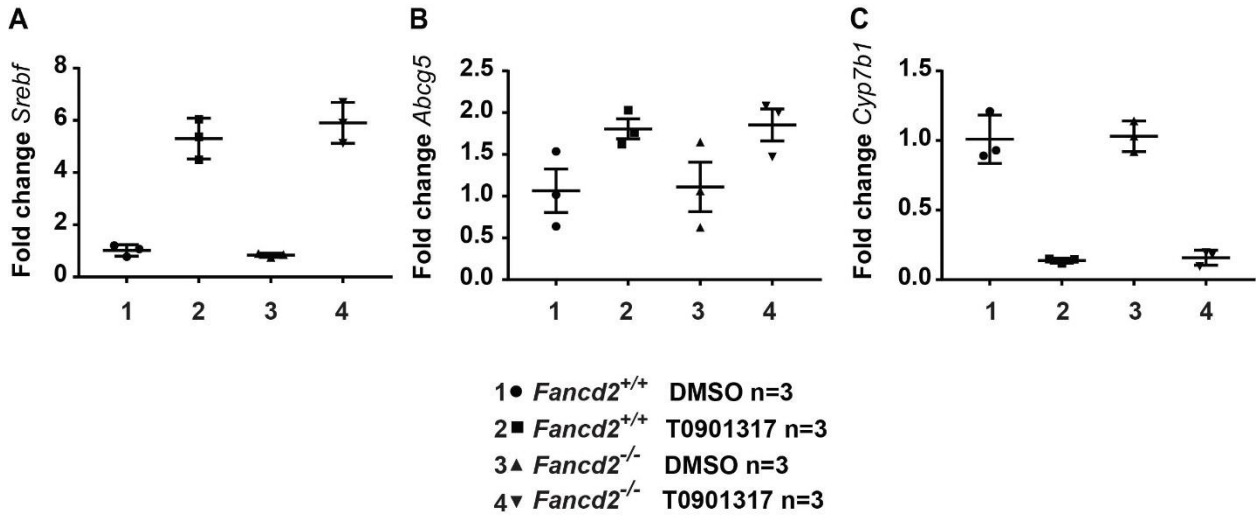

Figure 3.S13: **Elevated expression of select LXR target genes following T0901317 administration does not appear to be *Fancd2*-dependent.** The synthetic LXR agonist T0901317 or DMSO only control was administered to adult male WT and *Fancd2*$^{-/-}$ mice at 50 mg/kg daily for two days, followed by collection of liver tissue twelve hours after the second dose. Hepatic gene expression of LXR target genes *Srepbf* (**A**), *Abcg5* (**B**) and *Cyp7b1* (**C**) expressed as fold change relative to WT DMSO treated mice, showing similar response in gene expression to T0901317 in both genotypes. No post-hoc pairwise comparisons were statistically significant. Error bars represent SEM.

Figure 3.S14: Female wildtype (WT) and *Fancd2*$^{-/-}$ mice have similar trends towards increased hepatocellular DNA damage when fed Paigen diet (PD). PD or standard diet (SD) was fed for 50-55 days before liver collection for immunohistochemistry (IHC) or RNA extraction. Quantitative PCR comparisons expressed as fold change relative to the WT SD fed group. A: Quantification of positive hepatocytes as a percentage of total hepatocytes of IHC staining for the histone variant and DNA damage marker γH2AX, demonstrating a similar increase in positive hepatocytes upon PD feeding in both genotypes, though the difference was significant only for *Fancd2*$^{-/-}$ mice ($p = 0.048$). B: Quantification of TUNEL IHC of liver sections, which labels DNA nicks associated with apoptosis, as the percent of total hepatocytes. Female Fancd2$^{-/-}$ PD fed mice had a non-significant trend towards increased apoptotic hepatocytes. C: Expression of DNA damage response genes *Cdkn1a* (*p21*) and *Bbc3* (*PUMA*). D: Expression of translesion DNA synthesis polymerases encoding genes. Female WT and Fancd2$^{-/-}$ PD fed mice had trends towards increased expression of *Polκ* and *Polθ* relative to SD fed mice, though the difference were not statistically significant. E: Expression of genes encoding proteins involved in detoxifying superoxide radicals and glutathione metabolism. Error bars represent SEM. $p < 0.05$ for all pairwise comparison indicated.

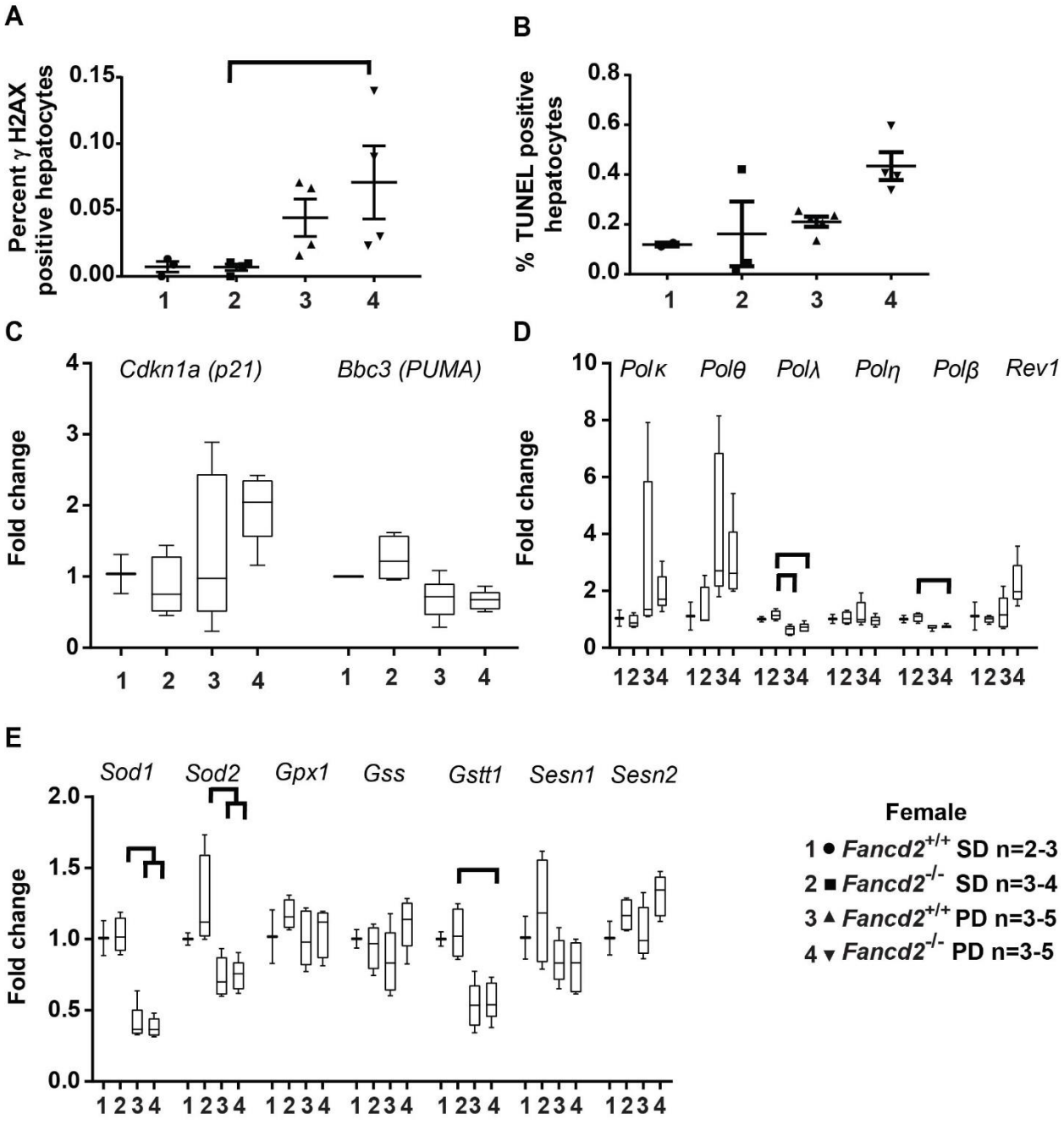
A
Percent γ H2AX positive hepatocytes
0.15
0.10
0.05
0.00
1 2 3 4
B
% TUNEL positive hepatocytes
0.8
0.6
0.4
0.2
0.0
1 2 3 4
C
Cdkn1a (p21)
Bbc3 (PUMA)
Fold change
4
3
2
1
0
1 2 3 4 1 2 3 4
D
Polκ Polθ Polλ Polη Polβ Rev1
Fold change
10
8
6
4
2
0
1234 1234 1234 1234 1234 1234
E
Sod1 Sod2 Gpx1 Gss Gstt1 Sesn1 Sesn2
Fold change
2.0
1.5
1.0
0.5
0.0
1234 1234 1234 1234 1234 1234 1234
Female
1 ● Fancd2+/+ SD n=2-3
2 ■ Fancd2-/- SD n=3-4
3 ▲ Fancd2+/+ PD n=3-5
4 ▼ Fancd2-/- PD n=3-5

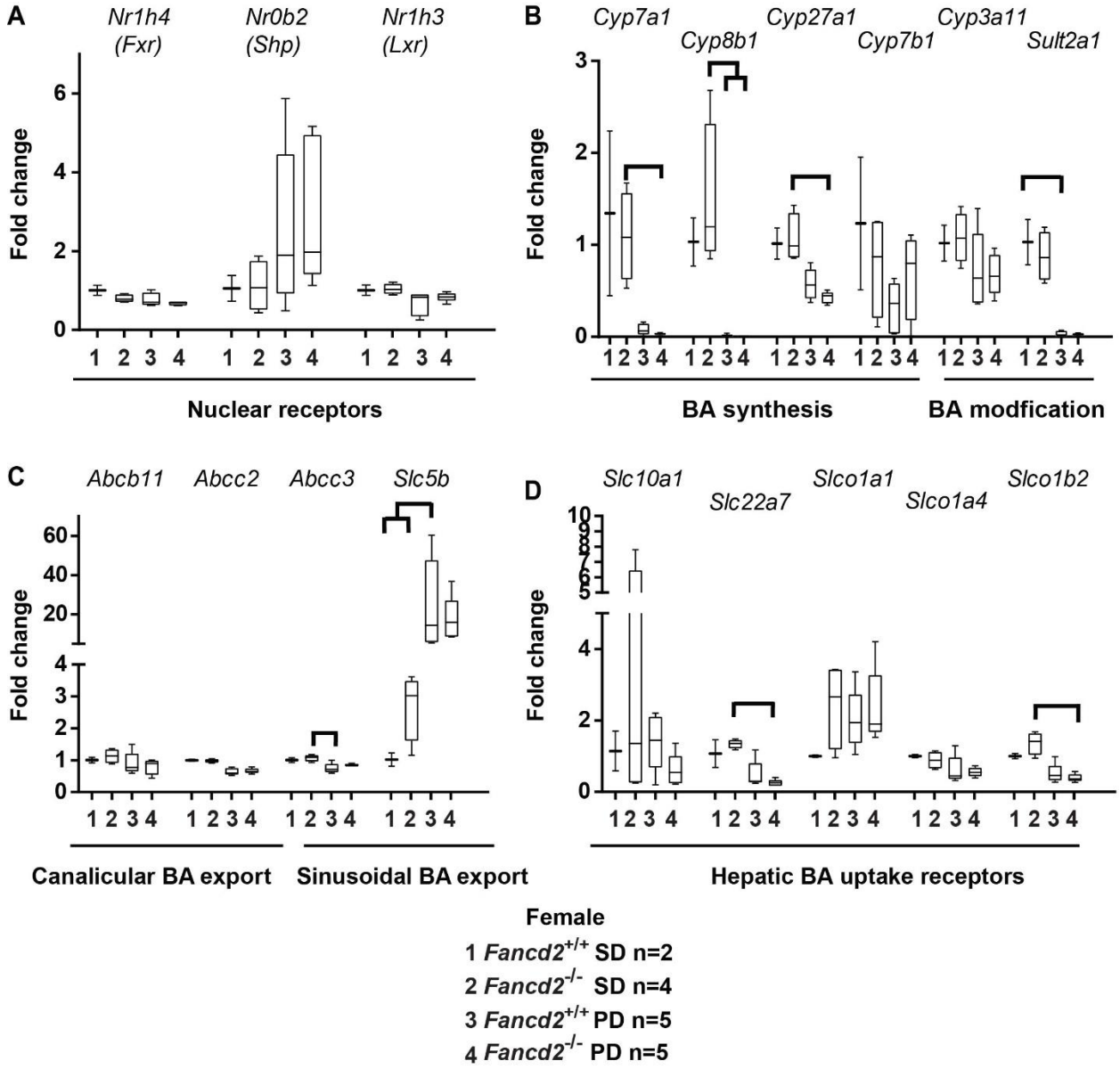

Figure 3.S15: Wildtype (WT) and *Fancd2*$^{-/-}$ female mice have similar expression patterns of genes regulating bile acid (BA) metabolism upon PD feeding. PD or standard diet (SD) was fed for 50-55 days before liver collection for RNA extraction. Quantitative PCR comparisons expressed as fold change relative to the WT SD fed group. A: Expression of nuclear receptors and transcription factors regulating BA and cholesterol metabolism. There was a non-statistically significant trend towards increased SHP expression upon PD feeding in both genotypes. B: Expression of genes encoding BA synthesis and

detoxification enzymes. WT and *Fancd2*$^{-/-}$ female mice downregulated expression of genes encoding BA synthesis enzymes when fed PD. In contrast to males, PD feeding was associated with a drastic decrease in expression of *Sult2a1*, encoding a BA modifying enzyme, in female mice of both genotypes. C: Expression of canalicular and sinusoidal BA exporters. The expression of the sinusoidal BA exporter encoding gene *Slc5b* increased upon PD feeding in both genotypes as in male mice. D: Female mice had less genotype-dependent differences in expression of genes encoding BA import receptors in contrast to male mice, however PD was associated with decreased expression of *Slc22a7* and *Slco1b2* in *Fancd2*$^{-/-}$ female mice. Box and whisker plots show 25th to 75th percentiles (box) and minimum and maximum (whiskers), with the median indicated by the horizontal bar. $p < 0.05$ for all pairwise comparison indicated.

Figure 3.S16: Female wildtype (WT) and Fancd2$^{-/-}$ mice have similar expression patterns of genes encoding proteins involved in cholesterol and lipid regulation upon Paigen diet (PD) feeding. PD or standard diet (SD) was fed for 50-55 days before liver collection for cholesterol or RNA extraction. Quantitative PCR comparisons expressed as fold change relative to the WT SD fed group. A: Total serum cholesterol increased with PD feeding in both genotypes in female mice. B: Expression of genes involved in cholesterol metabolism and transport. In contrast to males, in female mice, PD feeding was associated with similar decreases in expression of *Scp2/x* (encoding cholesterol transporters) in both genotypes. Also in contrast to males, female mice of both genotypes demonstrated similar increases in expression of *Abcg5/8,* genes encoding cholesterol exporters, upon PD feeding. LDL receptor (*Ldlr*) expression decreased in both genotypes upon PD feeding, in contrast to the pattern observed in male mice. C: Expression of genes involved in fatty acid and triglyceride metabolism. Unlike what was observed in male mice, PD feeding did not significantly impact expression of *Srebf1*, encoding a transcription factor regulating fatty acid synthesis, in either genotype. *Acat1*, *Fasn* and *Ppara* expression were similarly decreased upon PD feeding in both genotypes. Error bars represent SEM. Error bars in dot plots represent SEM. $p < 0.05$ for all pairwise comparison indicated. Box and whisker plots show 25th to 75th percentiles (box) and minimum and maximum (whiskers), with the median indicated by the horizontal bar.
$p < 0.05$ for all pairwise comparisons indicated.

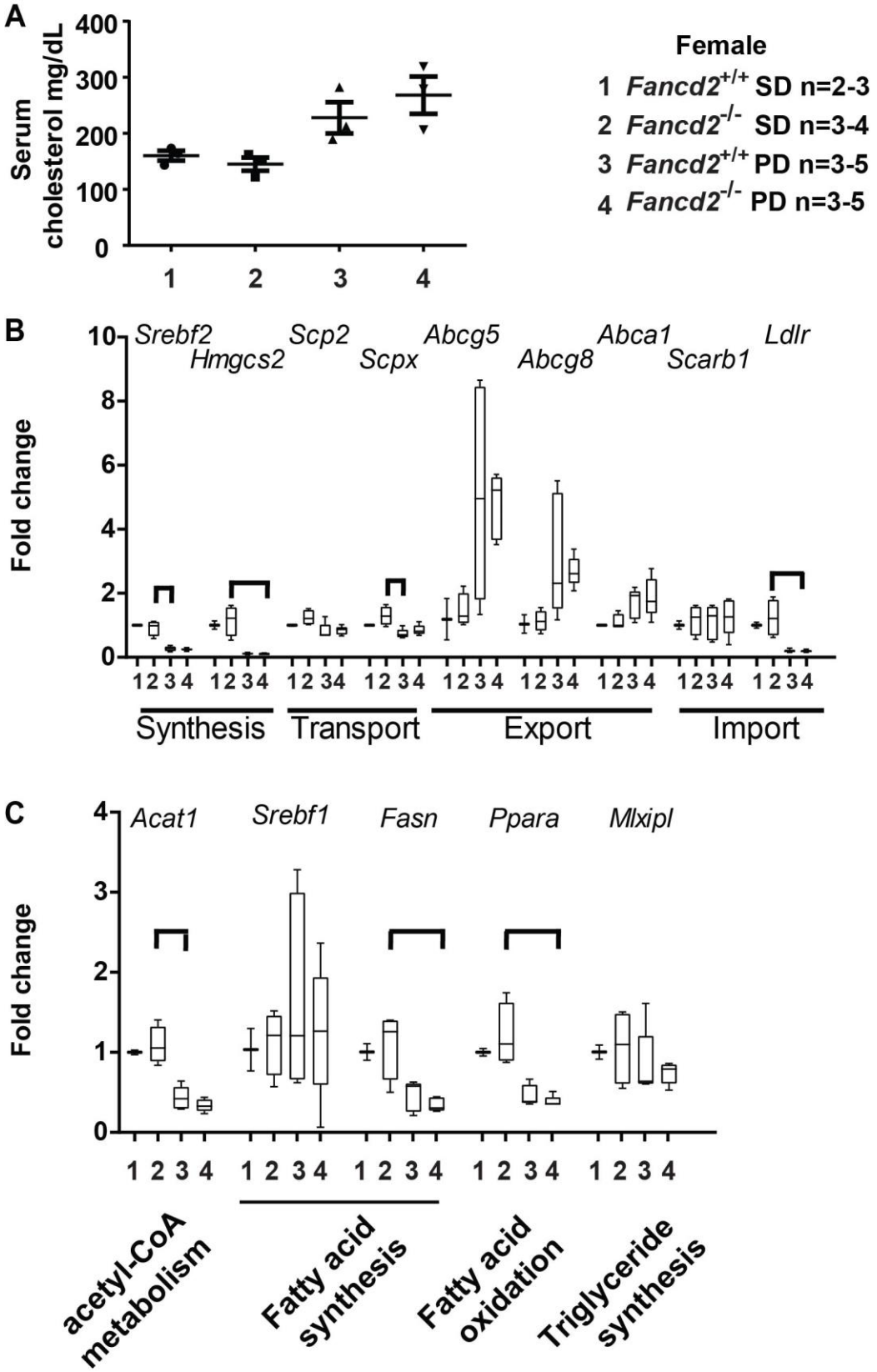
A
Serum cholesterol mg/dL
400
300
200
100
0
1
2
3
4
Female
1 Fancd2+/+ SD n=2-3
2 Fancd2-/- SD n=3-4
3 Fancd2+/+ PD n=3-5
4 Fancd2-/- PD n=3-5
B
Fold change
10
8
6
4
2
0
Srebf2
Hmgcs2
Scp2
Scpx
Abcg5
Abcg8
Abca1
Scarb1
Ldlr
1 2 3 4
Synthesis
Transport
Export
Import
C
Fold change
4
3
2
1
0
Acat1
Srebf1
Fasn
Ppara
Mlxipl
1 2 3 4
acetyl-CoA metabolism
Fatty acid synthesis
Fatty acid oxidation
Triglyceride synthesis

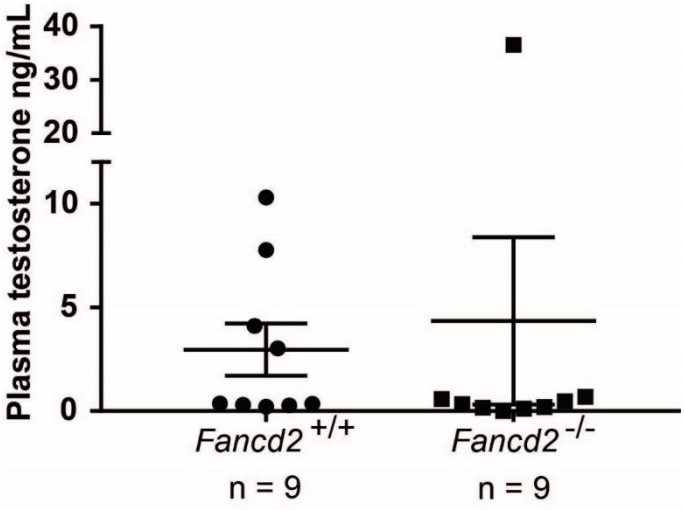

Figure S17: *Fancd2*$^{-/-}$ mice have a trend towards decreased plasma testosterone. Testosterone was measured via radioimmunoassay from heparinzized plasma. With the exception of one male, no *Fancd2*$^{-/-}$ mice had serum testosterone greater than 0. 7 ng/mL. Error bars represent SEM.

Table 3.S1: qPCR Primer Sequences

Gene	Forward 5' – 3'	Reverse 5' – 3'
Reference genes		
Rplp0 (Arbp)	GCTTTCTGGAGGGTGTCC	ACGCGCTTGTACCCATTGAT
Tbp	CTGGAATTGTACCGCAGCTT	GCAAATCGCTTGGGATTATATTCAG
Inflammatory markers		
Tgfb1	GAA CCA AGG AGA CGG AAT AC	GGC TGA TCC CGT TGA TTT
Tgfbr2	TGG AAG AGT GCA ACG ATT AC	CAC CCG TCA CTT GGA TAA TG
DNA damage markers		
Cdkn1a (*p21*)	CTT GTC GCT GTC TTG CAC TC	TAG AAA TCT GTC AGG CTG GTC
Bbc3 (*Puma*)	CCT AGT TGG GCT CCA TTT CTG	ACC TCA ACG CGC AGT AC
Translesion DNA polymerases		
Polq (*Polθ*)	CAT TGA GAC CCA AGC CTA TC	CTC CAT TCG GTG GTA ACT TT
Polk (*Polκ*)	GCT GTG AGT AAG GAG GTT AAG G	TCC TGC AAG TGC TGT GTT AT
Poll (*Polλ*)	TCA CAC CAG AGC TGT ATC T	CTT CTC CAT CGC TGG TTT C
Polh (*Polη*)	GGA ATC CAA ACT GAG TGG TC	TAC TCA GGA ACG CAG TGA TA
Polb (*Polβ*)	CGT GGA ACT CGC AAA CTT	TGT GGG TAC TTG GCT ATC A
Rev1	ACG TTG ATA TGG ACT GCT TC	TTC CCG TGC CTC TGT TA
Nuclear receptors		
Nr1h4 (*Fxr*)	CGA AGA CTC CCT CAC AGT TG	ACC TCT ACT TCA TCT CCT TCA CT
Nr0b2 (*Shp*)	ACG ATC CTC TTC AAC CCA GA	TGA TAG GGC GGA AGA AGA GA
Nr1h3 (*Lxr*)	TCA ATG CCT GAT GTT TCT CCT G	CTC CAA CCC TAT CCC TAA AGC
Bile acid synthesis		
Cyp7a1	AAC GAT ACA CTC TCC ACC TTT G	CTG CTT TCA TTG CTT CAG GG
Cyp8b1	GGA CAG CCT ATC CTT GGT GA	CGG AAC TTC CTG AAC AGC TC
Cyp27a1	GCCTCACCTATGGGATCTTCA	TCAAAGCCTGACGCAGATG
Cyp7b1	GCA TGG CCC TGA AAT TCT T	AGT GAG CCA CAG AAT GCA AA
Bile acid modifying enzymes		
Cyp3a11	TTC TGT CTT CAC AAA CCG GC	GGG GGA CAG CAA AGC TCT AT
Sult2a1	GAA GAA TCC AGG GTC ACT CG	CAT TCT CTC ATG GAC AGC CA
Bile acid transport		
Abcb11 (*Bsep*)	CAG TCC TCT CAT TGG GAT TG	GGC AAT AGA CCC AGC TTT AG
Abcc2	AGA AGG CAC TAA CCC TAT CT	GTA GTT GGT CAC GTC CAT TAG
Abcc3	CTG GGT CCC CTG CAT CTA C	GCC GTC TTG AGC CTG GAT AAC
Slc5b	GCA AAC AGA AAT CGA AAG AAG C	TCT GGC AGA AAG ACA AGT GAT

Slc10a1	ACT CCC ATA ATG CCC TTG G	TAA TCG GGC CAA CAA TCT TC
Slc22a7	GAT CAC TGC TCT GGT GGT GA	GAG TGC AGT GAA TCC CAT TCC
Slco1a1	TAG CTT GCC TCC AGT ATG CCTT	ACA GGC CAA ATG CTA TGT ATG C
Slco1a4	CAA GCT TTC TCC CTG CAC TCTT	TCC TTC GCA GTG AGC TTC ATT
Slco1b2	CTG GGA AGC ACT TCT CTT ATG	GGA GCT AGA ATT CCT CCT AGT
Cholesterol metabolism		
Srebf2	GCG TTC TGG AGA CCA TGG A	ACA AAG TTG CTC TGA AAA CAA ATCA
Hmgcs2	GCC GTG AAC TGG GTC GAA	GCA TAT ATA GCA ATG TCT CCT GCA A
Scp2	CAA GGC AAA CCT CGT CTT TA	CAG GGC CAT CTT TCA CTT T
*Scpx**	GAT GCA CAG ATC CCT TAC TC	CCA GTC AGT CCC AAA CTA TG
Abcg5	AGA GTC AGG ATG GCC TGT AT	ATG CTG AGC AGG GCC ACT AT
Abcg8	GAG AGC TTC ACA GCC CAC AA	GCC TGA AGA TGT CAG AGC GA
Abcb1 (*Mdr1*)	GCT CAT AGT TGC CTA CAT CC	CAC ATC AAA CCA GCC TAT CT
Abcg1	GCT CTT CTC CGG ATT CTT TG	CCG TAG ATG GAC AGG ATG A
Scarb1 (*Srb1* or *Hdlr*)	AGT GGG GGT GGG AGA GAA AC	CAA GCC TGT GAG CCT GAA GC
Ldlr	GGC CAT CTA TGA GGA CAA AG	TCA GCC ACC AAA TTC ACA T
Acetyl Co-A metabolism		
Acat1	GGC CAT TAA ACT TGG TAC TG	CAT TGC CCA TGT AGA CTT CC
Acat2	CGA ACG CAT CAG GAA TGA A	CTT GGG ACC AGG AGA CTA TT
Fatty acid metabolism		
Srebf1	CAT TCT CAC TCC CTC TGA TG	CAA CCA CTG GGT CCA ATT A
Scd1	CGT CTG GAG GAA CAT CAT TC	AGC GCT GGT CAT GTA GTA
Fasn	GAC TCG GCT ACT GAC ACG AC	CGA GTT GAG CTG GGT TAG CC
Ppara	CTG AAC ATC GAG TGT CGA ATA	CCG AAA GAA GCC CTT ACA G
Triglyceride synthesis		
Mlxipl	AGG GAA TAC ACG CCT ACA	TCT TGG TCT TAG GGT CTT CA
Glucose metabolism		
G6pc	GTC TGG ATT CTA CCT GCT AC	AAA GAC TTC TTG TGT GTC TGT C
Pck1	TAG GAG CAG CCA TGA GAT	CGA AGT TGT AGC CGA AGA A
Gck	TCA GGA GGC CAG TGT AAA	CCC AGG TCT AAG GAG AGA AA
Antioxidant		
Sod1	CAG GAG AGC ATT CCA TCA TT	CCC AGC ATT TCC AGT CTT T
Sod2	GCT GGC TTG GCT TCA ATA	GAA TAA GGC CTG TTG TTC CT
Gpx1	CGG GGT GGT GCT CGG TTT CCC G	CCA GGT CGG ACG TAC TTG AGG
Gss	CGG AAA AGT TGC TGT GGT GGTA CTT CC	CTC TAG CAT CAG GCG TGC TTC C
Gstt1	ACA ATA TCC CGT TCC AGA TGC	CAA GAT AGC CAC ACT CTC ACA C
Sesn1	GCA GTT ACA GGA ATC CGA GAG	CGG ACT GGT GTA ACT TCA TCA TCG TG
Sens2	CAC CTT CGC CTC CCA GTG A	CGC ACT GAA GCT GCC TCA TGC G

* *Scpx* primer will amplify *Scp2* and *Scpx*

Table 3.S2: Lipidomics filter criteria

Filter criteria	**Lipid class**
Main ion = M+H or M-HCOO	PC, LPC
Main ion = M+H or M+HCOO	Cer, CerG
Main ion = M+H	LSM, SM, So
Main ion = M+NH4	MG, DG, TG, Che
Main ion = M+H or M-H	PE, LPE, PS, LPS
Main ion = M+NH4 or M-H	PI, PG, LPI, LPG
Main ion = M-H	PA, LPA, DLCL, MLCL
Main ion = M-2H or M-H	CL
Main grade[a] = A, B, C	ALL

[a]A. Lipid class and fatty acid were completely identified; B: Lipid class and some of the fatty acid were identified; C: Lipid class or the fatty acid were identified

CHAPTER 4: SUMMARY AND FUTURE DIRECTIONS

The 9-1-1 complex is a critical component of the DDR, with separable roles in checkpoint signaling and DNA repair. Deficiency of HUS1 increases genomic instability and genotoxin sensitivity. Evidence suggest that the 9-1-1 clamp also supports high fidelity DSB repair. We examined the role of the 9-1-1 clamp in DSB repair by combining our *Hus1* hypomorphic mouse model with mice either lacking the HR component *Rad54*, or the NHEJ component *Prkdc* and observed strikingly different phenotypes in the two double mutant models. Double mutant $Rad54^{-/-}Hus1^{neo/\Delta 1}$ mice had decreased fitness, increased genomic instability, increased genotoxin sensitivity, and severe gonadal and fertility defects. Double mutant $Rad54^{-/-}Hus1^{neo/\Delta 1}$ MEFs had decreased proliferative capacity, increased chromosomal instability, and increased genotoxin sensitivity. This synergistic relationship suggests that both RAD54 and the 9-1-1 complex contribute to HR. In contrast, double mutant $Prkdc^{-/-}Hus1^{neo/\Delta 1}$ mice showed no significant worsening of fitness or spontaneous genomic instability relative to single mutant mice, outlived $Prkdc^{-/-}$ mice, and had a partial rescue in genotoxin sensitivity. Double mutant $Prkdc^{-/-}Hus1^{neo/\Delta 1}$ MEFs did not have a significant worsening in proliferative capacity or chromosomal instability relative to $Prkdc^{+}Hus1^{neo/\Delta 1}$ single mutant MEFs, had a partial rescue in sensitivity to aphidicolin, but did display an increased sensitivity to MMC and IR.

The observation that absence of *Prkdc*, and thus NHEJ deficiency, partially rescues genome instability in the context of *Hus1* deficiency suggests that HUS1 and the 9-1-1 complex and DNA-PK have some degree of an antagonistic relationship. Antagonistic relationships among players in different DSB repair pathways appear frequently, and deficiency of one protein can often be rescued by the loss of a competing/antagonizing protein. It is also possible that alternative DSB repair pathways are disinhibited in the absence of competent NHEJ and deficiency of the 9-1-1 clamp. This observation suggests that the 9-1-1 complex influences DSB repair pathway choice.

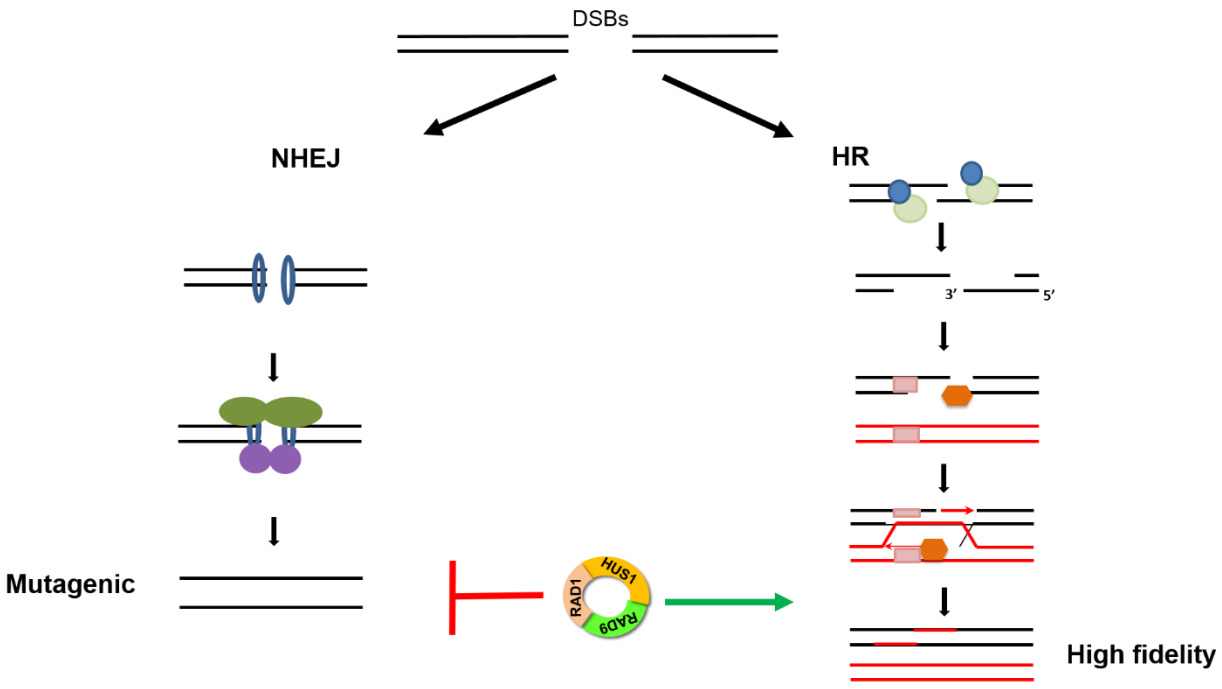

Figure 4.1: Proposed role of the 9-1-1 complex in DNA double strand break repair pathway choice. The partial rescue in genome stability observed in the combined absence of the NHEJ component *Prkdc* and deficiency of *Hus1* suggest that the 9-1-1 complex may have an NHEJ -inhibitory function. The increase in genome instability observed when *Hus1* deficiency was combined with absence of the HR component *Rad54* suggests that the 9-1-1 complex and RAD54 both contribute to the same high fidelity DSB repair.

It is not yet clear, however, whether the phenotypes observed in the combined *Hus1* deficient and *Rad54* or *Prkdc* null mouse models described here are attributable to roles of the 9-1-1 complex in checkpoint signaling or DNA repair (or both), as both functions are reduced in a *Hus1* hypomorphic background. Further, strong evidence suggests that in addition to influencing high fidelity DSB repair, the 9-1-1 complex is also required for replication fork protection (Patel et al., unpublished data). Indeed, this is a recurring theme, in which HR proteins have been identified to also play crucial roles in replication fork stability. RAD51, which catalyzes recombination via strand invasion during HR, is now understood

to regulate fork reversal and stability (reviewed in (455)). Other Fanconi Anemia proteins, such as BRCA1 and BRCA2, CtIP, and other HR proteins have also been shown to support stability of stalled and reversed replication forks (456-458). We used genotoxins (MMC and aphidicolin) that induce replication stress and replication fork stalling, and which also cause single and double strand DNA breaks. We cannot know what proportion of the phenotypes we observed in response to these genotoxins (in combination with absence of RAD54 or DNA-PK) is due to a role of 9-1-1 in replication fork protection vs DSB repair. It is interesting to consider that double mutant *Prkdc*$^{-/-}$*Hus1*$^{neo/\Delta 1}$ MEFs had increased sensitivity to IR and MMC, which both cause DSBs, but a rescue in sensitivity to the replication stress causing agent aphidicolin. This may reflect the varied roles of 9-1-1, though a rescue in sensitivity to both IR and MMC was seen in the *Prkdc*$^{-/-}$*Hus1*$^{neo/\Delta 1}$ mice.

Several strategies could be used to refine our understanding of the role the 9-1-1 complex plays in DSB repair and replication fork stability, and its relationship with other DNA repair proteins. HR efficiency reporter plasmids can be used to examine HR efficiency of an induced DSB via restoration of a GFP signal which is quantified by flow cytometry (459). Knockdown of HUS1 has been demonstrated to reduce HR efficiency (171). We could employ the DRGFP HR reporter plasmid to evaluate the efficiency of HR in cells deficient for HUS1 and lacking RAD54 or treated with a PRKDC inhibitor. I would predict that HR efficiency would be synergistically decreased in *Rad54*-targeted HUS1-deficient MEFs, which would support a model in which both proteins promote HR. I would predict HR efficiency in PRKDC inhibited HUS1-deficient MEFs to increase relative to untreated HUS1-deficient MEFs, fitting with a role of 9-1-1 in antagonizing NHEJ at DSBs. However, if the role of the 9-1-1 complex in promoting stability at stalled and reversed forks is predominating over its role in promoting HR at DSBs, the HR efficiency analysis may not reveal a significant change when HUS1 deficiency is combined absence of the other repair factors. The DSB induced in the reporter plasmids is also not in the context of a replication fork, and thus may not reflect the roles of the 9-1-1 clamp in that context.

A role of the 9-1-1 complex in replication fork stability could be assessed with DNA fiber analysis in cells also targeted for depletion of other DNA repair factors or treated with repair factor inhibitors. Assessing chromatin localization of DNA repair factors, such as RAD51, KU70/80, or endo

and exonucleases in the combined deficiency of HUS1 and absence/inhibition of other repair factors can also reveal roles of the 9-1-1 complex in recruiting or antagonizing other DDR components. Advancing our understanding of the role of the 9-1-1 complex and its interactions with other DDR factors will contribute to better understanding the mechanisms cells use to respond to replication stress and DSBs, which may yield beneficial insight in the development of therapeutic strategies for targeting cancer cells.

The Fanconi Anemia DNA repair pathway consists of twenty-two currently identified components, and is critical to multiple cell processes. Absence of an intact FA pathway causes deleterious phenotypes, including congenital defects, bone marrow failure, cancer predisposition, infertility, and endocrine and metabolic derangements. The FA pathway has critical functions in genome maintenance via participation in ICL repair, HR, checkpoint signaling, and mitosis, as well as functions outside the nucleus in mitochondrial homeostasis, energy metabolism, and lipid metabolism. We describe a novel role of the FA pathway in hepatic metabolism. When challenged with a high fat, high cholesterol Paigen diet, male *Fancd2*$^{-/-}$ mice had decreased survival and developed hepatobiliary disease characterized by increased hepatomegaly and hepatocellular swelling, increased serum bile acids, biliary hyperplasia, increased serologic markers of hepatic damage, and hepatic inflammation. The relatively mild increase in markers of DNA damage and hepatocellular apoptosis suggest the sensitivity of *Fancd2*$^{-/-}$ mice to Paigen diet does not arise from absence of canonical DNA repair roles of FANCD2. WT and *Fancd2*$^{-/-}$ mice had differential transcriptional responses of bile acid, cholesterol, and lipid metabolism genes, and different abundances of many lipid species, including sphingolipids, glycerophospholipids, and glycerolipids when challenged with a PD. We propose that the FA pathway has roles in hepatic metabolic homeostasis, and thus the *Fancd2*$^{-/-}$ mice were less able to tolerate a Paigen diet challenge.

Future studies could examine the etiology behind the sex specificity of the Paigen diet sensitivity. We hypothesize that testosterone may play a role in hepatic protection in this context. If this hypothesis is correct, exogenous administration of testosterone may decrease Paigen diet sensitivity in *Fancd2*$^{-/-}$ mice and castration of WT mice may sensitize them to Paigen diet feeding. Feeding additional diets could narrow down the metabolic challenges to which FA deficient mice are sensitive. Metabolomic studies

could reveal additional details of metabolic derangements in both challenged and unchallenged conditions. Lipidomic profiling in negative ionization mode could reveal additional differences in lipid metabolism, including fatty acid relative abundances. Functional analyses of cholesterol and lipid dynamics (synthesis, import, export) could be performed in primary hepatocytes or hepatocellular cell lines with knock out or knock down of *Fancd2* and exposure to various media nutrient/metabolite concentrations. It would also be important to evaluate human biologic samples for FA-dependent metabolic differences. Increasing our understanding of the role the FA pathway plays in cellular homeostasis can help us better understand, and hopefully prevent and treat, the mechanistic etiology behind FA phenotypes.

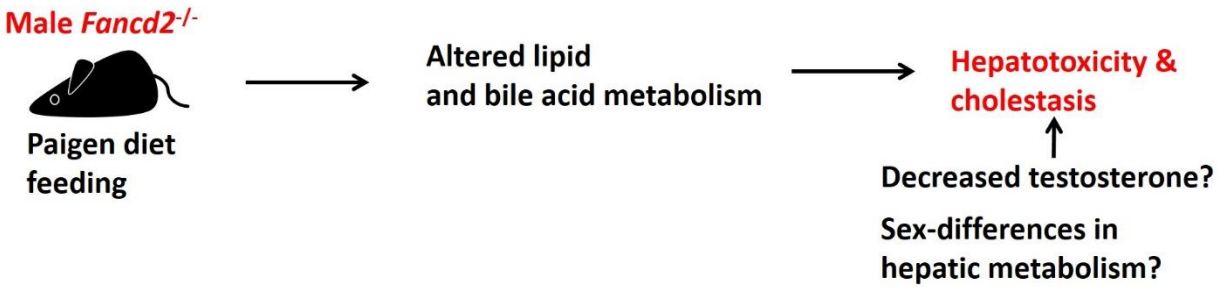

Figure 4.2: The FA pathway protects against hepatic damage in the face of Paigen diet-induced metabolic challenge in male mice.

Together, this work describes roles of DNA damage response pathways in double strand break repair, and in non-canonical regulation of hepatic metabolism. These studies suggest that the 9-1-1 DNA damage response clamp contributes to DSB repair and repair pathway choice, and adds to a growing body of evidence that the FA pathway is important in lipid and metabolic metabolism in addition to its canonical functions.

REFERENCES

1. Ciccia A, Elledge SJ. The DNA damage response: making it safe to play with knives. Mol Cell 2010;40:179-204.

2. Harper JW, Elledge SJ. The DNA damage response: ten years after. Mol Cell 2007;28:739-745.

3. Lindahl T. Instability and decay of the primary structure of DNA. Nature 1993;362:709-715.

4. Lindahl T, Wood RD. Quality control by DNA repair. Science 1999;286:1897-1905.

5. Hoeijmakers JH. DNA damage, aging, and cancer. N Engl J Med 2009;361:1475-1485.

6. Lavin MF, Shiloh Y. THE GENETIC DEFECT IN ATAXIA-TELANGIECTASIA. Annual Review of Immunology 1997;15:177-202.

7. Swift M, Reitnauer PJ, Morrell D, Chase CL. Breast and other cancers in families with ataxia-telangiectasia. N Engl J Med 1987;316:1289-1294.

8. Lee JH, Paull TT. ATM activation by DNA double-strand breaks through the Mre11-Rad50-Nbs1 complex. Science 2005;308:551-554.

9. Brown EJ, Baltimore D. ATR disruption leads to chromosomal fragmentation and early embryonic lethality. Genes Dev 2000;14:397-402.

10. de Klein A, Muijtjens M, van Os R, Verhoeven Y, Smit B, Carr AM, Lehmann AR, et al. Targeted disruption of the cell-cycle checkpoint gene ATR leads to early embryonic lethality in mice. Curr Biol 2000;10:479-482.

11. O'Driscoll M, Ruiz-Perez VL, Woods CG, Jeggo PA, Goodship JA. A splicing mutation affecting expression of ataxia-telangiectasia and Rad3-related protein (ATR) results in Seckel syndrome. Nat Genet 2003;33:497-501.

12. Cimprich KA, Cortez D. ATR: an essential regulator of genome integrity. Nat Rev Mol Cell Biol 2008;9:616-627.

13. Zou L, Liu D, Elledge SJ. Replication protein A-mediated recruitment and activation of Rad17 complexes. Proc Natl Acad Sci U S A 2003;100:13827-13832.

14. Haahr P, Hoffmann S, Tollenaere MA, Ho T, Toledo LI, Mann M, Bekker-Jensen S, et al. Activation of the ATR kinase by the RPA-binding protein ETAA1. Nat Cell Biol 2016;18:1196-1207.

15. Bass TE, Luzwick JW, Kavanaugh G, Carroll C, Dungrawala H, Glick GG, Feldkamp MD, et al. ETAA1 acts at stalled replication forks to maintain genome integrity. Nat Cell Biol 2016;18:1185-1195.

16. Lee YC, Zhou Q, Chen J, Yuan J. RPA-Binding Protein ETAA1 Is an ATR Activator Involved in DNA Replication Stress Response. Curr Biol 2016;26:3257-3268.

17. Zhou BB, Elledge SJ. The DNA damage response: putting checkpoints in perspective. Nature 2000;408:433-439.

18. Paulovich AG, Toczyski DP, Hartwell LH. When checkpoints fail. Cell 1997;88:315-321.
19. Painter RB, Young BR. Radiosensitivity in ataxia-telangiectasia: a new explanation. Proc Natl Acad Sci U S A 1980;77:7315-7317.

20. Larner JM, Lee H, Hamlin JL. Radiation effects on DNA synthesis in a defined chromosomal replicon. Mol Cell Biol 1994;14:1901-1908.

21. Kuzminov A. Collapse and repair of replication forks in Escherichia coli. Mol Microbiol 1995;16:373-384.

22. Weinert TA, Kiser GL, Hartwell LH. Mitotic checkpoint genes in budding yeast and the dependence of mitosis on DNA replication and repair. Genes Dev 1994;8:652-665.

23. McClintock B. The Stability of Broken Ends of Chromosomes in Zea Mays. Genetics 1941;26:234-282.

24. Ma C, Martin S, Trask B, Hamlin JL. Sister chromatid fusion initiates amplification of the dihydrofolate reductase gene in Chinese hamster cells. Genes Dev 1993;7:605-620.
25. Shiloh Y. ATM and ATR: networking cellular responses to DNA damage. Curr Opin Genet Dev 2001;11:71-77.

26. Matsuoka S, Huang M, Elledge SJ. Linkage of ATM to cell cycle regulation by the Chk2 protein kinase. Science 1998;282:1893-1897.

27. Sanchez Y, Wong C, Thoma RS, Richman R, Wu Z, Piwnica-Worms H, Elledge SJ. Conservation of the Chk1 checkpoint pathway in mammals: linkage of DNA damage to Cdk regulation through Cdc25. Science 1997;277:1497-1501.

28. Donzelli M, Draetta GF. Regulating mammalian checkpoints through Cdc25 inactivation. EMBO Rep 2003;4:671-677.

29. Falck J, Mailand N, Syljuasen RG, Bartek J, Lukas J. The ATM-Chk2-Cdc25A checkpoint pathway guards against radioresistant DNA synthesis. Nature 2001;410:842-847.

30. Yi C, He C. DNA repair by reversal of DNA damage. Cold Spring Harb Perspect Biol 2013;5:a012575.

31. Schermerhorn KM, Delaney S. A chemical and kinetic perspective on base excision repair of DNA. Acc Chem Res 2014;47:1238-1246.

32. Stivers JT, Jiang YL. A mechanistic perspective on the chemistry of DNA repair glycosylases. Chem Rev 2003;103:2729-2759.

33. Scharer OD. Nucleotide excision repair in eukaryotes. Cold Spring Harb Perspect Biol 2013;5:a012609.

34. Li GM. Mechanisms and functions of DNA mismatch repair. Cell Res 2008;18:85-98.

35. Jansen JG, Fousteri MI, de Wind N. Send in the clamps: control of DNA translesion synthesis in eukaryotes. Mol Cell 2007;28:522-529.

36. Chang DJ, Lupardus PJ, Cimprich KA. Monoubiquitination of proliferating cell nuclear antigen induced by stalled replication requires uncoupling of DNA polymerase and mini-chromosome maintenance helicase activities. J Biol Chem 2006;281:32081-32088.

37. Caldecott KW. Single-strand break repair and genetic disease. Nat Rev Genet 2008;9:619-631.
38. Hossain MA, Lin Y, Yan S. Single-Strand Break End Resection in Genome Integrity: Mechanism and Regulation by APE2. Int J Mol Sci 2018;19.

39. Ame JC, Spenlehauer C, de Murcia G. The PARP superfamily. Bioessays 2004;26:882-893.
40. Lindahl T, Satoh MS, Poirier GG, Klungland A. Post-translational modification of poly(ADP-ribose) polymerase induced by DNA strand breaks. Trends Biochem Sci 1995;20:405-411.

41. Caldecott KW. Mammalian single-strand break repair: mechanisms and links with chromatin. DNA Repair (Amst) 2007;6:443-453.

42. Hoeijmakers JH. Genome maintenance mechanisms for preventing cancer. Nature 2001;411:366-374.

43. Meek K, Dang V, Lees-Miller SP. DNA-PK: the means to justify the ends? Adv Immunol 2008;99:33-58.

44. Chen L, Trujillo K, Sung P, Tomkinson AE. Interactions of the DNA Ligase IV-XRCC4 Complex with DNA Ends and the DNA-dependent Protein Kinase. Journal of Biological Chemistry 2000;275:26196-26205.

45. Menon V, Povirk LF. End-processing nucleases and phosphodiesterases: An elite supporting cast for the non-homologous end joining pathway of DNA double-strand break repair. DNA Repair 2016;43:57-68.

46. Muñoz-Galván S, López-Saavedra A, Jackson SP, Huertas P, Cortés-Ledesma F, Aguilera A. Competing roles of DNA end resection and non-homologous end joining functions in the repair of replication-born double-strand breaks by sister-chromatid recombination. Nucleic Acids Res 2013;41:1669-1683.

47. Frit P, Barboule N, Yuan Y, Gomez D, Calsou P. Alternative end-joining pathway(s): bricolage at DNA breaks. DNA Repair (Amst) 2014;17:81-97.

48. Howard SM, Yanez DA, Stark JM. DNA damage response factors from diverse pathways, including DNA crosslink repair, mediate alternative end joining. PLoS Genet 2015;11:e1004943.
49. Audebert M, Salles B, Calsou P. Involvement of poly(ADP-ribose) polymerase-1 and XRCC1/DNA ligase III in an alternative route for DNA double-strand breaks rejoining. J Biol Chem 2004;279:55117-55126.

50. Mansour WY, Rhein T, Dahm-Daphi J. The alternative end-joining pathway for repair of DNA double-strand breaks requires PARP1 but is not dependent upon microhomologies. Nucleic Acids Res 2010;38:6065-6077.

51. Zhang Y, Jasin M. An essential role for CtIP in chromosomal translocation formation through an alternative end-joining pathway. Nat Struct Mol Biol 2011;18:80-84.

52. Xie A, Kwok A, Scully R. Role of mammalian Mre11 in classical and alternative nonhomologous end joining. Nat Struct Mol Biol 2009;16:814-818.

53. McVey M, Lee SE. MMEJ repair of double-strand breaks (director's cut): deleted sequences and alternative endings. Trends in Genetics 2008;24:529-538.

54. Williams RS, Williams JS, Tainer JA. Mre11–Rad50–Nbs1 is a keystone complex connecting DNA repair machinery, double-strand break signaling, and the chromatin template. Biochemistry and Cell Biology 2007;85:509-520.

55. Jazayeri A, Balestrini A, Garner E, Haber JE, Costanzo V. Mre11–Rad50–Nbs1-dependent processing of DNA breaks generates oligonucleotides that stimulate ATM activity. The EMBO Journal 2008;27:1953-1962.

56. You Z, Bailis JM. DNA damage and decisions: CtIP coordinates DNA repair and cell cycle checkpoints. Trends in Cell Biology 2010;20:402-409.

57. Huen MSY, Sy SMH, Chen J. BRCA1 and its toolbox for the maintenance of genome integrity. Nat Rev Mol Cell Biol 2010;11:138-148.

58. Bolderson E, Tomimatsu N, Richard DJ, Boucher D, Kumar R, Pandita TK, Burma S, et al. Phosphorylation of Exo1 modulates homologous recombination repair of DNA double-strand breaks. Nucleic Acids Res 2010;38:1821-1831.

59. Wold MS. Replication protein A: a heterotrimeric, single-stranded DNA-binding protein required for eukaryotic DNA metabolism. Annu Rev Biochem 1997;66:61-92.

60. West SC. Molecular views of recombination proteins and their control. Nat Rev Mol Cell Biol 2003;4:435-445.

61. Suwaki N, Klare K, Tarsounas M. RAD51 paralogs: roles in DNA damage signalling, recombinational repair and tumorigenesis. Semin Cell Dev Biol 2011;22:898-905.

62. Ceballos SJ, Heyer WD. Functions of the Snf2/Swi2 family Rad54 motor protein in homologous recombination. Biochim Biophys Acta 2011;1809:509-523.

63. Fekairi S, Scaglione S, Chahwan C, Taylor ER, Tissier A, Coulon S, Dong MQ, et al. Human SLX4 is a Holliday junction resolvase subunit that binds multiple DNA repair/recombination endonucleases. Cell 2009;138:78-89.

64. Ip SC, Rass U, Blanco MG, Flynn HR, Skehel JM, West SC. Identification of Holliday junction resolvases from humans and yeast. Nature 2008;456:357-361.

65. Munoz IM, Hain K, Declais AC, Gardiner M, Toh GW, Sanchez-Pulido L, Heuckmann JM, et al. Coordination of structure-specific nucleases by human SLX4/BTBD12 is required for DNA repair. Mol Cell 2009;35:116-127.

66. Svendsen JM, Smogorzewska A, Sowa ME, O'Connell BC, Gygi SP, Elledge SJ, Harper JW. Mammalian BTBD12/SLX4 assembles a Holliday junction resolvase and is required for DNA repair. Cell 2009;138:63-77.

67. Zeman MK, Cimprich KA. Causes and consequences of replication stress. Nat Cell Biol 2014;16:2-9.

68. Marnef A, Cohen S, Legube G. Transcription-Coupled DNA Double-Strand Break Repair: Active Genes Need Special Care. J Mol Biol 2017;429:1277-1288.

69. Initial sequencing and analysis of the human genome. Nature 2001;409:860-921.

70. Sakofsky CJ, Malkova A. Break induced replication in eukaryotes: mechanisms, functions, and consequences. Crit Rev Biochem Mol Biol 2017;52:395-413.

71. Mao Z, Bozzella M, Seluanov A, Gorbunova V. DNA repair by nonhomologous end joining and homologous recombination during cell cycle in human cells. Cell Cycle 2008;7:2902-2906.

72. Paques F, Haber JE. Multiple pathways of recombination induced by double-strand breaks in Saccharomyces cerevisiae. Microbiol Mol Biol Rev 1999;63:349-404.

73. Takata M, Sasaki MS, Sonoda E, Morrison C, Hashimoto M, Utsumi H, Yamaguchi-Iwai Y, et al. Homologous recombination and non-homologous end-joining pathways of DNA double-strand break repair have overlapping roles in the maintenance of chromosomal integrity in vertebrate cells. The EMBO Journal 1998;17:5497-5508.

74. Ferreira MG, Cooper JP. Two modes of DNA double-strand break repair are reciprocally regulated through the fission yeast cell cycle. Genes Dev 2004;18:2249-2254.

75. Limbo O, Chahwan C, Yamada Y, de Bruin RAM, Wittenberg C, Russell P. Ctp1 is a Cell Cycle-Regulated Protein that Functions with Mre11 Complex to Control Double-Strand Break Repair by Homologous Recombination. Mol Cell 2007;28:134-146.

76. Aylon Y, Liefshitz B, Kupiec M. The CDK regulates repair of double-strand breaks by homologous recombination during the cell cycle. The EMBO Journal 2004;23:4868-4875.

77. Ira G, Pellicioli A, Balijja A, Wang X, Fiorani S, Carotenuto W, Liberi G, et al. DNA end resection, homologous recombination and DNA damage checkpoint activation require CDK1. Nature 2004;431:1011-1017.

78. Seeber A, Hauer M, Gasser SM. Nucleosome remodelers in double-strand break repair. Current Opinion in Genetics & Development 2013;23:174-184.

79. Price Brendan D, D'Andrea Alan D. Chromatin Remodeling at DNA Double-Strand Breaks. Cell;152:1344-1354.

80. Llorente B, Symington LS. The Mre11 nuclease is not required for 5' to 3' resection at multiple HO-induced double-strand breaks. Mol Cell Biol 2004;24:9682-9694.

81. Langerak P, Russell P. Regulatory networks integrating cell cycle control with DNA damage checkpoints and double-strand break repair. Philos Trans R Soc Lond B Biol Sci 2011;366:3562-3571.

82. Pierce AJ, Hu P, Han M, Ellis N, Jasin M. Ku DNA end-binding protein modulates homologous repair of double-strand breaks in mammalian cells. Genes Dev 2001;15:3237-3242.

83. Roth DB, Wilson JH. Relative rates of homologous and nonhomologous recombination in transfected DNA. Proc Natl Acad Sci U S A 1985;82:3355-3359.

84. Richardson C, Jasin M. Coupled Homologous and Nonhomologous Repair of a Double-Strand Break Preserves Genomic Integrity in Mammalian Cells. Mol Cell Biol 2000;20:9068-9075.

85. Rothkamm K, Kruger I, Thompson LH, Lobrich M. Pathways of DNA double-strand break repair during the mammalian cell cycle. Mol Cell Biol 2003;23:5706-5715.

86. Shibata A, Conrad S, Birraux J, Geuting V, Barton O, Ismail A, Kakarougkas A, et al. Factors determining DNA double-strand break repair pathway choice in G2 phase. Embo j 2011;30:1079-1092.

87. Goedecke W, Eijpe M, Offenberg HH, van Aalderen M, Heyting C. Mre11 and Ku70 interact in somatic cells, but are differentially expressed in early meiosis. Nat Genet 1999;23:194-198.

88. Van Dyck E, Stasiak AZ, Stasiak A, West SC. Binding of double-strand breaks in DNA by human Rad52 protein. Nature 1999;398:728-731.

89. Frank-Vaillant M, Marcand S. Transient stability of DNA ends allows nonhomologous end joining to precede homologous recombination. Mol Cell 2002;10:1189-1199.

90. Ristic D, Modesti M, Kanaar R, Wyman C. Rad52 and Ku bind to different DNA structures produced early in double-strand break repair. Nucleic Acids Res 2003;31:5229-5237.

91. Shibata A, Jeggo P, Lobrich M. The pendulum of the Ku-Ku clock. DNA Repair (Amst) 2018.

92. Foster SS, Balestrini A, Petrini JH. Functional interplay of the Mre11 nuclease and Ku in the response to replication-associated DNA damage. Mol Cell Biol 2011;31:4379-4389.

93. Balestrini A, Ristic D, Dionne I, Liu XZ, Wyman C, Wellinger RJ, Petrini JH. The Ku heterodimer and the metabolism of single-ended DNA double-strand breaks. Cell Rep 2013;3:2033-2045.

94. Langerak P, Mejia-Ramirez E, Limbo O, Russell P. Release of Ku and MRN from DNA ends by Mre11 nuclease activity and Ctp1 is required for homologous recombination repair of double-strand breaks. PLoS Genet 2011;7:e1002271.

95. Teixeira-Silva A, Ait Saada A, Hardy J, Iraqui I, Nocente MC, Freon K, Lambert SAE. The end-joining factor Ku acts in the end-resection of double strand break-free arrested replication forks. Nat Commun 2017;8:1982.

96. Garcia V, Phelps SE, Gray S, Neale MJ. Bidirectional resection of DNA double-strand breaks by Mre11 and Exo1. Nature 2011;479:241-244.

97. Clerici M, Mantiero D, Guerini I, Lucchini G, Longhese MP. The Yku70-Yku80 complex contributes to regulate double-strand break processing and checkpoint activation during the cell cycle. EMBO Rep 2008;9:810-818.

98. Wu D, Topper LM, Wilson TE. Recruitment and dissociation of nonhomologous end joining proteins at a DNA double-strand break in Saccharomyces cerevisiae. Genetics 2008;178:1237-1249.

99. Chanut P, Britton S, Coates J, Jackson SP, Calsou P. Coordinated nuclease activities counteract Ku at single-ended DNA double-strand breaks. Nat Commun 2016;7:12889.

100. Rothkamm K, Kruger I, Thompson LH, Lobrich M. Pathways of DNA double-strand break repair during the mammalian cell cycle. Mol Cell Biol. 2003;23.

101. Mirza-Aghazadeh-Attari M, Mohammadzadeh A, Yousefi B, Mihanfar A, Karimian A, Majidinia M. 53BP1: A key player of DNA damage response with critical functions in cancer. DNA Repair (Amst) 2018.

102. Zhang J. The role of BRCA1 in homologous recombination repair in response to replication stress: significance in tumorigenesis and cancer therapy. Cell Biosci 2013;3:11.

103. Chapman JR, Sossick AJ, Boulton SJ, Jackson SP. BRCA1-associated exclusion of 53BP1 from DNA damage sites underlies temporal control of DNA repair. J Cell Sci 2012;125:3529-3534.

104. Chapman JR, Barral P, Vannier JB, Borel V, Steger M, Tomas-Loba A, Sartori AA, et al. RIF1 is essential for 53BP1-dependent nonhomologous end joining and suppression of DNA double-strand break resection. Mol Cell 2013;49:858-871.

105. Isono M, Niimi A, Oike T, Hagiwara Y, Sato H, Sekine R, Yoshida Y, et al. BRCA1 Directs the Repair Pathway to Homologous Recombination by Promoting 53BP1 Dephosphorylation. Cell Rep 2017;18:520-532.

106. Zhang H, Liu H, Chen Y, Yang X, Wang P, Liu T, Deng M, et al. A cell cycle-dependent BRCA1-UHRF1 cascade regulates DNA double-strand break repair pathway choice. Nat Commun 2016;7:10201.

107. Escribano-Diaz C, Orthwein A, Fradet-Turcotte A, Xing M, Young JT, Tkac J, Cook MA, et al. A cell cycle-dependent regulatory circuit composed of 53BP1-RIF1 and BRCA1-CtIP controls DNA repair pathway choice. Mol Cell 2013;49:872-883.

108. Feng L, Fong KW, Wang J, Wang W, Chen J. RIF1 counteracts BRCA1-mediated end resection during DNA repair. J Biol Chem 2013;288:11135-11143.

109. Bouwman P, Aly A, Escandell JM, Pieterse M, Bartkova J, van der Gulden H, Hiddingh S, et al. 53BP1 loss rescues BRCA1 deficiency and is associated with triple-negative and BRCA-mutated breast cancers. Nat Struct Mol Biol 2010;17:688-695.

110. Bunting SF, Callen E, Wong N, Chen HT, Polato F, Gunn A, Bothmer A, et al. 53BP1 inhibits homologous recombination in Brca1-deficient cells by blocking resection of DNA breaks. Cell 2010;141:243-254.

111. Cao L, Xu X, Bunting SF, Liu J, Wang RH, Cao LL, Wu JJ, et al. A selective requirement for 53BP1 in the biological response to genomic instability induced by Brca1 deficiency. Mol Cell 2009;35:534-541.

112. al-Khodairy F, Carr AM. DNA repair mutants defining G2 checkpoint pathways in Schizosaccharomyces pombe. Embo j 1992;11:1343-1350.

113. al-Khodairy F, Fotou E, Sheldrick KS, Griffiths DJ, Lehmann AR, Carr AM. Identification and characterization of new elements involved in checkpoint and feedback controls in fission yeast. Mol Biol Cell 1994;5:147-160.

114. Kostrub CF, al-Khodairy F, Ghazizadeh H, Carr AM, Enoch T. Molecular analysis of hus1+, a fission yeast gene required for S-M and DNA damage checkpoints. Mol Gen Genet 1997;254:389-399.

115. Dufault VM, Oestreich AJ, Vroman BT, Karnitz LM. Identification and characterization of RAD9B, a paralog of the RAD9 checkpoint gene. Genomics 2003;82:644-651.

116. Hang H, Zhang Y, Dunbrack RL, Jr., Wang C, Lieberman HB. Identification and characterization of a paralog of human cell cycle checkpoint gene HUS1. Genomics 2002;79:487-492.

117. Aravind L, Walker DR, Koonin EV. Conserved domains in DNA repair proteins and evolution of repair systems. Nucleic Acids Res 1999;27:1223-1242.

118. Thelen MP, Venclovas C, Fidelis K. A sliding clamp model for the Rad1 family of cell cycle checkpoint proteins. Cell 1999;96:769-770.

119. Caspari T, Dahlen M, Kanter-Smoler G, Lindsay HD, Hofmann K, Papadimitriou K, Sunnerhagen P, et al. Characterization of Schizosaccharomyces pombe Hus1: a PCNA-related protein that associates with Rad1 and Rad9. Mol Cell Biol 2000;20:1254-1262.

120. Lieberman HB, Hopkins KM, Nass M, Demetrick D, Davey S. A human homolog of the Schizosaccharomyces pombe rad9+ checkpoint control gene. Proc Natl Acad Sci U S A 1996;93:13890-13895.

121. Bluyssen HA, van Os RI, Naus NC, Jaspers I, Hoeijmakers JH, de Klein A. A human and mouse homolog of the Schizosaccharomyces pombe rad1+ cell cycle checkpoint control gene. Genomics 1998;54:331-337.

122. Weiss RS, Kostrub CF, Enoch T, Leder P. Mouse Hus1, a homolog of the Schizosaccharomyces pombe hus1+ cell cycle checkpoint gene. Genomics 1999;59:32-39.

123. Xu M, Bai L, Gong Y, Xie W, Hang H, Jiang T. Structure and functional implications of the human rad9-hus1-rad1 cell cycle checkpoint complex. J Biol Chem 2009;284:20457-20461.

124. Dore AS, Kilkenny ML, Rzechorzek NJ, Pearl LH. Crystal structure of the rad9-rad1-hus1 DNA damage checkpoint complex--implications for clamp loading and regulation. Mol Cell 2009;34:735-745.

125. Sohn SY, Cho Y. Crystal structure of the human rad9-hus1-rad1 clamp. J Mol Biol 2009;390:490-502.

126. Venclovas C, Thelen MP. Structure-based predictions of Rad1, Rad9, Hus1 and Rad17 participation in sliding clamp and clamp-loading complexes. Nucleic Acids Res 2000;28:2481-2493.

127. Navadgi-Patil VM, Burgers PM. The unstructured C-terminal tail of the 9-1-1 clamp subunit Ddc1 activates Mec1/ATR via two distinct mechanisms. Mol Cell 2009;36:743-753.

128. Kaur R, Kostrub CF, Enoch T. Structure-function analysis of fission yeast Hus1-Rad1-Rad9 checkpoint complex. Mol Biol Cell 2001;12:3744-3758.

129. Zou L, Cortez D, Elledge SJ. Regulation of ATR substrate selection by Rad17-dependent loading of Rad9 complexes onto chromatin. Genes Dev 2002;16:198-208.

130. Ellison V, Stillman B. Biochemical characterization of DNA damage checkpoint complexes: clamp loader and clamp complexes with specificity for 5' recessed DNA. PLoS Biol 2003;1:E33.

131. Bermudez VP, Lindsey-Boltz LA, Cesare AJ, Maniwa Y, Griffith JD, Hurwitz J, Sancar A. Loading of the human 9-1-1 checkpoint complex onto DNA by the checkpoint clamp loader hRad17-replication factor C complex in vitro. Proc Natl Acad Sci U S A 2003;100:1633-1638.

132. Majka J, Burgers PM. The PCNA-RFC families of DNA clamps and clamp loaders. Prog Nucleic Acid Res Mol Biol 2004;78:227-260.

133. Xu X, Guardiani C, Yan C, Ivanov I. Opening pathways of the DNA clamps proliferating cell nuclear antigen and Rad9-Rad1-Hus1. Nucleic Acids Res 2013;41:10020-10031.

134. Lim PX, Patel DR, Poisson KE, Basuita M, Tsai C, Lyndaker AM, Hwang BJ, et al. Genome Protection by the 9-1-1 Complex Subunit HUS1 Requires Clamp Formation, DNA Contacts, and ATR Signaling-independent Effector Functions. J Biol Chem 2015;290:14826-14840.

135. Moldovan GL, Pfander B, Jentsch S. PCNA, the maestro of the replication fork. Cell 2007;129:665-679.

136. Eichinger CS, Jentsch S. 9-1-1: PCNA's specialized cousin. Trends Biochem Sci 2011;36:563-568.

137. Han SH, Hahm SH, Tran AH, Chung JH, Hong MK, Paik HD, Kim KS, et al. A physical association between the human mutY homolog (hMYH) and DNA topoisomerase II-binding protein 1 (hTopBP1) regulates Chk1-induced cell cycle arrest in HEK293 cells. Cell Biosci 2015;5:50.

138. Wang W, Brandt P, Rossi ML, Lindsey-Boltz L, Podust V, Fanning E, Sancar A, et al. The human Rad9-Rad1-Hus1 checkpoint complex stimulates flap endonuclease 1. Proc Natl Acad Sci U S A 2004;101:16762-16767.

139. Li T, Wang Z, Zhao Y, He W, An L, Liu S, Liu Y, et al. Checkpoint protein Rad9 plays an important role in nucleotide excision repair. DNA Repair (Amst) 2013;12:284-292.

140. He W, Zhao Y, Zhang C, An L, Hu Z, Liu Y, Han L, et al. Rad9 plays an important role in DNA mismatch repair through physical interaction with MLH1. Nucleic Acids Res 2008;36:6406-6417.

141. Pandita RK, Sharma GG, Laszlo A, Hopkins KM, Davey S, Chakhparonian M, Gupta A, et al. Mammalian Rad9 plays a role in telomere stability, S- and G2-phase-specific cell survival, and homologous recombinational repair. Mol Cell Biol 2006;26:1850-1864.

142. Weiss RS, Leder P, Vaziri C. Critical role for mouse Hus1 in an S-phase DNA damage cell cycle checkpoint. Mol Cell Biol 2003;23:791-803.

143. Sabbioneda S, Minesinger BK, Giannattasio M, Plevani P, Muzi-Falconi M, Jinks-Robertson S. The 9-1-1 checkpoint clamp physically interacts with polzeta and is partially required for spontaneous polzeta-dependent mutagenesis in Saccharomyces cerevisiae. J Biol Chem 2005;280:38657-38665.

144. Helt CE, Wang W, Keng PC, Bambara RA. Evidence that DNA damage detection machinery participates in DNA repair. Cell Cycle 2005;4:529-532.

145. Wang W, Lindsey-Boltz LA, Sancar A, Bambara RA. Mechanism of stimulation of human DNA ligase I by the Rad9-rad1-Hus1 checkpoint complex. J Biol Chem 2006;281:20865-20872.

146. Friedrich-Heineken E, Toueille M, Tannler B, Burki C, Ferrari E, Hottiger MO, Hubscher U. The two DNA clamps Rad9/Rad1/Hus1 complex and proliferating cell nuclear antigen differentially regulate flap endonuclease 1 activity. J Mol Biol 2005;353:980-989.

147. Kai M, Wang TS. Checkpoint activation regulates mutagenic translesion synthesis. Genes Dev 2003;17:64-76.

148. Sabbioneda S, Minesinger BK, Giannattasio M, Plevani P, Muzi-Falconi M, Jinks-Robertson S. The 9-1-1 Checkpoint Clamp Physically Interacts with Polζ and Is Partially Required for Spontaneous Polζ-dependent Mutagenesis in Saccharomyces cerevisiae. Journal of Biological Chemistry 2005;280:38657-38665.

149. Giannattasio M, Lazzaro F, Longhese MP, Plevani P, Muzi-Falconi M. Physical and functional interactions between nucleotide excision repair and DNA damage checkpoint. EMBO J 2004;23:429-438.

150. Bai H, Madabushi A, Guan X, Lu AL. Interaction between Human Mismatch Repair Recognition Proteins and Checkpoint sensor Rad9-Rad1-Hus1. DNA Repair 2010;9:478-487.

151. Weiss RS, Enoch T, Leder P. Inactivation of mouse Hus1 results in genomic instability and impaired responses to genotoxic stress. Genes Dev 2000;14:1886-1898.

152. Weiss RS, Leder P, Enoch T. A conserved role for the Hus1 checkpoint protein in eukaryotic genome maintenance. Cold Spring Harb Symp Quant Biol 2000;65:457-466.

153. Levitt PS, Zhu M, Cassano A, Yazinski SA, Liu H, Darfler J, Peters RM, et al. Genome maintenance defects in cultured cells and mice following partial inactivation of the essential cell cycle checkpoint gene Hus1. Mol Cell Biol 2007;27:2189-2201.

154. Balmus G, Lim PX, Oswald A, Hume KR, Cassano A, Pierre J, Hill A, et al. HUS1 regulates in vivo responses to genotoxic chemotherapies. Oncogene 2016;35:662-669.

155. Zou L, Elledge SJ. Sensing DNA damage through ATRIP recognition of RPA-ssDNA complexes. Science 2003;300:1542-1548.

156. You Z, Kong L, Newport J. The role of single-stranded DNA and polymerase alpha in establishing the ATR, Hus1 DNA replication checkpoint. J Biol Chem 2002;277:27088-27093.

157. St Onge RP, Besley BD, Pelley JL, Davey S. A role for the phosphorylation of hRad9 in checkpoint signaling. J Biol Chem 2003;278:26620-26628.

158. Ohashi E, Takeishi Y, Ueda S, Tsurimoto T. Interaction between Rad9-Hus1-Rad1 and TopBP1 activates ATR-ATRIP and promotes TopBP1 recruitment to sites of UV-damage. DNA Repair (Amst) 2014;21:1-11.

159. Kumagai A, Lee J, Yoo HY, Dunphy WG. TopBP1 activates the ATR-ATRIP complex. Cell 2006;124:943-955.

160. Delacroix S, Wagner JM, Kobayashi M, Yamamoto K, Karnitz LM. The Rad9-Hus1-Rad1 (9-1-1) clamp activates checkpoint signaling via TopBP1. Genes Dev 2007;21:1472-1477.

161. Paulovich AG, Armour CD, Hartwell LH. The Saccharomyces cerevisiae RAD9, RAD17, RAD24 and MEC3 genes are required for tolerating irreparable, ultraviolet-induced DNA damage. Genetics 1998;150:75-93.

162. Yang XH, Zou L. Dual functions of DNA replication forks in checkpoint signaling and PCNA ubiquitination. Cell Cycle 2009;8:191-194.

163. Huang TT, Nijman SM, Mirchandani KD, Galardy PJ, Cohn MA, Haas W, Gygi SP, et al. Regulation of monoubiquitinated PCNA by DUB autocleavage. Nat Cell Biol 2006;8:339-347.

164. Chapman JR, Taylor MR, Boulton SJ. Playing the end game: DNA double-strand break repair pathway choice. Mol Cell 2012;47:497-510.

165. Ngo GH, Balakrishnan L, Dubarry M, Campbell JL, Lydall D. The 9-1-1 checkpoint clamp stimulates DNA resection by Dna2-Sgs1 and Exo1. Nucleic Acids Res 2014;42:10516-10528.

166. Ngo GHP, Lydall D. The 9-1-1 checkpoint clamp coordinates resection at DNA double strand breaks. Nucleic Acids Res 2015;43:5017-5032.

167. Tsai F-L, Kai M. The checkpoint clamp protein Rad9 facilitates DNA-end resection and prevents alternative non-homologous end joining. Cell Cycle 2014;13:3460-3464.

168. Hanlon Newell AE, Hemphill A, Akkari YM, Hejna J, Moses RE, Olson SB. Loss of homologous recombination or non-homologous end-joining leads to radial formation following DNA interstrand crosslink damage. Cytogenet Genome Res 2008;121:174-180.

169. McCabe KM, Olson SB, Moses RE. DNA Interstrand Crosslink Repair in Mammalian Cells. Journal of cellular physiology 2009;220:569-573.

170. Iliakis G, Wang H, Perrault AR, Boecker W, Rosidi B, Windhofer F, Wu W, et al. Mechanisms of DNA double strand break repair and chromosome aberration formation. Cytogenet Genome Res 2004;104:14-20.

171. Wang X, Hu B, Weiss RS, Wang Y. The effect of Hus1 on ionizing radiation sensitivity is associated with homologous recombination repair but is independent of nonhomologous end-joining. Oncogene 2006;25:1980-1983.

172. Lange J, Yamada S, Tischfield SE, Pan J, Kim S, Zhu X, Socci ND, et al. The Landscape of Mouse Meiotic Double-Strand Break Formation, Processing, and Repair. Cell 2016;167:695-708.e616.

173. Lyndaker AM, Lim PX, Mleczko JM, Diggins CE, Holloway JK, Holmes RJ, Kan R, et al. Conditional inactivation of the DNA damage response gene Hus1 in mouse testis reveals separable roles for components of the RAD9-RAD1-HUS1 complex in meiotic chromosome maintenance. PLoS Genet 2013;9:e1003320.

174. Vasileva A, Hopkins KM, Wang X, Weisbach MM, Friedman RA, Wolgemuth DJ, Lieberman HB. The DNA damage checkpoint protein RAD9A is essential for male meiosis in the mouse. J Cell Sci 2013;126:3927-3938.

175. Warburg O, Wind F, Negelein E. THE METABOLISM OF TUMORS IN THE BODY. J Gen Physiol 1927;8:519-530.

176. Pavlova NN, Thompson CB. The Emerging Hallmarks of Cancer Metabolism. Cell Metab 2016;23:27-47.

177. Turgeon MO, Perry NJS, Poulogiannis G. DNA Damage, Repair, and Cancer Metabolism. Front Oncol 2018;8:15.

178. Miller JL, Grant PA. The role of DNA methylation and histone modifications in transcriptional regulation in humans. Subcell Biochem 2013;61:289-317.

179. Jeggo PA, Downs JA. Roles of chromatin remodellers in DNA double strand break repair. Exp Cell Res 2014;329:69-77.

180. Sharma AK, Hendzel MJ. The relationship between histone posttranslational modification and DNA damage signaling and repair. Int J Radiat Biol 2018:1-12.

181. Niculescu MD, Zeisel SH. Diet, methyl donors and DNA methylation: interactions between dietary folate, methionine and choline. J Nutr 2002;132:2333s-2335s.

182. Reid MA, Dai Z, Locasale JW. The impact of cellular metabolism on chromatin dynamics and epigenetics. Nat Cell Biol 2017;19:1298-1306.

183. Jiang Y, Qian X, Shen J, Wang Y, Li X, Liu R, Xia Y, et al. Local generation of fumarate promotes DNA repair through inhibition of histone H3 demethylation. Nat Cell Biol 2015;17:1158-1168.

184. Kunz BA, Kohalmi SE, Kunkel TA, Mathews CK, McIntosh EM, Reidy JA. International Commission for Protection Against Environmental Mutagens and Carcinogens. Deoxyribonucleoside triphosphate levels: a critical factor in the maintenance of genetic stability. Mutat Res 1994;318:1-64.

185. Reichard P. Interactions between deoxyribonucleotide and DNA synthesis. Annu Rev Biochem 1988;57:349-374.

186. Aye Y, Li M, Long MJ, Weiss RS. Ribonucleotide reductase and cancer: biological mechanisms and targeted therapies. Oncogene 2015;34:2011-2021.

187. Kretschmer S, Wolf C, Konig N, Staroske W, Guck J, Hausler M, Luksch H, et al. SAMHD1 prevents autoimmunity by maintaining genome stability. Ann Rheum Dis 2015;74:e17.

188. Lu SC. Regulation of glutathione synthesis. Mol Aspects Med 2009;30:42-59.

189. Yang M, Vousden KH. Serine and one-carbon metabolism in cancer. Nat Rev Cancer 2016;16:650-662.

190. Gorrini C, Baniasadi PS, Harris IS, Silvester J, Inoue S, Snow B, Joshi PA, et al. BRCA1 interacts with Nrf2 to regulate antioxidant signaling and cell survival. J Exp Med 2013;210:1529-1544.

191. Cosentino C, Grieco D, Costanzo V. ATM activates the pentose phosphate pathway promoting anti-oxidant defence and DNA repair. Embo j 2011;30:546-555.

192. Aird KM, Worth AJ, Snyder NW, Lee JV, Sivanand S, Liu Q, Blair IA, et al. ATM couples replication stress and metabolic reprogramming during cellular senescence. Cell Rep 2015;11:893-901.

193. Jeong SM, Xiao C, Finley LW, Lahusen T, Souza AL, Pierce K, Li YH, et al. SIRT4 has tumor-suppressive activity and regulates the cellular metabolic response to DNA damage by inhibiting mitochondrial glutamine metabolism. Cancer Cell 2013;23:450-463.

194. Budanov AV, Karin M. p53 target genes sestrin1 and sestrin2 connect genotoxic stress and mTOR signaling. Cell 2008;134:451-460.

195. Matoba S, Kang JG, Patino WD, Wragg A, Boehm M, Gavrilova O, Hurley PJ, et al. p53 regulates mitochondrial respiration. Science 2006;312:1650-1653.

196. Li H, Jogl G. Structural and biochemical studies of TIGAR (TP53-induced glycolysis and apoptosis regulator). J Biol Chem 2009;284:1748-1754.

197. Yahagi N, Shimano H, Matsuzaka T, Najima Y, Sekiya M, Nakagawa Y, Ide T, et al. p53 Activation in adipocytes of obese mice. J Biol Chem 2003;278:25395-25400.

198. Berkers CR, Maddocks OD, Cheung EC, Mor I, Vousden KH. Metabolic regulation by p53 family members. Cell Metab 2013;18:617-633.

199. Lobitz S, Velleuer E. Guido Fanconi (1892-1979): a jack of all trades. Nat Rev Cancer 2006;6:893-898.

200. Rosenberg PS, Tamary H, Alter BP. How high are carrier frequencies of rare recessive syndromes? Contemporary estimates for Fanconi Anemia in the United States and Israel. Am J Med Genet A 2011;155a:1877-1883.

201. Mehta PA, Tolar J: Fanconi Anemia. In: Adam MP, Ardinger HH, Pagon RA, Wallace SE, Bean LJH, Stephens K, Amemiya A, eds. GeneReviews((R)). Seattle (WA): University of Washington, Seattle University of Washington, Seattle. GeneReviews is a registered trademark of the University of Washington, Seattle. All rights reserved., 1993.

202. Shimamura A, Alter BP. Pathophysiology and management of inherited bone marrow failure syndromes. Blood Rev 2010;24:101-122.

203. Petryk A, Kanakatti Shankar R, Giri N, Hollenberg AN, Rutter MM, Nathan B, Lodish M, et al. Endocrine disorders in Fanconi anemia: recommendations for screening and treatment. J Clin Endocrinol Metab 2015;100:803-811.

204. Rose SR, Myers KC, Rutter MM, Mueller R, Khoury JC, Mehta PA, Harris RE, et al. Endocrine phenotype of children and adults with Fanconi anemia. Pediatr Blood Cancer 2012;59:690-696.

205. Wajnrajch MP, Gertner JM, Huma Z, Popovic J, Lin K, Verlander PC, Batish SD, et al. Evaluation of growth and hormonal status in patients referred to the International Fanconi Anemia Registry. Pediatrics 2001;107:744-754.

206. Giri N, Batista DL, Alter BP, Stratakis CA. Endocrine abnormalities in patients with Fanconi anemia. J Clin Endocrinol Metab 2007;92:2624-2631.

207. Elder DA, D'Alessio DA, Eyal O, Mueller R, Smith FO, Kansra AR, Rose SR. Abnormalities in glucose tolerance are common in children with fanconi anemia and associated with impaired insulin secretion. Pediatr Blood Cancer 2008;51:256-260.

208. Li J, Sipple J, Maynard S, Mehta PA, Rose SR, Davies SM, Pang Q. Fanconi anemia links reactive oxygen species to insulin resistance and obesity. Antioxid Redox Signal 2012;17:1083-1098.

209. Alter BP, Frissora CL, Halperin DS, Freedman MH, Chitkara U, Alvarez E, Lynch L, et al. Fanconi's anaemia and pregnancy. Br J Haematol 1991;77:410-418.

210. Nabhan SK, Bitencourt MA, Duval M, Abecasis M, Dufour C, Boudjedir K, Rocha V, et al. Fertility recovery and pregnancy after allogeneic hematopoietic stem cell transplantation in Fanconi anemia patients. Haematologica 2010;95:1783-1787.

211. Cheng NC, van de Vrugt HJ, van der Valk MA, Oostra AB, Krimpenfort P, de Vries Y, Joenje H, et al. Mice with a targeted disruption of the Fanconi anemia homolog Fanca. Hum Mol Genet 2000;9:1805-1811.

212. Nadler JJ, Braun RE. Fanconi anemia complementation group C is required for proliferation of murine primordial germ cells. Genesis 2000;27:117-123.

213. Aynsley-Green A, Zachmann M, Werder EA, Illig R, Prader A. Endocrine studies in Fanconi's anaemia. Report of 4 cases. Arch Dis Child 1978;53:126-131.

214. Sherafat-Kazemzadeh R, Mehta SN, Care MM, Kim MO, Williams DA, Rose SR. Small pituitary size in children with Fanconi anemia. Pediatr Blood Cancer 2007;49:166-170.

215. Fanconi Anemia Research Fund I. Fanconi Anemia: Guidelines for Diagnosis and Management. In: Hays L, editor.; 2014.

216. Rio P, Segovia JC, Hanenberg H, Casado JA, Martinez J, Gottsche K, Cheng NC, et al. In vitro phenotypic correction of hematopoietic progenitors from Fanconi anemia group A knockout mice. Blood 2002;100:2032-2039.

217. Whitney MA, Royle G, Low MJ, Kelly MA, Axthelm MK, Reifsteck C, Olson S, et al. Germ cell defects and hematopoietic hypersensitivity to gamma-interferon in mice with a targeted disruption of the Fanconi anemia C gene. Blood 1996;88:49-58.

218. Carreau M, Gan OI, Liu L, Doedens M, Dick JE, Buchwald M. Hematopoietic compartment of Fanconi anemia group C null mice contains fewer lineage-negative CD34+ primitive hematopoietic cells and shows reduced reconstruction ability. Exp Hematol 1999;27:1667-1674.

219. Li Y, Chen S, Yuan J, Yang Y, Li J, Ma J, Wu X, et al. Mesenchymal stem/progenitor cells promote the reconstitution of exogenous hematopoietic stem cells in Fancg-/- mice in vivo. Blood 2009;113:2342-2351.

220. Navarro S, Meza NW, Quintana-Bustamante O, Casado JA, Jacome A, McAllister K, Puerto S, et al. Hematopoietic dysfunction in a mouse model for Fanconi anemia group D1. Mol Ther 2006;14:525-535.

221. Parmar K, D'Andrea A, Niedernhofer LJ. Mouse models of Fanconi anemia. Mutat Res 2009;668:133-140.

222. Chen M, Tomkins DJ, Auerbach W, McKerlie C, Youssoufian H, Liu L, Gan O, et al. Inactivation of Fac in mice produces inducible chromosomal instability and reduced fertility reminiscent of Fanconi anaemia. Nat Genet 1996;12:448-451.

223. Yang Y, Kuang Y, Montes De Oca R, Hays T, Moreau L, Lu N, Seed B, et al. Targeted disruption of the murine Fanconi anemia gene, Fancg/Xrcc9. Blood 2001;98:3435-3440.

224. Koomen M, Cheng NC, van de Vrugt HJ, Godthelp BC, van der Valk MA, Oostra AB, Zdzienicka MZ, et al. Reduced fertility and hypersensitivity to mitomycin C characterize Fancg/Xrcc9 null mice. Hum Mol Genet 2002;11:273-281.

225. Gari K, Constantinou A. The role of the Fanconi anemia network in the response to DNA replication stress. Crit Rev Biochem Mol Biol 2009;44:292-325.

226. Hira A, Yoshida K, Sato K, Okuno Y, Shiraishi Y, Chiba K, Tanaka H, et al. Mutations in the gene encoding the E2 conjugating enzyme UBE2T cause Fanconi anemia. Am J Hum Genet 2015;96:1001-1007.

227. Ishiai M, Kitao H, Smogorzewska A, Tomida J, Kinomura A, Uchida E, Saberi A, et al. FANCI phosphorylation functions as a molecular switch to turn on the Fanconi anemia pathway. Nat Struct Mol Biol 2008;15:1138-1146.

228. Collins NB, Wilson JB, Bush T, Thomashevski A, Roberts KJ, Jones NJ, Kupfer GM. ATR-dependent phosphorylation of FANCA on serine 1449 after DNA damage is important for FA pathway function. Blood 2009;113:2181-2190.

229. Singh TR, Ali AM, Paramasivam M, Pradhan A, Wahengbam K, Seidman MM, Meetei AR. ATR-dependent phosphorylation of FANCM at serine 1045 is essential for FANCM functions. Cancer Res 2013;73:4300-4310.

230. Meetei AR, de Winter JP, Medhurst AL, Wallisch M, Waisfisz Q, van de Vrugt HJ, Oostra AB, et al. A novel ubiquitin ligase is deficient in Fanconi anemia. Nat Genet 2003;35:165-170.

231. Ciccia A, Ling C, Coulthard R, Yan Z, Xue Y, Meetei AR, Laghmani el H, et al. Identification of FAAP24, a Fanconi anemia core complex protein that interacts with FANCM. Mol Cell 2007;25:331-343.

232. Kee Y, D'Andrea AD. Molecular pathogenesis and clinical management of Fanconi anemia. J Clin Invest 2012;122:3799-3806.

233. Wang LC, Gautier J. The Fanconi anemia pathway and ICL repair: implications for cancer therapy. Crit Rev Biochem Mol Biol 2010;45:424-439.

234. Garcia-Higuera I, Taniguchi T, Ganesan S, Meyn MS, Timmers C, Hejna J, Grompe M, et al. Interaction of the Fanconi anemia proteins and BRCA1 in a common pathway. Mol Cell 2001;7:249-262.

235. Liang CC, Zhan B, Yoshikawa Y, Haas W, Gygi SP, Cohn MA. UHRF1 is a sensor for DNA interstrand crosslinks and recruits FANCD2 to initiate the Fanconi anemia pathway. Cell Rep 2015;10:1947-1956.

236. Oestergaard VH, Langevin F, Kuiken HJ, Pace P, Niedzwiedz W, Simpson LJ, Ohzeki M, et al. Deubiquitination of FANCD2 is required for DNA crosslink repair. Mol Cell 2007;28:798-809.

237. Liang Q, Dexheimer TS, Zhang P, Rosenthal AS, Villamil MA, You C, Zhang Q, et al. A selective USP1-UAF1 inhibitor links deubiquitination to DNA damage responses. Nat Chem Biol 2014;10:298-304.

238. Andreassen PR, D'Andrea AD, Taniguchi T. ATR couples FANCD2 monoubiquitination to the DNA-damage response. Genes Dev 2004;18:1958-1963.

239. Collis SJ, Barber LJ, Clark AJ, Martin JS, Ward JD, Boulton SJ. HCLK2 is essential for the mammalian S-phase checkpoint and impacts on Chk1 stability. Nat Cell Biol 2007;9:391-401.

240. Bogliolo M, Lyakhovich A, Callen E, Castella M, Cappelli E, Ramirez MJ, Creus A, et al. Histone H2AX and Fanconi anemia FANCD2 function in the same pathway to maintain chromosome stability. Embo j 2007;26:1340-1351.

241. Taniguchi T, Garcia-Higuera I, Xu B, Andreassen PR, Gregory RC, Kim ST, Lane WS, et al. Convergence of the fanconi anemia and ataxia telangiectasia signaling pathways. Cell 2002;109:459-472.

242. Cheung RS, Taniguchi T. Recent insights into the molecular basis of Fanconi anemia: genes, modifiers, and drivers. Int J Hematol 2017;106:335-344.

243. Huang M, D'Andrea AD. A new nuclease member of the FAN club. Nat Struct Mol Biol 2010;17:926-928.

244. Yamamoto KN, Kobayashi S, Tsuda M, Kurumizaka H, Takata M, Kono K, Jiricny J, et al. Involvement of SLX4 in interstrand cross-link repair is regulated by the Fanconi anemia pathway. Proc Natl Acad Sci U S A 2011;108:6492-6496.

245. Ciccia A, McDonald N, West SC. Structural and functional relationships of the XPF/MUS81 family of proteins. Annu Rev Biochem 2008;77:259-287.

246. Haynes B, Saadat N, Myung B, Shekhar MP. Crosstalk between translesion synthesis, Fanconi anemia network, and homologous recombination repair pathways in interstrand DNA crosslink repair and development of chemoresistance. Mutat Res Rev Mutat Res 2015;763:258-266.

247. Nakanishi K, Yang YG, Pierce AJ, Taniguchi T, Digweed M, D'Andrea AD, Wang ZQ, et al. Human Fanconi anemia monoubiquitination pathway promotes homologous DNA repair. Proc Natl Acad Sci U S A 2005;102:1110-1115.

248. Zhang N, Liu X, Li L, Legerski R. Double-strand breaks induce homologous recombinational repair of interstrand cross-links via cooperation of MSH2, ERCC1-XPF, REV3, and the Fanconi anemia pathway. DNA Repair (Amst) 2007;6:1670-1678.

249. Duquette ML, Zhu Q, Taylor ER, Tsay AJ, Shi LZ, Berns MW, McGowan CH. CtIP is required to initiate replication-dependent interstrand crosslink repair. PLoS Genet 2012;8:e1003050.

250. Moynahan ME, Pierce AJ, Jasin M. BRCA2 is required for homology-directed repair of chromosomal breaks. Mol Cell 2001;7:263-272.

251. Xia B, Sheng Q, Nakanishi K, Ohashi A, Wu J, Christ N, Liu X, et al. Control of BRCA2 cellular and clinical functions by a nuclear partner, PALB2. Mol Cell 2006;22:719-729.

252. Litman R, Peng M, Jin Z, Zhang F, Zhang J, Powell S, Andreassen PR, et al. BACH1 is critical for homologous recombination and appears to be the Fanconi anemia gene product FANCJ. Cancer Cell 2005;8:255-265.

253. Sommers JA, Rawtani N, Gupta R, Bugreev DV, Mazin AV, Cantor SB, Brosh RM, Jr. FANCJ uses its motor ATPase to destabilize protein-DNA complexes, unwind triplexes, and inhibit RAD51 strand exchange. J Biol Chem 2009;284:7505-7517.

254. French CA, Masson JY, Griffin CS, O'Regan P, West SC, Thacker J. Role of mammalian RAD51L2 (RAD51C) in recombination and genetic stability. J Biol Chem 2002;277:19322-19330.

255. Liu Y, Tarsounas M, O'Regan P, West SC. Role of RAD51C and XRCC3 in genetic recombination and DNA repair. J Biol Chem 2007;282:1973-1979.

256. Ceccaldi R, Sarangi P, D'Andrea AD. The Fanconi anaemia pathway: new players and new functions. Nat Rev Mol Cell Biol 2016;17:337-349.

257. Howlett NG, Taniguchi T, Durkin SG, D'Andrea AD, Glover TW. The Fanconi anemia pathway is required for the DNA replication stress response and for the regulation of common fragile site stability. Hum Mol Genet 2005;14:693-701.

258. Molina B, Marchetti F, Gomez L, Ramos S, Torres L, Ortiz R, Altamirano-Lozano M, et al. Hydroxyurea induces chromosomal damage in G2 and enhances the clastogenic effect of mitomycin C in Fanconi anemia cells. Environ Mol Mutagen 2015;56:457-467.

259. Chen X, Bosques L, Sung P, Kupfer GM. A novel role for non-ubiquitinated FANCD2 in response to hydroxyurea-induced DNA damage. Oncogene 2016;35:22-34.

260. Zhu W, Dutta A. An ATR- and BRCA1-mediated Fanconi anemia pathway is required for activating the G2/M checkpoint and DNA damage repair upon rereplication. Mol Cell Biol 2006;26:4601-4611.

261. Spardy N, Duensing A, Charles D, Haines N, Nakahara T, Lambert PF, Duensing S. The human papillomavirus type 16 E7 oncoprotein activates the Fanconi anemia (FA) pathway and causes accelerated chromosomal instability in FA cells. J Virol 2007;81:13265-13270.

262. Ridpath JR, Nakamura A, Tano K, Luke AM, Sonoda E, Arakawa H, Buerstedde JM, et al. Cells deficient in the FANC/BRCA pathway are hypersensitive to plasma levels of formaldehyde. Cancer Res 2007;67:11117-11122.

263. Lossaint G, Larroque M, Ribeyre C, Bec N, Larroque C, Decaillet C, Gari K, et al. FANCD2 binds MCM proteins and controls replisome function upon activation of s phase checkpoint signaling. Mol Cell 2013;51:678-690.

264. Schlacher K, Christ N, Siaud N, Egashira A, Wu H, Jasin M. Double-strand break repair-independent role for BRCA2 in blocking stalled replication fork degradation by MRE11. Cell 2011;145:529-542.

265. Schlacher K, Wu H, Jasin M. A distinct replication fork protection pathway connects Fanconi anemia tumor suppressors to RAD51-BRCA1/2. Cancer Cell 2012;22:106-116.

266. Chen YH, Jones MJ, Yin Y, Crist SB, Colnaghi L, Sims RJ, 3rd, Rothenberg E, et al. ATR-mediated phosphorylation of FANCI regulates dormant origin firing in response to replication stress. Mol Cell 2015;58:323-338.

267. Chan KL, Palmai-Pallag T, Ying S, Hickson ID. Replication stress induces sister-chromatid bridging at fragile site loci in mitosis. Nat Cell Biol 2009;11:753-760.

268. Naim V, Rosselli F. The FANC pathway and BLM collaborate during mitosis to prevent micro-nucleation and chromosome abnormalities. Nat Cell Biol 2009;11:761-768.

269. Centurion SA, Kuo HR, Lambert WC. Damage-resistant DNA synthesis in Fanconi anemia cells treated with a DNA cross-linking agent. Exp Cell Res 2000;260:216-221.

270. Pichierri P, Rosselli F. The DNA crosslink-induced S-phase checkpoint depends on ATR-CHK1 and ATR-NBS1-FANCD2 pathways. Embo j 2004;23:1178-1187.

271. Somyajit K, Subramanya S, Nagaraju G. Distinct roles of FANCO/RAD51C protein in DNA damage signaling and repair: implications for Fanconi anemia and breast cancer susceptibility. J Biol Chem 2012;287:3366-3380.

272. Freie BW, Ciccone SL, Li X, Plett PA, Orschell CM, Srour EF, Hanenberg H, et al. A role for the Fanconi anemia C protein in maintaining the DNA damage-induced G2 checkpoint. J Biol Chem 2004;279:50986-50993.

273. Yu X, Chini CC, He M, Mer G, Chen J. The BRCT domain is a phospho-protein binding domain. Science 2003;302:639-642.

274. Nalepa G, Enzor R, Sun Z, Marchal C, Park SJ, Yang Y, Tedeschi L, et al. Fanconi anemia signaling network regulates the spindle assembly checkpoint. J Clin Invest 2013;123:3839-3847.

275. Lee H, Trainer AH, Friedman LS, Thistlethwaite FC, Evans MJ, Ponder BA, Venkitaraman AR. Mitotic checkpoint inactivation fosters transformation in cells lacking the breast cancer susceptibility gene, Brca2. Mol Cell 1999;4:1-10.

276. D'Angiolella V, Mari C, Nocera D, Rametti L, Grieco D. The spindle checkpoint requires cyclin-dependent kinase activity. Genes Dev 2003;17:2520-2525.

277. Mi J, Qiao F, Wilson JB, High AA, Schroeder MJ, Stukenberg PT, Moss A, et al. FANCG is phosphorylated at serines 383 and 387 during mitosis. Mol Cell Biol 2004;24:8576-8585.

278. Vinciguerra P, Godinho SA, Parmar K, Pellman D, D'Andrea AD. Cytokinesis failure occurs in Fanconi anemia pathway-deficient murine and human bone marrow hematopoietic cells. J Clin Invest 2010;120:3834-3842.

279. Shen Y, Lee YH, Panneerselvam J, Zhang J, Loo LW, Fei P. Mutated Fanconi anemia pathway in non-Fanconi anemia cancers. Oncotarget 2015;6:20396-20403.

280. Chen H, Zhang S, Wu Z. Fanconi anemia pathway defects in inherited and sporadic cancers. Transl Pediatr 2014;3:300-304.

281. Bogdanova N, Helbig S, Dork T. Hereditary breast cancer: ever more pieces to the polygenic puzzle. Hered Cancer Clin Pract 2013;11:12.

282. Antoniou A, Pharoah PD, Narod S, Risch HA, Eyfjord JE, Hopper JL, Loman N, et al. Average risks of breast and ovarian cancer associated with BRCA1 or BRCA2 mutations detected in case Series unselected for family history: a combined analysis of 22 studies. Am J Hum Genet 2003;72:1117-1130.

283. Fackenthal JD, Olopade OI. Breast cancer risk associated with BRCA1 and BRCA2 in diverse populations. Nat Rev Cancer 2007;7:937-948.

284. van der Heijden MS, Yeo CJ, Hruban RH, Kern SE. Fanconi anemia gene mutations in young-onset pancreatic cancer. Cancer Res 2003;63:2585-2588.

285. Taniguchi T, D'Andrea AD. Molecular pathogenesis of Fanconi anemia: recent progress. Blood 2006;107:4223-4233.

286. Tischkowitz M, Ameziane N, Waisfisz Q, De Winter JP, Harris R, Taniguchi T, D'Andrea A, et al. Bi-allelic silencing of the Fanconi anaemia gene FANCF in acute myeloid leukaemia. Br J Haematol 2003;123:469-471.

287. Taniguchi T, Tischkowitz M, Ameziane N, Hodgson SV, Mathew CG, Joenje H, Mok SC, et al. Disruption of the Fanconi anemia-BRCA pathway in cisplatin-sensitive ovarian tumors. Nat Med 2003;9:568-574.

288. Thomashevski A, High AA, Drozd M, Shabanowitz J, Hunt DF, Grant PA, Kupfer GM. The Fanconi anemia core complex forms four complexes of different sizes in different subcellular compartments. J Biol Chem 2004;279:26201-26209.

289. Mi J, Kupfer GM. The Fanconi anemia core complex associates with chromatin during S phase. Blood 2005;105:759-766.

290. Hoshino T, Wang J, Devetten MP, Iwata N, Kajigaya S, Wise RJ, Liu JM, et al. Molecular chaperone GRP94 binds to the Fanconi anemia group C protein and regulates its intracellular expression. Blood 1998;91:4379-4386.

291. Youssoufian H, Auerbach AD, Verlander PC, Steimle V, Mach B. Identification of cytosolic proteins that bind to the Fanconi anemia complementation group C polypeptide in vitro. Evidence for a multimeric complex. J Biol Chem 1995;270:9876-9882.

292. Futaki M, Igarashi T, Watanabe S, Kajigaya S, Tatsuguchi A, Wang J, Liu JM. The FANCG Fanconi anemia protein interacts with CYP2E1: possible role in protection against oxidative DNA damage. Carcinogenesis 2002;23:67-72.

293. Nordenson I. Effect of superoxide dismutase and catalase on spontaneously occurring chromosome breaks in patients with Fanconi's anemia. Hereditas 1977;86:147-150.

294. Joenje H, Arwert F, Eriksson AW, de Koning H, Oostra AB. Oxygen-dependence of chromosomal aberrations in Fanconi's anaemia. Nature 1981;290:142-143.

295. Pagano G, Talamanca AA, Castello G, Pallardo FV, Zatterale A, Degan P. Oxidative stress in Fanconi anaemia: from cells and molecules towards prospects in clinical management. Biol Chem 2012;393:11-21.

296. Takeuchi T, Morimoto K. Increased formation of 8-hydroxydeoxyguanosine, an oxidative DNA damage, in lymphoblasts from Fanconi's anemia patients due to possible catalase deficiency. Carcinogenesis 1993;14:1115-1120.

297. Schultz JC, Shahidi NT. Detection of tumor necrosis factor-alpha in bone marrow plasma and peripheral blood plasma from patients with aplastic anemia. Am J Hematol 1994;45:32-38.

298. Dusre L, Rajagopalan S, Eliot HM, Covey JM, Sinha BK. DNA interstrand cross-link and free radical formation in a human multidrug-resistant cell line from mitomycin C and its analogues. Cancer Res 1990;50:648-652.

299. Iyer VN, Szybalski W. Mitomycins and porfiromycin: chemiccal mechanism of activation and cross-linking of DNA. Science 1964;145:55-58.

300. Korkina LG, Deeva IB, De Biase A, Iaccarino M, Oral R, Warnau M, Pagano G. Redox-dependent toxicity of diepoxybutane and mitomycin C in sea urchin embryogenesis. Carcinogenesis 2000;21:213-220.

301. Castillo P, Bogliolo M, Surralles J. Coordinated action of the Fanconi anemia and ataxia telangiectasia pathways in response to oxidative damage. DNA Repair (Amst) 2011;10:518-525.

302. Kruyt FA, Hoshino T, Liu JM, Joseph P, Jaiswal AK, Youssoufian H. Abnormal microsomal detoxification implicated in Fanconi anemia group C by interaction of the FAC protein with NADPH cytochrome P450 reductase. Blood 1998;92:3050-3056.

303. Cumming RC, Lightfoot J, Beard K, Youssoufian H, O'Brien PJ, Buchwald M. Fanconi anemia group C protein prevents apoptosis in hematopoietic cells through redox regulation of GSTP1. Nat Med 2001;7:814-820.

304. Mukhopadhyay SS, Leung KS, Hicks MJ, Hastings PJ, Youssoufian H, Plon SE. Defective mitochondrial peroxiredoxin-3 results in sensitivity to oxidative stress in Fanconi anemia. J Cell Biol 2006;175:225-235.

305. Li J, Du W, Maynard S, Andreassen PR, Pang Q. Oxidative stress-specific interaction between FANCD2 and FOXO3a. Blood 2010;115:1545-1548.

306. Du W, Rani R, Sipple J, Schick J, Myers KC, Mehta P, Andreassen PR, et al. The FA pathway counteracts oxidative stress through selective protection of antioxidant defense gene promoters. Blood 2012;119:4142-4151.

307. Zhang QS, Eaton L, Snyder ER, Houghtaling S, Mitchell JB, Finegold M, Van Waes C, et al. Tempol protects against oxidative damage and delays epithelial tumor onset in Fanconi anemia mice. Cancer Res 2008;68:1601-1608.

308. Zhang QS, Marquez-Loza L, Eaton L, Duncan AW, Goldman DC, Anur P, Watanabe-Smith K, et al. Fancd2-/- mice have hematopoietic defects that can be partially corrected by resveratrol. Blood 2010;116:5140-5148.

309. Hadjur S, Ung K, Wadsworth L, Dimmick J, Rajcan-Separovic E, Scott RW, Buchwald M, et al. Defective hematopoiesis and hepatic steatosis in mice with combined deficiencies of the genes encoding Fancc and Cu/Zn superoxide dismutase. Blood 2001;98:1003-1011.

310. Kumari U, Ya Jun W, Huat Bay B, Lyakhovich A. Evidence of mitochondrial dysfunction and impaired ROS detoxifying machinery in Fanconi anemia cells. Oncogene 2014;33:165-172.

311. Bogliolo M, Borghini S, Abbondandolo A, Degan P. Alternative metabolic pathways for energy supply and resistance to apoptosis in Fanconi anaemia. Mutagenesis 2002;17:25-30.

312. Sumpter R, Sirasanagandla S, Fernández ÁF, Wei Y, Dong X, Franco L, Zou Z, et al. Fanconi anemia proteins function in mitophagy and immunity. Cell 2016;165:867-881.

313. Jayabal P, Ma C, Nepal M, Shen Y, Che R, Turkson J, Fei P. Involvement of FANCD2 in Energy Metabolism via ATP5alpha. Sci Rep 2017;7:4921.

314. Schultz JC, Shahidi NT. Tumor necrosis factor-alpha overproduction in Fanconi's anemia. Am J Hematol 1993;42:196-201.

315. Rosselli F, Sanceau J, Gluckman E, Wietzerbin J, Moustacchi E. Abnormal lymphokine production: a novel feature of the genetic disease Fanconi anemia. II. In vitro and in vivo spontaneous overproduction of tumor necrosis factor alpha. Blood 1994;83:1216-1225.

316. Dufour C, Corcione A, Svahn J, Haupt R, Poggi V, Beka'ssy AN, Scime R, et al. TNF-alpha and IFN-gamma are overexpressed in the bone marrow of Fanconi anemia patients and TNF-alpha suppresses erythropoiesis in vitro. Blood 2003;102:2053-2059.

317. Justo GA, Bitencourt MA, Pasquini R, Castelo-Branco MT, Rumjanek VM. Increased IL10 plasmatic levels in Fanconi anemia patients. Cytokine 2013;64:486-489.

318. Suematsu N, Tsutsui H, Wen J, Kang D, Ikeuchi M, Ide T, Hayashidani S, et al. Oxidative stress mediates tumor necrosis factor-alpha-induced mitochondrial DNA damage and dysfunction in cardiac myocytes. Circulation 2003;107:1418-1423.

319. Aggarwal BB, Shishodia S, Ashikawa K, Bharti AC. The role of TNF and its family members in inflammation and cancer: lessons from gene deletion. Curr Drug Targets Inflamm Allergy 2002;1:327-341.

320. Nagakawa Y, Williams GM, Zheng Q, Tsuchida A, Aoki T, Montgomery RA, Klein AS, et al. Oxidative mitochondrial DNA damage and deletion in hepatocytes of rejecting liver allografts in rats: role of TNF-alpha. Hepatology 2005;42:208-215.

321. Rezzoug F, Huang Y, Tanner MK, Wysoczynski M, Schanie CL, Chilton PM, Ratajczak MZ, et al. TNF-alpha is critical to facilitate hemopoietic stem cell engraftment and function. J Immunol 2008;180:49-57.

322. Vanderwerf SM, Svahn J, Olson S, Rathbun RK, Harrington C, Yates J, Keeble W, et al. TLR8-dependent TNF-(alpha) overexpression in Fanconi anemia group C cells. Blood 2009;114:5290-5298.

323. Bijangi-Vishehsaraei K, Saadatzadeh MR, Werne A, McKenzie KA, Kapur R, Ichijo H, Haneline LS. Enhanced TNF-alpha-induced apoptosis in Fanconi anemia type C-deficient cells is dependent on apoptosis signal-regulating kinase 1. Blood 2005;106:4124-4130.

324. Dufour C, Corcione A, Svahn J, Haupt R, Battilana N, Pistoia V. Interferon gamma and tumour necrosis factor alpha are overexpressed in bone marrow T lymphocytes from paediatric patients with aplastic anaemia. Br J Haematol 2001;115:1023-1031.

325. Rathbun RK, Faulkner GR, Ostroski MH, Christianson TA, Hughes G, Jones G, Cahn R, et al. Inactivation of the Fanconi anemia group C gene augments interferon-gamma-induced apoptotic responses in hematopoietic cells. Blood 1997;90:974-985.

326. Haneline LS, Broxmeyer HE, Cooper S, Hangoc G, Carreau M, Buchwald M, Clapp DW. Multiple inhibitory cytokines induce deregulated progenitor growth and apoptosis in hematopoietic cells from Fac-/- mice. Blood 1998;91:4092-4098.

327. Zhang X, Sejas DP, Qiu Y, Williams DA, Pang Q. Inflammatory ROS promote and cooperate with the Fanconi anemia mutation for hematopoietic senescence. J Cell Sci 2007;120:1572-1583.

328. Zhou L, McMahon C, Bhagat T, Alencar C, Yu Y, Fazzari M, Sohal D, et al. Reduced SMAD7 leads to overactivation of TGF-beta signaling in MDS that can be reversed by a specific inhibitor of TGF-beta receptor I kinase. Cancer Res 2011;71:955-963.

329. Suragani RN, Cadena SM, Cawley SM, Sako D, Mitchell D, Li R, Davies MV, et al. Transforming growth factor-beta superfamily ligand trap ACE-536 corrects anemia by promoting late-stage erythropoiesis. Nat Med 2014;20:408-414.

330. Zhang H, Kozono DE, O'Connor KW, Vidal-Cardenas S, Rousseau A, Hamilton A, Moreau L, et al. TGF-beta Inhibition Rescues Hematopoietic Stem Cell Defects and Bone Marrow Failure in Fanconi Anemia. Cell Stem Cell 2016;18:668-681.

331. Cagnan I, Gunel-Ozcan A, Aerts-Kaya F, Ameziane N, Kuskonmaz B, Dorsman J, Gumruk F, et al. Bone Marrow Mesenchymal Stem Cells Carrying FANCD2 Mutation Differ from the Other Fanconi Anemia Complementation Groups in Terms of TGF-beta1 Production. Stem Cell Rev 2018;14:425-437.

332. Ravera S, Vaccaro D, Cuccarolo P, Columbaro M, Capanni C, Bartolucci M, Panfoli I, et al. Mitochondrial respiratory chain Complex I defects in Fanconi anemia complementation group A. Biochimie 2013;95:1828-1837.

333. Cappelli E, Cuccarolo P, Stroppiana G, Miano M, Bottega R, Cossu V, Degan P, et al. Defects in mitochondrial energetic function compels Fanconi Anaemia cells to glycolytic metabolism. Biochim Biophys Acta 2017;1863:1214-1221.

334. Chun MJ, Choi H, Jun DW, Kim S, Kim YN, Kim SY, Lee CH. Fanconi anemia protein FANCD2 is activated by AICAR, a modulator of AMPK and cellular energy metabolism. FEBS Open Bio 2017;7:284-292.

335. Chun MJ, Kim S, Hwang SK, Kim BS, Kim HG, Choi HI, Kim JH, et al. AMP-activated protein kinase is involved in the activation of the Fanconi anemia/BRCA pathway in response to DNA interstrand crosslinks. Oncotarget 2016;7:53642-53653.

336. Sanli T, Steinberg GR, Singh G, Tsakiridis T. AMP-activated protein kinase (AMPK) beyond metabolism: a novel genomic stress sensor participating in the DNA damage response pathway. Cancer Biol Ther 2014;15:156-169.

337. Fu X, Wan S, Lyu YL, Liu LF, Qi H. Etoposide induces ATM-dependent mitochondrial biogenesis through AMPK activation. PLoS One 2008;3:e2009.

338. Sanli T, Rashid A, Liu C, Harding S, Bristow RG, Cutz JC, Singh G, et al. Ionizing radiation activates AMP-activated kinase (AMPK): a target for radiosensitization of human cancer cells. Int J Radiat Oncol Biol Phys 2010;78:221-229.

339. Ravera S, Degan P, Sabatini F, Columbaro M, Dufour C, Cappelli E. Altered lipid metabolism could drive the bone marrow failure in fanconi anaemia. Br J Haematol 2018.

340. Romick-Rosendale LE, Hoskins EE, Privette Vinnedge LM, Foglesong GD, Brusadelli MG, Potter SS, Komurov K, et al. Defects in the Fanconi Anemia Pathway in Head and Neck Cancer Cells Stimulate Tumor Cell Invasion through DNA-PK and Rac1 Signaling. Clin Cancer Res 2016;22:2062-2073.

341. Zhao X, Brusadelli MG, Sauter S, Butsch Kovacic M, Zhang W, Romick-Rosendale LE, Lambert PF, et al. Lipidomic Profiling Links the Fanconi Anemia Pathway to Glycosphingolipid Metabolism in Head and Neck Cancer Cells. Clin Cancer Res 2018;24:2700-2709.

342. Mendez-Ferrer S, Michurina TV, Ferraro F, Mazloom AR, Macarthur BD, Lira SA, Scadden DT, et al. Mesenchymal and haematopoietic stem cells form a unique bone marrow niche. Nature 2010;466:829-834.

343. Amarachintha S, Sertorio M, Wilson A, Li X, Pang Q. Fanconi Anemia Mesenchymal Stromal Cells-Derived Glycerophospholipids Skew Hematopoietic Stem Cell Differentiation Through Toll-Like Receptor Signaling. Stem Cells 2015;33:3382-3396.

344. Ceccaldi R, Rondinelli B, D'Andrea AD. Repair Pathway Choices and Consequences at the Double-Strand Break. Trends Cell Biol 2016;26:52-64.

345. Aparicio T, Baer R, Gautier J. DNA double-strand break repair pathway choice and cancer. DNA Repair (Amst) 2014;19:169-175.

346. Shibata A. Regulation of repair pathway choice at two-ended DNA double-strand breaks. Mutat Res 2017;803-805:51-55.

347. Bosma GC, Custer RP, Bosma MJ. A severe combined immunodeficiency mutation in the mouse. Nature 1983;301:527-530.

348. Haines JW, Coster M, Bouffler SD. Impairment of the non-homologous end joining and homologous recombination pathways of DNA double strand break repair: Impact on spontaneous and radiation-induced mammary and intestinal tumour risk in Apc min/+ mice. DNA Repair (Amst) 2015;35:19-26.

349. Gao Y, Chaudhuri J, Zhu C, Davidson L, Weaver DT, Alt FW. A targeted DNA-PKcs-null mutation reveals DNA-PK-independent functions for KU in V(D)J recombination. Immunity 1998;9:367-376.

350. Taccioli GE, Amatucci AG, Beamish HJ, Gell D, Xiang XH, Torres Arzayus MI, Priestley A, et al. Targeted disruption of the catalytic subunit of the DNA-PK gene in mice confers severe combined immunodeficiency and radiosensitivity. Immunity 1998;9:355-366.

351. Kuhfittig-Kulle S, Feldmann E, Odersky A, Kuliczkowska A, Goedecke W, Eggert A, Pfeiffer P. The mutagenic potential of non-homologous end joining in the absence of the NHEJ core factors Ku70/80, DNA-PKcs and XRCC4-LigIV. Mutagenesis 2007;22:217-233.

352. Petukhova G, Van Komen S, Vergano S, Klein H, Sung P. Yeast Rad54 promotes Rad51-dependent homologous DNA pairing via ATP hydrolysis-driven change in DNA double helix conformation. J Biol Chem 1999;274:29453-29462.

353. Essers J, Hendriks RW, Swagemakers SM, Troelstra C, de Wit J, Bootsma D, Hoeijmakers JH, et al. Disruption of mouse RAD54 reduces ionizing radiation resistance and homologous recombination. Cell 1997;89:195-204.

354. Dronkert ML, Beverloo HB, Johnson RD, Hoeijmakers JH, Jasin M, Kanaar R. Mouse RAD54 affects DNA double-strand break repair and sister chromatid exchange. Mol Cell Biol 2000;20:3147-3156.

355. Essers J, van Steeg H, de Wit J, Swagemakers SM, Vermeij M, Hoeijmakers JH, Kanaar R. Homologous and non-homologous recombination differentially affect DNA damage repair in mice. Embo j 2000;19:1703-1710.

356. Symington LS. Role of RAD52 epistasis group genes in homologous recombination and double-strand break repair. Microbiol Mol Biol Rev 2002;66:630-670, table of contents.

357. Chu WK, Hanada K, Kanaar R, Hickson ID. BLM has early and late functions in homologous recombination repair in mouse embryonic stem cells. Oncogene 2010;29:4705-4714.

358. Couedel C, Mills KD, Barchi M, Shen L, Olshen A, Johnson RD, Nussenzweig A, et al. Collaboration of homologous recombination and nonhomologous end-joining factors for the survival and integrity of mice and cells. Genes Dev 2004;18:1293-1304.

359. Farmer H, McCabe N, Lord CJ, Tutt AN, Johnson DA, Richardson TB, Santarosa M, et al. Targeting the DNA repair defect in BRCA mutant cells as a therapeutic strategy. Nature 2005;434:917-921.

360. Newell AE, Akkari YM, Torimaru Y, Rosenthal A, Reifsteck CA, Cox B, Grompe M, et al. Interstrand crosslink-induced radials form between non-homologous chromosomes, but are absent in sex chromosomes. DNA Repair (Amst) 2004;3:535-542.

361. Karras GI, Fumasoni M, Sienski G, Vanoli F, Branzei D, Jentsch S. Noncanonical role of the 9-1-1 clamp in the error-free DNA damage tolerance pathway. Mol Cell 2013;49:536-546.

362. Carroll AM, Hardy RR, Petrini J, Bosma MJ. T cell leakiness in scid mice. Curr Top Microbiol Immunol 1989;152:117-123.

363. Bosma MJ. B and T cell leakiness in the scid mouse mutant. Immunodefic Rev 1992;3:261-276.

364. Balmus G, Zhu M, Mukherjee S, Lyndaker AM, Hume KR, Lee J, Riccio ML, et al. Disease severity in a mouse model of ataxia telangiectasia is modulated by the DNA damage checkpoint gene Hus1. Hum Mol Genet 2012;21:3408-3420.

365. Barlow C, Hirotsune S, Paylor R, Liyanage M, Eckhaus M, Collins F, Shiloh Y, et al. Atm-deficient mice: a paradigm of ataxia telangiectasia. Cell 1996;86:159-171.

366. Xu Y, Ashley T, Brainerd EE, Bronson RT, Meyn MS, Baltimore D. Targeted disruption of ATM leads to growth retardation, chromosomal fragmentation during meiosis, immune defects, and thymic lymphoma. Genes Dev 1996;10:2411-2422.

367. Schubert R, Schmitz N, Pietzner J, Tandi C, Theisen A, Dresel R, Christmann M, et al. Growth hormone supplementation increased latency to tumourigenesis in Atm-deficient mice. Growth Factors 2009;27:265-273.

368. Niedernhofer LJ. Tissue-specific accelerated aging in nucleotide excision repair deficiency. Mech Ageing Dev 2008;129:408-415.

369. Vlangos CN, O'Connor BC, Morley MJ, Krause AS, Osawa GA, Keegan CE. Caudal regression in adrenocortical dysplasia (acd) mice is caused by telomere dysfunction with subsequent p53-dependent apoptosis. Dev Biol 2009;334:418-428.

370. Goodship J, Gill H, Carter J, Jackson A, Splitt M, Wright M. Autozygosity mapping of a seckel syndrome locus to chromosome 3q22. 1-q24. Am J Hum Genet 2000;67:498-503.

371. Verloes A, Drunat S, Gressens P, Passemard S: Primary Autosomal Recessive Microcephalies and Seckel Syndrome Spectrum Disorders. In: Adam MP, Ardinger HH, Pagon RA, Wallace SE, Bean LJH, Stephens K, Amemiya A, eds. GeneReviews((R)). Seattle (WA): University of Washington, Seattle University of Washington, Seattle. GeneReviews is a registered trademark of the University of Washington, Seattle. All rights reserved., 1993.

372. Digweed M, Sperling K. Nijmegen breakage syndrome: clinical manifestation of defective response to DNA double-strand breaks. DNA Repair (Amst) 2004;3:1207-1217.

373. Triemstra J, Pham A, Rhodes L, Waggoner DJ, Onel K. A Review of Fanconi Anemia for the Practicing Pediatrician. Pediatr Ann 2015;44:444-445, 448, 450 passim.

374. Meetei AR, Sechi S, Wallisch M, Yang D, Young MK, Joenje H, Hoatlin ME, et al. A multiprotein nuclear complex connects Fanconi anemia and Bloom syndrome. Mol Cell Biol 2003;23:3417-3426.

375. Nakanishi K, Taniguchi T, Ranganathan V, New HV, Moreau LA, Stotsky M, Mathew CG, et al. Interaction of FANCD2 and NBS1 in the DNA damage response. Nat Cell Biol 2002;4:913-920.

376. Pichierri P, Averbeck D, Rosselli F. DNA cross-link-dependent RAD50/MRE11/NBS1 subnuclear assembly requires the Fanconi anemia C protein. Hum Mol Genet 2002;11:2531-2546.

377. Roques C, Coulombe Y, Delannoy M, Vignard J, Grossi S, Brodeur I, Rodrigue A, et al. MRE11-RAD50-NBS1 is a critical regulator of FANCD2 stability and function during DNA double-strand break repair. Embo j 2009;28:2400-2413.

378. Adamo A, Collis SJ, Adelman CA, Silva N, Horejsi Z, Ward JD, Martinez-Perez E, et al. Preventing nonhomologous end joining suppresses DNA repair defects of Fanconi anemia. Mol Cell 2010;39:25-35.

379. Pace P, Mosedale G, Hodskinson MR, Rosado IV, Sivasubramaniam M, Patel KJ. Ku70 corrupts DNA repair in the absence of the Fanconi anemia pathway. Science 2010;329:219-223.

380. Bunting SF, Callen E, Kozak ML, Kim J-M, Wong N, Lopez-Contreras AJ, Ludwig T, et al. BRCA1 functions independently of homologous recombination in DNA interstrand cross-link repair. Mol Cell 2012;46:125-135.

381. Thongthip S, Conti BA, Lach FP, Smogorzewska A. Suppression of non-homologous end joining does not rescue DNA repair defects in Fanconi anemia patient cells. bioRxiv 2017.

382. Patel AG, Sarkaria JN, Kaufmann SH. Nonhomologous end joining drives poly(ADP-ribose) polymerase (PARP) inhibitor lethality in homologous recombination-deficient cells. Proc Natl Acad Sci U S A 2011;108:3406-3411.

383. Mills KD, Ferguson DO, Essers J, Eckersdorff M, Kanaar R, Alt FW. Rad54 and DNA Ligase IV cooperate to maintain mammalian chromatid stability. Genes Dev 2004;18:1283-1292.

384. Tsai FL, Kai M. The checkpoint clamp protein Rad9 facilitates DNA-end resection and prevents alternative non-homologous end joining. Cell Cycle 2014;13:3460-3464.

385. Shima N, Hartford SA, Duffy T, Wilson LA, Schimenti KJ, Schimenti JC. Phenotype-based identification of mouse chromosome instability mutants. Genetics 2003;163:1031-1040.

386. Ridpath JR, Nakamura A, Tano K, Luke AM, Sonoda E, Arakawa H, Buerstedde J-M, et al. Cells Deficient in the FANC/BRCA Pathway Are Hypersensitive to Plasma Levels of Formaldehyde. Cancer Research 2007;67:11117-11122.

387. Langevin F, Crossan GP, Rosado IV, Arends MJ, Patel KJ. Fancd2 counteracts the toxic effects of naturally produced aldehydes in mice. Nature 2011;475:53-58.

388. Oberbeck N, Langevin F, King G, de Wind N, Crossan GP, Patel KJ. Maternal aldehyde elimination during pregnancy preserves the fetal genome. Mol Cell 2014;55:807-817.

389. Puzio-Kuter AM. The Role of p53 in Metabolic Regulation. Genes & Cancer 2011;2:385-391.

390. Kim DH, Lee JW. Tumor suppressor p53 regulates bile acid homeostasis via small heterodimer partner. Proc Natl Acad Sci U S A 2011;108:12266-12270.

391. Kim SH, Trinh AT, Larsen MC, Mastrocola AS, Jefcoate CR, Bushel PR, Tibbetts RS. Tunable regulation of CREB DNA binding activity couples genotoxic stress response and metabolism. Nucleic Acids Res 2016;44:9667-9680.

392. Pagano G, Talamanca AA, Castello G, d'Ischia M, Pallardo FV, Petrovic S, Porto B, et al. From clinical description, to in vitro and animal studies, and backward to patients: oxidative stress and mitochondrial dysfunction in Fanconi anemia. Free Radic Biol Med 2013;58:118-125.

393. Degan P, Cappelli E, Regis S, Ravera S. New Insights and Perspectives in Fanconi Anemia Research. Trends Mol Med 2019;25:167-170.

394. Ravera S, Degan P, Sabatini F, Columbaro M, Dufour C, Cappelli E. Altered lipid metabolism could drive the bone marrow failure in fanconi anaemia. Br J Haematol 2018:DOI 10.1111/bjh.15171.

395. Nepal M, Ma C, Xie G, Jia W, Fei P. Fanconi Anemia complementation group C protein in metabolic disorders. Aging (Albany NY) 2018;10:1506-1522.

396. Panneerselvam J, Xie G, Che R, Su M, Zhang J, Jia W, Fei P. Distinct Metabolic Signature of Human Bladder Cancer Cells Carrying an Impaired Fanconi Anemia Tumor-Suppressor Signaling Pathway. J Proteome Res 2016;15:1333-1341.

397. Degan P, Cappelli E, Longobardi M, Pulliero A, Cuccarolo P, Dufour C, Ravera S, et al. A Global MicroRNA Profile in Fanconi Anemia: A Pilot Study. Metab Syndr Relat Disord 2019;17:53-59.

398. Paigen B, Morrow A, Brandon C, Mitchell D, Holmes P. Variation in susceptibility to atherosclerosis among inbred strains of mice. Atherosclerosis 1985;57:65-73.

399. Reccia I, Kumar J, Akladios C, Virdis F, Pai M, Habib N, Spalding D. Non-alcoholic fatty liver disease: A sign of systemic disease. Metabolism 2017;72:94-108.

400. Wang DQ, Paigen B, Carey MC. Phenotypic characterization of Lith genes that determine susceptibility to cholesterol cholelithiasis in inbred mice: physical-chemistry of gallbladder bile. J Lipid Res 1997;38:1395-1411.

401. Daugherity EK, Balmus G, Al Saei A, Moore ES, Abi Abdallah D, Rogers AB, Weiss RS, et al. The DNA damage checkpoint protein ATM promotes hepatocellular apoptosis and fibrosis in a mouse model of non-alcoholic fatty liver disease. Cell Cycle 2012;11:1918-1928.

402. Grillari J, Katinger H, Voglauer R. Contributions of DNA interstrand cross-links to aging of cells and organisms. Nucleic Acids Res 2007;35:7566-7576.

403. Begriche K, Igoudjil A, Pessayre D, Fromenty B. Mitochondrial dysfunction in NASH: causes, consequences and possible means to prevent it. Mitochondrion 2006;6:1-28.

404. He H, Wang J, Yannie PJ, Kakiyama G, Korzun WJ, Ghosh S. Sterol carrier protein-2 deficiency attenuates diet-induced dyslipidemia and atherosclerosis in mice. J Biol Chem 2018;293:9223-9231.

405. Quazi F, Molday RS. Lipid transport by mammalian ABC proteins. Essays Biochem 2011;50:265-290.

406. Terasaka N: Chapter 10 - Sterol Efflux by ABCA1 and ABCG1. In: Komoda T, ed. The HDL Handbook. Boston: Academic Press, 2010; 199-214.

407. Wang N, Lan D, Chen W, Matsuura F, Tall AR. ATP-binding cassette transporters G1 and G4 mediate cellular cholesterol efflux to high-density lipoproteins. Proc Natl Acad Sci U S A 2004;101:9774-9779.

408. Fukao T, Mitchell G, Sass JO, Hori T, Orii K, Aoyama Y. Ketone body metabolism and its defects. J Inherit Metab Dis 2014;37:541-551.

409. Garcia-Bermudez J, Birsoy K. Drugging ACAT1 for Cancer Therapy. Mol Cell 2016;64:856-857.

410. Fan J, Lin R, Xia S, Chen D, Elf SE, Liu S, Pan Y, et al. Tetrameric Acetyl-CoA Acetyltransferase 1 Is Important for Tumor Growth. Mol Cell 2016;64:859-874.

411. Goldstein JL, DeBose-Boyd RA, Brown MS. Protein Sensors for Membrane Sterols. Cell;124:35-46.

412. Ntambi JM. Regulation of stearoyl-CoA desaturase by polyunsaturated fatty acids and cholesterol. J Lipid Res 1999;40:1549-1558.

413. Rog T, Vattulainen I. Cholesterol, sphingolipids, and glycolipids: what do we know about their role in raft-like membranes? Chem Phys Lipids 2014;184:82-104.

414. D'Angelo G, Capasso S, Sticco L, Russo D. Glycosphingolipids: synthesis and functions. Febs j 2013;280:6338-6353.

415. Hakomori S, Igarashi Y. Functional role of glycosphingolipids in cell recognition and signaling. J Biochem 1995;118:1091-1103.

416. Summers SA. Ceramides in insulin resistance and lipotoxicity. Prog Lipid Res 2006;45:42-72.

417. Chaurasia B, Summers SA. Ceramides - Lipotoxic Inducers of Metabolic Disorders. Trends Endocrinol Metab 2015;26:538-550.

418. Hla T, Kolesnick R. C16:0-ceramide signals insulin resistance. Cell Metab 2014;20:703-705.

419. DeLong CJ, Shen YJ, Thomas MJ, Cui Z. Molecular distinction of phosphatidylcholine synthesis between the CDP-choline pathway and phosphatidylethanolamine methylation pathway. J Biol Chem 1999;274:29683-29688.

420. Fast DG, Vance DE. Nascent VLDL phospholipid composition is altered when phosphatidylcholine biosynthesis is inhibited: evidence for a novel mechanism that regulates VLDL secretion. Biochim Biophys Acta 1995;1258:159-168.

421. Kabarowski JH, Xu Y, Witte ON. Lysophosphatidylcholine as a ligand for immunoregulation. Biochem Pharmacol 2002;64:161-167.

422. McMahon HT, Boucrot E. Membrane curvature at a glance. J Cell Sci 2015;128:1065-1070.

423. Han X. Lipidomics for studying metabolism. Nat Rev Endocrinol 2016;12:668-679.

424. Unger RH, Scherer PE. Gluttony, sloth and the metabolic syndrome: a roadmap to lipotoxicity. Trends Endocrinol Metab 2010;21:345-352.

425. Jornayvaz FR, Shulman GI. Diacylglycerol activation of protein kinase Cepsilon and hepatic insulin resistance. Cell Metab 2012;15:574-584.

426. Samuel VT, Petersen KF, Shulman GI. Lipid-induced insulin resistance: unravelling the mechanism. Lancet 2010;375:2267-2277.

427. Spector AA, Mathur SN, Kaduce TL. Role of acylcoenzyme A: cholesterol o-acyltransferase in cholesterol metabolism. Prog Lipid Res 1979;18:31-53.

428. Pagano G, Degan P, d'Ischia M, Kelly FJ, Pallardo FV, Zatterale A, Anak SS, et al. Gender- and age-related distinctions for the in vivo prooxidant state in Fanconi anaemia patients. Carcinogenesis 2004;25:1899-1909.

429. Kais Z, Rondinelli B, Holmes A, O'Leary C, Kozono D, D'Andrea AD, Ceccaldi R. FANCD2 Maintains Fork Stability in BRCA1/2-Deficient Tumors and Promotes Alternative End-Joining DNA Repair. Cell Rep 2016;15:2488-2499.

430. Ceccaldi R, Liu JC, Amunugama R, Hajdu I, Primack B, Petalcorin MIR, O'Connor KW, et al. Homologous recombination-deficient tumors are hyper-dependent on POLQ-mediated repair. Nature 2015;518:258-262.

431. Smid V, Petr T, Vanova K, Jasprova J, Suk J, Vitek L, Smid F, et al. Changes in Liver Ganglioside Metabolism in Obstructive Cholestasis - the Role of Oxidative Stress. Folia Biol (Praha) 2016;62:148-159.

432. Guyot C, Stieger B. Interaction of bile salts with rat canalicular membrane vesicles: evidence for bile salt resistant microdomains. J Hepatol 2011;55:1368-1376.

433. Morita SY, Ikeda N, Horikami M, Soda K, Ishihara K, Teraoka R, Terada T, et al. Effects of phosphatidylethanolamine N-methyltransferase on phospholipid composition, microvillus formation and bile salt resistance in LLC-PK1 cells. Febs j 2011;278:4768-4781.

434. Maqdasy S, Trousson A, Tauveron I, Volle DH, Baron S, Lobaccaro JM. Once and for all, LXRalpha and LXRbeta are gatekeepers of the endocrine system. Mol Aspects Med 2016;49:31-46.

435. Laffitte BA, Joseph SB, Walczak R, Pei L, Wilpitz DC, Collins JL, Tontonoz P. Autoregulation of the human liver X receptor alpha promoter. Mol Cell Biol 2001;21:7558-7568.

436. Schulman IG. Liver X receptors link lipid metabolism and inflammation. FEBS Lett 2017;591:2978-2991.

437. Turley SD, Schwarz M, Spady DK, Dietschy JM. Gender-related differences in bile acid and sterol metabolism in outbred CD-1 mice fed low- and high-cholesterol diets. Hepatology 1998;28:1088-1094.

438. Zhang Y, Klaassen CD. Effects of feeding bile acids and a bile acid sequestrant on hepatic bile acid composition in mice. J Lipid Res 2010;51:3230-3242.

439. Maxwell KN, Soccio RE, Duncan EM, Sehayek E, Breslow JL. Novel putative SREBP and LXR target genes identified by microarray analysis in liver of cholesterol-fed mice. J Lipid Res 2003;44:2109-2119.

440. Lorbek G, Perse M, Horvat S, Bjorkhem I, Rozman D. Sex differences in the hepatic cholesterol sensing mechanisms in mice. Molecules 2013;18:11067-11085.

441. Houghtaling S, Timmers C, Noll M, Finegold MJ, Jones SN, Meyn MS, Grompe M. Epithelial cancer in Fanconi anemia complementation group D2 (Fancd2) knockout mice. Genes Dev 2003;17:2021-2035.

442. Behling-Kelly E, Collins-Cronkright R. Increases in beta-lipoproteins in hyperlipidemic and dyslipidemic dogs are associated with increased erythrocyte osmotic fragility. Vet Clin Pathol 2014;43:405-415.

443. Folch J, Lees M, Sloane Stanley GH. A simple method for the isolation and purification of total lipides from animal tissues. J Biol Chem 1957;226:497-509.

444. Chong J, Xia J. MetaboAnalystR: an R package for flexible and reproducible analysis of metabolomics data. Bioinformatics 2018;34:4313-4314.

445. Chong J, Soufan O, Li C, Caraus I, Li S, Bourque G, Wishart DS, et al. MetaboAnalyst 4.0: towards more transparent and integrative metabolomics analysis. Nucleic Acids Res 2018;46:W486-w494.

446. Research IfLA. Guide for the care and use of laboratory animals. 8th ed. Washington, DC: National Acadamies Press, 2011.

447. Bolliger AP. Cytologic evaluation of bone marrow in rats: indications, methods, and normal morphology. Vet Clin Pathol 2004;33:58-67.

448. Vandesompele J, De Preter K, Pattyn F, Poppe B, Van Roy N, De Paepe A, Speleman F. Accurate normalization of real-time quantitative RT-PCR data by geometric averaging of multiple internal control genes. Genome Biol 2002;3:RESEARCH0034.

449. Noel G, Le Vee M, Moreau A, Stieger B, Parmentier Y, Fardel O. Functional expression and regulation of drug transporters in monolayer- and sandwich-cultured mouse hepatocytes. Eur J Pharm Sci 2013;49:39-50.

450. Fuchs M, Hafer A, Munch C, Kannenberg F, Teichmann S, Scheibner J, Stange EF, et al. Disruption of the sterol carrier protein 2 gene in mice impairs biliary lipid and hepatic cholesterol metabolism. J Biol Chem 2001;276:48058-48065.

451. Haeusler RA, Hartil K, Vaitheesvaran B, Arrieta-Cruz I, Knight CM, Cook JR, Kammoun HL, et al. Integrated control of hepatic lipogenesis versus glucose production requires FoxO transcription factors. Nat Commun 2014;5:5190.

452. Cheung RS, Taniguchi T. Recent insights into the molecular basis of Fanconi anemia: genes, modifiers, and drivers. International journal of hematology 2017;106:335-344.

453. Alnouti Y, Klaassen CD. Tissue distribution and ontogeny of sulfotransferase enzymes in mice. Toxicol Sci 2006;93:242-255.

454. Kocarek TA, Duanmu Z, Fang HL, Runge-Morris M. Age- and sex-dependent expression of multiple murine hepatic hydroxysteroid sulfotransferase (SULT2A) genes. Biochem Pharmacol 2008;76:1036-1046.

455. Bhat KP, Cortez D. RPA and RAD51: fork reversal, fork protection, and genome stability. Nat Struct Mol Biol 2018;25:446-453.

456. Mijic S, Zellweger R, Chappidi N, Berti M, Jacobs K, Mutreja K, Ursich S, et al. Replication fork reversal triggers fork degradation in BRCA2-defective cells. Nat Commun 2017;8:859.

457. Zadorozhny K, Sannino V, Belan O, Mlcouskova J, Spirek M, Costanzo V, Krejci L. Fanconi-Anemia-Associated Mutations Destabilize RAD51 Filaments and Impair Replication Fork Protection. Cell Rep 2017;21:333-340.

458. Przetocka S, Porro A, Bolck HA, Walker C, Lezaja A, Trenner A, von Aesch C, et al. CtIP-Mediated Fork Protection Synergizes with BRCA1 to Suppress Genomic Instability upon DNA Replication Stress. Mol Cell 2018;72:568-582.e566.

459. Pierce AJ, Johnson RD, Thompson LH, Jasin M. XRCC3 promotes homology-directed repair of DNA damage in mammalian cells. Genes Dev 1999;13:2633-2638.